A New Approach To Identifying Effectors and Regulators of Small GTPases

Jessica Inti Bertram

MRC Laboratory of Molecular Biology

Pembroke College

University of Cambridge

This thesis is submitted for the degree of Doctor of Philosophy

Under the supervision of Dr. Sean Munro

March 2021

Declaration

This thesis is submitted for the degree of Doctor of Philosophy. It is the result of my own work and work done in collaboration, except when declared in the text, and it is not substantially the same as any work that has already been submitted before for any degree or other qualification. This thesis does not exceed the prescribed 60.000-word limit for the Faculty of Biology Degree Committee.

Jessica Inti Bertram

30th March 2021

Abstract

A New Approach To Identifying Novel Effectors and Regulators of Small GTPases

Jessica Inti Bertram

Secretion and endocytosis are essential processes in eukaryotic cells, executed and tightly regulated by the cell's endomembrane system. It is widely accepted that small GTPases of the Ras superfamily are major regulators of membrane trafficking and signalling, ensuring specificity and efficiency through their spatiotemporal regulation.

Identifying the proteins interacting with small GTPases is vital for understanding how the small G proteins are regulated and where they function. With the aim of eliminating certain limitations posed by many traditional methods of studying protein-protein interactions, an adaptation of the recently developed *in vivo* proximity labelling technique BioID was used in this study. Here, BioID was redirected to the ectopic location of the surface of mitochondria (hereafter called MitoID) with the aim of restricting the non-specific background. Applying this method to 25 small GTPases of the Ras superfamily in their active and inactive states allowed for a direct and clean comparison between the putative interactomes, identifying both known effectors and regulators as well as putative novel interactors for most tested GTPases. Several potential novel interactions were validated through GST affinity chromatography and/or microscopy, namely with the Rab GTPases Rab2A (ARFGEF3/BIG3, STAMBPL1), Rab5A (OSBPL9, TBCK), Rab9A (HPS3, NDE1), and Rab11A/B (ALS2).

Furthermore, numerous novel interactors were identified for Rab1A and Rab1B, two mammalian paralogues of the yeast protein Ypt1 that are known to be key regulators in ER to Golgi trafficking and suggested to play a role in the regulation of autophagy. The newly identified proteins include Rabaptin5, which is a key player in the regulation of endosomal trafficking, PPP1R37, a protein of unknown function, CALCOCO1 and CLEC16A, which are potentially involved in autophagy, and several components of the phosphatidylinsositol-3-phospate kinase (PI3K) complex I, which is known to be a major autophagic regulator.

In collaboration with the Williams group, the PI3K complex I was shown to be a bona fide Rab1A regulator. Furthermore, direct binding assays showed that CALCOCO1, CLEC16A, and PPP1R37 all bind to Rab1A and Rab1B independently of adaptor proteins or other factors. More specifically, the Rab1 binding site on PPP1R37 was shown to be located on the C-terminal and central regions that contain multiple leucine rich repeats.

Collectively, this study has shown that MitoID is an effective and powerful tool to study protein-protein interactions, and has identified and confirmed several novel interactors of small GTPases which can aid in gaining understanding of how major processes such as vesicle trafficking and autophagy are regulated.

Table of contents

Chapter 1: General Introduction

There and Back Again – A Tale of Secretion and Endocytosis

Secretion and endocytosis are essential processes in eukaryotic cells, executed and tightly regulated by the cell's endomembrane system. The secretory pathway is responsible for the production, folding, and delivery of membrane proteins to their correct intracellular location, as well as the export of proteins to the extracellular environment or the lumen of endomembrane compartments (Barlowe & Miller, 2013) The endocytic pathway, on the other hand, regulates the recycling or degradation of extracellular proteins or membrane components (Scott et al., 2014). It is the main way of obtaining nutrients and regulating the vast array of molecules that cells present to their environment, and is essential in fundamental processes such as development, immunity, and cell signalling (Elkin et al., 2016).

1.1 The secretory pathway

1.1.1 The endoplasmic reticulum: protein translation and modification

The secretory pathway is initiated at the endoplasmic reticulum (ER), where secreted and integral membrane proteins, as well as a subpopulation of cytosolic proteins, are synthesised (Fig. 1.1) (Schwarz & Blower, 2016). Protein translation is executed by membrane-bound ribosomes lining a subsection of the ER surface called the rough ER. During or shortly after translation, the proteins are transported into the ER lumen where they are folded with the aid of chaperones and undergo modifications such as N-linked glycosylation and disulphide bond formation. Proteins that are terminally misfolded or unfolded will be transported to the cytosol and degraded by the proteasome in a process called ER-associated degradation (ERAD) (Ruggiano et al., 2014). Proteins that contain one or more hydrophobic stretches are incorporated into the lipid bilayer as integral membrane proteins, while proteins that are due to be secreted will be transported to the Golgi apparatus in membrane vesicles (Barlowe & Miller, 2013; Schwarz & Blower, 2016).

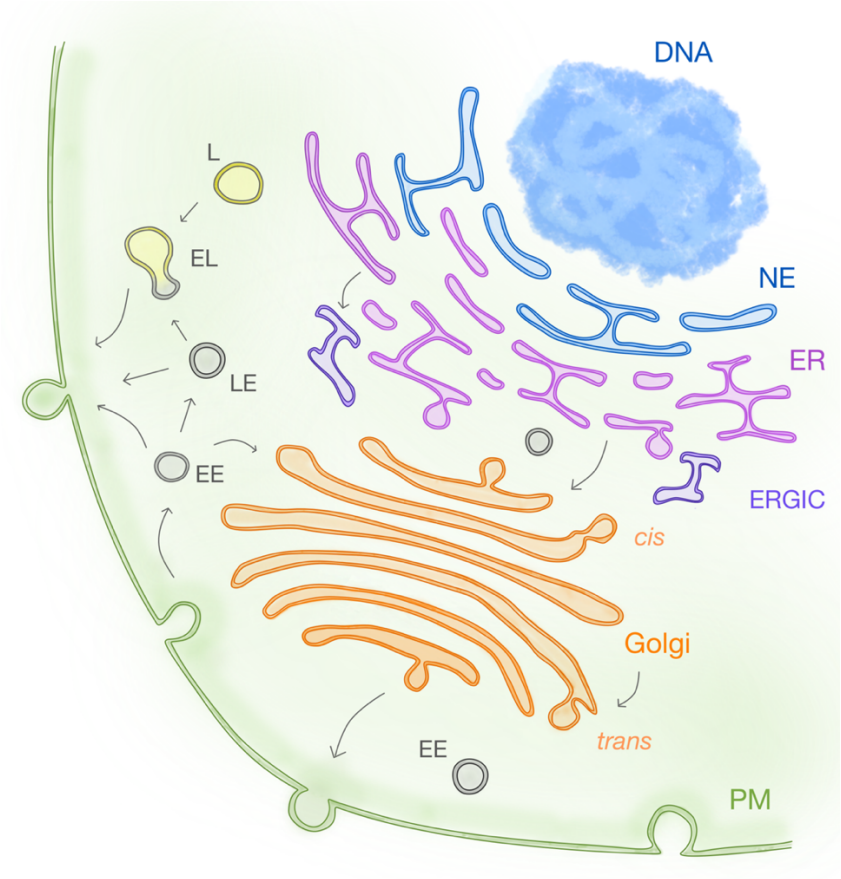

Figure 1.1. Schematic overview of the intracellular endomembrane system. Simplified overview of a mammalian cell, showing main components of the endomembrane system; the plasma membrane (PM, green), Golgi apparatus (orange, *cis*- and *trans*- sides indicated), ERGIC (ER-Golgi intermediate compartment, purple), Endoplasmic Reticulum (ER, lilac), nuclear envelope (NE, blue) early and late endosomes (EE, LE, grey), endo-lysosomes (EL, grey/yellow) and lysosomes (L, yellow). Arrows indicate potential routes of vesicle trafficking, both towards the plasma membrane (anterograde, secretion) or towards to the cell's interior (retrograde, endocytosis). Compartments not to scale.

1.1.2 From the ER to the Golgi: budding and fusing

1.1.2.1 Vesicle formation and budding

Proteins that were correctly synthesised and modified in the ER, can now be packaged and transported to the Golgi apparatus by membrane vesicles regulated and shaped by the COPII coat. The transport vesicles leaving the ER are formed at specialised zones called ER exit sites (ERES) or transitional ER (tER) (Kurokawa & Nakano, 2019). The formation of COPII-coated vesicles is initiated when the protein Sec12 activates the small GTPase Sar1 on the ER membrane (Barlowe & Miller, 2013). Small GTPases, or small G proteins, are a family of proteins which can be activated or inactivated by binding to GTP or GDP, respectively (more on small GTPases and their activation cycle in paragraph 1.3) (Wennerberg et al., 2005).

After Sec12 aids in the exchange of Sar1-assoiated GDP to GTP, the activated Sar1 is recruited to the membrane where it in turn recruits the heterodimeric complex of Sec23 and Sec24. Together, Sec23 and Sec24 form a stable concave complex which faces the membrane and together forms the inner layer of the COPII coat (Bi et al., 2002). The Sec23/Sec24 complex provides two different functions; while Sec23 deactivates Sar1 by aiding in the hydrolysis of its associated GTP, Sec24 allows cargo-binding by interacting with several sorting signals and ER export motifs, enriching cargo at the pre-budding site (Barlowe & Miller, 2013; Miller & Barlowe, 2010). Next, the heterotetrameric Sec13/Sec31 complex is recruited, which further stimulates the deactivation of Sar1 and comprises the outer layer of the COPII coat (Bi et al., 2007). Interestingly, Sec13 and Sec31 were shown to inherently self-assemble into a cage-like structure, independently of the presence of Sec23 and Sec24 (Stagg et al., 2006). However, later research by Stagg and colleagues indicated that Sec23/Sec24 complexes first oligomerise into clusters which define the site for Sec13/Sec31 cage formation, suggesting that Sec13/Sec31 might not be solely responsible for the structural roles of the COPII coat (Stagg et al., 2008).

After the planar ER membrane is transformed into a curved vesicle containing cargo ready for ER export, the budding vesicle will be released through scission. It is thought that COPII vesicle scission is driven by Sar1, but the exact mechanism behind this remains elusive; while certain studies suggests that Sar1 hydrolysis leads to fission by deforming the membrane, other studies have shown that a high concentration of Sar1 on the vesicle causes scission regardless of its activity state (Adolf et al., 2013; Hariri et al., 2014; M. C. S. Lee et al., 2005).

1.1.2.2 Vesicle tethering and fusion with the Golgi apparatus

The budded vesicles quickly encounter the first downstream sorting compartment, the ER-Golgi intermediate compartment (ERGIC) (Lord et al., 2013). The ERGIC is often found adjacent to ER exit sites, and mediates vesicle sorting both forwards to the Golgi and back to the ER (Ben-Tekaya et al., 2005). The COPII-coated vesicles can also fuse directly with the Golgi apparatus, specifically the ER-facing side called the *cis*-Golgi (Fig. 1.1). While a study in *S. cerevisiae* showed that the *cis*-Golgi can approach and contact the ERES to ensure efficient cargo transport, in general, the budded vesicles traverse the cytoplasm along cytoskeletal filaments and are guided to the *cis*-Golgi by certain tethering proteins (Kurokawa et al., 2014). Tethering proteins are categorised into two main groups, the multi-subunit tethering complexes and long coiled-coil proteins (Gillingham & Munro, 2019). Furthermore, tethers are generally only present on a specific membrane compartments where they recognise incoming vesicles, aiding towards the specificity of vesicle trafficking. Capture and tethering of ER-derived vesicles directed to the Golgi membrane arises through an interplay between COPII coat proteins, the small GTPase Rab1, the Rab1 activating protein

complex TRAPPIII, and the Rab1 effector and coiled-coil protein USO1/p115 (Lord et al., 2013). Small GTPase effectors are proteins that bind specifically to the activated form of the GTPase, thereby often setting in motion a cascade of events. After the TRAPPIII complex activates Rab1, the small GTPase becomes associated to the *cis*-Golgi membrane, where it recruits the long coiled-coil protein p115 (Lord et al., 2013). While the yeast ortholog of p115 (Uso1p) has been shown to be required for docking of ER-derived COPII vesicles at the Golgi, the exact mechanism through which p115 carries out this function is not yet fully understood (Cao et al., 1998). Several studies point towards p115 working together with the coiled-coil proteins GM130 and giantin, others indicate that p115 binds to monomeric SNARE proteins (Alvarez et al., 2001; Short et al., 2005; T. Wang et al., 2015). SNARE proteins (soluble N- ethylmaleimide-sensitive factor attachment protein receptors) are a group of proteins which aid membrane fusion by bringing two opposing membranes together through the interaction between SNAREs on vesicles (v-SNAREs) and SNAREs on the target membrane (t-SNAREs). Observing that p115 binds the v-SNARE sec22b and the t-SNARE rbet1, Wang and colleagues suggest a model in which p115 catalyses SNARE-SNARE interactions to mediate fusion (T. Wang et al., 2015). Further research is necessary to fully elucidate the mechanism of ER-derived vesicle docking and fusion at the *cis*-Golgi.

1.1.3 The Golgi apparatus

The Golgi apparatus is the main sorting station of the cell; central to both the secretory and endocytic pathways, it orchestrates the sorting and distribution of cargo originating from the ER and endocytic vesicles (Pantazopoulou & Glick, 2019). Consisting of stacks of distinct and polarised cisternae, the Golgi is organised from *cis*- to *trans*-, with the *cis*-side facing the ER and the *trans*-side facing outwards towards the cytoplasm and the plasma membrane (Fig. 1.2). Transport within the Golgi apparatus can occur from *cis*- to *trans*- (anterograde), as well as from the *trans*- to *cis*- (retrograde).

How intracellular membrane compartments maintain their identity, and how vesicle trafficking between these compartments and the plasma membrane is regulated, are topics of great interest and debate. One popular model that describes how this compartmentation could potentially be developed, is the cisternal maturation model, in which the *cis*-Golgi cisternae are formed *de novo* and then mature into *trans*-Golgi cisternae by undergoing certain biochemical changes. This model postulates cargo remains in a compartment and the arrival of certain enzymes converts *cis* cisternae into medial cisternae, and medial into *trans* cisternae. As the cisternae mature, they carry forward secretory cargoes and are remodelled into transport carriers at the *trans*-Golgi network (TGN), which means that each Golgi compartment would be viewed as a certain stage in the maturation process (Glick & Luini, 2011; Papanikou & Glick, 2014). However, while some studies point towards increased concentration of Golgi enzymes in transport vesicles

compared to the donor membrane, others observe that these vesicles are actually depleted of Golgi enzymes, which brings doubt to this model (Kweon et al., 2004; Lanoix et al., 1999).

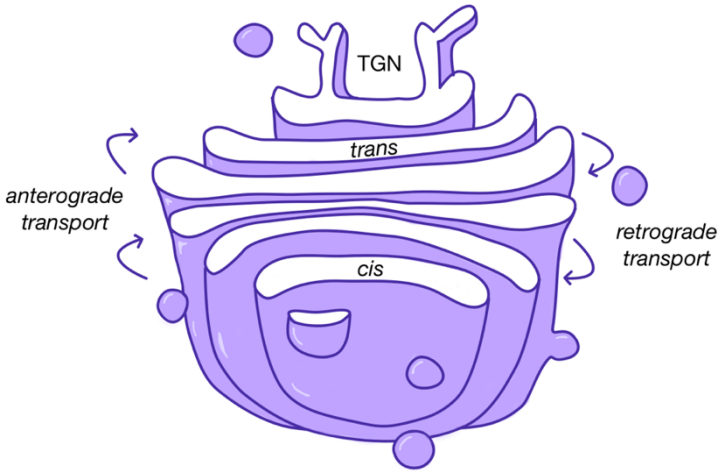

Figure 1.2. Schematic overview of the Golgi apparatus – a cross-section. A schematic representation of a cross-section of the mammalian Golgi apparatus. Cisternae are organised from *cis*- to *trans*-, terminating in a tubular structure called the *trans*-Golgi network (TGN). Cisternae are connected through continuous anterograde transport of cargo vesicles towards the TGN, while a retrograde flow of resident Golgi enzymes ensures that the cisternae retain their distinct organisation and function.

Another model suggests that the cisternae remain relatively stable and the cargo is transported between Golgi compartments by transport vesicles and/or tubules (Glick & Luini, 2011). While this model supports many aspects of observed Golgi morphology and function, the speed of vesicular transport that would be necessary to account for fast traffic of small cargoes also suggests that this model does not fully describe intra-Golgi transport.

In both the cisternal maturation and the vesicular transport models, the vesicles which transport either the Golgi enzymes or the cargo are coated by COPI. The COPI coat consists of seven components (αCOP, βCOP, β'COP, γCOP, δCOP, εCOP, ζCOP) forming a stable heteroheptameric complex called the coatomer (Popoff et al., 2011). Similar to the COPII coat, the assembly of the coatomer on vesicles is driven by a small GTPase of the Ras superfamily – Arf1. After Arf1 activation, most commonly by the protein GBF1, the GTP-bound Arf1 will anchor itself into the Golgi membrane and recruit the coatomer there (Beck et al., 2009). While Arf1 activation drives vesicle formation and budding, Arf1 hydrolysis by ArfGAPs leads to the shedding of the coat and allows the vesicle to fuse with the target membrane. Whether COPI-coated vesicles travel mostly anterograde or retrograde, and whether they largely carry protein cargo or Golgi enzymes remains disputed (Rabouille & Klumperman, 2005). A recent proteomic profiling study has found

numerous Golgi resident proteins, but hardly any anterograde cargo proteins, to be present in the proteomes of COPI vesicles, suggesting that COPI is mainly involved in retrograde traffic (Adolf et al., 2019). Further research toward COPI vesicle function could elucidate the potential roles of the cisternal maturation and the vesicle transport models.

Finally, the latest major model aimed at explaining intra-Golgi transport, the so-called cisternal progenitor model, is based on the observation that Rab GTPases can form distinct domains in endosomes (Sönnichsen et al., 2000). Furthermore, the previously described Rab cascades can drive a process called Rab conversion on endosomes, in which Rab cascades lead to the conversion of early to late endosomes (Rink et al., 2005). The cisternal progenitor model proposes that the Golgi is made up of stable compartments which are defined by distinct Rab GTPase domains (Pfeffer, 2010). These Rab domains can convert into a downstream Rab domain, after which the newly converted domain can fuse with the matching downstream Rab domain, creating a passageway for cargo to travel regardless of their size. While an intriguing proposition, this model provides no specific function for observed COPI vesicles and is also less appropriate for non-animal Golgi, which are generally observed in separate ministacks (Glick & Luini, 2011).

Even though the exact mechanism of developing and maintaining the *cis*- to *trans*-Golgi organisation remains elusive, it widely accepted that tight regulation of this process is necessary for proper Golgi function. One of the main reasons behind this is how anterograde traffic through the Golgi correlates with the sequential nature of glycan modifications on cargo proteins. In the secretory pathway, ER-derived vesicles dock at the *cis*-Golgi and traverse through the medial cisternae, where they may receive certain post-translational modifications (Jackson, 2009). While N-linked glycosylation mainly occurs in the ER, the Golgi apparatus is the main site of glycan processing, trimming, and addition, and is thus abundant with glycan modifying enzymes such as glycosyltransferases and glycosidases (Stanley, 2011; Welch & Munro, 2019). While glycosyltransferases catalyse the transfer of sugar groups onto proteins or lipids containing glycan acceptors, glycosidases may remove sugars to trim the glycan groups. Since the glycan modifications occur sequentially as the protein travels through the Golgi, the localisation of the enzymes relative to one another is key for providing the correct final modifications. It is thought that (specific) retrograde cisternal transport of resident Golgi enzymes ensures cisternal organisation and functionality while the Golgi is undergoing a continuous anterograde flow of cargo proteins (Fig 1.2) (Welch & Munro, 2019).

It is likely that multiple mechanisms are in place to facilitate the sorting and retention of Golgi enzymes, with a combination of factors contributing to maintaining proper Golgi organisation (Schoberer & Strasser, 2011; Welch & Munro, 2019). Firstly, an extensive comparison of transmembrane proteins has shown that the length of their transmembrane domains (TMDs) differs depending on which organelle the protein resides on – TMDs appeared to be shorter in the early secretory pathway and longer in the late secretory pathway (Sharpe et al., 2010). In line with these observations, it is thought that organelle membranes become increasingly thicker as they progress through the secretory pathway, possibly due to differing lipid compositions (Welch & Munro, 2019). It has previously been shown that increasing the length of the TMD decreases the efficiency of Golgi enzyme retention, which suggests that the Golgi enzymes are retained in the Golgi because their shorter TMDs favour the relatively thinner Golgi membranes (Munro, 1995). More recently, it has been shown that the cisternal membranes gradually increase in thickness from the *cis*- to *trans*-Golgi, suggesting that the thickness of membranes could not only be responsible for Golgi enzyme retention but also the sorting and organisation within cisternae (Bykov et al., 2017).

The rapid partitioning model, on the other hand, proposes that transport vesicles are sorted spatially due to self-organising lipid domains (Patterson et al., 2008). The variance of lipid composition and formation of distinct domains is suggested to be generated by the flux of proteins and lipids by intra-Golgi transport, as well as certain individual membrane properties. However, the mechanism described by Patterson and colleagues was disputed by Nilsson and colleagues, who suggest that the membrane proteins order the lipids surrounding them, rather than the other way around (Nilsson et al., 2009). Further research is necessary to elucidate the role of lipid composition in the sorting of glycan processing enzymes.

Another mechanism through which the Golgi enzymes can be organised and sorted to certain cisternae is through sorting motifs on the enzymes themselves. The main proteins identified to interact with certain well conserved motifs on glycosyltransferases are GOLPH3 and GOLPH3L (Tu et al., 2008). Furthermore, GOLPH3 and GOLPH3L have been found to bind directly to components of the COPI coat and interact with phosphatidylinositol-4-phosphate (PI4P), indicating that GOLPH3 and GOLPH3L could function as adaptor proteins to promote glycosyltransferase incorporation into COPI coated vesicles and transport them back to previous cisternae (Eckert et al., 2014; Tu et al., 2012; Welch & Munro, 2019).

Finally, the kin recognition mechanism postulates that Golgi enzymes resident to the *cis*- and medial cisternae oligomerise and form higher order complexes which prevents them from entering budding vesicles (Nilsson et al., 1993). Although the oligomerisation of medial Golgi enzymes (but not *trans*-Golgi enzymes) has been observed, a study using fluorescence recovery after photobleaching (FRAP) has shown that the

Golgi membrane composition recovers rapidly after photobleaching, indicating that the resident Golgi enzymes are not hindered in their mobility (Brandizzi et al., 2002; Opat et al., 2000). Further research towards this mechanism is crucial in understanding how the several proposed mechanisms could work together to generate and maintain Golgi enzyme sorting.

1.1.4 The journey after the Golgi

After navigating through the Golgi, the synthesised proteins reach the TGN where they will be sorted and packaged into transport carriers. The cargo sorting is a meticulous process involving coat proteins, adaptor proteins of the AP and GGA families, phosphatidylinositols, and the small GTPase Arf1 (Gadila & Kim, 2016). The general consensus of this process is as follows; active Arf1 can recruit phosphatidylinositol-4-kinase (PI4K) to the TGN membrane, which aids in the production of phosphatidylinositol-4-phosphate (PI4P). The presence of PI4P promotes the recruitment of the GGA adaptor proteins to the TGN by Arf1, which in turn recruits additional PI4K to the membrane, providing a positive feedback loop. When sufficient levels of PI4P are reached at the TGN, Arf1 will recruit and activate AP-1. AP-1 can then interact with sorting motifs present on cargos destined for endosomes and lysosomes, as well as recruit the clathrin coat on the budding vesicle (Gadila & Kim, 2016; Guo et al., 2014).

Besides transport to endosomes and lysosomes, proteins arrived at the Golgi can also be trafficked back to the ER. Retrograde Golgi-to-ER trafficking occurs generally to allow protein quality control in the ER, or to return trafficking machinery or ER-resident proteins, and is mediated by the COPI coat (Duden, 2009; Spang, 2013).

While clathrin-coated vesicles are the main carriers for endosome/lysosome-directed transport, and COPI-coated vesicles mediate the retrograde Golgi-to-ER trafficking, the main route of transport to the plasma membrane is through ‘pleomorphic tubular-vesicular carriers’ – lipid tubules and vesicles which are heterogenous in size and remain uncoated (Stalder & Gershlick, 2020). Bard and Malhotra suggest a model in which the transport carriers bud off from the membrane and grow in size, potentially through pulling by motor proteins, hereby forming tubules. Certain feedback loops and signalling cascades generate lipid domains on the TGN membrane, which lead to fission of the tubules and create the transport carriers (Bard & Malhotra, 2006).

1.2 The endocytic pathway

1.2.1 Internalisation via the plasma membrane

In the endocytic pathway, small membrane vesicles are generated that transport cargo from the plasma membrane into the interior of the cell. The cargo consist mainly of transmembrane proteins and their ligands, nutrients, and growth factors, although pathogens often exploit the endocytic pathway to mediate their internalisation (Doherty & McMahon, 2009).

1.2.1.1 Clathrin-mediated endocytosis

Most commonly, endocytosis is known to occur through the generation of clathrin-coated vesicles at the plasma membrane. Briefly, the proteins that make up the coat concentrate at the site of invagination, promoting membrane bending and resulting in a 'clathrin-coated pit' (Kaksonen & Roux, 2018). Certain protein components of the clathrin coat bind to cytosolic parts of different transmembrane cargo molecules, which mediates recruitment of cargo molecules to the prospective vesicle. Vesicle scission is generally catalysed by the GTPase dynamin, which forms a collar around the neck of the clathrin-coated pit, and snips it. The formation of the vesicle ends with the disassembly of the protein coat, after which the uncoated vesicle can fuse with early endosomes (Kaksonen & Roux, 2018).

1.2.1.2 Clathrin-independent endocytosis

Endocytosis can also occur via several clathrin-independent routes, of which the best characterised involves clathrin-independent carriers (CLICs) that can mature into glycosylphosphatidylinositol-anchored protein-enriched early endocytic compartments (GEECs). CLIC/GEEC endocytosis is regulated by the small GTPases Arf1 and Cdc42 and several other proteins including GTPase activating proteins, actin nucleation factors, and BAR-domain proteins (Shafaq-Zadah et al., 2020). It is thought that clathrin-independent routes of endocytosis are associated with cell polarity, since cargoes internalised via these routes are often found to be localised and internalised in a polarised manner. Furthermore, the clathrin-independent uptake machinery can show a polarised distribution itself; CLIC structures are preferentially found at the leading edge of migrating cells, as is the occurrence of clathrin-independent fast-endophilin-mediated endocytosis (FEME) (Casamento & Boucrot, 2020; Shafaq-Zadah et al., 2020).

1.2.2 endosomes: from early to late

Upon internalisation, endocytic vesicles fuse with early endosomes (EE), also known, appropriately, as sorting endosomes. Here, cargo is sorted into a variety of different endocytic pathways, including

degradation via endo-lysosomes, recycling either via recycling endosomes or directly back to the plasma membrane, or cargo redistribution via the Golgi apparatus, namely the *trans*-Golgi network (Fig. 1.1) (Huotari & Helenius, 2011).

Recycling of membrane components back to the plasma membrane is key in acquiring membrane homeostasis; an estimated 50-180% of plasma membrane surface area is cycled in and out of the cell every hour, highlighting the need for an efficient system of membrane recycling (Steinman et al., 1983). The recycling of plasma membrane components can occur directly via EE, allowing rapid turnover, or via recycling endosomes (RE). RE are often tubular in shape and are localised in the perinuclear region called the endocytic recycling complex (ERC) (Naslavsky & Caplan, 2018).

1.2.3 lysosomes and autophagosomes: degradation and recycling

If endocytosed proteins are targeted for degradation, the EE carrying the proteins will transport to late endosomes (LE) and fuse with lysosomes, forming endo-lysosomes (Fig. 1.1) (Scott et al., 2014). Lysosomes are membranous organelles that contain acid hydrolases and enzyme activators which can degrade different substrates (Ballabio & Bonifacino, 2020). The endo-lysosomal pathway is key in maintaining cell health, breaking down molecules to inactivate pathogens or clear up protein aggregates. Besides via the endocytic pathway, proteins and other macro-molecules can reach the lysosomes through the secretory, phagocytic, and autophagic pathways.

Autophagy is a key process in the cell and is induced upon cellular stress such as nutrient starvation, hypoxia, and infection. The main function of autophagy is to degrade cellular components and recycle them, mostly to meet energy requirements under starvation, but also to aid in the removal of misfolded proteins (K. H. Kim & Lee, 2014). It is a highly controlled and regulated process, and the key steps are largely homologous between mammalian cells and yeast.

Since the lysosomes are vital in mediating cellular catabolism, they are ideal hubs to sense the cell's nutritional status and health. One of the main signalling pathways related to nutrient starvation starts with the mTOR complex; mTORC1 is generally localised on lysosomes where it activates a signalling cascade that functions in cell survival (Ballabio & Bonifacino, 2020). Upon starvation or other autophagic cues, mTORC1 becomes inhibited which causes the dissociation of the ULK1 complex (ULK1, ATG13, ATG101, and FIP200) from mTORC1. ULK1 is then able to phosphorylate ATG13 and FIP200, hereby activating the ULK1 complex. The active ULK1 complex phosphorylates the protein AMBRA1, which then recruits the VPS34/VPS15/Beclin1 complex (specifically complex I, which additionally contains

ATG14L and NRBF2) to membranes. Notably, several other factors such as AKT and EGFR can also phosphorylate Beclin1 independently of mTORC1. The VPS34 complex functions by phosphorylating the lipid phosphatidylinositol to form phosphatidylinositol-3-phosphate (PI3P). Hence, the VPS34 complex is also called the PI3-kinase complex, or PI3K. PI3P then recruits numerous other proteins which together initiate the membrane formation that will ultimately form the phagophore (Fig. 1.3) (K. H. Kim & Lee, 2014; Ravanan et al., 2017). Besides in PI3K complex I, the VPS34/VPS15/Beclin1 components also exists in a separate but related complex – the class III PI3K complex II additionally contains UVRAG and Rubicon, and is mostly present on endosomal membranes (Ohashi et al., 2018).

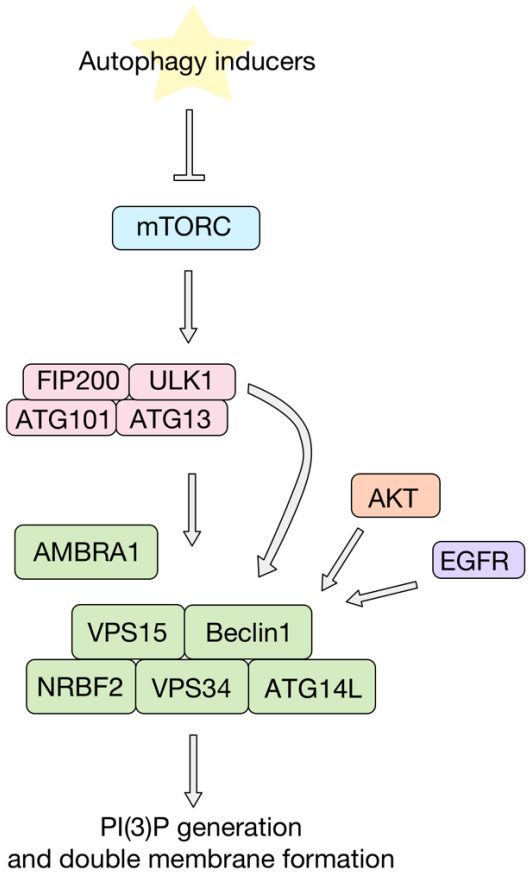

Figure 1.3. Schematic overview of signalling pathways involved in autophagy initiation. Schematic and simplified representation of initial molecular interaction and signalling pathways set in motion after detection of an autophagy inducer such as nutrient starvation.

After the initial phagophore membrane is formed, numerous autophagy-related proteins aid in the elongation, and eventually closure, of the phagophore (Fig. 1.4). The proteins ATG5, ATG12, and ATG16L1 form a complex that assists in forming the correct curvature of the double membrane structure.

Furthermore, ATG4B, ATG7, and ATG3 work together to lipidate LC3B, fully named MAP1LC3B (microtubule-associated protein 1A/1B light chain 3B) for its association with microtubules, but now mostly regarded as an autophagosome marker. The ATG5/ATG12/ATG16L1 complex then recruits the lipidated LC3B (LC3B-II) to the inner and outer membranes of the autophagosomes. Finally, autophagosomes fuse with lysosomes to form autolysosomes, this can happen either directly or by first fusing with endosomes to form amphisomes (K. H. Kim & Lee, 2014; Ravanan et al., 2017). Fusion with lysosomes allows the degradation of autophagosomal cargo by acidic lysosomal components, after which they can be recycled to help fulfil the cell's requirements for energy and amino acids.

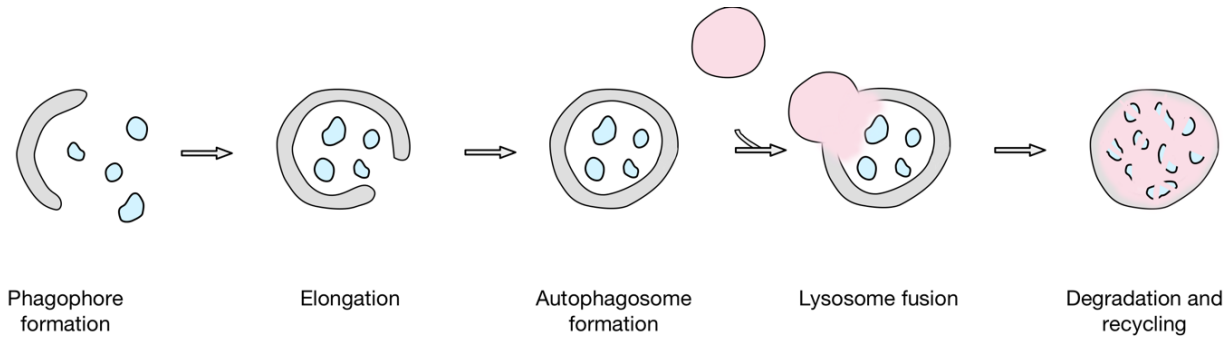

Figure 1.4. Schematic overview of autophagy initiation and progression. Schematic representation of initiation and progression of autophagy, starting at phagophore formation (grey), elongation of the phagophore to enclose cellular components (blue), closure of phagophore and autophagosome formation, fusion with the lysosome (pink), and ultimately degradation and recycling of degraded components.

Besides the aforementioned proteins, numerous other proteins are involved with the initiation, maturation, or regulation of autophagy. Several Rab GTPases have been found to show links to the regulation of autophagy, one of which is the previously mentioned Rab1. The yeast homologue of Rab1, Ypt1, has been shown to play an important role in autophagy, starting several decades ago when Ypt1 was shown to be necessary for the onset of autophagy and cell survival under starvation (Segev & Botstein, 1987). Since then, numerous studies have identified different ATG proteins as Ypt1 effectors, more specifically showing that Ypt1 is required for the recruitment of some of these proteins to the pre-autophagosomal structure, where the phagophore will be formed in yeast (Lipatova et al., 2012; Segev & Botstein, 1987; Juan Wang et al., 2013).

1.3 Small G proteins – a closer look

It is widely accepted that Arf and Rab GTPases from the Ras superfamily are key contributors to the regulation of membrane trafficking, which is vital for maintaining cell health. The Ras superfamily consists of the Ran, Ras, Rab, Rho, and Arf families, which all tend to have their own areas of expertise; while Rab and Arf proteins regulate membrane traffic, Ran is involved in nuclear trafficking, Ras family members are key cell cycle regulators, and members of the Rho family are mostly known to regulate actin formation (Donaldson & Jackson, 2011; Hall, 2012; Macaluso et al., 2002; Matchett et al., 2014).

Even though they affect various processes, all G-proteins in the Ras superfamily function in a similar way – they are all GTPases that act as molecular switches and set downstream effects in motion through their effectors. In their active state, the GTPases are GTP-bound, whereas inactive GTPases are associated with GDP. The activity cycle of GTPases is regulated by two groups of enzymes which catalyse the reactions; guanine nucleotide-exchange factors (GEFs) allow for GTP-association by opening up nucleotide interaction interface, while GTPase-activating proteins (GAPs) catalyse GTP hydrolysis by providing an extra residue to the active site (Hennig et al., 2015) (Fig. 1.5).

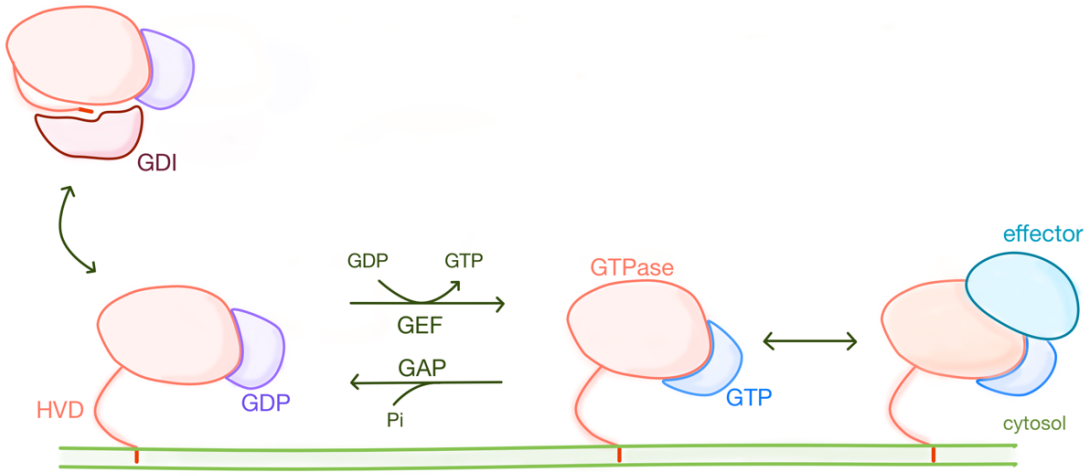

Figure 1.5. Schematic representation of the small GTPase activity cycle. Schematic representation of the activity cycle of small GTPases, in which the GTPases are activated by GTP association and inactivated by GTP hydrolysis. Guanine nucleotide-exchange factors (GEFs) exchange GDP for GTP, while GTPase activating proteins (GAPs) aid in the GTP hydrolysis. In its activated state, the small GTPase is membrane bound and can recruit effector proteins, while in its inactivate state, the GTPase becomes disassociated from the membrane aided by the GDP-dissociation inhibitors (GDIs) which protect the hydrophobic hypervariable domains (HVD) from the cytosol.

Most GTPases are incorporated into their target membrane through the prenylation of their C-terminal cysteines; enzymes called geranylgeranyl transferases catalyse the addition of a 20-carbon isoprenoid chain to cysteine residues which enables membrane association (Gutkowska & Swiezewska, 2012). Other small GTPases, such as members of the Arf family, receive their membrane-anchoring modifications at the N-terminus, while the GTPase Ran lacks the membrane targeting domain altogether (D'Souza-Schorey & Chavrier, 2006, Boudhraa, 2020). While active Rab GTPases generally remain associated with their distinct membrane compartments, inactive GTPases are solubilised by GDP-dissociation inhibitors (GDIs) (Fig. 1.5). GDIs specifically bind prenylated and inactive GDP-bound Rab proteins, ensuring extraction of the Rab proteins only after inactivation (Müller & Goody, 2017).

Small GTPases are generally allocated to specific intracellular membrane compartments and organelles. How the GTPases are targeted to specific membrane compartments remains a topic of great discussion, however more recent studies points towards GEFs being key players in GTPase targeting. In a literature review, Francis Barr proposes a model based on the continuous cycling of Rab GTPases membrane association state and the localisation of GEFs. Rab GTPases cycle between being soluble through GDI-association, and being incorporated in membranes they come across. Barr proposes that, once they encounter a membrane surface hosting its associated GEF, the Rab GTPases are activated and become resistant to GDI extraction, remaining in this membrane compartment (Barr, 2013).

This, importantly, means that the cycle of the GTPase's activity state is linked to its association to specific membrane compartments. Because GTPases predominantly interact with their effector proteins in their active, GTP-bound state, effectors are essentially recruited to specific intracellular membrane compartments where they are able to activate signalling pathways or set interaction cascades in motion (Zerial & McBride, 2001). One thoroughly investigated example shows how activated Rab5 recruits its effectors EEA1 and Rabaptin5 to early endosomes, where they have been shown to drive endosome fusion (Mills, et al., 1999). Active GTPases can also recruit motor proteins or motor protein adaptors, regulating the directed transport of organelles. For example, activated Rab7 on lysosomes and endosomes is able to recruit RILP (Rab-interacting lysosomal protein) and ORP1L (oxysterol-binding protein-related protein 1L), which together bind to the $p150^{glued}$ subunit of dynactin and the dynein light intermediate chain. This complex recruits the dynein-dynactin complex to the Rab7-positive vesicles for minus end-directed transport (Johansson et al., 2007).

Interestingly, certain effector proteins are able to bind multiple GTPases using distinct binding sites. For example, the aforementioned Rab5 effector Rabaptin5 was found to also bind to Rab4, thereby essentially

functioning as a molecular link between the two Rab GTPases (Vitale et al., 1998). This process is called a GTPase cascade, which can play essential roles in establishing membrane flow between intra-organelle compartments, such as endosome maturation or *cis*- to *trans*-Golgi flow (Pfeffer, 2017).

Another route through which GTPase cascades can be established is through the effector recruitment of regulators for downstream or upstream GTPases. A well-established example occurs in the conversion between Rab5- and Rab7-positive endosomes with the Mon1-Ccz1 complex, which is both a Rab5 effector and a Rab7 GEF. Upon Rab5 activation, the Mon1-Ccz1 complex is recruited to Rab5-positive early endosomes where they can recruit and activate Rab7, hereby driving the transition and maturation to Rab7-positive late endosomes and lysosomes (Langemeyer et al., 2020).
On the other hand, activated GTPases can also recruit GAPs of upstream GTPases. This leads to a cascade in which the activation of the second GTPase leads to inactivation of the first GTPase, hereby further allowing a proper GTPase transition. Continuing on with the previously mentioned example regarding endosome maturation, a study in yeast has identified that active Ypt7 (Rab7 homologue) recruits the BLOC-1 complex and the GAP Msb3, which together drive the inactivation of Vps21 (Rab5 homologue) (Rana et al., 2015). Together, this shows a sophisticated mechanism which drives endosome maturation.

1.4. Expanding the set of known Rab GTPase effectors

As previously discussed, membrane trafficking requires a high degree of regulation. Defects or alterations in these processes are known to be associated with numerous pathological conditions such as Parkinson's disease, Alzheimer's disease, and cancer (Goldenring, 2013; Rajendran & Annaert, 2012; Vidyadhara et al., 2019). However, since a multitude of diseases and conditions arise when the endocytic or secretory pathways are affected, these pathways in turn are possible therapeutic targets (Goldenring, 2013; Wright, 2008). Furthermore, bacteria and viruses target and hijack the host membrane machinery, which is essential for both the survival and pathogenesis of these infectious pathogens, further underscoring the importance of these processes in maintaining cell health (Armas-Rillo et al., 2016; Asrat et al., 2014).

Strict regulation of membrane trafficking is necessary to maintain cell health; a multitude of factors contribute to this regulation, with Rab GTPases being the largest protein family known to play key roles in membrane trafficking. With 66 members, the Rab GTPases are the largest family of small GTPases in humans, coordinating events such as the tethering and fusion of vesicles with their target membranes and

recruiting motor proteins necessary for intracellular transport (Mizuno-Yamasaki et al., 2012). It is therefore essential to maximise our understanding of their localisation, regulation, and downstream effectors, in order to better understand how vesicle trafficking is regulated and maintained. In order to investigate whether interacting proteins are Rab effectors or regulators, binding experiments are often preformed with the Rab GTPases in their active vs inactive states, since effectors and GAPs generally associate with GTPases in their active state, whereas GEFs interact mainly with inactive GTPases (Zerial & McBride, 2001). This can be achieved either by loading the GTPases with GDP and non-hydrolysable GTP, or by using mutations to lock the GTPases in GTP- or GDP-bound conformational states (Feig, 1999; G. Li & Stahl, 1993; Shirataki et al., 1992).

1.4.1 Traditional methods used to identify protein-protein interactions

The two main experimental approaches that are generally used to identify novel protein interactors are affinity chromatography and yeast two-hybrid screens. Affinity chromatography makes use of an affinity column which has the ability to selectively and reversibly bind to a target in the sample (Hage & Matsuda, 2015). One such (larger-scale) affinity chromatography study on Rab GTPases has previously been performed in the Munro lab (Gillingham et al., 2014). In that study, GST-based affinity chromatography experiments using *Drosophila melanogaster* Rab GTPases were performed, followed by mass spectrometry to identify their interactors. Their study resulted in the identification of a multitude of putative Rab interactors, a number of which were validated as novel effectors (Gillingham et al., 2014).

In addition to affinity chromatography, yeast two-hybrid is another traditional and widely-used method of studying binding interactions, and has previously been used to identify Rab GTPase interactors (Fukuda et al., 2008). Yeast two-hybrid uses a downstream reporter gene as output, splitting a transcription factor of the reporter gene in two and fusing these domains to two proteins of interest; if the proteins bind to each other, the two domains come into close contact and are able to activate the downstream reporter gene (Paiano et al., 2018). While yeast two-hybrid is generally used to study the interaction between one bait with one prey, the technique can also be used to screen for interaction partners (Simonsen et al., 1998).

These two approaches have had many successes in the past, but also come with limitations. Yeast two-hybrid requires the correct folding of both the GTPase and the potential effector in yeast, and does not allow for detection of protein complexes because single genes are tested. Even though affinity chromatography is able to detect protein complexes, it not only requires correct GTPase folding but also will have great difficulty detecting transient or weaker interactions due to repeated column washing in which the interactors might be lost.

1.4.2 In vivo proximity labelling

The continuous growth of novel experimental techniques and the increasing capacity for large-scale data analysis will greatly aid the journey towards maximising the set of known Rab GTPase effectors. One ground breaking method to study protein-protein interactions is by *in vivo* proximity labelling. By studying protein interactions *in vivo*, the endogenous environment remains mostly intact, ensuring correct protein folding.

The two most widely used proximity labelling methods, BioID (proximity-dependent biotin identification) and APEX (ascorbate peroxidase proximity labelling), both utilise biotin derivatives which can label proximal proteins through diffusion from the enzyme's active site (Trinkle-Mulcahy, 2019). Using biotinylation as a labelling method of choice, is largely due its strong interaction with streptavidin; since streptavidin-based affinity chromatography is used to isolate biotinylated proteins, and the interaction between biotin and streptavidin is tremendously strong and selective, the loss of interactions due to column washing is minimal (Dundas et al., 2013). Previously in the Munro lab, both APEX and BioID were compared for the identification of Rab GTPase interactors. The use of APEX resulted in much higher amounts of cytosolic background, compared to when BioID was used (personal communication). Hence, for this study, our focus lies on the BioID technique and the adaptions thereof.

BioID (proximity-dependent biotin identification) was developed by Roux and colleagues as a novel proximity-labelling technique (Roux et al., 2012). The BioID approach makes use of a promiscuous mutant of the biotin ligase BirA (R118G, hereafter named BirA*). Whereas wildtype BirA specifically biotinylates lysine residues in the biotin acceptor tag, BirA* prematurely releases biotinoyl-5'-AMP (bioAMP) after which it can be attached to available lysine residues within a ~10 nm radius (Roux et al., 2012). The BioID approach is a valuable addition to the repertoire of protein-protein interaction methods, firstly because proximity labelling allows for the identification of transient or less stable interactions. Secondly, the method is performed *in vivo* and in the native cell type, unlike the traditionally bacterially-expressed affinity chromatography and yeast two-hybrid. And thirdly, since biotin is used as a labelling agent, the extremely selective and stable interaction between biotin and streptavidin can be used to isolate biotinylated proteins from the sample (Dundas et al., 2013).

In practice, the BioID approach can be used to identify potential interaction partners by fusing a protein of interest to BirA*. After expressing the fusion protein in cells and allowing biotinylation to occur after addition of exogenous biotin, the biotinylated proteins are isolated using streptavidin-based affinity

chromatography and identified using mass spectrometry and/or SDS-PAGE followed by Western blotting (Fig. 1.6).

Like every experimental approach, BioID comes with a few internal drawbacks. Mainly, the nature of the promiscuous BirA* biotin ligase means that all proximal proteins with accessible lysines are biotinylated, meaning that proximal non-interacting proteins will be identified but are in fact background proteins. Distinguishing this non-specific background from true interactors is challenging – something we aimed to

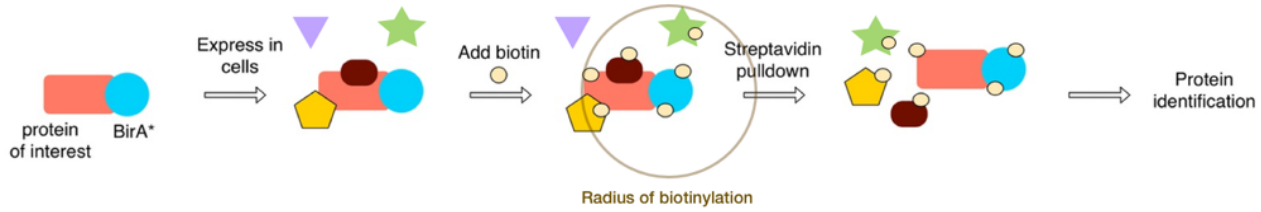

Figure 1.6 Schematic overview of the BioID method. The promiscuous mutant of the biotin ligase BirA (BirA*) is fused to a protein of interest and expressed in cells. Upon addition of biotin, proteins with available lysine residues and within the radius of biotinylation (~10 nm) are biotinylated. Biotinylated proteins are isolated using affinity chromatography and identified through mass spectrometry or SDS-PAGE resolution. Proteins, BirA*, biotin, and the radius of biotinylation are not to scale.

improve by adapting the BioID approach. By redirecting the BirA*-fused proteins to a stable, ectopic location, the mitochondria, we were able to develop a system in which the interactomes of many GTPases, in their distinct activity states, can be directly compared to one another. Performing these large-scale comparisons, we were able to more clearly distinguish true interactors from the background. In this study, the development and large-scale use of the adapted BioID (MitoID) approach was described. Numerous novel Rab GTPase interactors were validated and further examined, with a particularly in-depth look at the interactome of Rab1A and Rab1B.

1.5 Thesis lay-out

In Chapter 2, the use of BioID in combination with stable ectopic localisation will be examined, directing the BioID-tagged proteins to the outer mitochondrial membrane (MitoID) to considerably equalise the background landscape and aid in the identification of true interactors. In order to test the MitoID approach, the well-characterised Rab GTPase Rab5A was used and several potential Rab5A interactors were identified, two of which (TBCK and OSBPL9) were confirmed to be novel interactors.

In Chapter 3, this system will be used for a screen with a whole panel of Rab GTPases and various small GTPases of the Rho and Ras families, resulting in the identification of a multitude of putative novel effectors. Several putative effectors are studied further and validated as novel Rab GTPase effectors, namely ARFGEF3/BIG3 and STAMBPL1 for Rab2A, NDE1 and HPS3 for Rab9A and ALS2/Alsin for Rab11A and Rab11B.

In Chapter 4, several adaptations to the MitoID approach are examined, namely use of BioID2 and TurboID and how these compare to the original BioID, and whether MitoID can be used to study the effect of post-translational modifications on protein interactions.

In Chapter 5, the MitoID approach is applied to Rab1A and Rab1B, aiming to maximise the set of effectors. Numerous putative effectors are identified and several (GCC88, CALCOCO1, AKAP10, PPP1R37, and CLEC16A) are validated to be true novel Rab1 interactors.

In Chapter 6, Rab1 and its novel effectors are studied further to examine their role in vesicle trafficking and autophagy. In collaboration with the Roger Williams group (MRC LMB), Rab1 is identified as a specific activator of the class III phosphatidylinositol-3-kinase complex I, and its binding site is studied through mutagenesis. CLEC16A, CALCOCO1, and PPP1R37 are identified as direct binders Rab1A and Rab1B, of which CALCOCO1 and PPP1R37 are associated with autophagosomes and CLEC16A and PPP1R37 appear to play a role in maintaining Golgi morphology.

Note: a portion of the work done in Chapter 2 was done before the official start of my PhD. The screen was set up and started, and certain Rab GTPases were tested in duplicates (Rab1A, Rab2A, Rab5A, Rab6A, Rab8A, Rab11A, Rab18, Rab19B, Rab30B, Rab33B, Rab39B, Rab43). During my PhD, this was extended to add more Rab GTPases (Rab1B, Rab7A, Rab9A, Rab10, Rab11B, Rab21, Rab29), other small GTPases (Cdc42, Rac1, RhoA, RalB, Rheb, and N-Ras), and the whole screen was extended to triplicates. In addition, the bulk of the mass spec analysis and all the interactor validations were performed during my PhD. This study was done together with Alison Gillingham from the Munro Lab, and we contributed in equal measures. Experiments/analysis performed solely by Alison Gillingham or Sean Munro are credited where appropriate.

Chapter 2: Developing a novel mitochondrially-redirected proximity labelling approach

2.1 Introduction

In this study, we set out to use and adapt the proximity labelling technique BioID and perform this across a subset of small GTPases (Gillingham et al., 2014, 2019). Maximising the set of known Rab GTPases interactors will increase our knowledge on how they regulate membrane traffic.

As previously mentioned, different Rab GTPases can act on different membranes in their GTP-bound forms, ranging from early endosomes to the Golgi apparatus and recycling endosomes. Furthermore, in their GDP-bound forms, Rab GTPases are generally cytosolic. When comparing several baits to each other, the non-specific background can be identified by determining which proteins are present regardless of which bait is used and the bait's activity state. However, since active Rab GTPases are localised to a wide range of different cell compartments, and are largely cytosolic in their inactive states, their interactomes cannot be directly compared in order to identify the general background.

In order to overcome this, we have established a system which allows relocation of the BirA*-fusion proteins to a standard and consistent location – the mitochondrial outer membrane. In our adapted BioID (MitoID) assay, we have used a subset of the Ras superfamily that comprises 25 small GTPases, each containing point mutations which essentially lock the GTPases in permanently active or inactive states (Feig, 1999; G. Li & Stahl, 1993). Although these mutations have mostly been studied in Ras GTPases, it is thought that these mutations have similar effects on other small GTPases. Comparing the MitoID data of a large subset of small GTPases in their different activity states, will aid in the identification of true GTPase interactors and can significantly increase our knowledge on GTPase effectors and regulators.

2.2 Results

2.2.1 GTPase-BirA chimeras can be stably re-localised to mitochondria*

Re-localising GTPase-BirA* fusion proteins to a stable and ectopic location allows for a cleaner and more direct comparison between a large set of different baits and their mutations. Since mitochondria have been

proven useful for ectopic relocation of cytosolic proteins, we have replaced the C-terminal cysteines of the GTPases that receive lipid modifications, with the mitochondrial targeting sequence of monoamine oxidase (MAO) (Hoogenraad et al., 2003). Together, this results in a chimera schematically shown in Figure 2.1A, with the GTPase C-terminally fused with BirA*, an HA tag to allow for close examination of expression and localisation of the chimera, and finally the MAO targeting sequence to anchor the chimera into the mitochondrial membrane (Fig. 2.1A, right panel). Our aim is that these chimeras will allow recruitment of specific GTPase effectors and regulators to the mitochondria (Fig 2.1A, left panel), where they can be biotinylated and later identified. This technique is hereafter called MitoID (Gillingham et al., 2019).

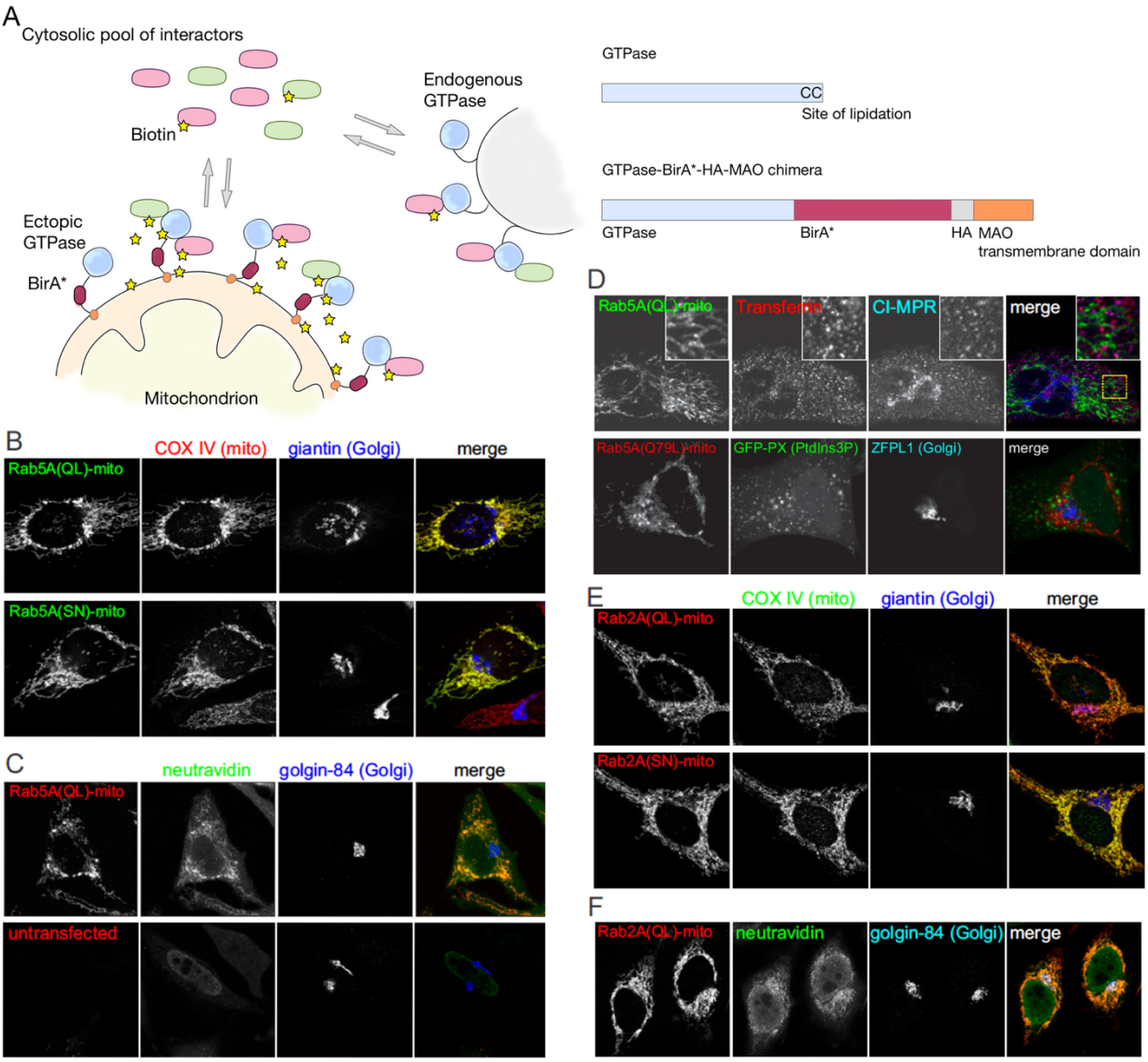

Figure legend on next page.

Figure 2.1. BirA*-tagged GTPases are re-localised and functional at the mitochondrial surface. (A) Schematic overview of the MitoID approach, in which the chimeras are anchored to the mitochondrial outer membrane, where they are able to recruit and biotinylate GTPase effectors. The right panel shows the MitoID chimera in which the C-terminal cysteines of a GTPase are replaced by the biotin ligase BirA*, an HA-tag and the mitochondrial targeting sequence MAO. (B) Confocal images of HeLa cells expressing Rab5A chimeras in either the GTP-form (QL) or the GDP-form (SN), and stained for the HA tag in the chimera as well as markers for the mitochondria (COXIV) and Golgi (giantin). (C) Confocal images of HeLa cells either un-transfected or expressing active Rab5A chimeras. Cells were stained for the chimera using HA-antibodies, in addition to the Golgi marker golgin-84 and the use of the biotin-binding neutravidin-488. (D) As (C) except that the cells were incubated with fluorescent transferrin prior to fixation to label endosomes, and then also stained for cation-independent mannose 6-phosphate receptor (CI-MPR) that recycles through endosomes (top panel). Lower panel shows confocal images of HeLa cells co-transfected with GTP-locked Rab5A chimera and GFP-PX (PI(3)P binding domain) and stained for the Golgi apparatus (ZFPL1). Data generated and collected by Alison Gillingham. (E) Confocal micrographs of HeLa cells expressing Rab2A chimeras in either the GTP-form (QL) or the GDP-form (SN) and stained for the chimera itself (HA), mitochondria (COXIV), and the Golgi (giantin). (F) Confocal images of HeLa cells expressing active Rab2A chimera (QL), stained for the chimera itself (HA), the Golgi (golgin-84), and using neutravidin-488 to stain biotinylated proteins.

To test the localisation and activity of these GTPase-chimeras, we transiently expressed both GTP- and GDP-locked mutants of the endosomal GTPase Rab5A in HeLa cells and found that both are efficiently ectopically localised to the mitochondria (Fig. 2.1B). Importantly, co-staining of the Golgi marker giantin shows that the presence of Rab5A on mitochondria does not result in disruption or fragmentation of the Golgi apparatus. Furthermore, the presence of biotinylated proteins on the mitochondria indicates that the BirA* has remained active and is able to biotinylate proximal proteins (Fig. 2.1C). Moreover, the mitochondrial localisation of the endosomal Rab5A does not result in the disruption or relocation of entire endosomes – the endosomal lipid PI(3)P is observed on endosomal vesicles and not at the mitochondria, as are the endosomal cargoes transferrin and CI-MPR (cation-independent mannose 6-phosphate receptor) (Fig. 2.1D, data generated by Alison Gillingham). This indicates that any potential Rab5A interactors we detect, are not biotinylated simply for being a part of the endosomal landscape but are true potential interactors.

The well-characterised Golgi GTPase, Rab2A, was also tested for the use of MitoID. Similar to Rab5A, chimeras in both activity states are efficiently re-localised to mitochondria, while retaining biotin ligase activity at the mitochondria and keeping the Golgi apparatus intact (Fig. 2.1E, F).

Finally, we tested whether transiently expressed mitochondrial chimeras induced mitochondrial stress by observing whether the ubiquitin ligase Parkin is accumulated there – a commonly used marker for mitochondrial stress (Lazarou et al., 2015). We observed clear Parkin accumulation when stress was induced by CCCP (a mitochondrial uncoupling agent), but no such Parkin accumulation after expression of

Rab2A or Rab5A chimeras, indicating that mitochondria remain functional and healthy (Fig. 2.2) (Georgakopoulos et al., 2017). Interestingly, a recent study has shown that Rab5A and its effector Alsin/ALS2 are recruited to mitochondria after induction of oxidative stress (Hsu et al., 2018). Even though we have shown that a major mitochondrial stress marker Parkin is not accumulated at the mitochondria, the relevance of these new potential stress markers to our study will be further examined in the discussion of this chapter.

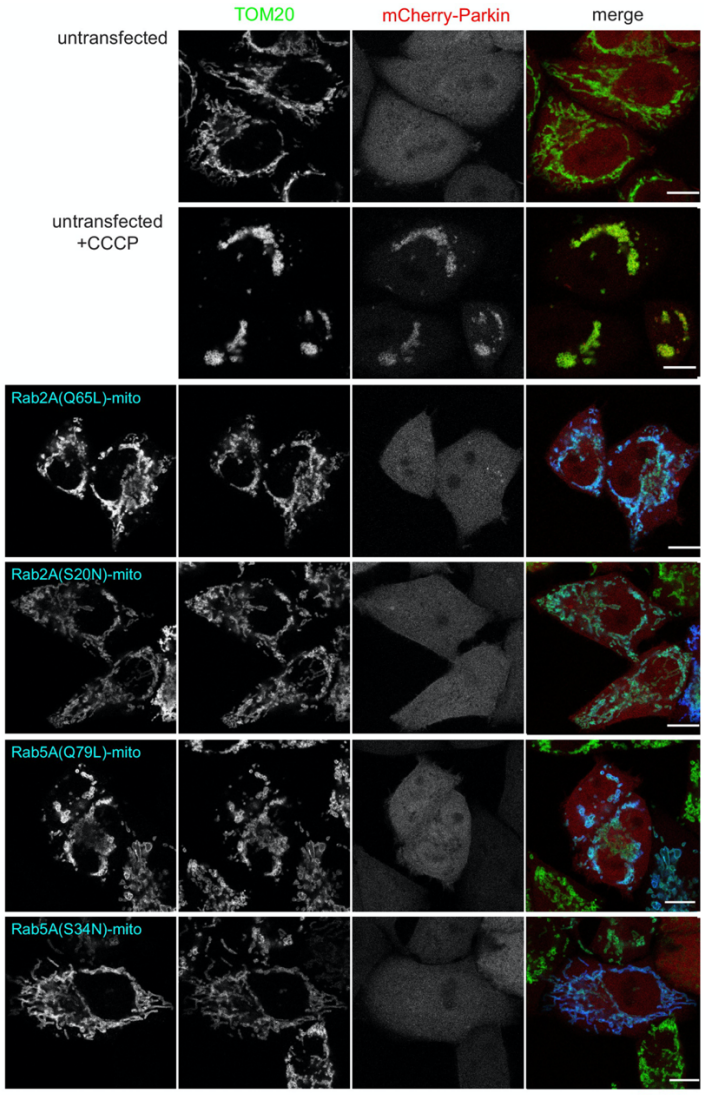

Figure 2.2. Expression of mitochondrial GTPase-chimeras does not induce mitochondrial stress. Confocal micrographs of HeLa cells stably expressing mCherry-parkin, either un-transfected or transfected with Rab2A- or Rab5A mitochondrial chimeras for 48 hours. As a positive control, un-transfected cells were treated with 10 μM CCCP (carbonyl cyanide *m*-chlorophenyl hydrazone, a mitochondrial uncoupling agent) for three hours prior to fixation. Scalebars: 10 μm.

Together, these data indicate that transiently expressing the GTPase chimeras results in efficient ectopic localisation of the small G protein, while retaining the chimera's biotin ligase activity and showing no disruption to the organelle of residence nor inducing mitochondrial stress.

2.2.2 Rab5A-BirA chimeras biotinylate interacting proteins at the mitochondria*

To determine whether the chimeras are able to biotinylate interacting proteins, we expressed Rab5A chimeras in wildtype HEK293T cells, added exogenous biotin, and isolated biotinylated proteins by streptavidin affinity chromatography. The MitoID experiments were performed according to the BioID protocol set out by Roux and colleagues, supplying 50µM biotin for 18-24 hours and performing the affinity chromatography protocol with the same buffers (Roux et al., 2012, detailed in the Materials and Methods). Next, we identified the proteins using tandem mass spectrometry, using the total number of spectra that match peptides from a certain protein (further referred to as spectral counts) as a semi-quantitative analysis method. We tested chimeras of both GTP- and GDP-locked Rab5, and performed these MitoID experiments in biological triplicates.

In order to visualise the identified proteins, the mean of the total spectral counts obtained from GTP-locked Rab5A triplicates was plotted against the mean of the GDP-locked Rab5 triplicates (Fig. 2.3A,B). As expected, the chimera itself (identified as Rab5A) is found in high and roughly equal amounts between the two forms. Other proteins that are high on the list and found in roughly equal amounts are endogenously biotinylated proteins such as Acetyl-CoA carboxylase 1 (ACACA) and Pyruvate carboxylase (PC) (Tong, 2012). Importantly, the fact that both the bait and several endogenously biotinylated proteins are found in roughly equal amounts is a good indicator that similar input levels were used (Fig. 2.3A).

Amongst the proteins specific for the GTP form of Rab5A were several proteins that are known to bind to active Rab5, such as EEA1, HTT/Huntingtin, APPL1/2 and RABEP1/Rabaptin-5 (Miaczynska et al., 2004; Pal et al., 2006; Simonsen et al., 1998; Stenmark et al., 1995). Furthermore, multiple subunits of the CORVET complex (VPS8, VPS18, VPS11) and the class III PI3-kinase complex (PIK3R4/VPS15, PIK3C3/VPS34, NRBF2, UVRAG, RUBCN/Rubicon) were identified (Fig. 2.3B) (Beek et al., 2019; Ohashi et al., 2018).

Furthermore, we were able to identify three known Rab5 GEFs, of which two (GAPVD1 and ALS2/Alsin) are predominantly present in the GDP-locked form (Hunker et al., 2006; Topp et al., 2004). The third known and identified Rab5 GEF, RABGEF1/Rabex-5, was found in similar levels in both mutants, which

can be explained by its ability to form a complex with the Rab5 effector Rabaptin-5 (Horiuchi et al., 1997; Z. Zhang et al., 2014). When examining the separate triplicate runs, we find that almost all of the identified

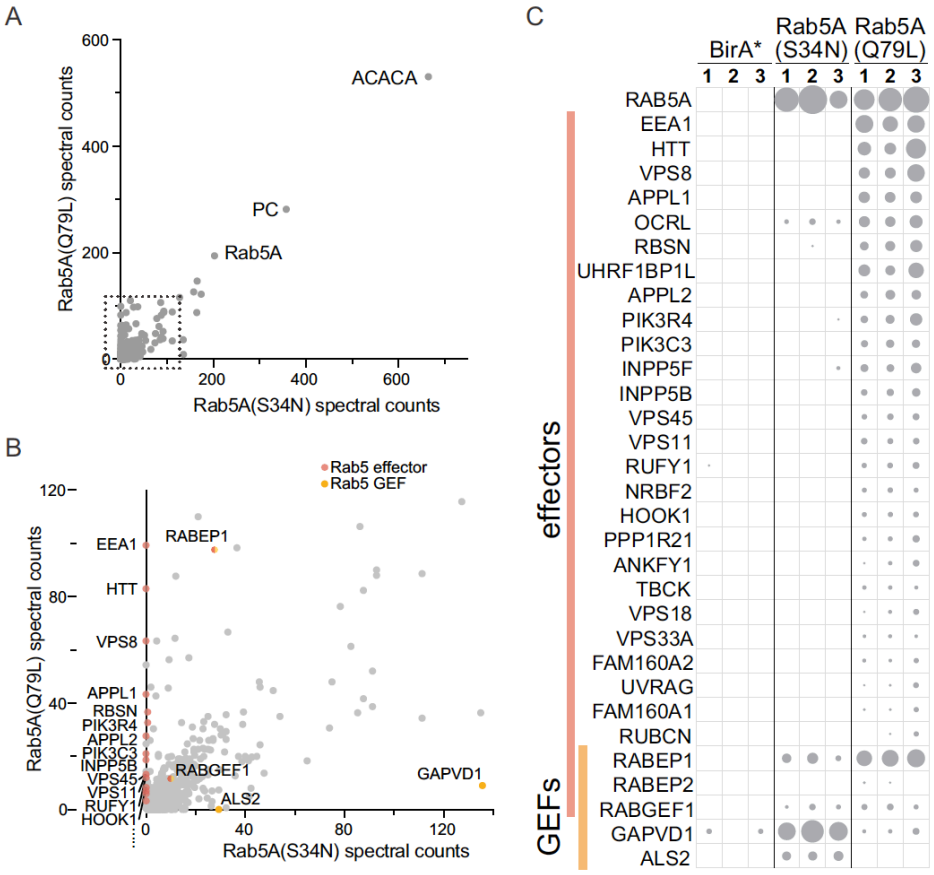

Figure 2.3. Mitochondrial Rab5A-BirA* chimeras are able to biotinylate Rab5 effectors and regulators. (A) Plot of spectral counts obtained by tandem mass spectrometry using streptavidin affinity chromatography samples from cells expressing Rab5A-BirA*-HA-MAO chimeras. These Rab5A chimeras were either GTP-locked (Q79L) or GDP-locked (S34N), and the counts represent means of triplicate biological repeats. (B) As (A) except only the region in the dashed box in (A) is shown. Known Rab5A effectors (red) and exchange factors (orange) are labelled as indicated by their gene names. (C) Spectral counts for known Rab5A interactors identified using the mitochondrial Rab5A chimeras in both GDP-locked (S34N) and GTP-locked (Q79L) mutants, as well as BirA*-HA-MAO as a control. Values from three biological replicates are shown, with the area of the circle proportional to the number of counts. Plots were generated by Sean Munro.

effectors and regulators were found across all three replicates, indicating that the approach is robust and reproducible. This is visualised by a so-called ‘bubble plot’, in which the area of the circles corresponds to the number of spectral counts (Fig. 2.3C).

Taken together, these results indicate that the Rab5A chimeras are able to recruit effectors and regulators to the mitochondria in a nucleotide-specific manner, where they can be biotinylated and identified.

2.2.3 Expanding the method: chimeras of a range of GTPases are efficiently expressed and re-localised

The results so far suggest that mitochondrial GTPase-BirA* chimeras are expressed well in mammalian cultured cells, are efficiently anchored at the mitochondria, are able to recruit nucleotide-specific effectors and regulators to the mitochondria, and are biotinylated there by the BirA* within the chimeras. Having examined the efficiency of the MitoID approach using the well-characterised Rab5A, we next aimed to expand this approach to a subset of 25 small GTPases from the Ras superfamily. Our studies are mainly focused on the family of Rab GTPases, investigating a number of Rabs from several intracellular membrane compartments.

The full set of Rab GTPases examined in this study are Rab1A, Rab1B, Rab2A, Rab6A, Rab8A, Rab10, Rab19B, Rab29/Rab7L1, Rab30, Rab33B, Rab39B, and Rab43 from the Golgi apparatus, Rab11A and Rab11B from recycling endosomes, Rab5A and Rab21 from early endosomes, and Rab7A and Rab9A from late endosomes (Hutagalung & Novick, 2011) (Huber et al., 1993). Rab18 can be found on lipid droplets as well as the Golgi (Hutagalung & Novick, 2011). In addition to Rab GTPases, we have also included the small GTPases Cdc42, RhoA, and Rac1 from the Rho family (known to regulate the actin cytoskeleton and cellular polarity and migration), and N-Ras, Rheb, and RalB from the Ras family (mainly involved in signalling cascades and cell proliferation) (Hall, 2012; Macaluso et al., 2002; Wennerberg et al., 2005). It should be noted that most small GTPases don't have just one resident organelle and their stated localisation might not be as distinct as originally thought. This will be further discussed later in this thesis, as we gain more knowledge on the interaction partners of the GTPases.

Notably, the Arf family of GTPases was not included in this study since, unlike the other small GTPases investigated here, Arf GTPases receive their membrane-tethering modifications on their N-terminus instead of the C-terminus (D'Souza-Schorey & Chavrier, 2006). This seemingly small distinction would force a change in the chimera's structure; switching from the C-terminal MAO-tag to an N-terminal mitochondrial localisation tag such as TOM70. Unfortunately, the N-terminal TOM70 tag has proven to be less efficient for the use of MitoID by several researchers in the Munro group (data not shown, personal communication). Since this would not allow a fair and equal comparison between the samples, we have decided to exclude Arf GTPases from this study.

All 25 small GTPases were expressed as chimeras (as in Figure 2.1A) either as wildtype proteins or with their known or predicted GTP-locked and GDP-locked mutations (Sup. Table 1). Wildtype Rab GTPases were used to examine the behaviour and stability of the mutants, but were not used for any further comparisons or investigations – all direct comparisons and further validations were performed with GTP- and GDP-locked mutants.

Immunoblotting showed that all chimeras were expressed at comparable levels, except for GDP-locked Rab7A, Rab18 and RhoA, which appear to be less stable (Sup. Fig. 2.1). This phenomenon has previously been reported for Rab27A and will be further examined in the discussion (Ramalho et al., 2002). Furthermore, all used chimeras were efficiently redirected to the mitochondria, with the Golgi apparatus remaining intact (several representative images shown in Sup. Fig. 2.2).

Taken together, this data indicates that the chimeras were expressed and localised as intended, with no noticeable negative effects on the Golgi apparatus. Next, MitoID experiments were performed across the whole panel of small GTPases, in both their locked activity states and in biological triplicates, as was done for Rab5A in Figure 2.3.

The appropriate scale with which to perform the MitoID experiments was investigated by testing the approach with either 1, 2, or 3 confluent T175 flasks of HEK293T cells expressing Rab2A-chimeras (equivalent to approximately 20-25 million cells per flask) (Fig. 2.4). Using our set-up, we found that using 1 flask of HEK cells leads to several true Rab2A hits being left out (such as BICD1 and OATL1/TBC1D25) and various others to be present in only very low amounts (such as BICD2, CCDC186, and GOLGA2/GM130) (data not shown). Bubble plots showing the top hits of these three scales also highlight an increase of non-Rab2A associated proteins/background proteins when using 1 T175 flask (Fig. 2.4A). We did not observe an absence of known hits or an increase in non-specific background proteins when comparing the use of 2 T175 flasks to 3 flasks (Fig. 2.4B,C). However, in the dataset of 3 T175 flasks, several background proteins are falsely annotated to be GTP-locked specific proteins such as Acetyl CoA Carboxylase 2 (ACACB) (Fig. 2.4C). It is likely that in using 3 T175 flasks, other proteins that are not as obviously background will also falsely be identified as interactors, making it a trade-off between more non-specific background versus more false positives. Hence, we have decided to perform all MitoID experiments in this study using 2 confluent HEK293T T175 flasks.

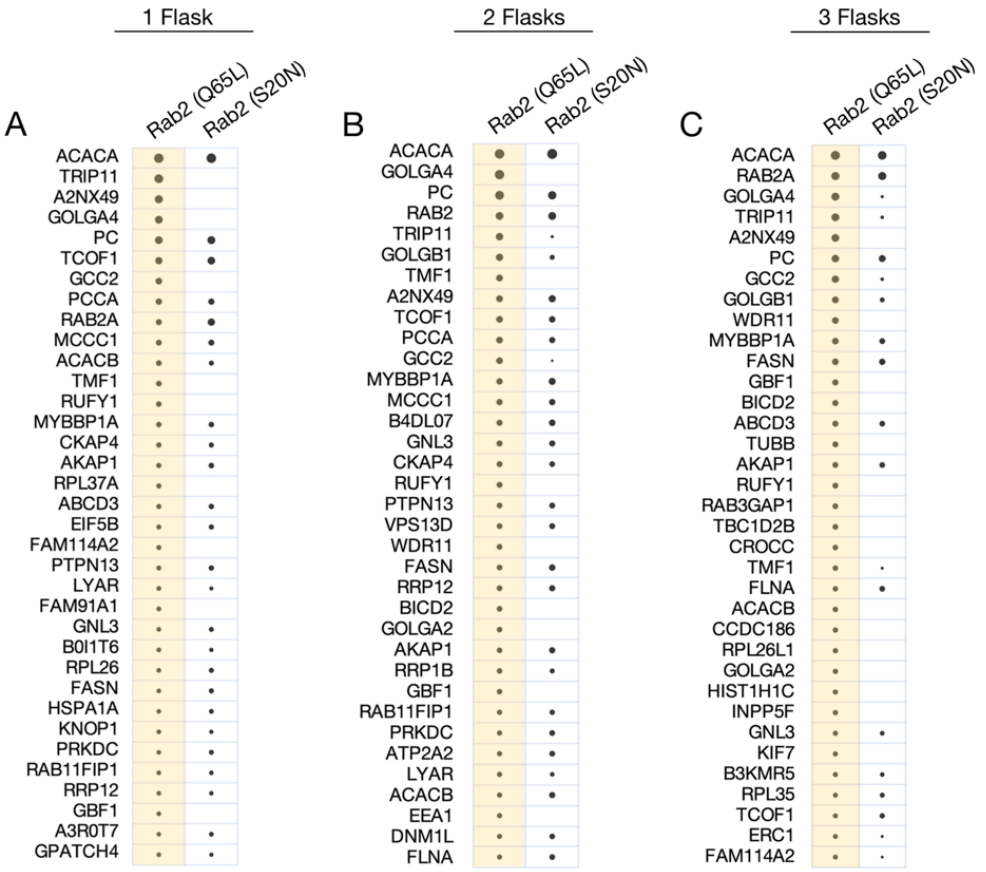

Figure 2.4. The use of approximately 50 million HEK293T cells per MitoID experiment is efficient and effective. (A-C). Bubble plots of MitoID experiments on GTP- and GDP-locked Rab2A chimeras, using either 1 confluent T175 flask/20-25M cells (A), 2 confluent T175 flasks/40-50M cells (B), or 3 confluent T175 flasks/80-100M cells (C) per sample. Circle area corresponds to WD-score of GTP-locked Rab2A compared to GDP-locked Rab2A within each sample. Top 35 hits are shown. All bubble plots are aligned for their GTP-locked Rab2A samples (yellow columns).

2.2.4. Analysing the MitoID data

Comparing the identified interactors across multiple baits can aid in the identification of true and specific interactors – for instance, proteins that are present in a nucleotide-independent manner across all baits will likely be proximal background and not putative interactors, whereas proteins interacting with one bait in a nucleotide-dependent manner are very likely to be true interactors. In this study, we applied a scoring system to aid in distinguishing background from interactors.

The analytic method is based on spectral count data obtained from mass-spectrometric analysis, and involves applying a scoring system from the CompPASS platform (Sowa et al., 2009). The scoring system we used on our data set is the WD-score:

$$WD_{i,j} = \sqrt{\left(\frac{k}{\sum_{i=1}^{i=k} f_{i,j}}\,\omega_j\right)^p X_{i,j}}$$

$$\omega_j = \left(\frac{\sigma_j}{\bar{X}_j}\right), \quad \bar{X}_j = \frac{\sum_{i=1, j=n}^{i=k} X_{i,j}}{k} \;; n = 1,2,\ldots m, \quad \begin{matrix} \text{if } \omega_j \le 1 \rightarrow \omega_j = 1 \\ \text{if } \omega_j > 1 \rightarrow \omega_j = \omega_j \end{matrix}$$

$$f_{i,j} = \begin{cases} 1 \;; X_{i,j} > 0 \\ X_{i,j} \end{cases}$$

where *i* is the bait number, *j* is the interactor, *Xi,j* is the total number of spectral counts for interactor *j* with bait *i*, *k* is the total number of baits in the dataset, *f* is the frequency that prey *i* interacts with the set of baits, *p* is the number of replicates in which the interactor is present, ω is a weighting factor, and σ is the standard deviation of *X*.

Applying this formula to our entire dataset, each datapoint will be assigned a score that takes into account how many times a protein is identified across a set of baits, how many times a protein is identified in the replicates of that certain bait, and the number of spectral counts of the protein in that certain bait. In our study we have decided to use the WD-score and not the original D-score, because the latter would assign lower than fair scores to proteins that are interactors for multiple small GTPases. The WD-score, however, gives an extra weight factor (ω) to proteins found in multiple baits with higher spectral counts than average for that protein, more accurately reflecting effectors that interact with multiple small GTPases. Thus, proteins that are enriched in all replicates of a certain bait but not in many (or any) other baits, will have the highest WD-scores.

After performing MitoID experiments on the entire panel of small GTPases, we analysed the mass spectrometry data using the WD-scoring system. To demonstrate the application, we will first examine the results of GTP-locked Rab5A.

2.2.5 MitoID analysis efficiently identifies both known and putative novel Rab5 effectors

Aligning the entire list of raw spectral count data to GTP-locked Rab5A, shows that many proteins that are found at the top of the list are also present in multiple other GTPases (Fig. 2.5A). These non-specific interactors include abundant cytosolic proteins and some mitochondrial proteins. After applying the WD-

scoring method on the spectral counts data, we observe a clear differentiation of specific protein interactors versus background (Fig. 2.5B). By applying the WD-scoring system, the known Rab5A interactors (red) become strongly enriched in the top hits, some of which were discussed in paragraph 2.2.2.

Though this data is analysed by comparing GTP-locked Rab5A against all other small GTPases, the visualisation in Figures 2.5A,B only shows Rab5A and the negative control in order to clearly observe which proteins are enriched in GTP-Rab5A in comparison to GDP-Rab5A. However, when we want to get a clear overview of which other small GTPases bind to a certain protein, we can observe the WD-score data of the entire panel of GTPases at once (Fig. 2.5C, Sup. Table 3 for separate triplicate runs). This overview not only allows for identification of overlap in the GTPase interactomes, but again clearly highlights the efficiency of this WD-score analysis to separate specific interactors from the background.

In addition to previously known Rab5A effectors, we were also able to identify a number of novel putative Rab5A effectors. These proteins include the TSC1 and TSC2 subunits of the Rheb GAP and the V-ATPase regulator WDR7, as well as the two subunits of the Rab3 GTPase activating protein RAB3GAP, which has also been shown to play a role in nuclear envelope formation at the ERGIC, as well as function as a Rab18 GEF (Gerondopoulos et al., 2014; Hantan et al., 2014; Manning & Cantley, 2003; Sethi et al., 2010) (Fig. 2.5B).

Other notable putative interactors include OSBPL9 and its closely related paralog OSBPL11 (Fig. 2.5B). These members of the oxysterol-binding protein (OSBP) family are known to regulate lipid transport and triglyceride stage, and have also been shown to heterodimerise and localise to the Golgi/late endosome interface (You Zhou et al., 2012). The protein KIAA1468/RELCH was also identified as a putative novel Rab5A interactor. Interestingly, RELCH was recently found to bind to Rab11 and OSBP proteins and we find both RELCH and OSBPL9/11 to specifically interact with Rab11 as well as Rab5A (Fig. 2.5C) (Sobajima et al., 2018). Another novel putative Rab5A effector is TBC1 domain-containing kinase (TBCK). Only limited knowledge exists on TBCK, though it is suggested to play possible roles in mTOR signalling, actin organisation and cell proliferation (Y. Liu et al., 2013). Interestingly, the presence of the TBC domain may indicate that TBCK could potentially function as a Rab GAP, however TBCK has been suggested to be inactive due to lack of catalytic domains (Y. Liu et al., 2013; Pan et al., 2006).

Next, we set out to validate the binding of OSBPL9 to Rab5A (novel interactor) and Rab11A (known interactor). We performed affinity chromatography with bacterially expressed GTP- and GDP-locked mutants of GST-Rab5A and GST-Rab11A and used wildtype HEK293T lysate as input.

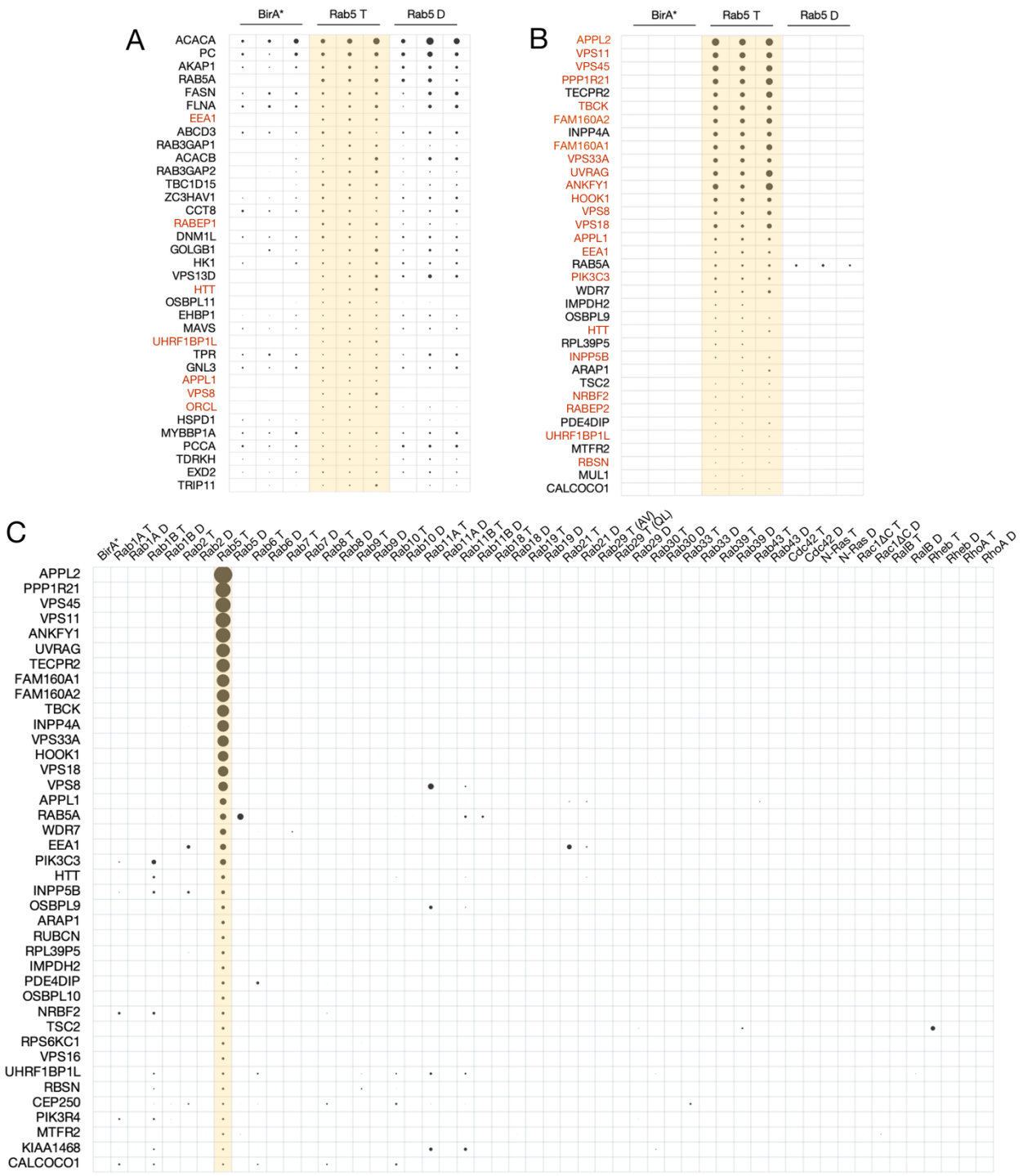

Figure 2.5. Analysis of Rab5A MitoID experiments highlights specific interactors. (A, B) Bubble plot of MitoID experiments of both the BirA* control and both Rab5A chimeras, aligned for GTP-locked Rab5A (second replicate). Circle area corresponds to total spectral counts (A) or WD-score (B). BirA* is a non-GTPase control at the mitochondria (BirA*-HA-MAO). Top 35 hits of all three biological replicates are shown. Known effectors are shown in red. (C) Bubble pot of MitoID experiments of the whole panel of studied GTPases, aligned for GTP-locked Rab5A. Circle area corresponds to average WD-score (average of the biological triplicates). T: GTP-locked mutant, D: GDP-locked mutant. Top 40 hits are shown. Yellow columns indicate alignment.

OSBPL9 is observed clearly binding to GTP-locked Rab5A and to a lesser extent to GTP-locked Rab11A, while not binding to their GDP-locked forms (Fig. 2.6A, data generated by Alison Gillingham). Interestingly, the affinity chromatography experiments suggest that the interaction with OSBPL9 is much stronger with Rab5A than with Rab11A, while similar levels of spectral counts are acquired by mass spectrometry (Fig. 2.5C, Fig. 2.6A). One possible reason for this disparity could be the difficulty of *in vitro* affinity chromatography to detect weaker and transient interactions, which can be identified through *in vivo* proximity labelling, suggesting that OSBPL9 binds more strongly or stably to Rab5A compared to Rab11A.

Finally, we probed the abovementioned blots with an antibody against TBCK, and found it to bind specifically to GTP-locked Rab5A and not to its GDP-locked form or to Rab11A (Fig. 2.6B, data generated by Alison Gillingham). To visualise this interaction, we co-expressed GFP-TBCK and the mitochondrial GTP-locked Rab5A chimera in wildtype HeLa cells. While expression of GFP-TBCK alone leads to dispersion throughout the cell, we observed a strong co-localisation of Rab5A and TBCK when the Rab5A chimera was co-expressed (Fig. 2.6C, data generated by Alison Gillingham).

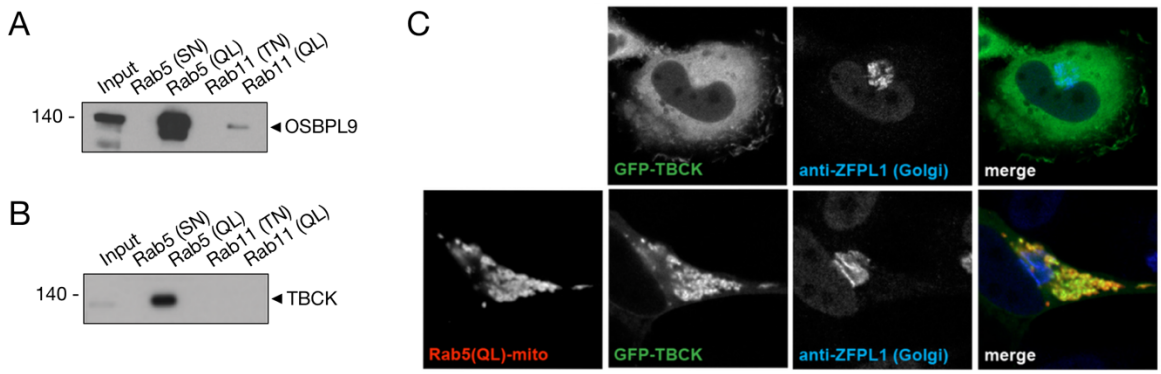

Figure 2.6. Analysis of Rab5A MitoID data identifies OSBPL9 and TBCK as novel Rab5A effectors. (A,B) Affinity chromatography of GST-tagged baits (indicated), probed with OSBPL9 (A) and TBCK (B) antibodies. Input: wildtype HEK293T lysate. Data obtained and analysed by Alison Gillingham. (C) Confocal micrographs of HeLa cells expressing GFP-TBCK (upper panel) or GFP-TBCK and Rab5QL-BirA*-HA-MAO (lower panel). Both panels are additionally probed for the Golgi marker ZFPL1. Data obtained and analysed by Alison Gillingham.

Taken together, this data shows that WD-score bubble plots illuminate which proteins are likely to be specific interactors and whether proteins bind to multiple GTPases, giving a clear overview of the entire panel of GTPases. We were able to identify both known and novel putative Rab5A effectors, two of which (OSBPL9 and TBCK) were validated using affinity chromatography and immunofluorescence. Together,

this shows that the MitoID approach can effectively and accurately identify both known and novel GTPase interactors.

2.3 Discussion

Rab GTPases are key regulators of vesicle trafficking and endomembrane organisation; in their active state they recruit effectors to specific intracellular membrane compartments where they can recruit further proteins and activate signalling pathways. Gaining more knowledge of the effectors and regulators of Rab GTPases will aid in better understanding the strictly regulated vesicle trafficking pathways and could ultimately result in the generation of treatments for pathologies ranging from cancer to neurodegenerative diseases.

In this study, we have adapted the *in vivo* proximity-labelling technique BioID by redirecting the chimeras containing BirA* to the mitochondria. The mitochondria were chosen as the ectopic location to which the small GTPase chimeras are re-localised, since previous studies have shown that mitochondria are useful for this purpose; they are ubiquitous membranous structures that are thought to not interfere with the studied trafficking pathways (Hoogenraad et al., 2003).

Importantly, overexpressing the mitochondrial chimeras does not appear to induce stress – our MitoID set-up does not lead to mitochondrial accumulation of the stress marker Parkin. Interestingly, a recent study has found that Rab5A and its effector Alsin/ALS2 are recruited to mitochondria when the cells are under stress (Hsu et al., 2018). In our study, Rab5A and Alsin are not found throughout the dataset, which suggests that they are not detected due to stress induced by overexpressing and ectopically localising the chimeras. If the presence of Rab5A and/or Alsin would indicate induction of mitochondrial stress, we would expect to observe this with the overexpression of every (or at least multiple) chimera(s), irrespective of nucleotide state. This suggests that where these proteins are identified, they are potential true interactors and not indicators of mitochondrial stress.

Stably re-localising the chimeras to the mitochondrial outer membrane is one of the methods we used to equalise – and ultimately reduce – the background in our BioID experiments. Since proximity-labelling techniques inherently have more non-specific background proteins, we aimed to minimise the presence of background proteins in the resulting data set through a combination of different factors. By stably re-

localising the chimeras to the same ectopic location, comparing the biotinylated proteins across a large panel of GTPases, internally comparing a GTPase between its GTP- and GDP-locked forms, performing biological triplicates, and applying a scoring systems to the resulting data, several possible novel Rab5A interactors stood out from the background. These proteins include TBCK and OSBPL9, both of which were subsequently validated to be true Rab5A effectors.

The mutations used to lock the GTPases in their GTP- or GDP-bound conformations, were based on many years of research done on members of the Ras superfamily (Feig, 1999; G. Li & Stahl, 1993). A number of these mutations were previously established, and these locations were used to generate mutations for less well studied GTPases. However, the use of some of these mutants has proven to be challenging for certain GTPases, especially the GDP-locked forms. When immunoblotting the MitoID samples for the chimeras, the GDP-locked mutants were sometimes found to be expressed at lower levels than their GTP-locked counterparts (Sup. Fig. 2.1). For most GTPases, this expression level difference was negligible, however for Rab7A, Rab18 and RhoA in particular this discrepancy was significantly larger. Interestingly, in these samples, the tubulin levels are extremely similar, as are the levels of the non-specific background band from the HA antibody (Sup. Fig. 2.1). This indicates that cells expressing the GDP-locked forms are not dying, but rather it is more likely that they break down the chimeras to protect the health of the cell. This phenomenon has previously been reported in *in vivo* mouse studies with Rab27, where the rapid degradation of the GDP-locked GTPase was observed using pulse-chase experiments (Ramalho et al., 2002).

The variation between the GTP- and GDP-locked forms of the same GTPase, can lead to challenges for the analysis of the data and conclusions drawn. Normalisation of spectral counts against background proteins such as Acetyl CoA carboxylase (ACACA) was considered, since this is a endogenously biotinylated protein and could work as a sample size control (normalising the number of cells used in each experiment). Alternatively, taking the amount of abundant background proteins such as fatty acid synthase (FASN) or filamin-A (FLNA) could be used to normalise for the amount of BioID-dependent biotinylation. However, neither of these normalisation methods would solve the problem of potentially missing proteins (even with normalisation, a zero remains zero). In this study, we have decided to examine the results for the GTPases described above on a case-by-case basis. The post-experimental analyses we have chosen are semi-quantitative, which means that we use the numbers obtained as a guideline only. When investigating the MitoID results, we are mainly interested in the ratios of the hits between the GTP- and GDP-locked mutants, in which case the expression levels of the GTPases as well as indicators such as ACACA, FASN, or FLNA can be taken into account to assess whether it is a potential interactor. This will be further discussed in the next chapter, where the datasets are thoroughly examined to identify GTPase interactors

Using different inactive mutations could potentially overcome the issue of degradation. In addition to the mutation that locks the protein's conformation in a GDP-bound state, there are known point mutations that mimic the nucleotide-free state, described in Rab3D as N135I (as opposed to the T36N GDP-locked mutation corresponding to the mutations used in this study) (X. Chen et al., 2003). Interestingly, the GDP-locked mutations used throughout this study function by perturbing binding of Mg^{2+} to the GTPase, which leads to the reduced binding affinity to guanine nucleotides. However, the protein's affinity for GDP is the deciding factor whether this 'GDP-locked' mutation functions as a GDP-bound GTPase, or a GTPase in a nucleotide-free state (Macia et al., 2004; Y.-C. Shin et al., 2016). This was underscored in a study on the GTPase Arf6, in which the 'GDP-locked' mutant T27N was found to be nucleotide-free, causing the GTPase to aggregate *in vivo* (Macia et al., 2004). Macia and colleagues developed a novel dominant negative mutant, T44N, which only affected GTP-binding and not GDP-binding, hereby functioning as a true GDP-locked mutant. In addition, a study on Rab11 has shown similar findings; the traditionally used 'GDP-locked' mutant of Rab11A functioned as a nucleotide-free mutant because of low GDP affinity, causing the mutant to be unstable (Y.-C. Shin et al., 2016). It appears that the stability and affinity for GDP is GTPase-dependent, leading us to speculate that the expression level variations of the GDP-locked mutants could be due to instability caused by these specific mutations. The study performed by Macia and colleagues indicate that similar point mutations in other GTPases could be found that do give the desired outcome; a mutation that only affects GTP- binding, but not GDP-binding affinity (Macia et al., 2004). Testing various mutations of residues in switch 1 that interact with GTP, could potentially improve the instability of dominant-negative mutants.

While an increased background is a major inherent BioID pitfall that we were able to strongly improve by redirecting to a stable, ectopic location and several internal controls, there remain several pitfalls to the BioID approach that we were unable to address with this adaptation. One main problem is the availability of free lysines; proximal proteins are biotinylated on their available lysines, if there are no available lysines on an interacting protein it will not be biotinylated and thus not identified as a potential interactor. This can be taken into account when confirming a certain interaction, but when searching for novel interactors this could become problematic. Second, the semi-quantitative mass spectrometry analysis is built upon the number of spectral counts (how many times a certain protein fragment belonging to that protein is identified in the mass spectrometer), but this number will be skewed highly towards larger proteins. Larger proteins can be fragmented in more peptides, each of which would count as a spectral count in the spectrometer. Thus, larger proteins would (sometimes misleadingly) be detected as being present in higher amounts than smaller proteins would. Since this is an intrinsic mass spectrometry challenge, perhaps the best way to overcome this would be to normalise the spectral counts against the size of the protein. We have not

performed this analysis here, since addressing this issue would leave other related issues unaddressed, such as protein abundancy in the cell.

Finally, a note on another family of vesicle trafficking regulators – Arf GTPases. As previously mentioned, Arf and Rab GTPases both play key roles in regulating intracellular membrane trafficking, however, throughout this study, our main focus has been on the Rab family of GTPases (Donaldson & Jackson, 2011; Stenmark, 2009). Arf GTPases differ from other small GTPases in their main structure; instead of being membrane-anchored through a C-terminal modification such as geranylgeranylation, the Arf GTPases associate with the membrane through myristoylation of an N-terminal amphipathic helix (Nawrotek et al., 2016). This seemingly straightforward reversal means that the GTPase needs to be fused to a mitochondrial targeting sequence on its N-terminus instead of its C-terminus, which lends better to the use of a N-terminal TOM70 sequence than a C-terminal MAO sequence (Backes et al., 2018; Iacovino et al., 2018). Previous work in our group has indicated that TOM70-HA-BirA*-Arf chimeras are not as effective as the MAO sequence tagged GTPases in MitoID experiments (personal communication, Munro Lab). Whether this discrepancy is due to the TOM70 targeting sequence (and why) remains unknown. However, the inability to accurately compare the Arf GTPases to the other small GTPases, has led us to exclude the Arf GTPases from the MitoID study.

All in all, our MitoID adaptation of the BioID approach appears promising; we are able to identify both previously known and putative novel interactors for the well-characterised Rab5A. Next, we will examine several datasets generated by MitoID experiments and study whether this approach remains effective and accurate with other small GTPases of the Ras superfamily.

Chapter 3: Identifying small GTPase interactors by applying the MitoID approach

3.1 Introduction

The previous chapter has shown that the MitoID approach is an effective and accurate method to identify Rab5A effectors and regulators. By comparing triplicate runs of the GTP- and GDP-locked forms of 25 different small GTPases, we were able to distinguish putative Rab5A interactors from non-specific background. Here, several of the other tested small GTPases are examined, with the aim of identifying novel effectors or regulators.

3.2 Results

In addition to Rab5A, we have performed MitoID experiments on 18 other Rab GTPases, and 6 other small GTPases – 3 from the Ras family, and 3 from the Rho family – all in their known or suspected GTP- and GDP-locked forms. Here, the results of Rab2A, Rab9A, Rab11A, and Rab11B will be thoroughly examined, in addition to the results of the small GTPases of the Ras and Rho families. The full datasets – both the raw Mass Spectrometry data, and the analysed data – are available in Supplementary Tables 2 and 3. Furthermore, bubble plots of all GTP-locked GTPases not discussed below are available in Supplementary Figures 3.1 – 3.3, with the exception of Rab1A/B which will be discussed in detail in Chapter 5.

3.2.1 Rab2A

Rab2A is a highly conserved Rab GTPase which is mainly localised on the Golgi membrane, where it is proposed to be a key regulator of ER-to-Golgi trafficking. More recent studies have suggested that Rab2 is also involved in late endosomal and lysosomal pathways (Ailion et al., 2014; Lund et al., 2018).

Examining the bubble plot when aligned to GTP-locked Rab2A, several known interactors were present, including the golgins GOLGA2/GM130 and golgin-45, the coiled-coil protein CCDC186 and the dynein adapter Bicaudal D (BICD) (Fig. 3.1A) (Ailion et al., 2014; Ding et al., 2019; Gillingham et al., 2014). In addition, several high-scoring proteins are suspected to be involved in membrane trafficking, such as GBF1, RUFY1, USO1/p115 and ARFGEF3/BIG3 (Cormont et al., 2001; Grabski et al., 2012; Richter et al., 2014; X. Zhao et al., 2006). Furthermore, the Rab GAP TBC1D25 is also identified as interacting with Rab2A, which aligns with a previous report that TBC1D25, in addition to Rab33B, also has GAP activity on Rab2A (Itoh et al., 2006). Finally, in addition to a number of proteins involved with centrosomes and cilia (such as CEP250 and centrobin), we identified several proteins of unknown function (including STAMBPL1 and FAM184A) (Ambuj Kumar et al., 2013; Ogungbenro et al., 2018). The argininosuccinate synthetase enzyme (ASS1) seems unlikely to be valid, though it is interesting that it appears to bind specifically and consistently to GTP-locked Rab2A.

Interestingly, even though a study initially identified p115 as a potential Rab2 binding partner, direct yeast two-hybrid studies revealed that they do not directly interact (Short et al., 2001). Short and colleagues suggest that p115 was initially found to bind to Rab2 since both are known to bind to GM130, and it can thus act a bridge between the proteins (N. Nakamura et al., 1997). This highlights the importance of performing further validations after identifying potential binding partners, in particular when using techniques such as proximity labelling or other large-scale indirect binding experiments.

Further validations were performed for ARFGEF3, a member of the Sec7-domain family of Arf GEFs without GEF activity, and STAMBPL1, a deubiquitinase that localises to early endosomes (Y.-A. Chen et al., 2014; M. Nakamura et al., 2006). Firstly, we validated the interaction with ARFGEF3 by applying wildtype HEK293T lysate to beads coated with bacterially expressed Rab2A, and observing clear binding in the GTP-locked samples (Fig. 3.1B, data obtained by Alison Gillingham). For STAMBPL1, the mass spectrometry data was confirmed by Western blotting the MitoID samples, where the protein was found to be enriched in GTP-locked Rab2A samples (Fig 3.1C). Next, this interaction was validated by applying wildtype HEK293T lysate to bacterially expressed Rab2A, in a similar manner as was done for ARFGEF3 above (Fig. 3.1D, data obtained by Alison Gillingham). Furthermore, after expressing and isolating GFP-STAMBPL1 and GST-Rab from *E. coli*, we observed direct binding between STAMBPL1 and GTP-locked Rab2A, but not with GDP-locked Rab2A or Rab5A (Fig. 3.1E, data obtained by Alison Gillingham). In addition, confocal imaging of GFP-tagged ARFGEF3 and STAMBPL1 co-expressed with GTP-locked Rab2A chimera, showed distinct re-localisation of the interactors to the mitochondria (Fig. 3.1F, G, data obtained by Alison Gillingham).

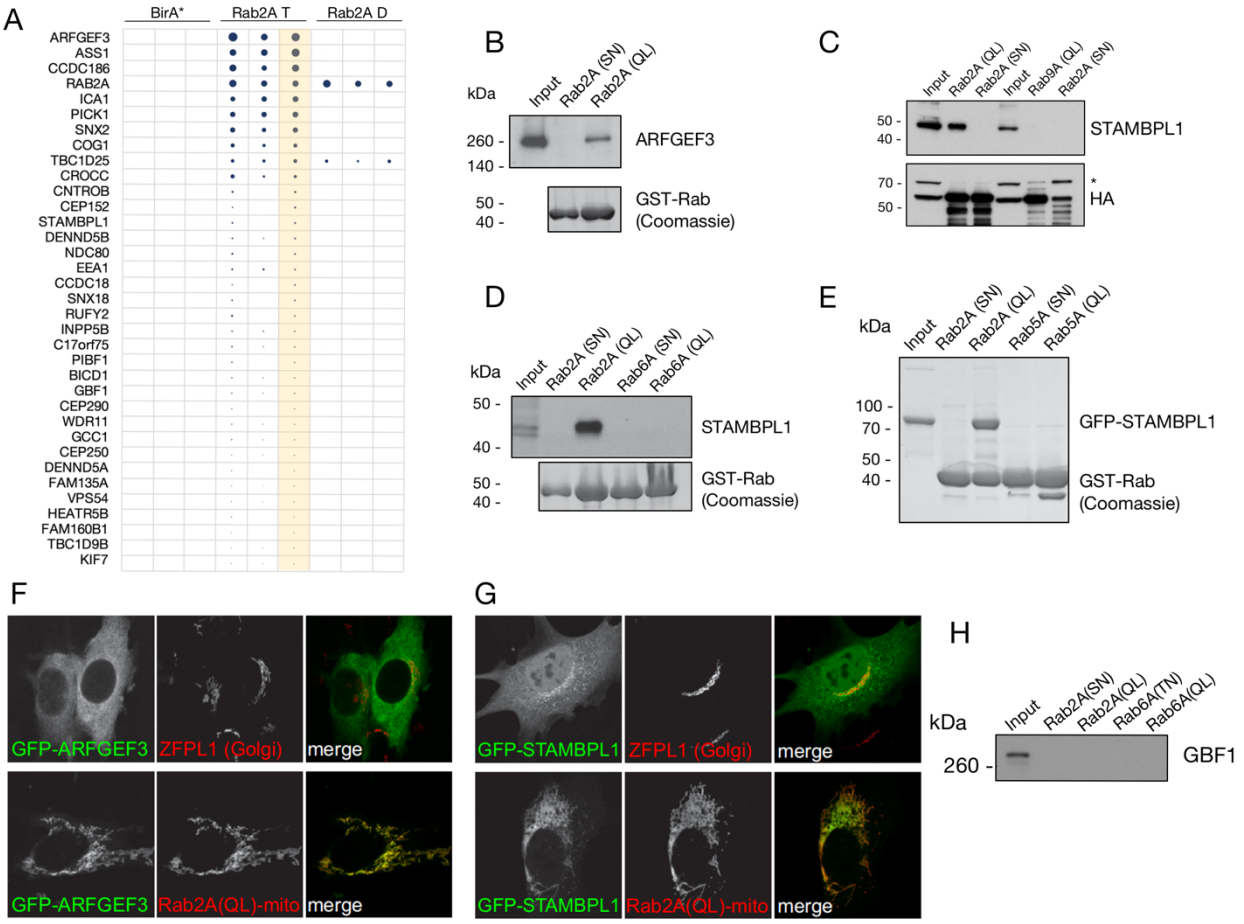

Figure 3.1. Rab2A MitoID analysis has identified ARFGEF3 and STAMBPL1 as novel Rab2A effectors. (A) Bubble plot aligned for the third replicate of GTP-locked Rab2A. Shown here are all three biological replicates of BirA* (BirA-HA-MAO control) and both Rab2A chimeras, though GTP-locked Rab2A was compared against all other GTPases in the full data list to generate this plot. Circle area corresponds to WD-score. The top 35 hits are shown. Yellow column indicates alignment. (B) Affinity chromatography in which HEK293T lysate was washed over GST-tagged Rab2A-coated beads. Resulting eluates were probed against ARFGEF3, the Coomassie staining shows expression levels of the baits. Wildtype HEK293T lysate is used as input. Data obtained by Alison Gillingham. (C) Western blots of MitoID samples of GTP- and GDP-locked Rab2A and Rab9A. Blots were probed with STAMBPL1 and HA (internal chimera epitope tag) antibodies. Asterisk (*) indicates non-specific background band of the HA antibody. Input: HEK293T lysate expressing GTP-locked Rab2A chimera. (D) Affinity chromatography of GST-tagged Rab2A and Rab6A with wildtype HEK293T lysate, resulting samples probed for STAMBPL1. Input: wildtype HEK293T lysate. Coomassie stained gels show bait expression levels. Data obtained by Alison Gillingham. (E) Coomassie stained gel of a direct binding experiment of bacterially-expressed GST-Rab2/5 with purified GFP-STAMBPL1. Indicated are GFP-STAMBPL1 and GST-Rab bands. Data obtained by Alison Gillingham. (F,G) Confocal micrographs of HeLa cells expressing GFP-ARFGEF3 (F) or GFP-STAMBPL1 (G), either co-expressed with GTP-locked Rab2A chimeras (lower panels) or co-stained with a Golgi marker (ZFPL1). Data obtained and analysed by Alison Gillingham. (H) Affinity chromatography of GST-tagged Rab2A and Rab6A with wildtype HEK293T lysate, probed with anti-GBF1. Input: wildtype HEK293T lysate. Data obtained by Alison Gillingham.

In addition to ARFGEF3 and STAMBPL1, we further examined the high scoring hit GBF1, a Sec7 domain containing Arf GEF that mainly functions at the Golgi and TGN (Bhatt et al., 2019). However, this interaction could not be validated by GST affinity chromatography (Fig. 3.1H, data obtained by Alison Gillingham). While this could mean that the interaction identified by MitoID is not a true interaction, this is not necessarily the case. Drawbacks to validating MitoID-identified interactions by GST-affinity chromatography will be examined in the discussion of this chapter.
It should be noted though, that although GBF1 is mainly known for its role in the secretory pathway, it has recently been reported to have a role in mitochondrial positioning and reorganisation (Walch et al., 2018). Even though this mitochondrial function of GBF1 might seem to indicate that this protein is simply mitochondrial background, this is not likely since the protein is not found consistently throughout all mitochondrially localised baits (Sup. Tables 2 and 3).

Together, these findings confirm that analysing MitoID experiments across large panel of small GTPases, allows us to identify of both previously known and novel putative Rab2A interactors. Furthermore, two relatively uncharacterised proteins – ARFGEF3 and STAMBPL1 – were validated to be true novel Rab2A effectors, highlighting the efficiency and large potential of this MitoID screen.

3.2.2 Rab9A

Active Rab9A is mainly associated to endosomes, entering the endosomal pathway at the stage between early Rab5-positive and late Rab7-positive endosomes (Kucera et al., 2016). In addition to the known Rab9A effector GCC2/golgin-185, we were able to identify numerous proteins known to be involved with the endocytic pathway. These proteins include the coiled-coil scaffolding protein GRIPAP1/GRASP1, the endosomal and lysosomal sorting nexins SNX13 and SNX14, and the A-kinase anchoring proteins and Arf GEFs BIG1/ARFGEF1 and BIG2/ARFGEF2 (Fig. 3.2A) (Akizu et al., 2015; Boal & Stephens, 2010; Henne et al., 2015; Hoogenraad et al., 2010; Hoogenraad & Sluijs, 2010; STINTON et al., 2005). Interestingly, while BLOC-3 (Biogenesis of Lysosome-related Organelles Complex-3) is reported to interact with Rab9A, we find GTP-locked Rab9A to interact with HPS3, a subunit to the related BLOC-2 (Fig. 3.2A) (Gautam et al., 2004; Kloer et al., 2010).

The dynein interactor NDE1/NudE is also identified as a putative Rab9A interactor (Fig. 3.2A). Interestingly, although NDE1 has previously been recorded to interact with Rab9B by yeast two-hybrid, co-precipitation did not result in nucleotide-specific binding (Bradshaw & Hayashi, 2016).

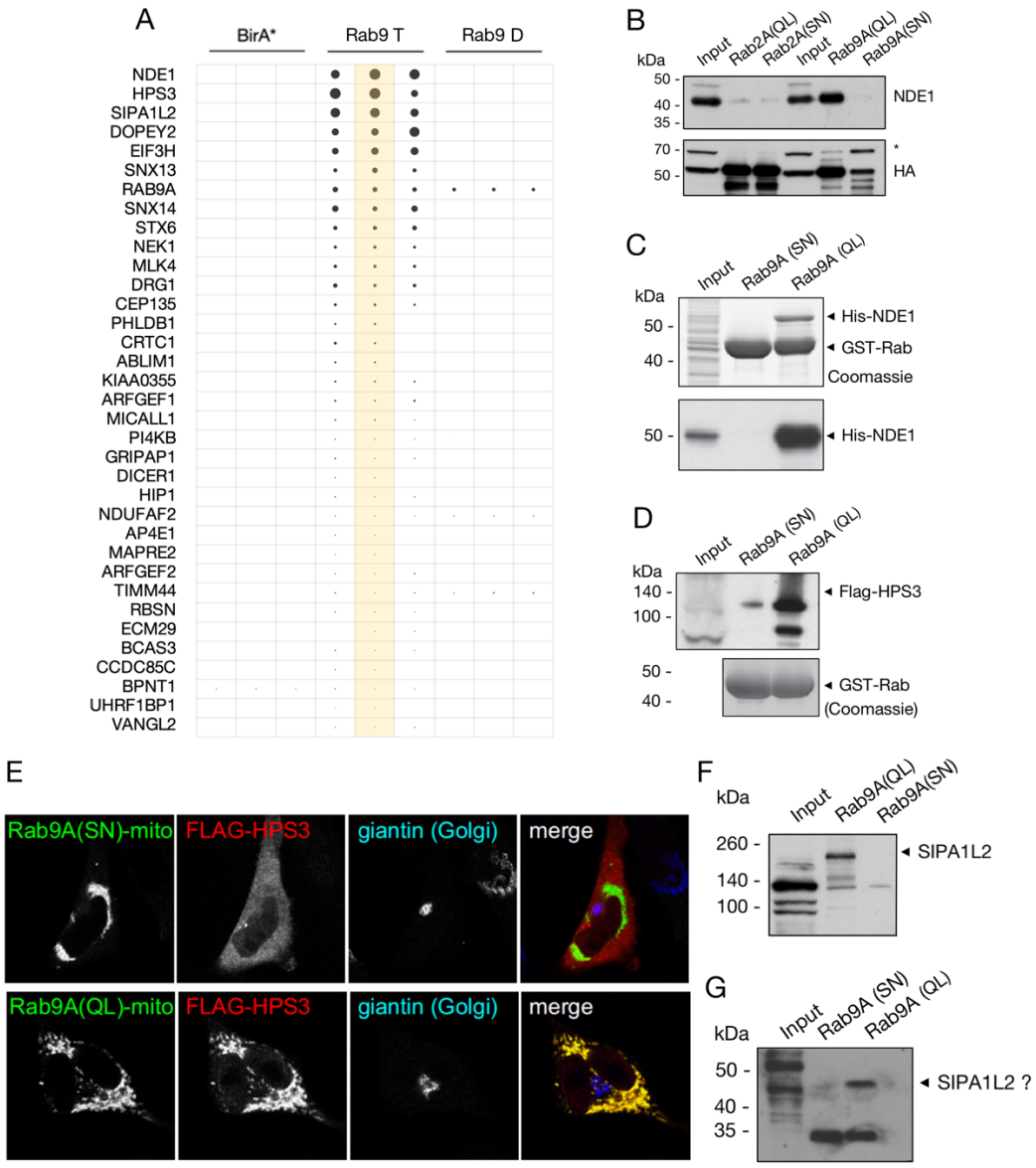

Figure 3.2. Analysis of Rab9A MitoID experiments have identified NDE1 and HPS3 as novel effectors. (A) Bubble plot aligned for the second replicate of GTP-locked Rab9A. Shown here are all three biological replicates of BirA* (BirA-HA-MAO control) and both Rab9A chimeras, though GTP-locked Rab9A was compared against all other GTPases in the full data list to generate this plot. Circle area corresponds to WD-score. The top 35 hits are shown. Yellow column indicates alignment. (B) Western blots of MitoID samples from Rab9A-chimeras, probed with antibodies against NDE1 and HA. Asterisk (*) indicates HA antibody background band. Input: HEK293T lysate expressing GTP-locked Rab9A chimera. (C) Affinity chromatography Coomassie-stained gel of GST-Rab9A with wildtype HEK293T lysate, showing both GST-Rab9A levels and His_6-tagged NDE1. The lower panel shows a Western blot of this sample probed with anti-His. Data obtained by Alison Gillingham. (D) Affinity chromatography of GST-tagged Rab9A, using HEK293T lysate expressing FLAG-HPS3 cell lysate. Blot probed for FLAG to show FLAG-HPS3, Coomassie gel showing GST-Rab levels in lower panel. Data obtained by Alison Gillingham. (E) Confocal micrographs of HeLa cells co-expressing GDP- or GTP-locked Rab9A-chimeras and FLAG-HPS3, and stained for giantin (Golgi). Data obtained and analysed by Alison Gillingham. (F) Western blot of MitoID samples using Rab9A chimeras, probed against SIPA1L2. Input: HEK293T lysate expressing GTP-locked Rab9A chimera (G) Affinity chromatography of bacterially purified GST-tagged Rab9A with wildtype HEK293T lysate, probed against SIPA1L2. Input: wildtype HEK293T lysate. Data obtained by Alison Gillingham.

Finally, the Rap GAP SIPA1L2 is consistently in the top 3 highest WD-scoring proteins (Fig. 3.2A). A recent study showed SIPA1L2 to be involved in neuronal retrograde trafficking of autophagosomal organelles called amphisomes, and several studies link variations in the SIPA1L2 gene to Parkinson's disease or Charcot-Marie-Tooth disease type 1A, though the function of SIPA1L2 in non-neuronal cells is unknown (Andres-Alonso et al., 2019; Tao et al., 2019).

Putative effectors SIPA1L2, HPS3, and NDE1 were chosen for further validation. Firstly, a Western blot of the Rab9A MitoID samples confirmed the presence of NDE1 in the GTP-locked Rab9A sample, thereby validating the mass spectrometry data (Fig. 3.2B). Next, GST-Rab9A was purified from *E. coli* and mixed with *E. coli* lysate expressing His_6-tagged NDE1. NDE1 was found to bind to purified GTP-locked Rab9A, indicating a direct interaction between the two proteins (Fig. 3.2C, data obtained by Alison Gillingham). Next, the interaction with HPS3 was examined by performing a similar affinity chromatography experiment, but this time using lysate of HEK293T cells expressing epitope-tagged HPS3 since no effective HPS3 antibodies were available. A clear enrichment of HPS3 was observed with the GTP-locked Rab9A compared to GDP-locked Rab9A, validating the interaction of the novel effector with Rab9A (Fig. 3.2D, data obtained by Alison Gillingham). Finally, this interaction was corroborated by the recruitment of epitope-tagged HPS3 to GTP-locked mitochondrial Rab9 chimeras (Fig. 3.2E, data obtained by Alison Gillingham).

The presence of the putative interactor SIPA1L2 in MitoID samples was confirmed by Western blot, showing a clear band near the expected size of 190kDa (Fig. 3.2F). This interaction was examined further *in vitro* by mixing wildtype HEK293T lysate with bacterially expressed and purified GST-Rab9A and performing a Western blot (Fig. 3.2G, data obtained by Alison Gillingham). However, even though the Western blot shows a clear band that is present only in GTP-locked Rab9A and not in GDP-locked Rab9A, it is not of the expected size but rather much smaller (approximately 45 kDa). Conversely, no SIPA1L2 bands are present at the expected size of 190 kDa. Further research needs to be performed to investigate whether this is a true interaction, for instance by repeating this experiment with overexpressed epitope-tagged SIPA1L2 in the HEK293T lysate.

Taken together, this data shows that MitoID can effectively identify new interactors for a Rab GTPase that previously had few known effectors, in this case Rab9A.

3.2.3 Rab11A/B

Rab11 is a conserved and relatively well-characterised Rab GTPase, mostly known to regulate membrane trafficking at recycling endosomes and the TGN (Wandinger-Ness & Zerial, 2014). It has two main paralogues, Rab11A, Rab11B, as well as the more distantly related Rab11C/Rab25 which we will not focus on in this study. While Rab11A is ubiquitously expressed, Rab11B is mostly expressed in the brain, testes and heart (Lai et al., 1994). Previous studies have shown that, despite having 89% amino acid sequence homology, Rab11A and B not only reside in different vesicular compartments, but are also able to differentially regulate endosomal sorting (Grimsey et al., 2015; Lapierre et al., 2003). Furthermore, a recent study found that deletion of Rab11A led to distinct morphological and functional defects of the endo-lysosomal system, whereas Rab11B did to a lesser extent (Zulkefli et al., 2019). To further examine the overlap and/or distinction of the two main Rab11 paralogs, we have included both proteins in our MitoID screen.

Among the top hits for Rab11A are numerous known Rab11 effectors, such as Rab3IP/Rabin8, Rab3IL1/GRAB, TBC1D12, AKAP10/D-AKAP2, and several subunits of the exocyst complex (namely EXOC3/Sec6 and EXOC5/Sec10) (Eggers et al., 2009; Horgan et al., 2013; Oguchi et al., 2017; Vetter et al., 2015; Welz et al., 2014) (Fig. 3.3A,B). Furthermore, WDR44 and RELCH/KIAA1468, two known Rab11 interactors with unknown function, and two known Rab11 GAPs, Evi5 and RABGAP1, are also identified (Fuchs et al., 2007; Häsler et al., 2020; Sobajima et al., 2018; C J Westlake et al., 2007). Interestingly, oxysterol binding protein 1 (OSBP) was recently identified as a RELCH-interactor, with RELCH mediating the interaction between OSBP and Rab11A (Sobajima et al., 2018). While we do not detect OSBP in our dataset, we do detect OSBP-like proteins OSBPL9 and OSBPL11 as high-scoring hits in GTP-locked Rab11A samples (Fig. 3.3A,B).

In addition to previously known Rab11A effectors, we were able to identify a number of proteins known to be involved with endosomal trafficking but not previously known to interact with Rab11A. These include the Rab4 and Rab14 effector RUFY1, the CORVET subunit VPS8, and the Syntaxin 6 binding partner UHRF1BP1L, as well as the previously discussed Rab5 interactors RABEP1 and RABGEF1 (Kunita et al., 2007; Markgraf et al., 2009; Otto et al., 2010; Yamamoto et al., 2010). Furthermore, we find ARFGEF1/BIG1 to bind to GTP-locked, but not GDP-locked, Rab11A. Even though this interaction hasn't yet been reported in mammalian cells, the yeast homologue of ARFGEF1, Sec7, is a known effector of the yeast Rab11 homologue, Ypt31/32 (McDonold & Fromme, 2014) (Fig. 3.3A,B).

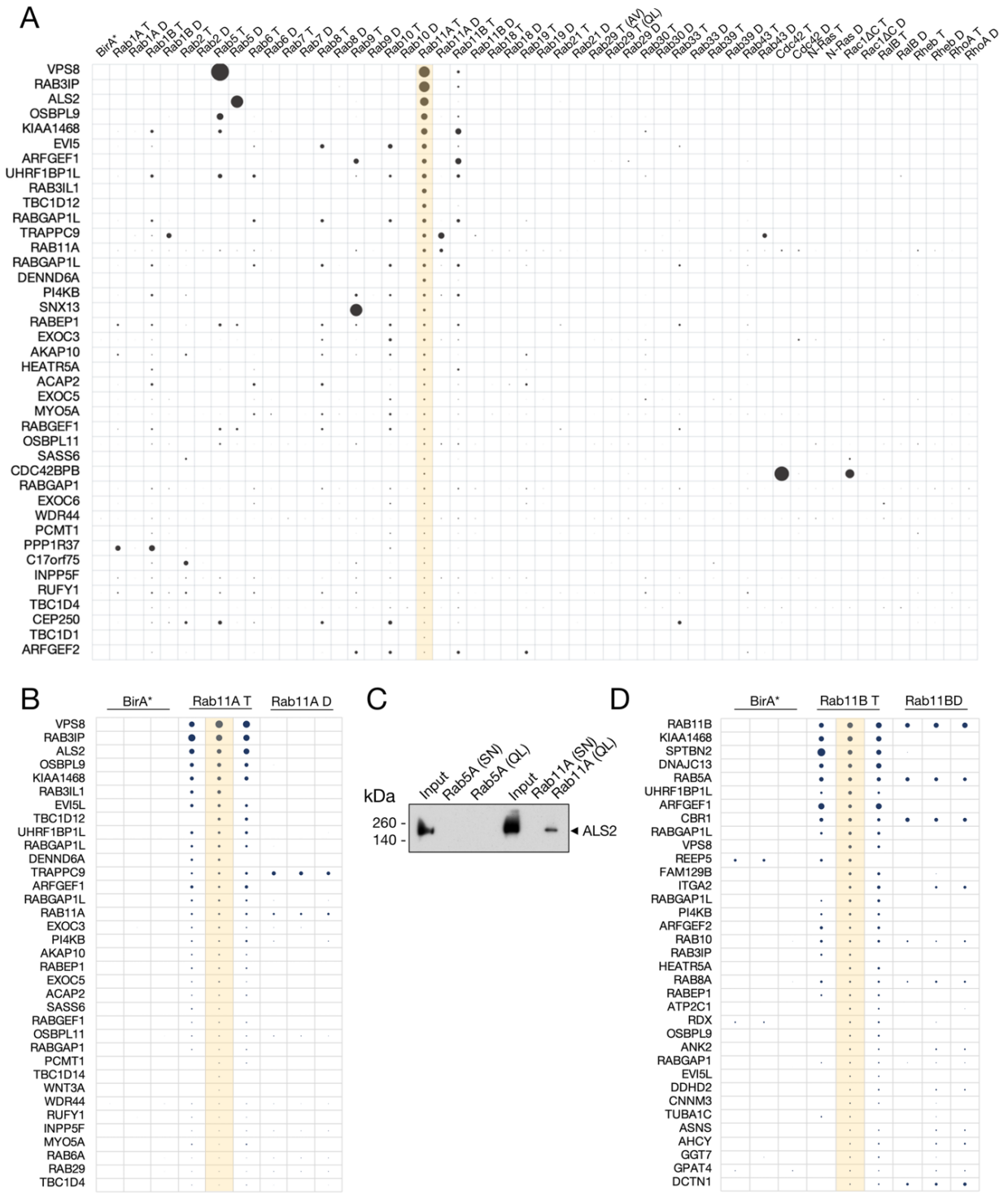

Figure 3.3. The MitoID approach highlights interactome differences and similarities between Rab11 paralogues. (A) Bubble pot of MitoID experiments of the whole panel of studied GTPases, aligned for GTP-locked Rab11A. Circle area corresponds to average WD-score (average of the biological triplicates). T: GTP-locked mutant, D: GDP-locked mutant. BirA* is an empty mitochondrial control. Top 40 hits are shown. Yellow column indicates alignment. (B) Bubble plot aligned for the third replicate of GTP-locked Rab11A. Shown here

Legend continued on next page.

are all three biological replicates of BirA* (BirA-HA-MAO control) and both Rab11A chimeras, though GTP-locked Rab11A was compared against all other GTPases in the full data list to generate this plot. Circle area corresponds to WD-score. The top 35 hits are shown. Yellow column indicates alignment (C) Affinity chromatography of bacterially expressed and purified GST-tagged Rab5A and Rab11A with wildtype HEK293T lysate, probed with ALS2 antibody. (D) As (B) but with Rab11B chimeras and aligned for GTP-locked Rab11B.

Interestingly, although the protein UHRF1BP1L remains largely uncharacterised, it is found to interact with several small GTPases in their GTP-locked forms (mainly Rab1B, Rab5A, Rab6A, Rab10, Rab11A and Rab11B) (Fig. 3.3A). Similarly to UHRF1BP1L, Rabaptin5 is also detected in multiple GTP-locked Rab GTPases, as is RABGAP1 and several other interactors such as RABGAP1L and AKAP10, indicating overlap of function between these Rab GTPases (Fig. 3.3A).

Furthermore, one of the highest scoring hits in GTP-locked Rab11A samples is the Rab5 GEF and Rac1 effector ALS2/Alsin (Fig. 3.3A,B). Although Alsin has been found to play a role in the regulation of the mitochondrial stress response (Hsu et al., 2018), it is highly unlikely that this is the reason that it is present in our dataset, since the protein is solely present in GTP-locked Rab11A and GDP-locked Rab5A and not across the whole panel, and we have formerly shown that our experimental set up does not induce mitochondrial stress, as was examined in the discussion of the previous chapter (Sup. Table 2 and 3, Fig. 2.2). The interaction between ALS2 and Rab11A was validated by affinity chromatography using bacterially expressed and purified GST-tagged Rab11A and wildtype HEK293T cell lysate (Fig. 3.3C, performed by Alison Gillingham).

Examining the top hits for Rab11B, we again identify many of the previously mentioned Rab11A interactors, such as RELCH, UHRF1BP1L, RABGAP1/1L, VPS8, ARFGEF1, and the exocyst components (Fig. 3.3D). However, when comparing the two Rab11 paralogues, we find that almost all effectors seem to have higher spectral counts for Rab11A than Rab11B (Fig. 3.3A). In particular Rab3IL1, AKAP10, Alsin and RABGEF1 stand out for being almost exclusively present in the Rab11A samples. Exceptions to this are RELCH, ARFGEF1, and RABEP1, which appear to interact with similar strengths to both paralogues, and ARFGEF2/BIG2, which is present in higher amounts in Rab11B samples than in Rab11A (Fig. 3.3A, Fig. 3.4A). Finally, RABEP1 and RABGEF1 are known to interact and form a protein complex, yet they do not seem to follow the same binding patterns to the Rab11 paralogues; Rab11A appears to interact with both RABEP1 and RABGEF1 at similar strengths, whereas Rab11B appears to interact only with RABEP1 (Fig. 3.3A). This suggests separate and additional functions for both proteins, besides the known Rab4-Rab5 activation bridge (Horiuchi et al., 1997; Kälin et al., 2015).

When comparing the top hits for Rab11A and B, we also identified several proteins that appear to bind to Rab11B alone, such as alpha-II spectrin (SPTAN1), which is involved in numerous neurological conditions, and DNAJC13/RME-8, an endocytic protein involved in Parkinson's disease and recently found to function as an autophagy regulator (Besemer et al., 2020; Girard et al., 2005; Roosen et al., 2019; Syrbe et al., 2017) (Fig. 3.3D, Fig. 3.4A). Carbonyl reductase 1 (CBR1) is unlikely to be a true Rab11B interactor due to its cellular function and the fact that it binds to both the GTP- and GDP-locked mutants, though it is interesting that it binds almost exclusively and consistently to Rab11B, Rac1, and Rheb (Sup. Tables 2 and 3).

Furthermore, Rab11B, but not Rab11A, interacts with Rab5A, Rab8A and Rab10 (Fig. 3.3D, Fig. 3.4A). Interestingly, Rab11A and Rab8A are coupled by Rabin8/RAB3IP –Rabin8 is a Rab11A effector and a Rab8A GEF, and thus mediates the Rab11A-Rab8A cascade (Vetter et al., 2015). Even though a biochemical interaction between Rab11B and Rabin8 has not yet been reported, and the MitoID data suggests a very reduced interaction affinity compared to Rab11A, Rab11B has shown some with degree of co-localisation with Rabin8 (Christopher J Westlake et al., 2011). Moreover, Rabin8 also activates Rab10, which, similarly to Rab8A, is very enriched in GTP-locked Rab11B samples compared to Rab11A and thus shows opposing interaction patterns (Fig. 3.4A) (Homma & Fukuda, 2016).

Even though Rab11A and Rabin8 are known to be in a complex with the Rab11-interacting protein Rab11FIP3 (FIP3), this latter protein is not detected in our study (Vetter et al., 2015). The absence of FIP3 in our dataset could be due to several reasons. One, FIP3 is simply too far away from the BirA* in our Rab11 chimeras, which prevents the protein from being biotinylated by the free biotin released by the BirA*. Two, the lysines of FIP3 are almost exclusively localised at the C-terminal domain, which is also the Rab11A binding region (Vetter et al., 2015). It is possible that the lysines are not available for biotinylation because they are blocked by the binding of Rab11. And finally, perhaps an intrinsic mass spectrometry fault has obstructed the identification of FIP3. In this specific case the latter seems most likely, since a recent study also failed to detect FIP3 by performing mass spectrometry on immunoprecipitated Rab11A (Walia et al., 2019). Notably, the same study observed that the interaction between FIP3 and Rab11A increases the binding affinity of Rabin8 fourfold, which makes the likelihood of FIP3 being present in this sample likely.

Interestingly, WDR44 is found to compete with FIP3 for the canonical binding site on Rab11, suggesting that WDR44 could interfere with the interaction between Rabin8 and Rab11A. In our study, WDR44 is found in similar amounts in both Rab11A and B, suggesting it has a similar role for both Rab11 paralogues (Fig. 3.3A) (Walia et al., 2019).

While Rab11B and Rab5A are occasionally found to function in similar pathways, an interaction between the two GTPases has as of yet remained unreported (Anand et al., 2020; Pavlos & Jahn, 2011). One possibility is that the two GTPases are involved in a Rab cascade with the Rab5A GEF ALS2. However, it would be more likely for this potential cascade to include Rab11A than Rab11B, since our data suggests that ALS2 preferentially interacts with Rab11A. Further research is necessary to uncover this interaction further.

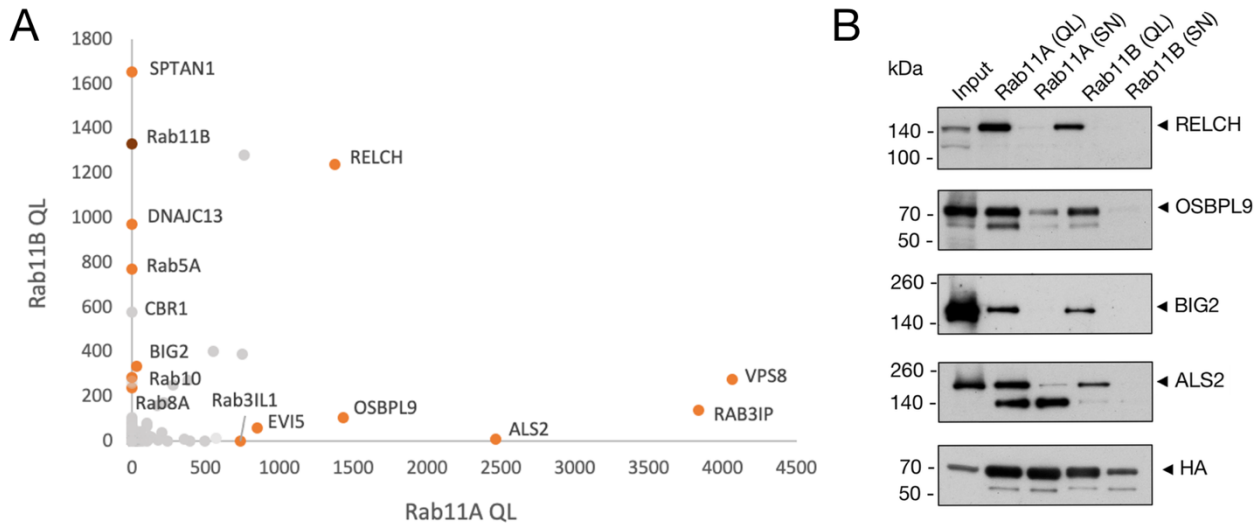

Figure 3.4. Different detection methods lead to discrepancies between identified Rab11A and Rab11B interactomes. (A) Plot of WD-scores of potential interactors of GTP-locked Rab11A and Rab11B. The WD-scores shown represent means of triplicate biological repeats. Several potential or known interactors that have higher WD-scores in one of the paralogues are highlighted in orange and labelled, as is RELCH which has high scores for both paralogues. (B) Western blots of MitoID samples of GTP- and GDP-locked Rab11A and Rab11B, probed with RELCH, OSBPL9, BIG2, ALS2 and HA antibodies, as indicated.

With the aim to validate the differences and similarities between the binding patterns of Rab11A and Rab11B, Western blots were performed on the MitoID samples and probed against RELCH, OSBPL9, BIG2, and ALS2 (Fig. 3.4B). While the mass spectrometry data shows OSBPL9 and ALS2 to be strongly enriched in Rab11A samples as opposed to Rab11B, the Western blots of the same samples show minimal differences in binding patterns (Fig. 3.4A,B). The very slight enrichment of OSBPL9 and ALS2 in Rab11A samples is likely due to the slightly higher expression levels of Rab11A chimeras as opposed to Rab11B (Fig. 3.4B, HA panel). This is corroborated by a similar level of RELCH enrichment in the Rab11A samples which mass spectrometry data have suggested are present in similar amounts in both paralogues (Fig. 3.4B). Contrarily, even though mass spectrometry detects higher levels of ARFGEF2/BIG2 in Rab11B samples compared to Rab11A, probing a Western blot for BIG2 again shows a slight enrichment in Rab11A samples

in line with chimera expression levels (Fig. 3.4A,B). Potential causes of the discrepancy between mass spectrometry output and biochemical analysis of the same samples will be examined in the Discussion of this chapter.

Together, this shows that the MitoID approach and subsequent analyses can highlight both similarities and differences between the interactomes of paralogues. However, we report discrepancies between mass spectrometry output and Western blotting of the same samples, which remains unexplained. Differences between detection methods highlight the necessity of validating the interactions through different approaches.

3.2.4 Rho family GTPases

Rab GTPases are one of five families of the Ras GTPase superfamily, the four other families being Ras, Rho, Ran and Arf GTPases (Wennerberg et al., 2005). To examine whether the MitoID approach is applicable to other small GTPases, we have tested the approach with three Rho family GTPases and three Ras family GTPases.

The Rho family of GTPases act mainly in the organisation and regulation of the actin cytoskeleton, which drive processes such as cell migration and morphogenesis (Hall, 2012). The MitoID approach was tested on three of the best characterised family members RhoA, Rac1, and Cdc42, using their known or predicted GTP- and GDP-locked mutants.

Cdc42 plays a large role in the regulation of actin dynamics and cell polarity, and thus affecting large scale processes like morphogenesis (Farhan & Hsu, 2015; Pichaud et al., 2019; Watson et al., 2016). The top hits for GTP-locked Cdc42 contains many known Cdc42 effectors, such as kinases (TNK2/ACK1, PAK2/4, and CDC42BPB/MRCKB), actin regulators (WASL and CDC42EP1/2/4 (BORG5/1/4), and scaffolding/ adaptor proteins (IQGAP1/2 and BAIAP2/IRSp53) (Fig. 3.5A) (Carlier et al., 1999; Farrugia & Calvo, 2016; Ha & Boggon, 2018; Hedman et al., 2015; Jung & Traugh, 2005; Lim et al., 2008; Moncrieff et al., 1999; Yokoyama & Miller, 2003). Known Cdc42 GAPs ARHGAP31/CDGAP and ARHGAP32/RICS are also high scoring hits for GTP-locked Cdc42 (Lamarche-Vane & Hall, 1998; Okabe et al., 2003). The motor protein myosin18A is also identified to be a potential Cdc42 effector, and, although this specific interaction has not been reported yet, myosin18A is reported to interact with the known Cdc42 effector MRCKB (Z. Zhao & Manser, 2015). Furthermore, KCTD3, mostly reported for its role in neurocognitive disease and selecting proteins for ubiquitination by cullin-RING ligases, is strongly enriched in GTP-locked Cdc42 samples (Teng et al., 2019). Interestingly, another KCTD family member, SHKBP1, is also found to interact

with active Cdc42 (Teng et al., 2019). Finally, several known regulators of other members of the Rho family are high scoring hits for Cdc42, such as ARHGEF11, ARHGEF12, and PLEKHG4 (Gupta et al., 2013; Kourlas et al., 2000; Rümenapp et al., 1999) (Fig. 3.5A). For instance, the RhoA GEF ARHGEF11 is enriched in both GTP- and GDP-locked Cdc42 samples. Interestingly, ARHGEF11 has been shown to interact with PAK4, though PAK4 only interacts with GTP-locked Cdc42; together this could suggest distinct roles of ARHGEF11 on both activity states of Cdc42 (Barac et al., 2003).

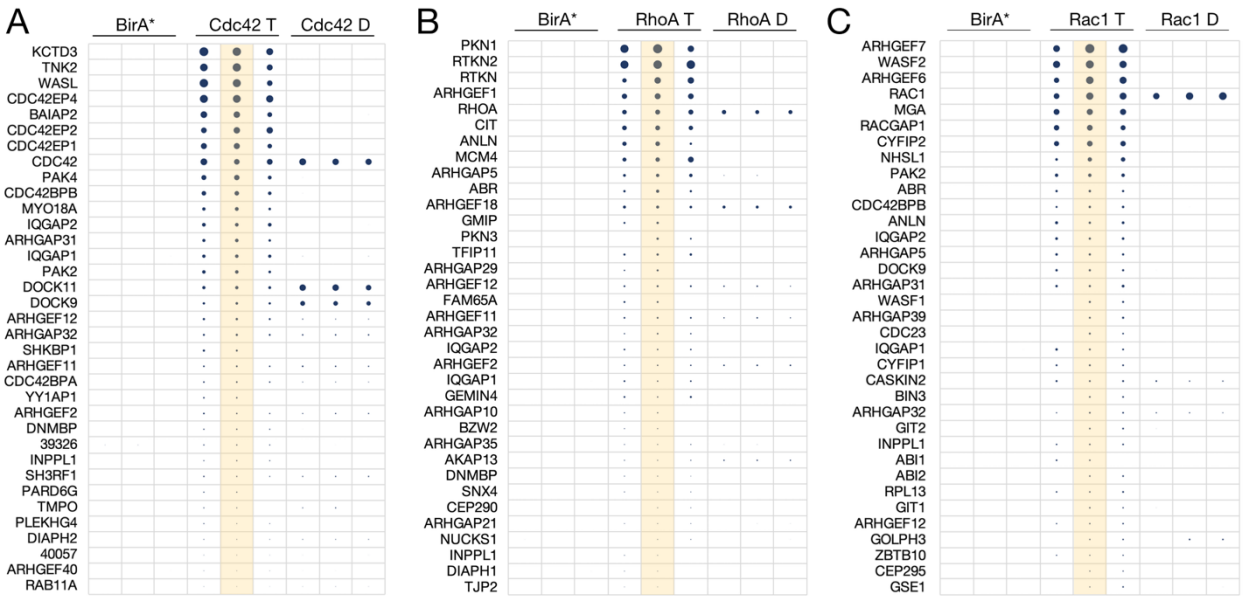

Figure 3.5. Identification of known and putative interactors of GTPases from the Rho family. (A) Bubble plot aligned for the second replicates of GTP-locked Cdc42. Shown here are all three biological replicates of BirA* (BirA-HA-MAO control) and both chimeras of Cdc42, though GTP-locked Cdc42 was compared against all other GTPases in the full data list to generate this plot. Circle area corresponds to WD-score. The top 35 hits are shown. Yellow column indicates alignment. (B) as (A) but showing RhoA chimeras and aligned for the second replicate of GTP-locked RhoA. (C) as (A) but showing Rac1ΔC chimeras and aligned for the second replicate of GTP-locked Rac1ΔC.

Similar to the other Rho family GTPases, RhoA functions by regulating the actin cytoskeleton (Nguyen et al., 2016). Numerous previously known effectors are detected in GTP-locked RhoA samples, which include kinases (PKN1, PKN3/PKNbeta and CIT/Citron), scaffolding/adaptor proteins (RTKN/Rhotekin, RTKN2/Rhotekin-2, and ANLN/Anillin), and phosphatases (INPPL1/SHIP2) (Fig. 3.5B) (Collier et al., 2004; Ito et al., 2018; Kato et al., 2012; Madaule et al., 1995; Reyes et al., 2014; Shibata et al., 2001; F. Wang et al., 2017). Moreover, the known Rho GAPs ABR, ARHGAP32/GRIT, GMIP, and both isoforms of p190RhoGAP (ARHGAP5 and ARHGAP35), are identified to be present in either GTP-locked or both

GTP- and GDP-locked RhoA samples (ARESTA et al., 2002; T. H. Chuang et al., 1995; Héraud et al., 2019; T. Nakamura et al., 2002). As for potential novel RhoA interactors, the Rac1 and Cdc42 effector IQGAP2 is strongly enriched in GTP-locked RhoA, which has so far remained unreported (Ozdemir et al., 2018). Finally, other high scoring hits that are as of yet unreported to interact with RhoA include the Cdc42 GEF DNMBP/Tuba, the sorting nexin SNX4, and several DNA or RNA binding proteins which are likely to be unspecific background (Fig. 3.5B) (Salazar et al., 2003).

Rac1 also plays a role in actin polymerisation and cell migration (Nguyen et al., 2016), however, after initial application of the MitoID approach to Rac1 chimeras, a multitude of DNA or RNA binding proteins were detected independently of their nucleotide-state (Fig. 3.6A). For this analysis we used peak intensity data obtained from mass spectrometry and analysed this with the Perseus platform (Keilhauer et al., 2014). Here, intensities of the peptide spectra within the replicates of GTP-locked Rac1 are compared to the intensities of that peptide for all tested GDP-locked GTPases, which results in a fold enrichment and a statistical confidence for that enrichment. Plotting fold enrichment and statistical confidence against each other results in so called 'volcano plots', which highlight proteins that sit high on both axes and are thus proteins that are likely to be specific interactors. In this analysis, GTP-locked Rac1 was compared against all GDP-locked baits with the aim of reducing the chance of incorrectly assigning proteins as background due to them being true interactors to multiple baits. This is based on the grounds that effectors generally bind only to the active/GTP-locked form and not to the inactive/GDP-locked form (Zerial & McBride, 2001). The GDP-locked baits were also compared to the other GDP-locked baits, because it is very unlikely that GEFs regulate multiple Rab GTPases due to the fact that several factors together contribute to GEF specificity (Pylypenko et al., 2017).

Several small GTPases in the Rho and Ras families have a C-terminal polybasic region, which promotes the association with membranes and can also serve as a nuclear localisation signal (Williams, 2003). Rac1 contains such a polybasic region, and is now brought to the ectopic and less acidic location of the outer mitochondrial membrane, which could lead the polybasic stretch to associate with nucleic acids. To test this, we repeated the MitoID approach with Rac1 lacking the C-terminal basic region (Rac1ΔC). Comparing these two MitoID experiments, we indeed detected fewer nucleic acid binding proteins with the Rac1ΔC version, without affecting the effector interactions, and thus this version was used for further analysis (Fig. 3.6B).

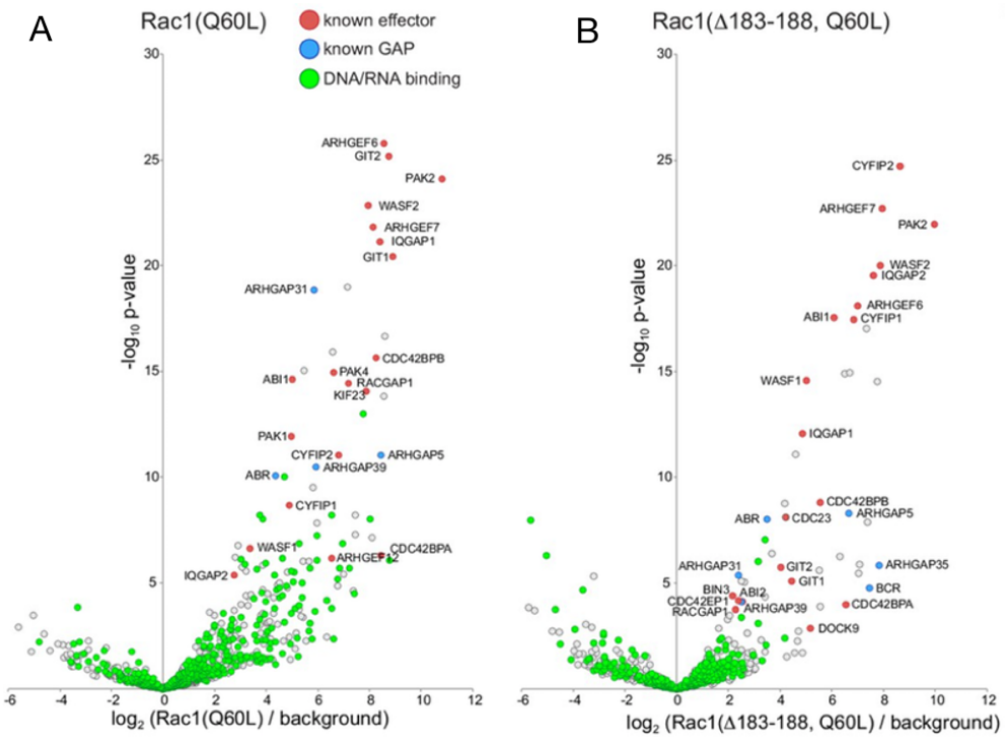

Figure 3.6. Deletion of Rac1 C-terminal polybasic stretch reduces the number of detected DNA/RNA binding proteins. (A,B) Volcano plots of GTP-locked Rac1 (A) and GTP-locked Rac1ΔC (Rac1 from which six basic residues have been deleted (Δ183-188)) plotted against all tested GDP-locked GTPases. Data was generated by MitoID proximity labelling and consecutive streptavidin affinity chromatography experiments, after which the peak intensity data was obtained through mass spectrometry. Red: known effectors, blue: known GAPs, green: DNA/RNA binding proteins. Data analysed by Alison Gillingham, plots generated by Sean Munro.

The top hits of GTP-locked Rac1ΔC contain numerous previously known Rac1 effectors, including kinases (PAK2, CDC42BP/MRCK), scaffolding/adaptor proteins (IQGAP1/2) and actin regulators (WAVE1/WASF2, WAVE2/WASF2, ABI1/2, CYFIP1/Sra1, and CYFIP2/PIR121)(B. Chen et al., 2017; Dubielecka et al., 2010; Flaiz et al., 2009; Hedman et al., 2015; Ozdemir et al., 2018; Z. Zhao & Manser, 2015) (Fig. 3.5C). Furthermore, all the components of the GIT/PIX complex (GIT1, GIT2, ARHGEF6/PIXA, and ARHGEF7, PIXB) are specifically enriched in GTP-locked Rac1ΔC(W. Zhou et al., 2016) (Fig. 3.5C). Besides numerous previously identified RhoA effectors such as Anillin and INPPL1/SHIP2, the Nance-Horan syndrome (NHS) protein family member, NHSL1, was identified as one of the putative novel Rac1 effectors. Interestingly, the NHS family proteins contain a WAVE homology domain, and function in actin remodelling and cell morphology (Brooks et al., 2010).

3.2.5 Ras family GTPases

The Ras family of GTPases function mainly in the regulation of signalling cascades, cell proliferation and differentiation, and we have selected three of the well characterised members for further analysis; N-Ras, RalB, and Rheb (Wennerberg et al., 2005).

The Ras family proteins are quite extensively studied due to their activity as oncogenes, and we are able to identify a number of known Ras effectors in our GTP-locked N-Ras samples (Hobbs et al., 2016). Among the highest scoring hits are the kinases RAF1/c-RAF and BRAF1, the Ras GAP neurofibromin/NF1, and Rap GEFs RAPGEF2/CNrasGEF and RAPGEF6/RA-GEF-2 (Fig. 3.7A) (Gao et al., 2001; G. A. Martin et al., 1990; Pham et al., 2000; Weber et al., 2001). Furthermore, the tumour suppressor RASSF5/NORE1A has been reported to bind to N-Ras in a GTP-dependent manner, which we can confirm by RASSF5 enrichment in two out of three GTP-locked N-Ras samples (Zinatizadeh et al., 2019) (Fig. 3.7A). UniProt has annotated CBARP/C19orf26 as a voltage-dependent calcium channel beta subunit-associated regulatory protein, although no reports have been published on the exact function of CBARP or how it could relate to N-Ras signalling. In addition, two centrosomal proteins are enriched in N-Ras samples; CEP104, involved in ciliogenesis, is specifically present in GTP-locked N-Ras, whereas CEP192, involved in centrosome maturation and spindle assembly, is enriched in both GTP- and GDP-locked samples (Fig. 3.7A) (Gomez-Ferreria & Sharp, 2008; Tammana et al., 2013).

The Ral family of GTPases regulate several key cellular processes such as exosome secretion, cell migration, and gene expression (Gentry et al., 2014; Hyenne et al., 2016). Since RalB is known to interact with the exocyst, the high degree of enrichment of several subunits (EXOC6, 7, and 8) and presence of many others (EXOC1, 2, 3, 4, 5) in our GTP-locked RalB samples is no surprise (Fig. 3.7B, Sup. Tables 2 and 3) (Fenwick et al., 2010; Moskalenko et al., 2003; Rossé et al., 2006). Other high scoring hits are the known effector RLIP76/RalBP1, its binding partner REPS1, and two known Ral GAPs (RALGAPA1/2 and RALGAPB) (Fenwick et al., 2010; Shirakawa et al., 2009; Yamaguchi et al., 1997). Interestingly, we detect high amounts of N-Ras in GTP-locked RalB samples but not in GDP-locked samples, and, contrarily, we do not observe any RalB in the N-Ras samples (Fig. 3.7A,B). It has been reported that Ras and Ral are involved in a GTPase cascade, in which active Ras binds to the Ral GEFs RGL1 and 2 which activate RalB (Zago et al., 2018). However, intriguingly, the aforementioned Ral GEFs are not identified in our dataset. It is unclear whether RGL1 and 2 are not detected by mass spectrometry, or if there is another link between Ras and Ral that is as of yet unidentified. Finally, several other significant hits are DNA- and RNA-binding proteins, which are unlikely to be true interactors.

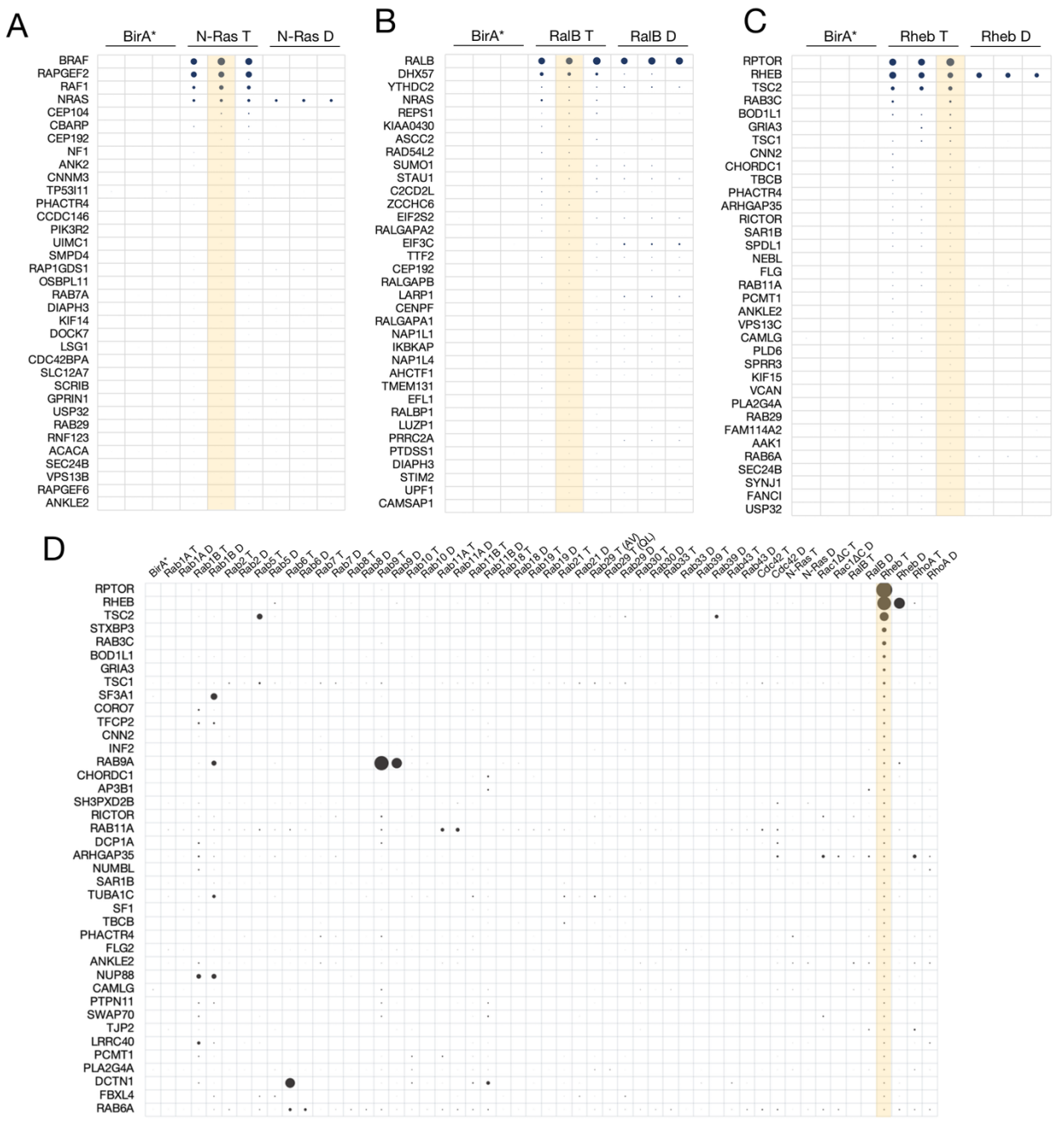

Figure 3.7. Identification of known and putative interactors of GTPases from the Ras family. (A) Bubble plot aligned for the second replicate of GTP-locked N-Ras. Shown here are all three biological replicates of BirA* (BirA-HA-MAO control) and both chimeras of N-Ras, though GTP-locked N-Ras was compared against all other GTPases in the full data list to generate this plot. Circle area corresponds to WD-score. The top 35 hits are shown. (B) as (A) but showing RalB chimeras and aligned for the second replicate of GTP-locked RalB. (C) as (A) but showing Rheb chimeras and aligned for the third replicate of GTP-locked Rheb. (D) Bubble pot of MitoID experiments of the whole panel of studied GTPases, aligned for GTP-locked Rheb. Circle area corresponds to average WD-score (average of the biological triplicates). T: GTP-locked mutant, D: GDP-locked mutant. BirA* is an empty mitochondrial control. Top 40 hits are shown. Yellow columns indicate alignment.

Rheb is an activator of mTORC, controlling protein synthesis and cell growth, and thus it is reassuring that one of the highest scoring proteins we detect in the GTP-locked Rheb samples is the mTORC1 subunit Raptor/RPTOR (Fig. 3.7C) (Heard et al., 2014). Moreover, we find the tumour suppressor gene encoded subunits of the Rheb GAP complex, TSC1 and TSC2, as very significant hits (Manning & Cantley, 2003). Interestingly, a third subunit of this complex, TBC1D7, is not detected in our study. Perhaps, since TBC1D7 is found to interact with the complex through TSC1, the protein is not proximal enough to the BirA* in our Rheb chimera to be biotinylated (Dibble et al., 2012). This is corroborated by TSC2 containing the active GAP domain, and TSC2 having significantly more spectral counts than TSC1 in our GTP-locked Rheb samples (Sup. Table 2, Fig. 3.7D shows scores) (Huang & Manning, 2008). Finally, one of the top scoring hits is Rab3C (Fig. 3.7C). Although it is only detected by 4 spectral counts, Rab3C is consistently present throughout the three replicates in GTP-locked and not in GDP-locked Rheb samples. It is not consistently detected with other baits, which suggests it could be a true interactor (Fig. 3.7D). There is no known link between active Rheb and Rab3C, with Rab3C mostly functioning on synaptic and secretory vesicles, and more research needs to be done to investigate this putative interaction further (Schlüter et al., 2002). Finally, even though Ral and Rheb proteins have been shown to both work on mTOR signalling and the TSC1/TSC2 complex, there is no clear overlap between their MitoID results (T. D. Martin et al., 2014).

Taken together, we are able to identify both known and novel potential interaction partners for all the tested Rho and Ras family members. In addition, we have detected both numerous GTPase-specific interactors as well as certain overlapping interactors between the members of each GTPase family. This shows that the MitoID approach is successful in identifying effectors of different families of small GTPases.

3.2.6 The MitoID approach allows for identification of small GTPase GEFs

As previously mentioned, there are two broad categories of GTPase regulators: the GTP bound to small GTPases is hydrolysed by GAPs (GTPase activating proteins), whereas GEFs (guanine nucleotide exchange factors) reactivate the GTPase by catalysing the dissociation of GDP and the association of a free GTP molecule. GEFs have been shown to interact more strongly with the nucleotide-free or GDP-associated form than with the GTP form, which means that mutations that interfere with GTP-binding should show an increase of exchange factor binding (Koch et al., 2016; Langemeyer et al., 2014; Müller & Goody, 2017). Since the conserved P-loop is necessary for GTP-binding, we have used mutations where the serine or threonine is replaced by an asparagine. Similar mutations have shown to both prevent GTP-binding as well as reduce affinity for GDP, which makes these mutations a hybrid between GDP-bound and nucleotide-free forms (John et al., 1993; Koch et al., 2016). Performing the entire MitoID screen on mitochondrially-localised chimeras with these mutations, we aimed to identify known GEFs and perhaps identify new

candidates. Contrary to our successful GTP-locked Rab results, it appeared to be more challenging to identify GEFs using the GDP-locked Rab GTPases, with more candidates identified with the GDP-locked GTPases of the Rho and Ras family. Bubble plots of GDP-locked GTPases not discussed below are available in Supplementary Figures 3.4 - 3.6, with the exception of Rab1A/B which will be discussed in detail in Chapter 5.

Focusing on the Rab GTPases discussed above for their GTP-locked forms, GDP-locked Rab2A showed specific enrichment of the autophagy regulator CLEC16A, which has previously been reported with the *C. elegans* homologue (GOP-1) activating Rab2A homologue UNC-108 (Fig. 3.8A) (Tam et al., 2017; Yin et al., 2017).

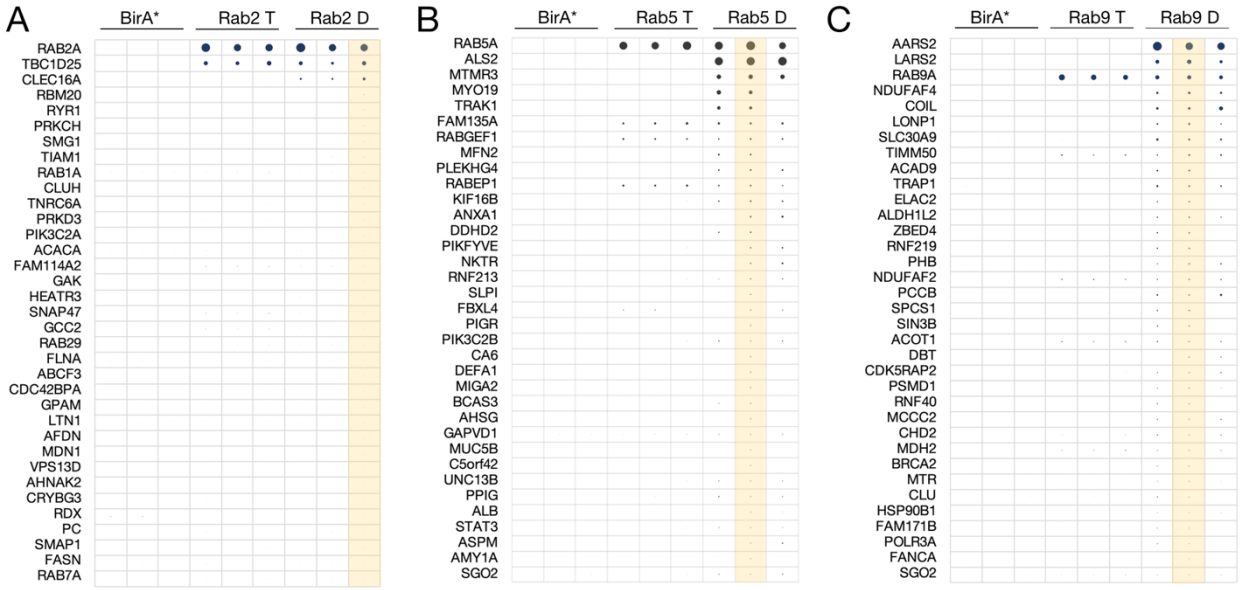

Figure 3.8. Analysis of GDP-locked Rab GTPases illuminates putative novel Rab regulators. (A) Bubble plot aligned for the third replicate of GDP-locked Rab2A. Shown here are all three biological replicates of BirA* (BirA-HA-MAO control) and both chimeras of Rab2A, though GDP-locked Rab2A was compared against all other GTPases in the full data list to generate this plot. Circle area corresponds to WD-score. The top 35 hits are shown. Yellow column indicates alignment. (B) as (A) but showing Rab5A chimeras and aligned for the second replicate of GDP-locked Rab5A. (C) as (A) but showing Rab9A chimeras and aligned for the second replicate of GDP-locked Rab9A.

The previously mentioned Rab5A GEFs (Alsin/ALS2, GAPVD1, and the RABEP1-RABGEF1 complex) are all high scoring hits for the GDP-form of Rab5A (Fig. 3.8B) (Horiuchi et al., 1997; Hunker et al., 2006; Topp et al., 2004; Z. Zhang et al., 2014). Furthermore, the unconventional myosin MYO19 and the kinesin-

adaptor protein TRAK1/Milton are both enriched in GDP-locked Rab5A samples, however, upon closer inspection both proteins appear to be related to mitochondrial trafficking and are thus possible contaminants (Shneyer et al., 2015; van Spronsen et al., 2013). Finally, the myotubularin-related protein MTMR3 is specifically present in GDP-locked Rab5A samples, though it is mostly known to play a role in autophagy regulation and there are no reports that this protein might function as an exchange factor (Fig. 3.8B) (Hao et al., 2015).

Rab9A results did not show any potential GEF candidates – GDP-locked Rab9A samples contained specific enrichment of mitochondrial factors such as tRNA ligases, NADH dehydrogenases, and proteases, as well as COIL/coilin which is a main component of nuclear bodies and the zinc transporter SLC30A9 (Fig. 3.8C).

Two known Rab11A GEFs are very strong hits in GDP-locked Rab11A samples; SH3BP5/SH3BP5L and the C9 and C10 subunits of the TRAPPII complex (Fig. 3.9A) (Riedel et al., 2017; Sato et al., 2016). Intriguingly, we detect high levels of Rab43 in our GDP-locked Rab11A samples, which could potentially be explained by two possibilities – it is possible that both Rab11A and Rab43 are a part of a Rab cascade, but it is more likely that they are in close contact with each other due to them both being activated by the same regulator. This latter explanation is corroborated by the presence of TRAPPC8 and TRAPPC9 as high scoring hits for GDP-locked Rab43. (Sup. Fig. 3.6D). Interestingly, while Rab11A is technically present in Rab43 samples, it is not specifically enriched when compared to background levels.

A number of these high-scoring Rab11A hits are not detected in GDP-locked Rab11B samples, including Rab43, TRAPPC10 and RalGAPA2 (Fig. 3.9B). However, since the TRAPPII complex subunit TRAPPC9 is present in Rab11B (although in significantly lower amounts than in Rab11A) it is possible that the TRAPPII complex is in fact a GEF for both Rab11 paralogues but has a lower affinity to Rab11B (Fig. 3.9C). The other known Rab11 GEFs, SH3BP5 and SH3BP5L, are detected in GDP-locked Rab11B samples in similar amounts as for Rab11A (Fig. 3.9C). Other high-scoring GDP-locked Rab11B hits include many proteins that are likely to be unspecific background, such as transcription factors BTF3 and TAF7 and protein modifier enzymes NMT1 and PPID.

The binding patterns of SH3BP5L and TRAPPC10 to the Rab11 paralogues were further examined, first by performing Western blots on the MitoID samples which confirmed SH3BP5L to be enriched in both GDP-locked Rab11A and B (Fig. 3.9D). Since a sufficient TRAPPC10 antibody was lacking, MitoID experiments were then performed in HEK293T cells transiently expressing FLAG-tagged SH3BP5L or

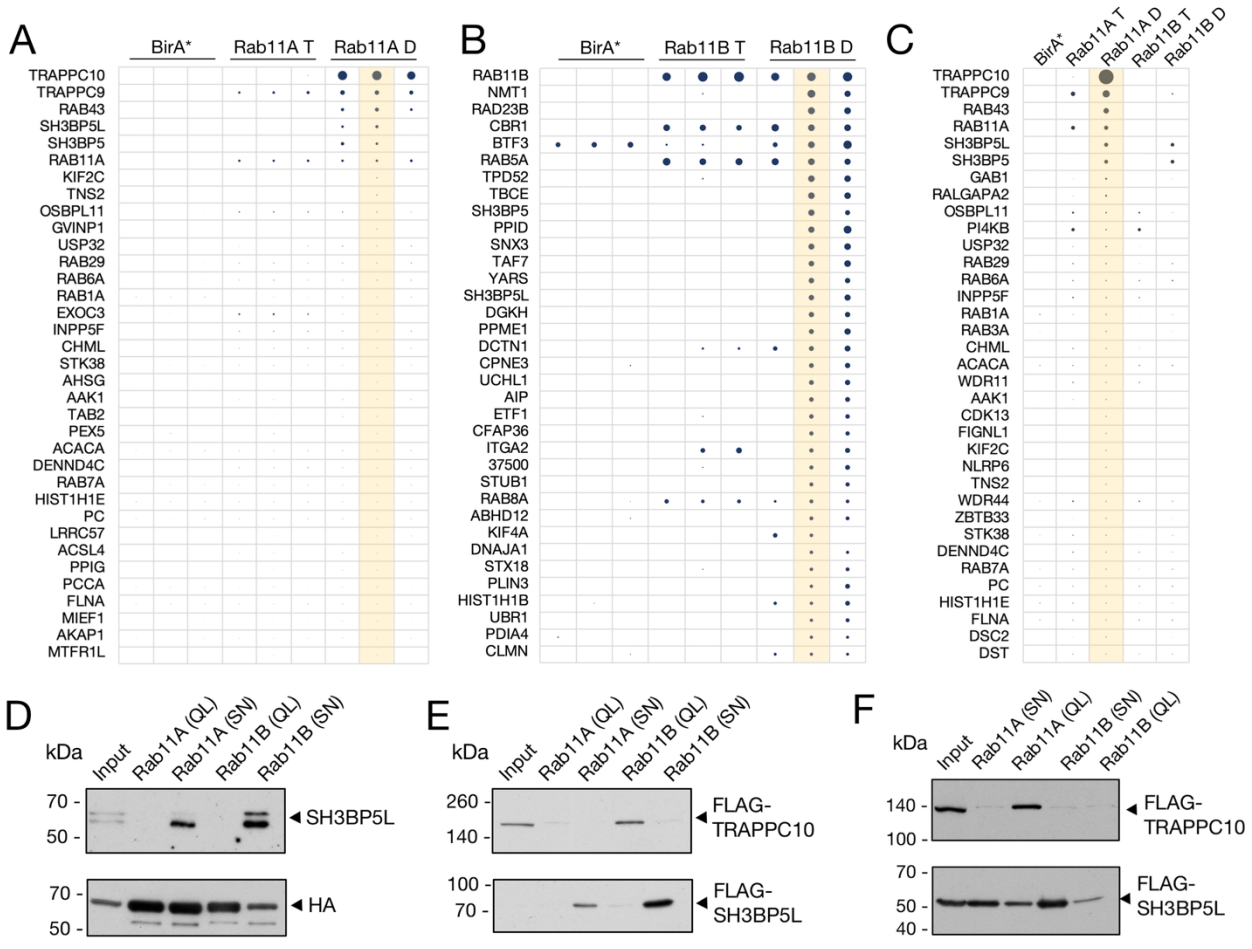

Figure 3.9. Differences and similarities between regulators of Rab11 paralogues. (A) Bubble plot aligned for the second replicate of GDP-locked Rab11A. Shown here are all three biological replicates of BirA* (BirA-HA-MAO control) and both chimeras of Rab11A, though GDP-locked Rab11A was compared against all other GTPases in the full data list to generate this plot. Circle area corresponds to WD-score. The top 35 hits are shown. Yellow column indicates alignment. (B) as (A) but showing Rab11B chimeras and aligned for the second replicate of GDP-locked Rab11B. (C) Bubble plot of MitoID experiments with Rab11 paralogues. Circle area corresponds with WD-score, generated by comparing against the full list of tested GTPases. T: GTP-locked form, D: GDP-locked form, BirA*: empty mitochondrial control. Yellow column indicates alignment. (D) Western blots of MitoID experiments on Rab11 paralogues, probed with SH3BP5L and HA (bait) antibodies. Input: wildtype HEK293T lysate. (E) Western blots of MitoID experiments on Rab11 paralogues, performed in HEK293T cells transiently expressing FLAG-TRAPPC10 (upper panel) or FLAG-SH3BP5L (lower panel). Blots are probed with FLAG antibody. Input: lysate of HEK293T cells overexpressing indicated FLAG-tagged protein. (F) Affinity chromatography of bacterially expressed and purified GST-Rab11 paralogues with HEK293T lysate transiently expressing FLAG-TRAPPC10 (upper panel) or FLAG-SH3BP5L (lower panel). Blots are probed with FLAG antibody. Input: lysate of HEK293T cells overexpressing indicated FLAG-tagged proteins. Performed by Alison Gillingham.

TRAPPC10. Western blots of these samples again confirmed the presence of SH3BP5L in the GDP-locked Rab11 paralogues, while, surprisingly, TRAPPC10 appeared to be enriched only in GTP-locked Rab11A

(Fig. 3.9E). While the mass spectrometry analysis indeed suggests that TRAPPII interacts with Rab11A and not (or much less) with Rab11B, it is expected to interact with the inactive, GDP-locked form. Affinity chromatography experiments were performed to investigate this further; bacterially expressed GST-Rab11 paralogues were purified and mixed with HEK293T lysate expressing FLAG-tagged SH3BP5L or TRAPPC10 (performed by Alison Gillingham). Western blotting of these samples validated the interactions described above; SH3BP5L interacts with both Rab11A and B and is enriched in their GDP-locked forms, whereas TRAPPC10 interacts with GTP-locked Rab11A (Fig. 3.9F). Even though TRAPPII was shown to activate *Drosophila melanogaster* Rab11, the study by Riedel and colleagues does not include binding or interaction comparisons between GTP- or GDP-bound forms of Rab11 (Riedel et al., 2017). Furthermore, since *D. melanogaster* Rab11 does not exist in multiple paralogues, a comparison between the fly orthologs of Rab11A and Rab11B could not be made (Riedel et al., 2017).
It is possible that TRAPPII interacts with GTP-bound Rab11A as well as being a Rab11A GEF, essentially forming a positive feedback loop, similar to Rabex-5/RABGEF1 with Rab5A. Such an interaction could involve another Rab11A effector, just like Rabex-5 binds to active Rab5A through Rabaptin5. Further research is necessary to elucidate the potential interaction pattern of the TRAPPII complex with Rab11A.

As mentioned above, identifying proteins specifically interacting with inactive GTPases was a lot more effective for small GTPases of the Rho and Ras families compared to those of the Rab families, with the exception of RalB and Rheb. GDP-locked N-Ras showed enrichment of SOS1 (son of sevenless homologue 1), a well-characterised Ras GEF, in 2 out of 3 replicates (Fig. 3.10A) (Tian & Feig, 2001). Furthermore, the previously mentioned Rho and Ras family GEF RAP1GDS1/smgGDS is present in both GDP- and GTP-locked N-Ras samples, although, interestingly, previous reports have been unable to detect GEF activity towards N-Ras *in vitro* (Vikis et al., 2002).

A subset of DOCK family members are well-characterised GEFs for several small GTPases. Cdc42 is known to be activated by DOCK-D (DOCK9, 10, and 11), and DOCK-C (DOCK6, 7, and 8) is thought to have dual specificity for both Rac1 and Cdc42 (Gadea & Blangy, 2014; Kang et al., 2019; Kukimoto-Niino et al., 2019; Lin et al., 2006; Miyamoto et al., 2007; Shiraishi et al., 2016; Yeyun Zhou et al., 2013). With the exception of DOCK10, we are able to detect all of these DOCK proteins with high numbers of spectral counts (Fig. 3.10B) (Gadea & Blangy, 2014; Kang et al., 2019; Lin et al., 2006; Miyamoto et al., 2007; Shiraishi et al., 2016; Yeyun Zhou et al., 2013). In addition, certain members of the DOCK family have recently been found to interact with LRCH proteins, of which we found two (LRCH2 and LRCH3) very specifically enriched in inactive Cdc42 samples (O'Loughlin et al., 2018). The scaffolding protein DNMBP/Tuba is also a known Cdc42 GEF, though, interestingly, we detect DNMBP in GTP-locked, but

not in GDP-locked, Cdc42 samples (Fig. 3.10B) (Salazar et al., 2003). This can be explained by the complex formation of DNMBP and Cdc42 with the adaptor protein PAR6; PAR6 is known to bind solely to active Cdc42, so this could explain why DNMBP is also present in GTP-locked Cdc42 samples (Noda et al., 2001). To corroborate this, we detect the PAR6 subunit PAR6G/PARD6G enriched in 2 out of 3 GTP-locked Cdc42 samples (Fig. 3.10B). The known Cdc42 GEF AKAP13/Brx is also detected in GDP-locked Cdc42 samples (Rubino et al., 1998). Finally, the Rho GEFs ARHGEF11/LARG and ARHGEF12/PDZ-RhoGEF bind to Cdc42 in a nucleotide independent manner, while, interestingly, the Rho famly GAP ARHGAP35/p190RhoGAP appears to bind specifically to inactive Cdc42 (Fig. 3.10B) (Kourlas et al., 2000; Lévay et al., 2013; Rümenapp et al., 1999).

The known Rho GEFs ARHGEF11 and ARHGEF12 are high scoring hits for RhoA (Fig. 3.10C) (Kourlas et al., 2000; Rümenapp et al., 1999). Similarly to Rho GEFs ARHGEF18 and ARHGEF2, ARHGEF11 and ARHGEF12 appear to bind RhoA in a nucleotide independent manner, which suggests that they are also effectors that can act in a positive feedback loop (Medina et al., 2013; Niu et al., 2003; Pathak & Dermardirossian, 2013). The Cdc42 effector Cdc42BPA/MRCKA appears to interact with GDP-locked RhoA, suggesting this could be a novel RhoA GEF and potentially function as a link in a RhoA and Cdc42 cascade.

The DOCK protein family has been previously mentioned as GEFs for Cdc42, but are also known to be Rac1 activators. More specifically, DOCK-A (DOCK1, 2, and 5) and DOCK-B (DOCK 3 and 4) are Rac1 activators, while DOCK-C (DOCK6, 7, and 8) is suspected of having dual specificity for Rac1 and Cdc42 (Gadea & Blangy, 2014; Kiyokawa et al., 1998; Kukimoto-Niino et al., 2019; Miyamoto et al., 2007; Namekata et al., 2004; Vives et al., 2011; Xiao et al., 2013). Multiple subunits of each of these DOCK families are present at high levels in the GDP-locked Rac1 samples, namely DOCK1, 3, 4, 5, 6, and 7 (Fig. 3.10D). The presence of DOCK-C subunits in both Cdc42 and Rac1 GDP-locked samples, corroborates the suggestion that DOCK-C has dual specificity for both small GTPases. In addition, PDLIM7/Enigma, a member of the PDZ-LIM family, is specifically enriched in GDP-locked Rac1 samples (Fig. 3.10D). Even though there are as yet no reports showing that PDLIM7 can function as a GEF, another member of the PDZ-LIM family has been shown to regulate Cdc42 activation, suggesting that PDLIM7 could share this function (Z. Liu et al., 2014; Velthuis & Bagowski, 2007).

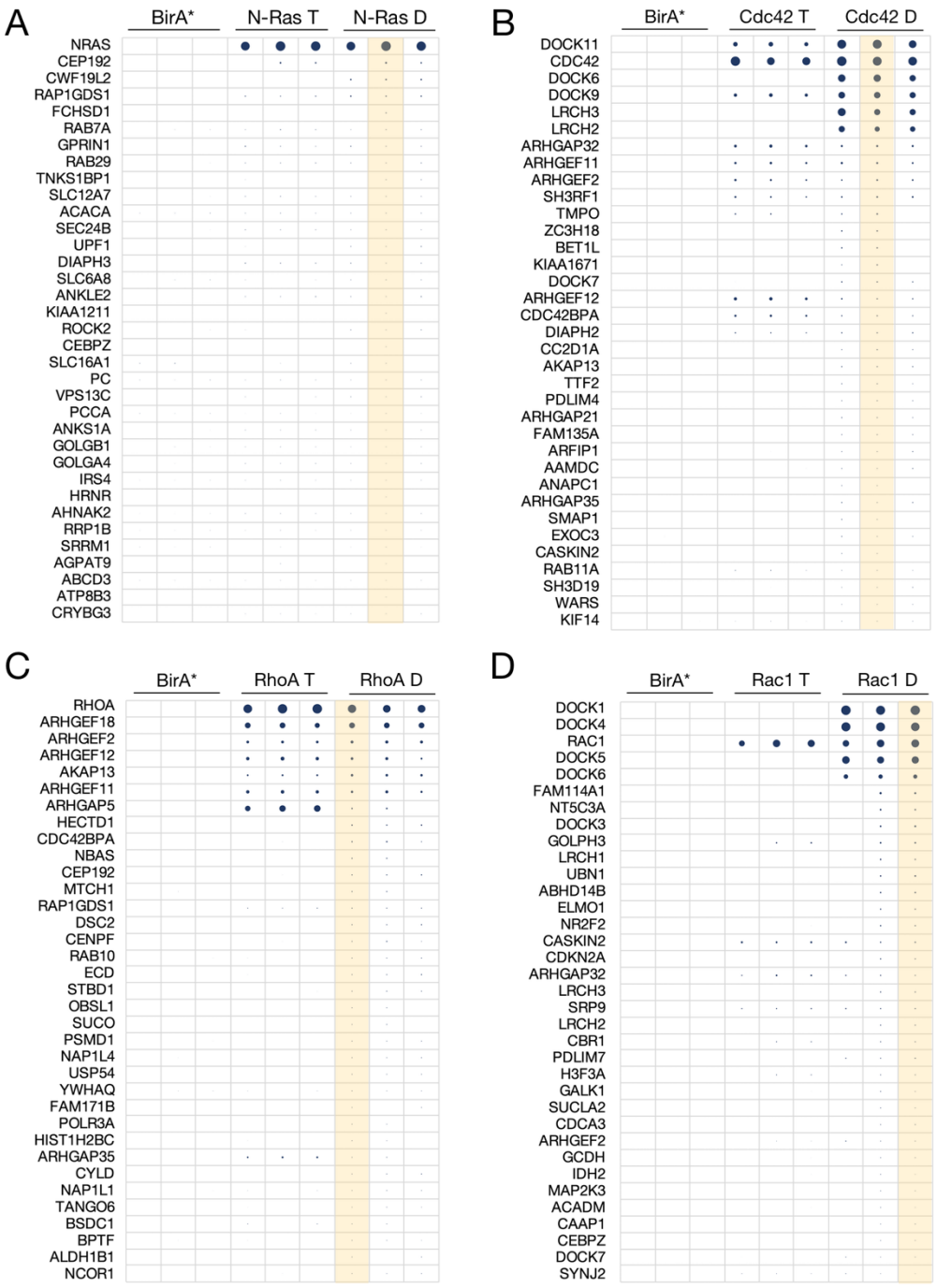

Figure 3.10. Analysis of GDP-locked GTPases illuminates novel putative regulators. (A) Bubble plot aligned for the second replicates of GDP-locked N-Ras. Shown here are all three biological replicates of BirA* (BirA-HA-MAO control) and both chimeras of N-Ras, though GDP-locked Rab2A was compared against all other GTPases in the full data list to generate this plot. Circle area corresponds to WD-score. The top 35 hits are shown. Yellow column indicates alignment. (B) as (A) but showing Cdc42 chimeras and aligned for the second replicate of GDP-locked Cdc42. (C) as (A) but showing RhoA chimeras and aligned for the first replicate of GDP-locked RhoA. (D) as (A) but showing Rac1ΔC chimeras and aligned for the third replicate of GDP-locked Rac1ΔC.

Taken together, these results show that MitoID can effectively detect exchange factors of some small GTPases of the Rab, Ras and Rho families. One possible reason why this is not as effective for all small GTPases tested could be the dominant negative mutations that were used. Several of the mutations used have been well established and used in numerous laboratories, however, certain dominant negative mutations we have developed ourselves, based on the sequence of the protein and the location of its residues in the P-loop. The mass spectrometry data shows a clear difference between the constitutively active and dominant negative mutations, though it is possible that the conformational change of the protein is not identical to what the GEFs of certain GTPases require for binding. Taking this into consideration, further research needs to be done to identify exchange factors of the other G-proteins, by testing multiple mutations and performing MitoID experiments on these chimeras.

3.3 Discussion

By applying the MitoID approach to a subset of 25 small GTPases from the Rab, Rho, and Ras families, we were able to identify numerous previously known and potentially novel interactors. An in-depth examination of Rab2A, Rab9A and Rab11 has led to the validation of several novel effectors, namely ARFGEF3/BIG3 and STAMBPL1 for Rab2A, NDE1 and HPS3 for Rab9A and ALS2/Alsin for Rab11A.

Interestingly, certain small GTPases appear to have a more expansive set of known and/or potential interactors than others. A multitude of factors could have contributed to this discrepancy. A biological explanation would be that small GTPases with fewer identified interactors, just naturally have fewer interactors; while certain small GTPases – such as Rab2A and Rab5A – are known to be essential key regulators with an extensive network of interactors, other GTPases play a less extensive role in the cell, and are thus bound to have fewer binding partners. In addition, the functionality of GTP- and GDP-locked mutations could also have contributed in the discrepancy between the different G proteins. The possibility of using different mutations was examined in the discussion of the previous chapter, and could potentially increase the efficiency and validity of the MitoID approach on these GTPases.

Throughout this study, I have chosen to transiently express the mitochondrially-localised GTPase chimeras. As is evident from the data presented above, transiently expressing the chimeras is sufficient to identify both known and novel interactors. Furthermore, overexpressing the chimeras does not appear to disrupt the mitochondria to the extent of inducing stress, nor does it seem to disrupt any essential cellular processes or

cause cell death. That being said, stably expressing the chimeras could potentially enhance the MitoID approach further – creating stable cell lines using the CRISPR-Cas9 technique would mean that expression efficiency would be ubiquitous and the expression levels would be more similar to the endogenous GTPases present in the genome (Doudna & Charpentier, 2014). With the continued increase of the ease and efficiency of stable genome editing methods such as the FLP recombinase or the PiggyBac transposase systems, using stable expression could be an excellent option for future studies (Ivics, 2016; Shah et al., 2015).

As mentioned above, the localisation patterns of small GTPases are not necessarily as distinct as traditionally thought. Collectively, we continuously gain more information on the function, interaction partners, and localisation of small GTPases, which leads us to continuously adjust our knowledge base. A relatively recent example of this is Rab2A; traditionally known as a Rab GTPase involved in ER-to-Golgi trafficking, until studies reported a role of Rab2A in endosomal-lysosomal fusion and dense-core vesicle maturation (Ailion et al., 2014; Lőrincz et al., 2017; Lund et al., 2018; Sandoval & Simmen, 2012; Sumakovic et al., 2009). Our study has highlighted two novel Rab2A effectors, one of which (ARFGEF3/BIG3) is found to be localised to lysosomes in neurons and thus aligns with the known localisation of Rab2 (Tao Liu et al., 2016). However, STAMBPL1, another novel Rab2A effector, is known to localise to early endosomes, which potentially places Rab2A at this previously unreported location (M. Nakamura et al., 2006). This shows that gaining more knowledge on the interaction partners of small GTPases can potentially increase our knowledge on their localisation patterns, placing the proteins at previously unreported intracellular membrane compartments.

Arf GTPases were excluded from this study due to inherent differences between them and other families of small GTPases, as explained in the discussion of Chapter 2. However, besides Arf GTPases, the other tested families of small GTPases do not appear to show family-specific differences in efficiency. While several hits do recur in multiple members of the same family, the ability of the MitoID approach to identify interactors seems to be protein-dependent, not family-dependent. The family of Rab GTPases highlight this distinction clearly; belonging to the same family of GTPases, there is a clear disparity between the datasets produced by for instance Rab2A or Rab5A (many known and novel hits) versus for instance Rab33B or Rab19B (very few known and novel hits) (data not displayed, raw data in Table 2-4).

One of the key aspects of performing a screen is an effective method of validation. In this study, we have identified numerous potential GTPase interactors, of which several were validated by biochemistry or immunofluorescence experiments. However, several tested putative interactors could not be validated through these methods. While it is possible that this means that they are in fact not true interactors, failure

to validate binding through affinity chromatography could also be due to one of the intrinsic draw backs of this latter method. When using affinity chromatography with bacterially expressed and purified proteins, incorrect folding could occur which interrupts the effector binding site or certain essential post-translational modifications (PTMs) could be missing due to bacterial expression. Another factor is the stability of the interaction; if the interaction is transient or weak, the protein can be washed off the Rab-coated beads more easily which results in it not being detected in the resulting sample. While using microscopy techniques to examine protein interactions is a possibility in theory, applying this to our small GTPase chimeras has proven to be challenging. Immunofluorescence antibody probing for possible interactors has not resulted in any visible relocation to the mitochondrially-localised GTPases, even for well-established interactions such as GTP-locked Rab2A and GMAP-210 (data not shown) (Sinka et al., 2008). In the cases where confocal microscopy was successful in validating interactions, we had overexpressed tagged versions of both bait and prey. While confocal microscopy, even with overexpression of the proteins involved, is a satisfactory way of validating interactions, weaker or transient interactions are unlikely to be detected. Perhaps redirecting the baits to a more densely localised organelle could aid in this, or implementing split-GFP to stabilise the interaction once it occurs (Cabantous et al., 2013).

While, in this study, the MitoID protein samples were resolved by Western blot solely to verify the accuracy of the mass spectrometry output, this method can also be used as a validation method in and of itself. Even though validating the presence of proteins in the tested MitoID samples will not definitively show whether the interactions are physical or whether the proteins are simply proximal, the context can indicate the likelihood of this being an interaction of interest – if a bait and a prey are consistently observed, and validated, to be proximal (~10 nm distance) solely when the bait is in its active state, this finding would be considered highly interesting regardless of whether these proteins physically interact.

Interestingly, we have occasionally come across discrepancies between the mass spectrometry output and the biochemical analysis of the same samples. For example, in Figure 3.4A we have shown that the mass spectrometry output indicates that OSBPL9 is almost exclusively present in Rab11A samples while BIG2 is solely present in Rab11B samples. However, Figure 3.4B shows that resolving these same samples by SDS-Page and Western blotting shows a very different interaction pattern; both OSBPL9 and BIG2 appear to be present approximately equally in both Rab11 paralogues. It is likely that this discrepancy reflects a shortcoming of the semi-quantitative mass spectrometry approach, underscoring the necessity of validating the found interactions through other methods. If more quantitative methods are needed, the MitoID approach could be combined with stable isotope labelling techniques such as SILAC (stable isotope labelling by amino acids in cell culture) or TMT (tandem mass tags) (Chahrour et al., 2015).

Taken together, we believe that the MitoID approach is highly valuable. It allows for efficient detection of weaker and transient interactions, which conventional methods such as affinity chromatography and yeast two-hybrid could miss. With the unique benefits of proximity labelling combined with internal larger-scale comparisons, we believe MitoID should be added to the general repertoire of widely used protein-protein interaction examination methods.

Chapter 4: Investigating adaptations of the MitoID method

4.1 Introduction

After performing a MitoID screen on a wide range of small GTPases, we aimed to test several ways to alter, adapt, or even improve this method. Adaptations that were tested include the ability of MitoID to examine differences in interactomes due to post-translational modifications (PTMs) of the bait protein, testing new possible nucleotide-locked mutations, and comparing the use of different generations of the biotin ligase BirA.

4.2 Results

4.2.1 MitoID analysis allows detection of differences in the interactome based on phospho-mutations

As previous chapters have shown, MitoID has proven to be a very effective method for identifying protein interactors. We set out to test whether this approach also allows for the rapid testing of sequence variants, such as mutations other than the nucleotide-locked forms examined above. One prime example of point-mutations leading to functional adaptations are phosphomimetics – point-mutations that mimic either the phosphorylated or unphosphorylated state of a certain protein residue.

Rab GTPases can be phosphorylated by kinases such as the leucine-rich repeat kinase LRRK2, which has recently gained a lot of attention due its role in pathological aspects of Parkinson's disease (Seol et al., 2019). Recently, a study found that, in addition to the well-known LRRK2 substrates Rab8A and Rab10, 12 other Rab GTPases are regulated by LRRK2, including Rab5A upon overexpression (Steger et al., 2017). In order to test whether the MitoID approach is effective in identifying differences in Rab GTPase interactions due to modifications such as phosphorylation, we used phosphomimetics to create mutants of Rab5A, Rab8A, and Rab10, and examined their interactomes.

We substituted the Serine/S or Threonine/T on the identified phosphorylation site for non-phosphorylated amino acids that are negatively charged (Glutamate/E) or unable to be phosphorylated (Alanine/A), which mimics phosphorylation or non-phosphorylation, respectively (Dissmeyer & Schnittger, 2011; Eidenmüller et al., 2000). These sites are S84 for Rab5A, T72 For Rab8A, and T73 for Rab10 (Lis et al., 2018).

After performing triplicate MitoID experiments with these phospho-mutant Rab chimeras, the samples were examined by tandem mass spectrometry and spectral count data was gathered, in an identical manner as the MitoID experiments explained in chapters 2 and 3. Importantly, for these experiments the wildtype, S/T→A and S/T→E versions of the GTP-locked mutants were tested, in order to more efficiently identify specific interactors.

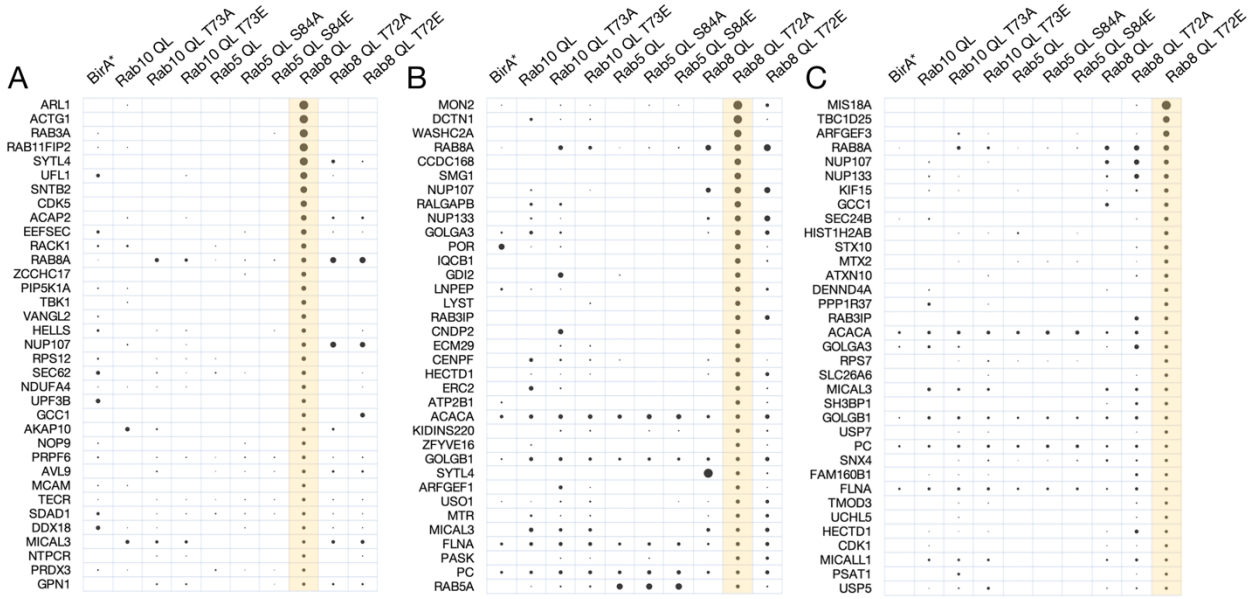

Figure 4.1. MitoID can detect differences in interactomes after phosphomimetic point mutations on Rab8A. (A-C) Bubble plots showing MitoID results of BirA* control (BirA*-HA-MAO) and GTP-locked Rab5A, Rab8A, and Rab10, as indicated. Point mutations were made on S84 (Rab5A), T72 (Rab8A), and T73 (Rab10), substituting them for either Glutamate/E or Alanine/A to mimic phosphorylation or non-phosphorylation, respectively. Bubble plots are aligned for GTP-locked Rab8 (A), Rab8 T72A (B), and Rab8 T72E (C). Circle area corresponds to WD-score. Yellow columns indicate alignment.

Rab8A functions in the formation of actin-containing structures such as lamellipodia, filopodia, and primary cilia, and is known to play a role in membrane recycling (Peränen, 2011). It is therefore unsurprising that several Rab8A top hits include proteins involved in actin regulation, endosomal trafficking, and cytoskeletal adaptors. A number of proteins stand out for interacting solely with the non-mutated protein and not with either phospho-mutant, such as the known Rab8A interactors SYTL4, Rab11FIP2, and VANGL1/2 (Fig.

4.1A) (Hampson et al., 2013; Hatakeyama et al., 2014; Machesky, 2019). Interestingly, Rab3A is also found to specifically bind to wildtype GTP-locked Rab8A, which could be explained by both Rab8A and Rab3A being known to interact with SYTL4 (Fukuda, 2003). There are also a number of cytoskeletal/trafficking proteins enriched for the phospho-mutants, such as MON2, DCTN1/Dynactin subunit 1, and the WASH complex subunit WASHC2A for the non-phosphorylated (T72A) mutant (Fig. 4.1B) and MIS18A, TBC1D25/OATL1, and ARFGEF3/BIG3 for the phospho-mimicking mutant (T72E) (Fig. 4.1C) (Carter et al., 2016; Tao Liu et al., 2016; Mahajan et al., 2019; Panarella et al., 2016; Spiller et al., 2017; Jing Wang et al., 2018). In addition, the golgin GCC1/GCC88 appears to bind to the wildtype and the phospho-mimicked mutant, but not to the non-phosphorylated mutant, suggesting that GCC88 requires phosphorylation (or the possibility of phosphorylation) to bind.

Since Rab8 and Rab10 stem from a gene duplication and have related functions, it is not surprising that Rab10 is also found to interact with many cytoskeletal and membrane trafficking-related proteins (Peränen, 2011). Proteins that solely bind to non-mutated GTP-locked Rab10 but not the phospho-mutants of GTP-locked Rab10 include CLASP1 and exocyst subunits EXOC5, 6, and 7, which are both involved in the regulation of endomembrane organisation and trafficking (Fig. 4.2A) (Boal & Stephens, 2010; Bouchet et al., 2016; Hong et al., 2018; Wu & Guo, 2015). Conversely, not many proteins stand out for solely binding to the phospho-mutants of GTP-locked Rab10 except for the Rab GDP dissociation inhibitor GDI2 and the actin bundler PLS1 for T73A and COPB2 and MAP4K2 for T73E (H.-C. Chuang et al., 2015; Shisheva et al., 1999; L. Wang et al., 2020; Y. Wang et al., 2017; T. Zhang et al., 2020) (Fig. 4.2B,C). The Arf GEF ARFGEF2/BIG2 is detected in both the non-mutated Rab10 and the non-phosphorylated mutant (T73A), which suggests that BIG2 strongly favours binding when Rab10 is unphosphorylated (Fig. 4.2A,B). This distinction detected by mass spectrometry was confirmed by Western blotting of the samples (Fig. 4.2D). The known Rab10 interactors KIF13A/B are also detected in GTP-locked Rab10 samples (Etoh & Fukuda, 2019) (Fig. 4.2A). Interestingly, although both KIF13 isoforms have been reported to interact with Rab10, they show different binding patterns when phospho-mutations are introduced; while KIF13A is strongly enriched in non-mutated GTP-locked Rab10 compared to the two phospho-mutants, KIF13B appears to interact with all three GTP-locked Rab10 samples indeterminately. Further research is necessary to determine whether this discrepancy indicates slightly separate functions for both isoforms.

Finally, we tested the two phospho-mutants for Rab5A, since it is perhaps the best characterised Rab GTPase with many known effectors, which allows for more in depth examination of the differential interactomes. Several known effectors show equal affinity to all three tested Rab5A forms, showing that substitution of that residue does not affect binding of those effectors. These proteins include VPS8, EEA1,

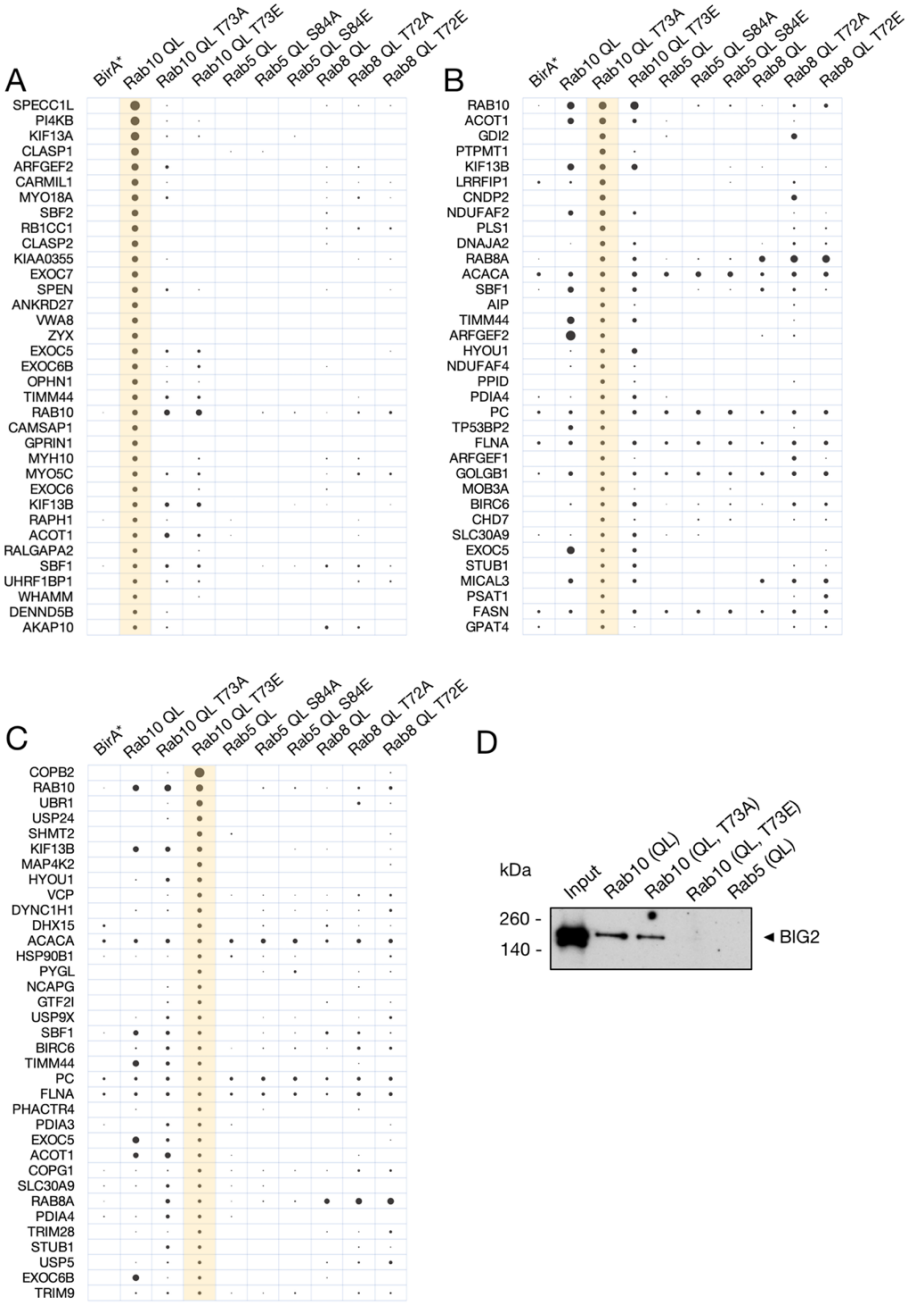

Figure 4.2. MitoID can detect differences in interactomes after phosphomimetic point mutations on and Rab10. (A-C) Bubble plots showing MitoID results of BirA* control (BirA*-HA-MAO) and GTP-locked Rab5A, Rab8A, and Rab10, as indicated. Point mutations were made on S84 (Rab5A), T72 (Rab8A), and T73 (Rab10), substituting them for either Glutamate/E or Alanine/A to mimic phosphorylation or non-phosphorylation, respectively. Bubble plots are aligned for GTP-locked Rab10 (A), Rab10 T73A (B), and Rab10 T73E (C). Circle area corresponds to WD-score. Yellow columns indicate alignment. (D). Western blot of MitoID samples of GTP-locked Rab10 with and without phospho-mutations, as indicated. GTP-locked Rab5A was used as a negative control. Input: wildtype HEK293T lysate. Blot was probed with BIG3 antibodies.

TSC1/2 and two of the core components of the class III PI3-kinase complex; PIK3R4/VPS15 and PIK3C3/VPS34 (Fig. 4.3A-C) (Huang & Manning, 2008; Markgraf et al., 2009; Ohashi et al., 2018; Simonsen et al., 1998). Interestingly, the two class III PI3K complex II-specific subunits (UVRAG and Rubicon) are strongly enriched in wildtype GTP-locked Rab5A samples compared to the two phospho-mutants (Fig. 4.3A) (Itakura et al., 2008; Matsunaga et al., 2009). Notably, no complex I-specific subunits are detected in any of the Rab5A samples, even though Rab5A is known to interact with both complexes (to be discussed in detail in Chapter 6). Other proteins that are preferentially present in non-mutated GTP-locked Rab5 samples include OSBPL9, KIAA1468/RELCH and the CORVET/HOPS subunits (and recently also identified as E3 ubiquitin ligases) VPS11 and VPS18 (Fig. 4.3A) (Xinwei Liu & Ridgway, 2014; Segala et al., 2019; Sobajima et al., 2018). Intriguingly, Rab11A is also present in this list, which can perhaps be explained by OSBPL9 and RELCH also being strong Rab11A interactors (Fig. 3.4C).

The strongest interactor with the non-phosphorylated mutant (S84A) is the centrosomal protein CEP192, a regulator of the microtubule organising centre (MTOC), which is not detected in the other two Rab5 samples (Fig. 4.3B) (Gomez-Ferreria & Sharp, 2008; O'Rourke et al., 2014). Contrarily, the phospho-mimicking Rab5 mutant (S84E) appears to interact specifically with proteins including the centrosomal protein CEP290, and the cytoskeletal regulators FLNC/filamin-C and BCAS3 (Fig. 4.3C) (Jain et al., 2012; Ambuj Kumar et al., 2013; Mao & Nakamura, 2020). Interestingly, APPL1/2 and WDR7 are strongly enriched in non-mutated and S84A samples, but not in S84E, implying that these proteins interact with GTP-locked Rab5A when it is not phosphorylated (Fig. 4.3A-C) (Kawabe et al., 2003; Miaczynska et al., 2004).

The selective interactor response of phospho-mutated GTP-locked Rab5A was further examined by probing Western blots of the MitoID samples against EEA1, PIK3R4, OSBPL9, and HA (internal chimera epitope tag). We were able to confirm that whilst introducing phospho-mutants into Rab5A does not affect its binding to EEA1 and PIK3R4, it does indeed affect its binding to OSBPL9 (Fig. 4.3D). OSBPL9 shows a significantly decreased binding pattern when Rab5A is mutated to mimic either a non-phosphorylated or constitutively phosphorylated state.

Together, this data shows that MitoID is able to detect differential changes in effector binding due to point mutations and residue modifications. Comparing multiple mutations with the wildtype protein allows for closer examination of the effect of the mutants and the nature of the interactions. These results are promising and suggest that MitoID can be effective when testing the effect that point mutations have on the protein's interactome.

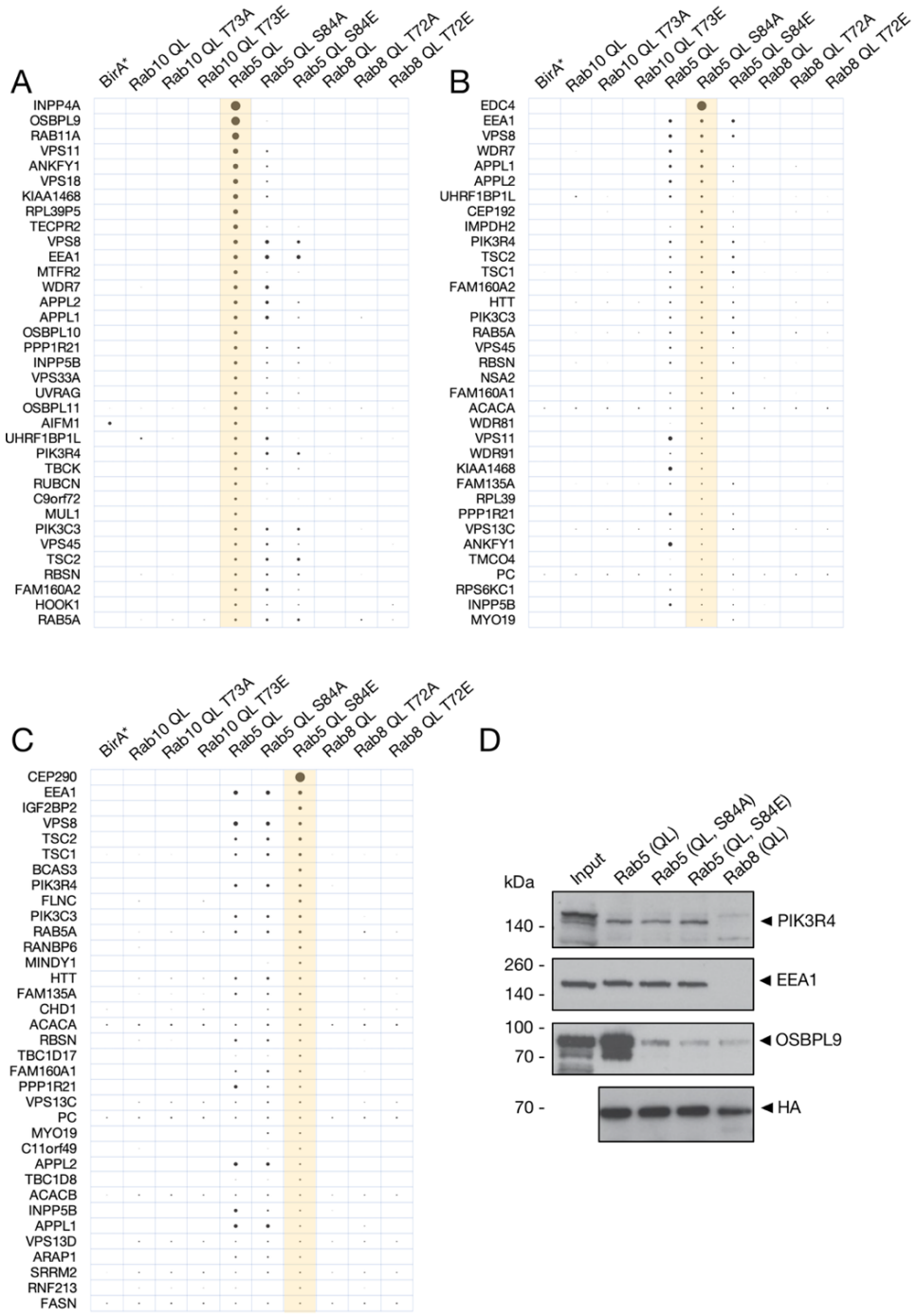

Figure 4.3. MitoID can detect differences in interactomes after phosphomimetic point mutations on Rab5A. (A-C) Bubble plots showing MitoID results of BirA* control (BirA*-HA-MAO) and GTP-locked Rab5A, Rab8A, and Rab10, as indicated. Point mutations were made on S84 (Rab5A), T72 (Rab8A), and T73 (Rab10), substituting them for either Glutamate/E or Alanine/A to mimic phosphorylation or non-phosphorylation, respectively. Bubble plots are aligned for GTP-locked Rab5A (A), Rab5 S84A (B), Rab8 S84E (C). Circle area corresponds to WD-score. Yellow columns indicate alignment. (D). Western blots of MitoID samples from indicated mutants of GTP-locked Rab5. Blots were probed against PIK3R4, EEA1, OSBPL9, and the epitope tag present in the chimera (HA) as an expression level control. Input: wildtype HEK293T lysate. GTP-locked Rab8 sample was used as a negative control.

4.2.2 Investigating the validity of a novel GTP-locked Rab29 mutant

As previously mentioned, the leucine-rich repeat kinase LRRK2 is strongly involved in the occurrence of Parkinson's disease (Kluss et al., 2019). Above, several Rab GTPases that are known substrates for LRRK2 were further investigated by generating phospho-mutants and examining their interactomes by comparative MitoID. In addition to Rab5A, Rab8A and Rab10, eleven other Rab GTPases are known to be regulated by LRRK2, including Rab29 (also known as Rab7L1) (Seol et al., 2019; Steger et al., 2017). Furthermore, Rab29 was found to be one of the 5 genes located on the PARK16 locus, which is also linked to Parkinson's disease and is found mutated in patients (Purlyte et al., 2017). With the aim of gaining more knowledge on the function and interactors of Rab29, the Rab GTPase was included in our list of tested GTPases for the MitoID screen. However, an issue arose when creating a GTP-locked mutant for Rab29/Rab7L1. Throughout our study, the GTP- and GDP-locked mutations we have used for Rab GTPases were Q→L (GTP-locked) and S/T→N (GDP-locked). However, a study has shown that while Rab29 T21N is indeed deficient in GTP binding (and thus an excellent GDP-locked mutant), Rab29 Q67L has a 10-fold increased nucleotide dissociation rate (Beilina et al., 2014). Due to this inability to retain GTP, Beilina and colleagues concluded that both Rab29 mutants function as loss-of-function mutants. In this study, we aimed to create a bona fide GTP-locked mutant to compare against the GDP-locked T21N. The GTPases RalB and Cdc42 are mutated on a different residue to create their GTP-locked forms, namely RalB G23V and Cdc42 G12V. These known mutations were utilised to generate Rab29 A16V, a corresponding mutation which we hoped would lock Rab29 in a GTP-bound conformational state.

After performing MitoID experiments on all three discussed Rab29 mutants and analysing the generated datasets, we found that the main Rab29 interactors are not present (Fig. 4.4A,B). Missing from the GTP-locked samples are for instance the Parkinson's disease associated LRRK2 kinase, the transport protein IFT20, the SNARE BET1L/GS15 and the golgin TGN46/TGOLN2 (Onnis et al., 2015; Purlyte et al., 2017; S. Wang et al., 2014). However, Rab11 is known to interact with Rab29, which is reflected in our results by Rab11B interacting specifically with A16V and to a lesser extend with Q67L, while not being present in the GDP-locked form (Fig. 4.4A) (Onnis et al., 2015). Similarly, C9orf72 is a known Rab29 effector that, even though it is present in both A16V and Q67L, is only detected in very low amounts (Sup. Tables 2 and 3) (Aoki et al., 2017). We are able to detect a number of previously unreported potential Rab29 interactors in the A16V form, including the non-centrosomal microtubule binder CAMSAP3, the V-snare VTIB, and CEP44, a centrosomal protein known to be involved in centriole to centrosome conversion and centrosome cohesion (Fig. 4.4A) (Atorino et al., 2020; Hossain et al., 2020; Nozawa et al., 2016; Jing Wang et al., 2017).

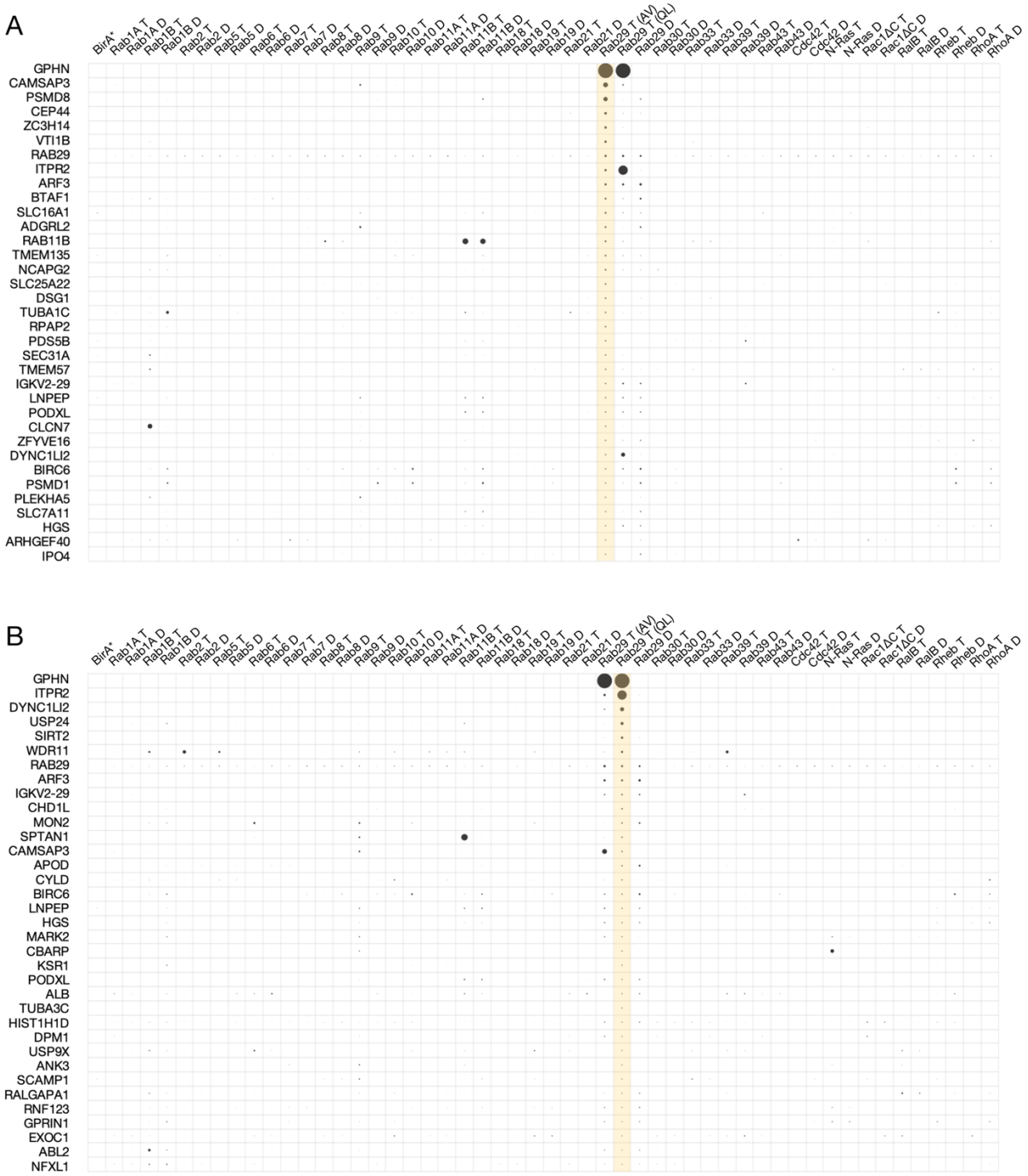

Figure 4.4. MitoID can be used to investigate novel nucleotide-locked mutations of GTPases (A,B) Bubble plots showing MitoID results of BirA* control (BirA*-HA-MAO) and all tested GTP- and GDP-locked GTPases, as indicated. Plots aligned for Rab29 A16V (A) and Rab29 Q67L (B). Circle area corresponds to average WD-score from three biological replicates. Yellow columns indicate alignment. T: GTP-locked form, D: GDP-locked form.

Moreover, several identified hits have specific neuronal functions, such as the scaffolding protein GPHN/Gephyrin in both A16V and Q67L mutants, and Neurobeachin/NBEA and ZNF106 (Fig. 4.4A,B) (Celona et al., 2017; Farzana et al., 2015; Groeneweg et al., 2018). Finally, Arf3 is found to interact with all three forms of Rab29, which could be due to both proteins being active at the *trans*-Golgi (Manolea et al., 2010; S. Wang et al., 2014) (Fig. 4.4A,B).

Taken together, while several potential Rab29 interactors are identified, most known Rab29 interactors are not identified in the MitoID samples of either of the 'GTP-locked' forms, which is reason for concern regarding these specific samples. Further research is necessary to examine the accuracy and validity of the Rab29 mutations. However, these results do show the potential of assessing the validity of other potential nucleotide-locked mutations by comparing interactomes against a wide range of similar baits.

4.2.3 Various biotin ligase generations function slightly differently

Since the original publication describing the use of a mutated, promiscuous biotin ligase to create the BioID approach, numerous studies have reported adaptations of this approach. One common adjustment to BioID is the substitution of the original promiscuous biotin ligase (R118G, resulting in biotin ligase called BirA*) to other, possibly more efficient, promiscuous mutations. The two most commonly used BioID adaptations are called BioID2 and TurboID, both generated to result in more efficient labelling, better localisation, and a decreased need for exogenous biotin (Branon et al., 2018; D. I. Kim et al., 2016). BioID2 makes use of a biotin ligase humanised from *A. aeolicus,* which is substantially smaller than its counterpart from *E. coli.* The mutation R40G within the biotin catalytic domain results in a promiscuity similar to BirA* (D. I. Kim et al., 2016). TurboID, on the other hand, was generated by using directed evolution on the *E. coli* biotin ligase with the promiscuous mutation R118S (Branon et al., 2018). To compare the efficiency of these three BioID generations, we have performed MitoID experiments on three different Rab GTPases (Rab1A, Rab6A and Rab11A) with each of the biotin ligase enzymes, following our original MitoID protocol and chimera lay-out (Rab-BirA-HA-MAO) and using the same biotinylation duration throughout. Results for the Rab1A MitoIDs will be discussed extensively in Chapter 5.

Rab6A plays a role in both *trans*-Golgi regulation and vesicular cytoskeletal transport, and it is thus unsurprising that many top hits for Rab6A include either endosomal or cytoskeletal proteins (Fridmann-Sirkis et al., 2004; Grigoriev et al., 2007; P. L. Lee et al., 2015; Miserey-Lenkei et al., 2017; Short et al., 2002). A few well-characterised Rab6A interactors are present in all three biotin ligase samples, namely the previously identified effectors ERC1/ELKS, bicaudal-D1/BICD1, and GCC2/GCC185, as well as the putative novel interactor MB21D2/C3orf59 (Fig. 4.5A-C) (Fernandes et al., 2009; Grigoriev et al., 2007;

Matanis et al., 2002, 2002). The presence of MB21D2 in all three GTP-locked Rab6A experiments underscores the likely validity of this protein as a Rab6A interactor. Unfortunately, we were unable to validate this interaction by affinity chromatography, possibly due to one of multiple possible explanations given in the discussion of Chapter 3 (data not shown). Further investigations are necessary to assess whether MB21D2 is indeed a true novel Rab6A interactor.

Numerous previously identified Rab6A interactors are observed in the original BioID and BioID2 samples, but not in TurboID samples. These include the dynactin subunit p150-glued (DCNT1), the Rab GEFs DENND5A/B, and myotubularin related protein 1 (MTMR1) which has been highlighted as a potential interactor in comparisons against the full set of tested GTPases (Fig. 4.5A-B, Sup. Fig. 3.1A) (Fukuda et al., 2011; Short et al., 2002). There is no significant overlap found between samples of the original BioID and TurboID, as well as between BioID2 and TurboID, indicating that TurboID appears to biotinylate a different set of interactors.

In order to gain more insight of the efficiency and quality of the three GTP-locked Rab6A samples, the samples were examined separately. Proteins solely identified in the original BioID sample include several cytoskeletal proteins such as kinesin light chain KLC1 and the cytoskeletal regulator RUFY2 (Fig. 4.5A) (DeBoer et al., 2008; Kitagishi & Matsuda, 2013). Specific GTP-locked Rab6A BioID2 hits include centrosomal proteins (CEP290, CEP135, and CEP250), cytoskeletal regulators (ERC2, CLASP2, and MICALL1), and motor proteins (the kinesin KIF15 and the myosin MYO18A) (Fig. 4.5B) (Arancibia et al., 2019; Buschman & Field, 2017; Frémont et al., 2017; Ko et al., 2006; Lawrence et al., 2018; McHugh et al., 2018). Conversely, proteins solely identified in the TurboID sample include proteins involved in DNA repair (BLM, ERCC6), the Rab6-interacting golgin GORAB, and the E3 ubiquitin-protein ligase HERC1 (Fig. 4.5C) (J.-W. Liu et al., 2013; Patel et al., 2017; Schneider et al., 2018; Witkos et al., 2019). Importantly, when aligning the bubble plot for GTP-locked Rab6 with TurboID, it immediately becomes apparent that the top hits include fewer Rab6-specific interactors and more background proteins (Fig. 4.5C).

When assessing GDP-locked Rab6A samples, we find that the only previously reported Rab6A GEF – RAP1GDS1/smgGDS – is identified in the original BioID and BioID2 samples, but not in TurboID (Fig. 4.5D) (Hamel et al., 2011; Shimizu et al., 2017). No other potential GEFs are identified with TurboID samples (Sup. Tables 2 and 3).

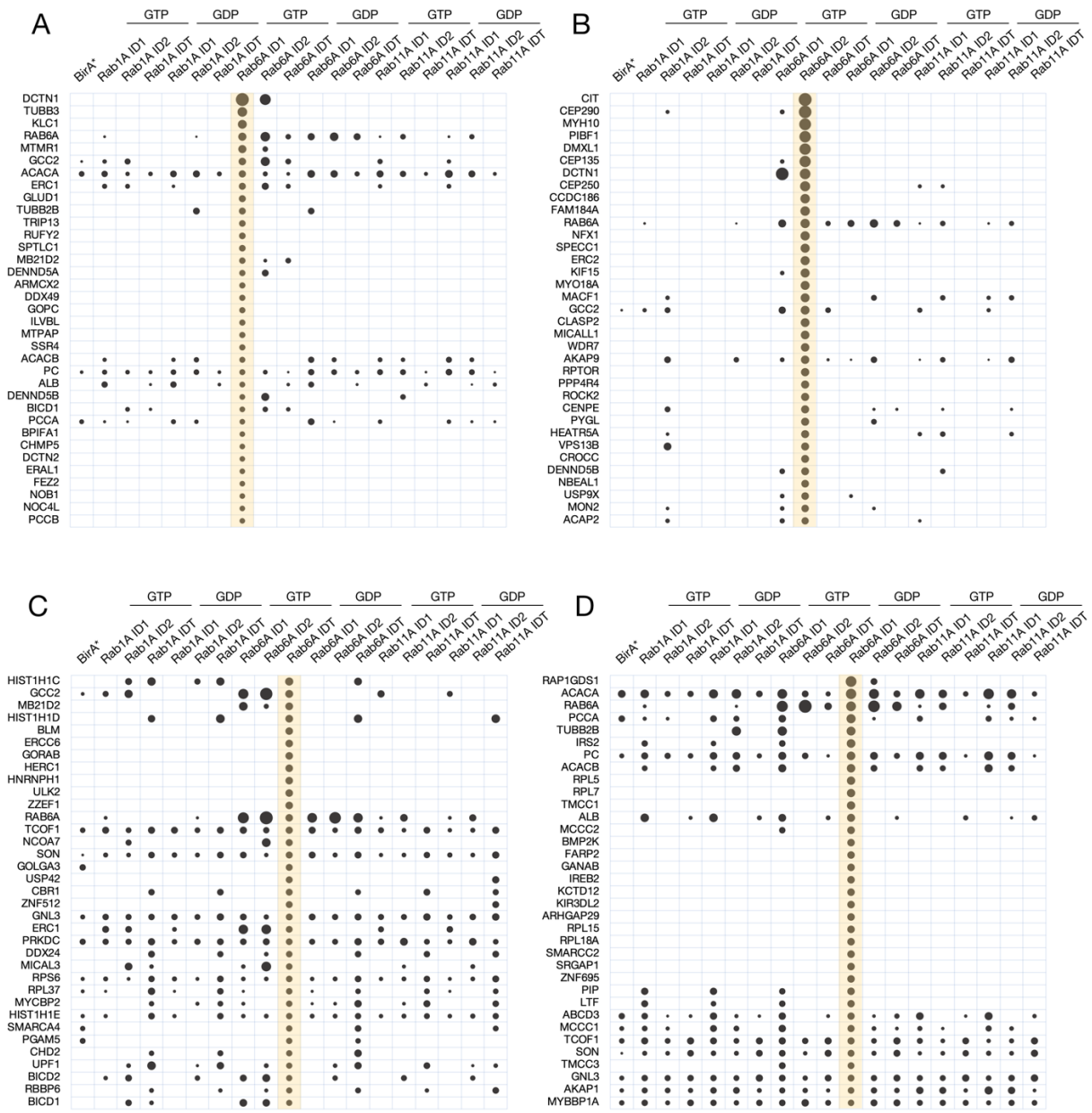

Figure 4.5. Several generations of BioID produce a different sets of potential interactors for Rab6A. (A-D) Bubble plots showing MitoID results of GTP- and GDP-locked Rab1A, Rab6A and Rab11A. Different BirA* generations were cloned into Rab-BirA*-HA-MAO constructs, using ID1 (original BioID), ID2 (BioID2) and IDT (TurboID). Circle area corresponds to WD-score, calculated by comparing single replicates of the baits shown. BirA* is a control showing mitochondrial background levels (BirA*-HA-MAO) and contains the original BioID biotin ligase. Plots are aligned for GTP-locked Rab6A chimeras containing original BioID (A), BioID2 (B), and TurboID (C), and the original GDP-locked Rab6A (D) (yellow columns). Top 35 hits are shown.

Similarly to Rab6A, MitoID experiments were performed on Rab11A using the three aforementioned biotin ligase enzymes. When examining the results, we only detected one previously known Rab11A effector in

all three samples; KIAA1468/RELCH (Sobajima et al., 2018) (Fig. 4.6A-C). The Rab6A GAP RABGAP1/GAPCenA and the Rab5A effector RABEP1/Rabaptin5 are also detected in all three GTP-locked Rab11A samples, indicating they could have a second function as a Rab11A GAP or effector (Cuif et al., 1999; Stenmark et al., 1995). As previously mentioned, the Rab11A hit UHRF1BP1L is also found to interact with other GTP-locked GTPases such as Rab1B, Rab5A, Rab6A, Rab10, and Rab11B (Fig. 3.3A). However, throughout our study the highest WD-scores for UHRF1BP1L arise for Rab11A, and we are able to detect the protein in all three MitoID experiments with different biotin ligases, suggesting it to be a true Rab11A interactor (Fig. 4.6A-C).

The Rab5A effector OSBPL9 is detected in GTP-locked Rab11A samples when using original BioID and BioID2, but not when using TurboID (Fig. 4.6A,B). Similarly to what we observed for Rab6A, there is no overlap found between Rab11 samples when using TurboID compared to the other two biotin ligases. Proteins that are solely detected in TurboID include the senescence regulators UBN1 and UBN2, and several proteins involved in trafficking (GOLPH3L and SYTL4) (Hampson et al., 2013; Ng et al., 2013; Ricketts et al., 2019; Xiong et al., 2018; Y.-L. Zhao et al., 2019). However, the vast majority of proteins identified with Rab11A-TurboID appear to be background proteins, as becomes apparent when examining the full list (Fig. 4.6C).

When comparing the GTP-locked Rab11A interactomes identified through the original BioID and BioID2, we detect numerous proteins that are only present in either one of the samples. Proteins that are solely present in the original BioID sample include the known Rab11 effectors RAB3IP/Rabin8 and Rab3IL1/GRAB, as well as potential Rab11 interactors ALS2, ARFGEF1/BIG1, VPS8, and C9orf72, which are all known to be involved with endo-lysosomal trafficking, as previously discussed in paragraph 3.2.3 (Fig. 4.6A) (Boal & Stephens, 2010; Horgan et al., 2013; Kunita et al., 2007; Markgraf et al., 2009; Topp et al., 2004; Vetter et al., 2015; Webster et al., 2018). Proteins solely present in the BioID2 sample also include numerous possible Rab11 interactors which act on the endosomal pathway, such as LYST, DENND5A/B and Ccd42BPA (Fig. 4.6B) (Sepulveda et al., 2015; Yoshimura et al., 2010; Z. Zhao & Manser, 2015).

Together, this suggests that, in this set-up, BioID and BioID2 are more effective than TurboID in detecting Rab6A- and Rab11A-specific interactors. The output of BioID and BioID2 seem mostly consistent with each other, detecting proteins that largely align with the literature, whereas using TurboID appears to create more background than the other biotin ligases. The use of different generations of biotin ligases for different types of experiments will be examined in the discussion of this chapter.

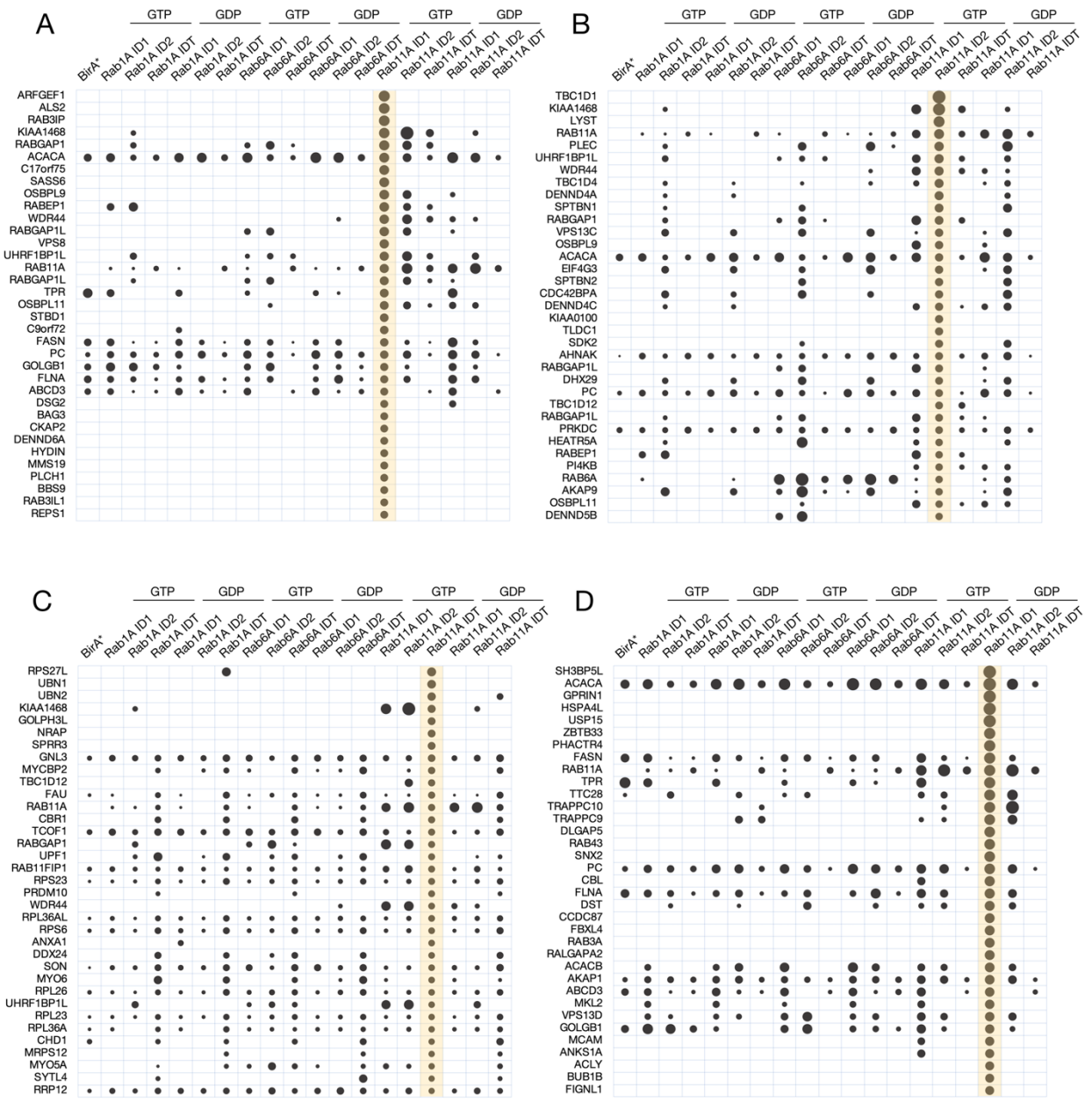

Figure 4.6. Several generations of BioID produce a different sets of potential interactors for Rab11A. (A-D) Bubble plots showing MitoID results of GTP- and GDP-locked Rab1A, Rab6A and Rab11A. Different BirA* generations were cloned into Rab-BirA*-HA-MAO constructs, using ID1 (original BioID), ID2 (BioID2) and IDT (TurboID). Circle area corresponds to WD-score, calculated by comparing single replicates of the baits shown. BirA* is a control showing mitochondrial background levels (BirA*-HA-MAO) and contains the original BioID biotin ligase. Plots are aligned for GTP-locked Rab11A chimeras containing original BioID (A), BioID2 (B), and TurboID (C), and the original GDP-locked Rab11A (D) (yellow columns). Top 35 hits are shown.

4.3 Discussion

Small changes to canonical sequences can have large effects on the functionality of the protein in question. Point-mutations can increase or disrupt binding to interaction partners, cause misfolding, or alter the intracellular localisation of the protein (Krauss et al., 2009; Adesh Kumar & Biswas, 2019; Shanthirabalan et al., 2018). In this study, we have generated specific point-mutants that mimic phosphorylation of certain residues in order to examine whether the MitoID approach can assess differential changes to interactions. Indeed, numerous changes in binding patterns are observed, several of which are confirmed by Western blotting of the samples. Although further research is necessary to validate these differential changes, these results are promising and suggest that MitoID can be effective when testing the effect that point mutations have on a protein's interactome.

A major aspect of this MitoID study is the use of nucleotide-locked mutations to internally compare active and inactive GTPases to search for effectors and regulators. One of the baits we intended on studying, Rab29/Rab7L1, has not been reported with a true GTP-locked mutation – the traditionally used Q→L mutation has been shown to function as a loss-of-function mutation rather being constitutively active (Beilina et al., 2014). After generating a different possible GTP-locked mutation of Rab29, A16V, we examined using the MitoID approach to test the functionality of mutations such as these. Performing biological triplicates of Rab29 chimeras in the three different mutations (T21N, Q67L, and A16V) and compare these against the full data set of small GTPases, we were able to assess the functionality of the A16V mutation as a true GTP-locked mutation. Unfortunately, in this case, most known Rab29 interactors are not identified in the MitoID samples of the A16V mutation. The results of Rab29 A16V resemble those of Rab29 Q67L, which does not appear to function as a true constitutively active Rab29. While this is a reason for concern regarding these specific samples, these results do show the potential of assessing the validity of other potential nucleotide-locked mutations by comparing interactomes against a wide range of similar baits.

Finally, we performed MitoID experiments using three different generations of BirA biotin ligases with the aim of comparing their functionality and efficiency. With BioID, BioID2 and TurboID being the most used biotin ligases at the time of our study, we compared these three ligases on Rab1A, Rab6A and Rab11A (with Rab1A being discussed in Chapter 5). We have been able to show that, while able to detect certain known effectors, the use of TurboID in our MitoID experiments decreased the number of putative effectors identified and drastically increased background levels. On the other hand, using the original BioID and BioID2 led to similar datasets which contain numerous known effectors and several putative novel

interactors. Interestingly though, both biotin ligases appear to biotinylate several proteins that the other does not, suggesting that one biotin ligase is not superior over the other, but rather that they might be suitable for different types of experiments. Interestingly, several proteins are found to bind to multiple Rab GTPases only when using the same biotin ligase; for instance, DENND4A, VPS13C and Cdc42BPA are found in almost all BioID2 samples, highlighting how different biotin ligases function slightly differently (Fig. 4.6B). The steep decrease in interactors identified by TurboID compared to BioID and BioID2 could theoretically be due to a number of reasons; a. the proteins do not interact when TurboID is fused, b. the proteins did not get biotinylated, or c. the proteins interacted and got biotinylated, but were not identified by mass spectrometry. Since the amount of non-specific background proteins drastically increased in TurboID samples, I believe it most likely that the proteins were properly biotinylated but got missed by the mass spectrometry analysis because of the vast amount of background proteins overflowing the machine. Perhaps dialling down the speed of the mass spectrometric flow could allow for more careful analysis of all proteins in the sample.

Since TurboID and BioID2 were generated to be more time efficient and require less biotin addition, those ligases could be used for shorter duration experiments or whenever adding exogenous biotin is challenging. Troubleshooting the specific requirements of these methods will most definitely lead to better results than those presented here, since these experiments were performed with a protocol optimised for the original BioID biotin ligase. Furthermore, it should be noted that the BirA* control in this experiment was performed using the original BioID, not the other two generations of the biotin ligase. Even though distinguishing the background proteins is done mainly based on the comparison with other samples and mutations, adding in an empty mitochondrial control specific for that biotin ligase could aid in this process.

Chapter 5: Maximising the set of known Rab1 effectors

5.1 Introduction

The MitoID study described in the previous chapters has identified many novel putative GTPase interactors, showing that MitoID is an effective tool for examining protein interactomes. In this chapter, we set out to use the MitoID approach to maximise the set of known Rab1 effectors and study this GTPase in more depth.

Rab1 is an essential and highly conserved Rab GTPase, with orthologues present in most eukaryotes, ranging from protozoa to plants and humans (Klöpper et al., 2012). In mammals, Rab1 exists as two paralogues – Rab1A and Rab1B – which are predominantly found at the ER and Golgi membranes (X.-Z. Yang et al., 2016). While Rab1 is mainly known for being a key regulator of ER-to-Golgi membrane trafficking by tethering COPII-coated vesicles to the *cis*-Golgi, it is also reported to be one of the main targets of a *Legionella pneumophila* infection, an mTORC1 activator, and an oncogene (Hardiman & Roy, 2014; Moyer et al., 2001; J. D. Thomas et al., 2014). Furthermore, mammalian Rab1 is found to localise to autophagosomes, specialised vesicles containing cellular contents to be degraded by autophagy (Zoppino et al., 2010).

Even though many studies have investigated the role of the yeast orthologue of Rab1, Ypt1, in autophagy, a thorough understanding of the role of mammalian Rab1 in the initiation and regulation of autophagy is lacking. Relatively recent reports show contradicting results regarding the general effect Rab1A and Rab1B have on autophagy. One study reports that not only do GTP-locked and wildtype Rab1B co-localise with LC3, their expression levels affect the amount of autophagosomes in the cell; overexpression of GTP-locked or wildtype Rab1B leads to an increase in autophagosomes and LC3-II levels, whereas depleting Rab1B with RNAi leads to a decrease in autophagosomes and LC3-II levels (Zoppino et al., 2010). However, Winslow and colleagues found the opposite to be true, observing an increase of LC3-II after Rab1B depletion (Winslow et al., 2010). Furthermore, yet another study reports Rab1A and Rab1B to co-localise to ATG9-positive vesicles, and Rab1B to co-localise with LC3B and p62, another autophagosome marker (Kakuta et al., 2017). Of note, the lack of evidence of Rab1A co-localising with LC3B and other autophagy markers is due to a lack of a good Rab1A-specific antibody, not because of negative results. Interestingly, this study also reports that depletion of Rab1B increases the number and intensity of LC3B and p62 vesicles, which contradicts Zoppino and colleagues, while they also report that depleting Rab1A

not only decreases LC3B levels but also inhibits the recruitment of ATG9 to autophagosomes, contradicting Winslow and colleagues (Kakuta et al., 2017; Winslow et al., 2010; Zoppino et al., 2010). Comparing these results, it becomes apparent that research into the roles of Rab1A and Rab1B has led to discrepancies and contradictions within the field.

Several other studies show links of mammalian Rab1 to autophagy that have remained undisputed. For instance, Webster and colleagues observed that GTP-bound Rab1A interacts with C9orf72, which functions as a link between Rab1A and the ULK1 complex and aids in the recruitment of the ULK1 complex to the phagophore (Webster et al., 2016, 2018). Furthermore, Mochizuki and colleagues have reported that Rab1B interacts with and regulates the localisation of MTMR6, a myotubularin-related protein known to play a role in autophagy (Mochizuki et al., 2013).

Taken together with the yeast studies showing a link between Ypt1 and autophagy, these reports indicate that Rab1 has an additional, non-secretory function in the pathway leading to autophagy. Even though large gaps in knowledge remain regarding the function of Rab1 in autophagy, identifying novel Rab1 effectors and thus maximising the set of known effectors identified by the MitoID approach, could greatly aid in increasing our understanding of autophagy regulation. This is crucial because mis-regulation of autophagy can result in a range of human pathological conditions (Levine & Kroemer, 2008, 2019). Furthermore, it is not clear how Rab1 is able to distinctively regulate both autophagy and vesicle trafficking; whether this is regulated by specific and defined sets of Rab1 interactors or if certain interactors adjust their functions according to the stress state of the cell. In this study, we aim to find clarity in this intriguing phenomenon.

Unfortunately, investigating Rab1 can be challenging due to the difficulty of performing certain traditional experimental methods such as depletion experiments and generating Rab1 knock-outs. Since Rab1 is essential, knocking out or severely depleting both paralogues would lead to significant cell death. However, Rab1A and Rab1B have 92% sequence similarity and they are partially redundant, which means that the effect of depleting only one of the two paralogues could be masked by the function of the other (Homma et al., 2019; Touchot et al., 1989).

Furthermore, performing *in vitro* affinity chromatography experiments with Rab1 GTPases has proven to be challenging. Difficulties applying *in vitro* methods to Rab1 possibly arise because of the lack of necessary post-translational modifications (PTMs) when expressing Rab1 GTPases in bacteria (personal communication, Munro group). Moreover, certain proteins might not fold correctly when expressed in bacteria, since bacteria do not express the proteins which usually aid in this folding. One example of these

proteins is Mss4, a mammalian protein which has been reported to interact with several Rab GTPases including Rab1A and Rab1B and potentially function as a chaperone (Wixler et al., 2011). Challenges regarding commonly used experimental methods probably account for a number of contradicting results, as previously highlighted, and a relatively low number of published reports for a master regulator of two vital cellular processes.

I aimed to shed light on the roles of Rab1A and Rab1B on autophagy, and investigate how these Rab GTPases are able to distinctively regulate vesicle trafficking and autophagy. In this study, I used the previously mentioned MitoID screen to identify and validate novel Rab1A and Rab1B interactors, hereby maximising the set of known Rab1 effectors and allowing for a thorough investigation into Rab1 function. Using *in vivo* methods such as MitoID, I hope to overcome previous issues regarding protein folding and missing PTMs.

5.2 Results

5.2.1 MitoID analysis identifies known and potential novel Rab1A effectors

Utilising the MitoID screen, we were able to identify approximately 800 and 1200 proteins potentially interacting with Rab1A and Rab1B, respectively. Broadly examining the full list of Rab1A interactions, we observe a clear overlap between the Rab1A and Rab1B interactomes, suggesting a degree of redundancy (Fig. 5.1A). Moreover, the pattern of interactions with Rab1A shows some similarities to those of Rab5A, Rab8A, and Rab10, indicating that the Rab GTPases may function in the same or overlapping processes. Interestingly, aligning the full list for Rab1B reveals a much lesser degree of overlap with Rab5A, Rab8A, Rab10, and most interestingly Rab1A (Fig. 5.1B). This could either point to Rab1B having additional, isoform-specific functions, or to the Rab1B chimera picking up on a distinct set of background proteins, a difference that we will examine later in this section.

5.2.1.1 Rab1A

Looking closer at the triplicate runs of the Rab1A and Rab1B samples, several high-scoring proteins were identified which are known to interact with Rab1 (Fig. 5.2). For GTP-locked Rab1A, this includes the vesicle tether giantin (GOLGB1), the COG-complex component COG4, the inositol phosphatase OCRL,

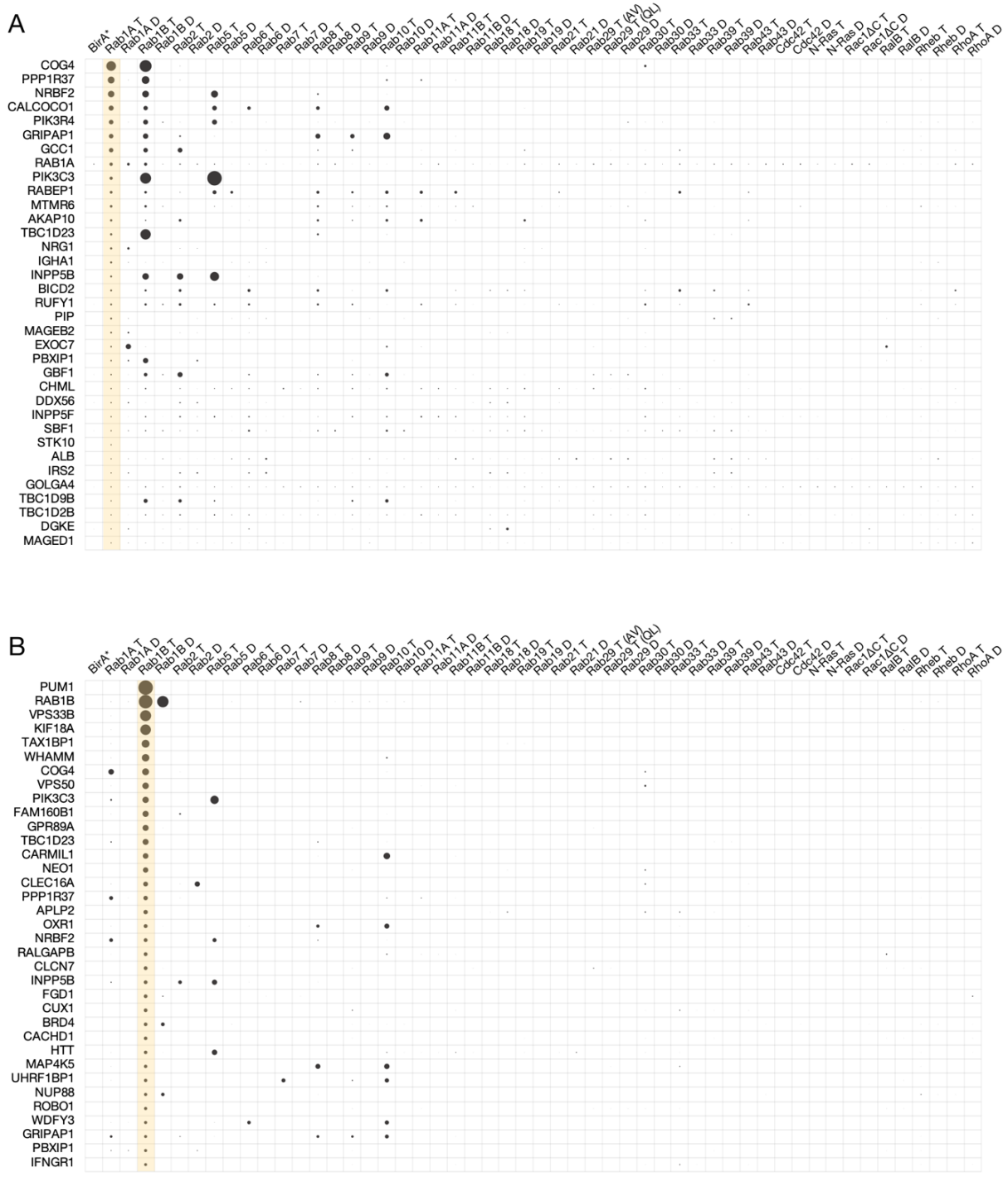

Figure 5.1. Overview of putative interactomes and binding patterns of Rab1A and Rab1B. (A,B) Bubble plots showing MitoID results of BirA* control (BirA*-HA-MAO) and all tested GTP- and GDP-locked GTPases, as indicated. Plots aligned for Rab1A Q70L (A) and Rab1B Q67L (B) (yellow columns). Circle area corresponds to average WD-score from three biological replicates. T: GTP-locked form, D: GDP-locked form. Top 35 hits are shown.

and the Arp2/3 activator WHAMM (Fig. 5.2A) (Guo & Linstedt, 2013; Hayes et al., 2009; Hyvola et al., 2006; Rosing et al., 2007; Russo et al., 2016; Saraste, 2016).

Whereas the Arf GEF GBF1 has previously been reported to be a Rab1B interactor, no such binding experiments were done for Rab1A (Dumaresq-Doiron et al., 2010; Monetta et al., 2007). Akam and colleagues do show that Rab1A plays a role in GBF1 recruitment to the Golgi, hence it is perhaps unsurprising that we have found GBF1 to be enriched in GTP-locked samples of both Rab1A and Rab1B, compared to their inactive forms (Fig. 5.2A,B).

While the presence of these previously known interactors indicates that the method is effective at identifying Rab1A interactors, our primary interest lays in the identification of putative novel interactors. One of the proteins enriched in GTP-locked Rab1A and Rab1B samples is GCC1/GCC88, a golgin known to play a role in retrograde trafficking from endosomes to the Golgi (Fig. 5.2A,B, Fig. 5.3) (Wong et al., 2017). GCC88 has also recently been shown to regulate Golgi ribbon structure, through which it affects mTOR signalling and autophagosome formation, indicating a link to both vesicle trafficking and autophagy (Gosavi et al., 2018). While an interaction between GCC88 and Rab1 has at the time of writing not been previously reported, our data suggests that GCC88 is a novel effector for both Rab1A and Rab1B.

GRIPAP1, also known as GRASP-1, was also found to interact with GTP-locked Rab1A and Rab1B but not with the GDP-locked Rab1 paralogues (Fig. 5.2A,B, Fig. 5.3). GRIP (glutamate receptor interacting protein 1) associated protein is known to function as a neuronal scaffolding protein and RasGEF (Ye et al., 2000, 2007). In neurons, GRIPAP1 has been shown to promote endosome maturation by facilitating the transition between Rab4- and Rab11-positive recycling endosomes (Chiu et al., 2017). To date, an interaction between Rab1 and GRIPAP1 has not yet been reported, though our data suggests GRIPAP1 to be a putative effector for Rab1A and Rab1B – possibly playing a role in endosomes or in autophagosome interaction with the endocytic pathway (Fig. 5.2A,B, Fig. 5.3).

AKAP10 (A-kinase anchoring protein 2/D-AKAP2) is a member of a family of scaffold proteins known as A-kinase anchoring proteins. AKAP10 binds the regulatory subunit of cAMP-dependent protein kinase A (PKA) and targets the kinase to various intracellular locations (A. S. Edwards & Scott, 2000). AKAP10 has previously been shown to have a nucleotide-dependent localisation to Rab4- and Rab11-positive endosomes, in addition to playing a role in the regulation of Rab4- and Rab11-positive recycling endosome morphology and Rab11 vesicle exocytosis (Sorvina et al., 2016). Our data suggests a previously unreported

interaction between AKAP10 and the GTP-locked mutants of Rab1A and Rab1B, suggesting that AKAP10 is a novel Rab1 effector functioning in endosomal trafficking (Fig. 5.2A,B, Fig. 5.3).
Interestingly, both GRIPAP1 and AKAP10 have been linked to the Rab4- and Rab11-positive endosomes, suggesting a link of this endosome subset with the Rab1 paralogues. Indeed, Rab1 has previously been recorded to function in the same cellular process with Rab4 and Rab11 – Rab1 has been shown to regulate transferrin recycling, which involves Rab4- and Rab11-positive endosomes (Mukhopadhyay et al., 2014). Further research is necessary to assess whether GRIPAP1 and AKAP10 are involved in these processes or whether they have additional functions as Rab1 effectors.

Another protein that we have identified with the GTP-locked Rab1 isoforms but not to their GDP-locked states, is TBC1D23 (Fig. 5.2A,B, Fig. 5.3). While TBC1D23 is a member of the TBC (Tre-2/Bub2/Cdc16) family of Rab GAPs, it appears to lack GAP activity when tested on a broad panel of Rab GTPases (Marin-Valencia et al., 2017). Even though it is still possible that the Rab GAP domain of TBC1D23 interacts with Rab GTPases in a non-regulatory capacity, a recent study by Shin and colleagues identified TBC1D23 as a bridging factor between golgins and endocytic vesicles, where the N-terminal Rab GAP domain of TBC1D23 interacts with golgins at the *trans*-Golgi, while the C-terminal domain interacts with the WASH complex on the surface of endosomes (J. J. H. Shin et al., 2017). Thus, while interactions between Rab GTPases and TBC1D23 have not yet been reported, it is not surprising that we have identified several possible interactions – TBC1D23 is enriched in GTP-locked Rab1A, Rab1B, and Rab8A samples, and to a much lesser extent in GTP-locked Rab10 and both GTP- and GDP-locked and Rab39 samples (Fig. 5.1A,B). The strongest enrichment of TBC1D23 is identified in GTP-locked Rab1B samples, where it is found consistently in all three triplicates, while the potential interactor is found in two out of three triplicates for active Rab1A. (Fig. 5.2B).

Rabaptin5 (RABEP1) is a well-characterised Rab5 effector, mostly known for its role in the regulation of early endosome trafficking ((Kälin et al., 2015, 2016)). We have found Rabaptin5 to be enriched specifically in GTP-locked Rab1A and Rab1B (Fig. 5.2A, Fig. 5.3), suggesting it to be a novel putative Rab1 effector.

The protein phosphatase inhibitor PPP1R37, also called leucine-rich repeat-containing protein 68 (LRRC68), is also found to be enriched in GTP-locked Rab1A and Rab1B samples, suggesting it plays a role as a Rab1 effector (Fig. 5.2A,B, Fig. 5.3). Besides the presence of five central leucine-rich repeats and a proline-rich stretch near the C-terminus, the protein remains largely uncharacterised and its function unclear, making it an intriguing potential Rab1 interactor to further investigate.

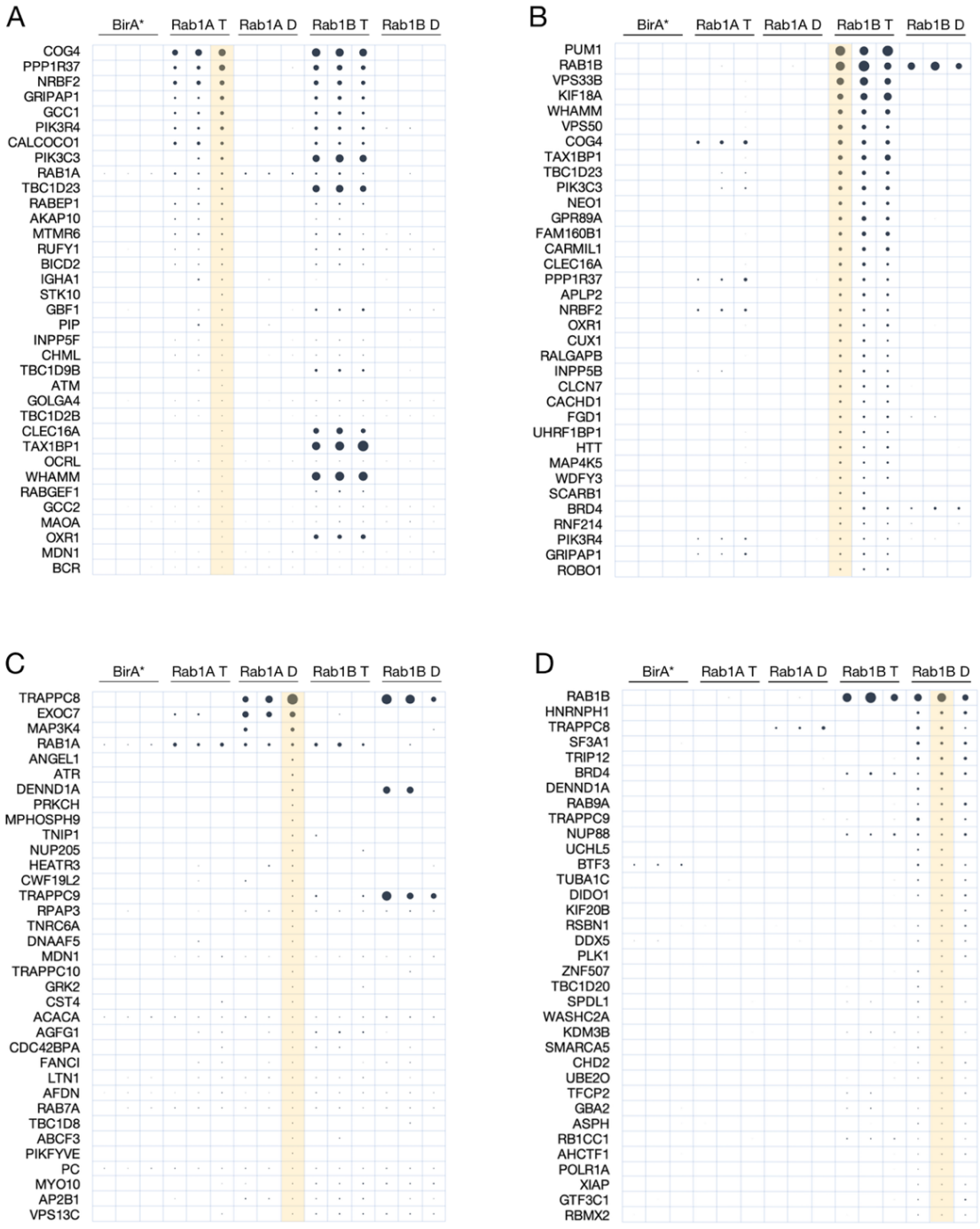

Figure 5.2. Identifying novel Rab1 effectors through MitoID. (A-D) Bubble plots showing MitoID results of GTP- and GDP-locked Rab1A and Rab1B and the BirA* control (BirA*-HA-MAO). Circle area corresponds to WD-score, calculated by comparing triplicates of all previously tested small GTPases. Plots are aligned for one of the triplicates using baits Rab1A Q70L (A), Rab1B Q67L (B), Rab1A S25N (C), and Rab1B S22N (D), as indicated by yellow columns. Top 35 hits are shown.

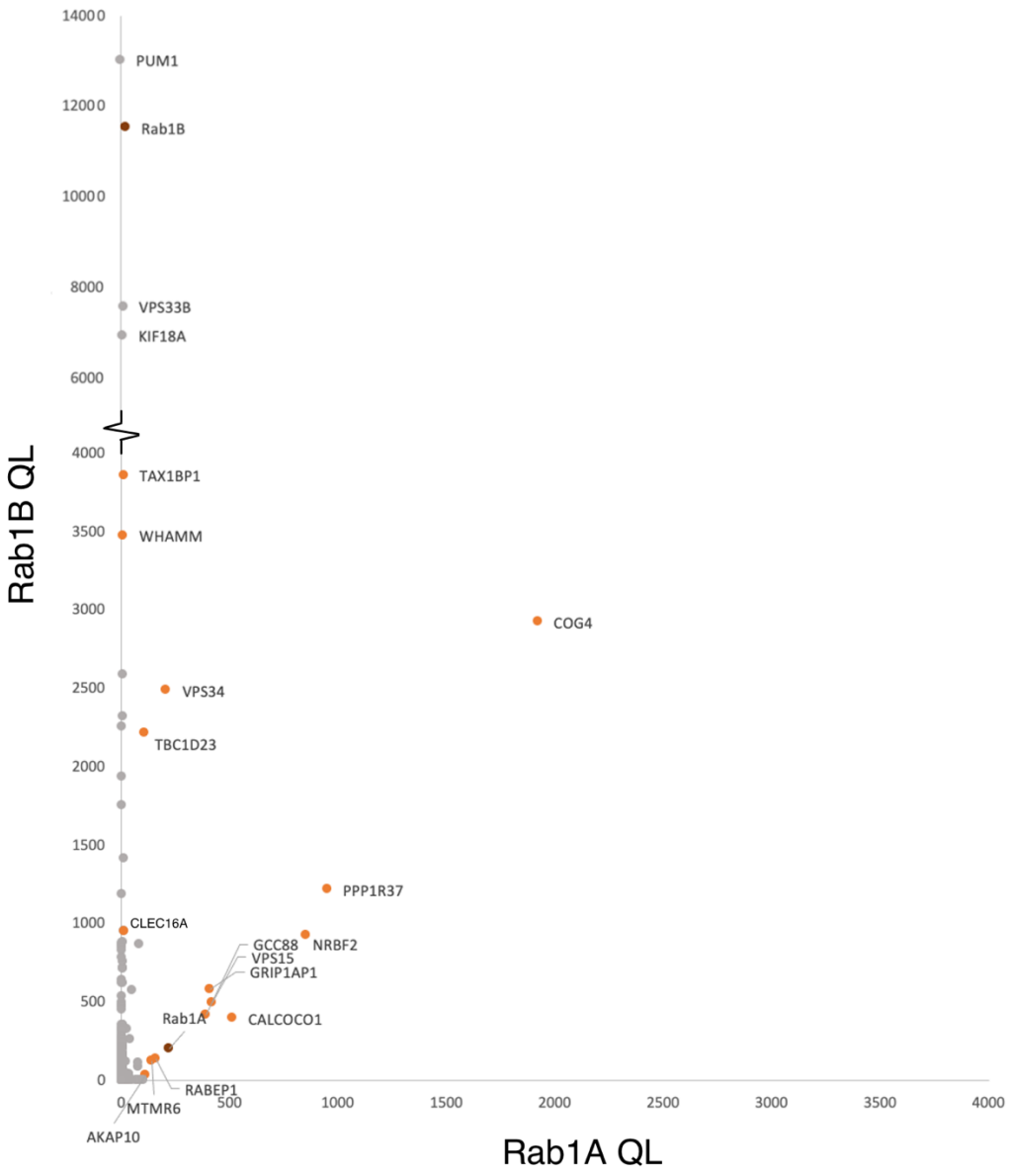

Figure 5.3. Comparing the interactomes of GTP-locked Rab1A and Rab1B. (A) Plot of WD-scores of potential interactors of GTP-locked Rab1A and Rab1B. The WD-scores shown represent means of triplicate biological repeats. Several potential or known interactors are highlighted in orange and labelled, whereas Rab1A/B themselves are labelled in dark brown. The y-axis (GTP-locked Rab1B) shifts in increments after the break, as annotated.

The myotubularin PI3-phosphatase MTMR6 has been found to interact with the GTP-locked mutants of both Rab1A and Rab1B (Fig. 5.2A,B, Fig. 5.3). Previously, MTMR6 has been shown to be regulated by Rab1B in both secretory and autophagic pathways, however, our data suggests that MTMR6 associates with both Rab1A and Rab1B to possibly regulate both vesicle trafficking and autophagy (Mochizuki et al., 2013).

Another novel putative Rab1A and Rab1B effector is CALCOCO1 (calcium-binding and coiled-coil domain-containing protein 1), a protein of unknown function (Fig. 5.2A,B, Fig. 5.3). CALCOCO1 contains 3 relatively large coiled-coil domains and an N-terminal SKICH domain. BLAST alignments show that this domain scheme is also present in the autophagy receptors NDP52 (CALCOCO2) and TAX1BP1 (CALCOCO3), suggesting that CALCOCO1 plays a role in the regulation of autophagy (Y. Yang et al., 2015). Interestingly, TAX1BP1 is specifically enriched in GTP-locked Rab1B samples, suggesting it to be a Rab1B specific effector (Fig. 5.2B, Fig. 5.3).

Interestingly, we also identified multiple subunits of a class III phosphatidylinositol 3-kinase (PI3K) complex that bind to active Rab1A and Rab1B. The PI3K complexes contains 7 subunits, which are able to form two related complexes, both of which share a core of PIK3C3 (VPS34), PIK3R4 (VPS15) and BECN1 (Beclin-1) (Ohashi et al., 2018). ATG14L and NRBF2 form an autophagy-specific complex (complex I) on phagophore membranes along with the core three subunits, whereas the complex existing of the core, UVRAG, and RUBCN, is present on endosomal membranes (complex II) (Ma et al., 2017; Ohashi et al., 2016). We identified the two core subunits PIK3C3 and PIK3R4 and the complex I-specific subunit NRBF2 to be enriched in GTP-locked Rab1A and Rab1B samples compared to their GDP-locked forms (Fig. 5.2A,B, Fig. 5.3). Notably, the three mentioned PI3K subunits have also been consistently identified in GTP-locked Rab5A samples, which is unsurprising since Rab5 is known to be involved in PI3K activity (Fig. 5.1A,B) (H.-W. Shin et al., 2005).

Finally, examining GDP-locked Rab1A, we find the TRAPPIII component TRAPPC8 to be enriched in both GDP-locked Rab1A and Rab1B (Fig. 5.2C,D). TRAPPIII is a known GEF for the yeast homologue of Rab1 (Ypt1) and *Drosophila melanogaster* Rab1, and while this interaction has not yet been reported for mammalian Rab1, it is likely to be a conserved function (Riedel et al., 2017; L. L. Thomas et al., 2018).

Another protein that is enriched in GDP-locked Rab1A, is the exocyst component EXOC7 (Fig. 5.2C). The exocyst is a multi-subunit protein complex that mediates tethering of secretory vesicles to the plasma membrane (Mei & Guo, 2018). A recent study has shown that Rab1 activation is necessary for the recruitment of the exocyst complex to *Legionella*-containing vacuoles (LCVs), in mammalian cells with a *Legionella pneumophila* infection (Arasaki et al., 2018). While the role of Rab1 on LCVs is studied extensively, and it is known that the *Legionella* protein DrrA functions as a Rab1 GEF, the link between GDP-locked Rab1A and the exocyst has not yet been reported. Interestingly, the original study showing the functionality as DrrA as a Rab1 GEF uses both Rab1A and Rab1B tools for different experiments, which suggests that DrrA functions as a GEF for both Rab1 paralogues and thus also that both Rab1 paralogues

are involved with LCVs (Murata et al., 2006). However, our data indicate that only GDP-locked Rab1A interacts with the exocyst, of which the only reported link to date is the LCVs. Since only one component of the exocyst complex is identified, further research is necessary to study whether the Rab1A-exocyst interaction is true, and whether this interaction has a function outside of a *Legionella*-infection background.

5.2.1.2 Rab1B

Although a lot of overlap is found between the interaction partners of GTP-locked Rab1A and Rab1B, there are also stark differences. At first glance, the amount of non-specific background appears to be strongly reduced in the Rab1B samples when compared to Rab1A (Fig. 5.1, Fig. 5.2). Upon closer examination, however, we find that a several of the 'specific' Rab1B hits appear to be DNA/RNA-binding proteins (such as PUM1, CUX1, and BRD4) and proteins thought to be linked to voltage-dependent membrane channels (such as GPR89A, CACHD1, and CLCN7), indicating non-specific background (Fig. 5.2B). These (likely) background proteins possibly appear to be top hits because they are not found in other baits in the MitoID screen, the cause of this discrepancy is unclear – it is unlikely that the Rab1B chimeras are less stable than Rab1A, since many Rab1 interactors bind more strongly to Rab1B than to Rab1A.

Numerous proteins stand out for being possible Rab1B-specific effectors. Interestingly, the MitoID method has picked up many more potential Rab1B-specific effectors than for Rab1A (Fig. 5.2A,B, Fig. 5.3). This could be explained by Rab1B being approximately four times more abundant than Rab1A in cultured HEK293T cells; since endogenous Rab1B is more abundant than endogenous Rab1A, it is likely that its effectors are also more abundant, which increases the likelihood of identifying them (Georg Borner, personal communication). The discrepancies and similarities between the Rab1A and Rab1B interactomes identified through MitoID are visualised in Figure 5.3 (note the different increments in the axes).

While the C-type lectin family 16 member A (CLEC16A) is also present in one of the GTP-locked Rab1A triplicates, it is consistently enriched in GTP-locked Rab1B samples (Fig. 5.2A,B, Fig. 5.3). CLEC16A is a membrane-associated endo-lysosomal protein which regulates mitophagy (Soleimanpour et al., 2014). Previously, CLEC16A has been shown to down-regulate starvation induced autophagy by stimulating mTOR activity (Tam et al., 2017). Interestingly, Tam and colleagues also found CLEC16A to relocate to the Golgi upon starvation. Although the *Drosophila melanogaster* ortholog of CLEC16A has been found to interact with *D. melanogaster* Rab39, a close relative of human Rab2, no interaction with Rab1 has been reported. Our data suggests CLEC16A to be a putative novel Rab1A and Rab1B effector, possibly functioning in autophagy initiation or regulation.

Interestingly, several proteins involved in cytoskeletal regulation are specifically and consistently enriched in GTP-locked Rab1B samples. For example, CARMIL1 (LRRC16A) is known to bind barbed end actin capping proteins, is involved in Rac1 activation, and is necessary for cell migration (M. Edwards et al., 2013; Liang et al., 2009). Moreover, the actin nucleation promoting factor WHAMM (WASP homologue associated protein with actin, membranes and microtubules) is known to bind to (and be regulated by) Rab1 (Russo et al., 2016). In addition, WHAMM is also known to bind to microtubules and intracellular membranes and has recently been shown to function on autophagosomes; initiating autophagosome tubulation by promoting actin polymerisation (Dai et al., 2019; Tianyang Liu et al., 2017). Finally, one of the top hits for Rab1B is the motor protein KIF18A which has recently gained notoriety as a negative outcome marker for several types of cancer (Alfarsi et al., 2019; F.-T. Chen & Zhong, 2019; Luo et al., 2018). In healthy cells, KIF18A is mostly reported to be involved with mitotic spindle assembly (Janssen et al., 2018; F. Yang et al., 2015) (Fig. 5.2B, Fig. 5.3).

Furthermore, the potential Rab1B-specific effectors neogenin (NEO1) and FAM160B1 both show links to neuronal differentiation or pathologies (Fig. 5.2B). While the function of FAM160B1 remains elusive, a cellular deficit of this protein is associated with neurological pathologies such as microcephaly and severe intellectual disability (Mavioğlu et al., 2019). Neogenin, on the other hand, is known to be a transmembrane receptor expressed by differentiating neurons in the central nervous system, and has been shown to bind to the axon guiding molecule RGM (repulsive guidance molecule) (Wilson & Key, 2007). It remains unknown why several potential Rab1B interactors act on neuronal cells and processes, further research is necessary to elucidate whether they are true effectors and what function they fulfil.

Interestingly, we also identify several components of multi-subunit protein complexes involved in endosomal trafficking to be potential Rab1B effectors. Vps50/Syndetin is a component of the EARP (endosome-associated recycling protein) complex, which was found to be specifically enriched in GTP-locked Rab1B samples (Fig. 5.2B). Vps50 is known to localise to Rab4-positive recycling endosomes, promoting the recycling of internalised transferrin receptor (Schindler et al., 2015; Spang, 2016). The CHEVI (class C homologues in endosome-vesicle interaction) complex component VPS33B is also enriched in GTP-locked Rab1B samples (Fig. 5.2B, Fig. 5.3). While the exact function and composition of CHEVI remain elusive, the tethering complex is thought to be involved in recycling and the biogenesis of certain lysosome related organelles (Beek et al., 2019; Rogerson & Gissen, 2016).
Similarly to Rab1A, inactive Rab1B also interacts with components of the TRAPPIII complex – both TRAPPC8 and TRAPPC9 are enriched in GDP-locked Rab1B samples (Fig. 5.2D). While TRAPPIII is a known Rab1 GEF, several novel proteins stand out for being enriched specifically in GDP-locked Rab1B

samples (L. L. Thomas et al., 2018). Several top hits appear to be DNA/RNA-binding proteins (HNRNPH1 and SF3A1) and are thus unlikely to be true GEFs (Fig. 5.2D) (Y. Li et al., 2018; Martelly et al., 2019). The same is true for the E3-ubiquitin ligase TRIP12, which is known to function in DNA damage response and thus unlikely to function as a Rab GEF (Fig. 5.2D) (Xiaoliang Liu et al., 2016).The most likely of these being a true Rab1 GEF, is the known Rab35 GEF DENND1A (Langemeyer et al., 2014) (Fig. 5.2D). Rab35 shows high sequence overlap with Rab1A and Rab1B, especially in the N-terminal and mid domains, and is therefore also called Rab1C (Klinkert & Echard, 2016). Although no interaction has been reported between Rab1A/Rab1B and DENND1A, the high degree of similarity with Rab35 makes it possible that they share certain interactors or regulators, and it is thus conceivable that DENND1A could function as a Rab1 effector or GEF. Interestingly, a study examining DENN domain exchange factors reported no detectable GEF activity of DENND1A on Rab1A or Ra1B (Yoshimura et al., 2010). However, it should be noted that the Rab GTPases used in this study were purified from bacteria, which could cause Rab1 to not be capable of being activated in their assay.

Taken together, we were able to identify several known Rab1 effectors, validating the effectiveness of the method, and identify numerous putative novel Rab1A and Rab1B interactors. Many potential interactors appear to bind to both Rab1A and Rab1B, though a subset of the hits seem to be paralogue-specific. Next, we aim to increase the set of known Rab1 effectors by performing validation experiments on the aforementioned hits.

5.2.1.3 Comparing identified interactomes with different biotin ligase generations

As previously discussed for Rab6A and Rab11A in paragraph 4.2.3, we tested different generations of the BirA* biotin ligase with the aim of identifying different interactors. In order to pursue this, we used the same chimera lay-out and simply exchanged the biotin ligase for that of a different generation, meaning that all these tested chimeras are redirected to the mitochondria and should have similar expression levels. Even though we expect the comparison between the biotin ligases to be similar for Rab1A as we found for Rab6A and Rab11A, it is valuable to investigate this since novel effectors could possibly be identified. Previously, we have found that BioID and BioID2 are more effective than TurboID in detected Rab6A- and Rab11A-specific interactors; the hits detected through BioID and BioID2 show overlap with each other and align with literature, whereas TurboID appears to create more background.

We find that the proteins that are specific for the original BioID and GTP-locked Rab1A include several proteins that are involved with microtubule/cilia; even though the seemingly specific occurrence of TUBA1C/tubulin alpha is most likely an anomaly, the axonemal proteins DNAAF5/dynein assembly factor 5 and DNAH5/dynein heavy chain 5 are potential true interactors (Fig. 5.4A). Moreover, several BioID-

specific hits are known to play in role in vesicle trafficking, including the GTPase-activating protein CHN2/ARHGAP3, OPTN/optineurin, and SNX4, all of which are potential true effectors. Finally, multiple proteins that are enriched only in the original BioID samples are likely background proteins, such as the ER mannosidase MAN1B1, the zinc transporter SLC30A1, and RNA/DNA binding proteins MCM7 and EIF4A2. Interestingly, none of these proteins are picked up by the empty mitochondrial BirA* control, which is probably due to the fact that hits that appear in fewer columns get a higher WD-score and will thus appear higher in the list.

Examining proteins that are enriched only in the BioID2 sample with GTP-locked Rab1A, we identified multiple potential novel Rab1A interactors. These include several proteins related to vesicle sorting and tethering (UHRF1BP1, VPS13B, VPS33B, VPS54, GGA2, and FCHSD2) and potential Rab GAPs TBC1D5 and TBC1D13 (Fig. 5.4B). Furthermore, the previously mentioned CALCOCO1-related TAX1BP1, the scaffolding protein AKAP9, and the F-actin uncapping protein CARMIL1/LRRC16A are also potential Rab1 effector candidates. As expected, several proteins that are specifically enriched in the BioID2 sample are likely non-specific background proteins, such as the mitochondrial proteins ATAD3B and ALDH1L2, the oxidative damage regulator OXR1, and the oxidoreductase DHRS7B.

However, the GTP-locked Rab1A TurboID samples include many more proteins that are likely to be non-specific background, such as the DNA-binding proteins DNASE2B, ZNF512B, and LRRFIP1, nuclear import factor KPNA3, mitochondrial import factor TIMM44, and NADPH reductase CBR1 (Fig. 5.4C). Potential true Rab1 effectors that are enriched solely in the TurboID samples are PAK2, an effector of Cdc42 and Rac1, and AP3B1, a subunit of the AP3 complex which is involved in vesicle cargo sorting.

Numerous proteins are enriched in multiple GTP-locked Rab1A samples. The three main hits that are identified with all three biotin ligase generations are the PI3K component PIK3R4, the myotubularin related protein MTMR6, and the vesicle bridging factor TBC1D23, all of which have been discussed above (Fig. 5.4A-C). Furthermore, the known Rab1A GEF subunit TRAPPC8 is found in all three GDP-locked Rab1A samples, further confirming its validity (Fig. 5.4D).

Although there is hardly any overlap between the interactomes identified by TurboID and the other biotin ligases, there is significant overlap between the original BioID and BioID2. Numerous proteins that are enriched in both GTP-locked Rab1A samples are either previously known Rab1A effectors or are proteins that we have previously discussed in detail. These proteins include COG4, CALCOCO1, INPP5B, NRBF2, PIK3C3, RABEP1, USO1/p115, and GRIPAP1 (Fig. 5.4A,B).

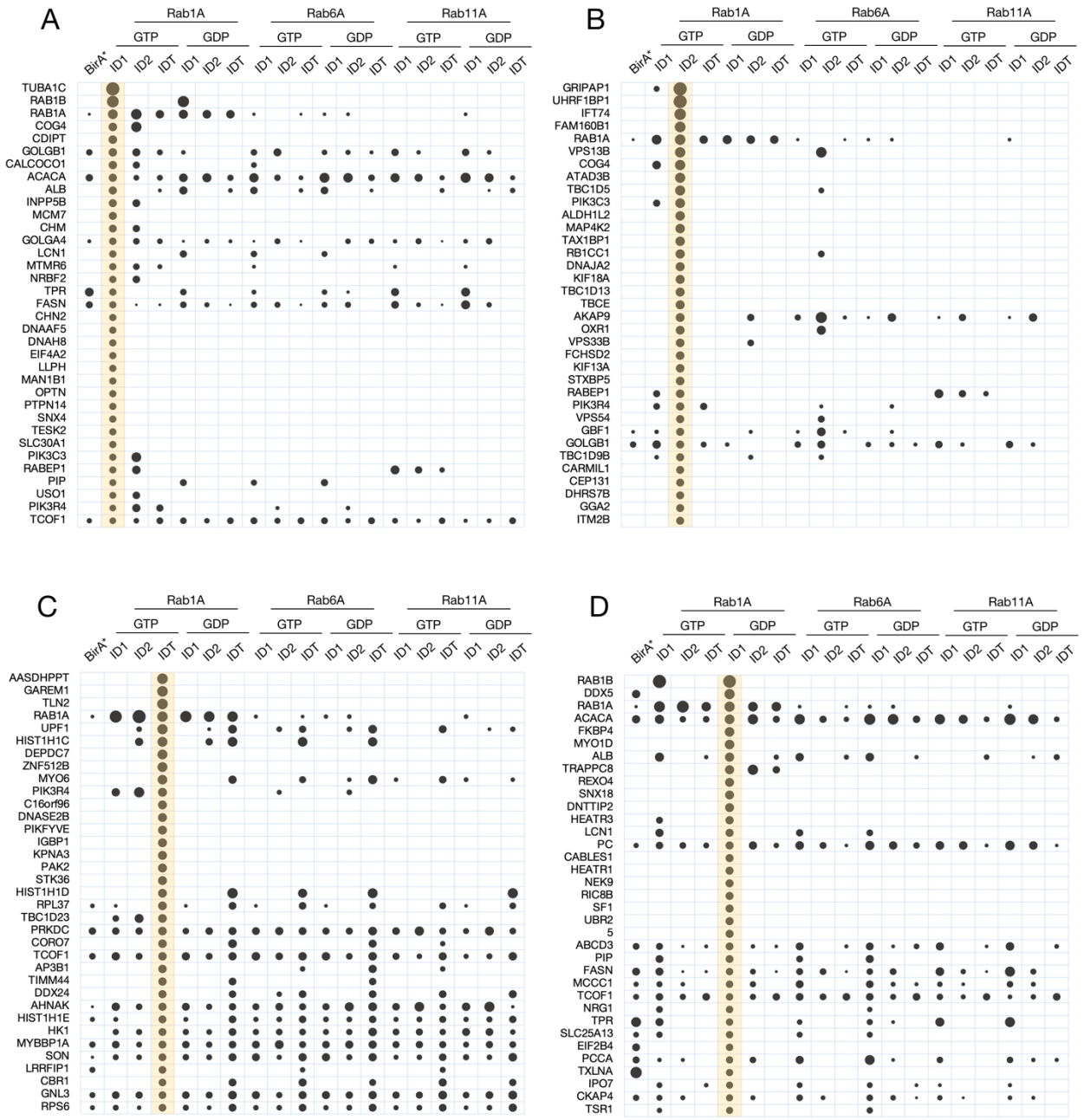

Figure 5.4. Several generations of BioID produce a different sets of potential interactors for Rab1A. (A-D) Bubble plots showing MitoID results of GTP- and GDP-locked Rab1A, Rab6A and Rab11A. Different BirA* generations were cloned into Rab-BirA*-HA-MAO constructs, to give ID1 (BioID), ID2 (BioID2) and IDT (TurboID). Circle area corresponds to S-score, calculated by comparing single replicates of the baits shown. BirA* is a control showing mitochondrial background levels (BirA*-HA-MAO) and contains the original BioID biotin ligase. Plots are aligned for GTP-locked Rab1A chimeras containing BioID (A), BioID2 (B), and TurboID (C), and the BioID-GDP-locked Rab1A (D) (yellow columns). Top 35 hits are shown.

It should be noted that several possible Rab1 effectors that were picked up by BioID2 or TurboID but not the original BioID, were in fact picked up in one or more of the triplicate runs in the MitoID screen using the original BioID. For instance, TAX1BP1 is strongly enriched in all three GTP-locked Rab1B samples and in one of the GTP-locked Rab1A samples, while in our biotin ligase comparison experiment it was only identified when BioID2 was used (Fig. 5.2B, Fig. 5.4B). This discrepancy is likely due to this experiment only consisting of a single run per biotin ligase, which will be less likely to pick up less abundant interactors than duplicate or triplicate runs are. While this would indicate that our biotin ligase comparison experiment is not as conclusive, it does give us a rough idea of the efficiency and specificity of the biotin ligases. Interestingly, other similar proteins were originally identified as possible Rab1B – but not Rab1A – binders, including UHRF1BP1, VPS33B, and CARMIL1, whereas they are enriched in GTP-locked Rab1A samples when BioID2 was used (Fig. 5.2B, Fig. 5.4B). The validity of the identified interactors can be tested by, for instance, Western blotting, to determine whether the proteins are present in GTP-locked Rab1A samples.

Together, these results lead to similar conclusions as previously drawn in paragraph 4.2.3 – using the original BioID and BioID2 lead to a large degree of overlap in the interactors they identify, whereas the use of TurboID causes more suspected background proteins to be enriched. However, as mentioned in the discussion of Chapter 4, the use of BioID2 and TurboID have not been optimised to the same degree as the original BioID in this set-up. Furthermore, it is likely that the different generations of BirA biotin ligases are useful in different types of experiments, as also discussed in Chapter 4. Taken together, the proteins that most intrigued us as potential Rab1A and/or Rab1B interactors are GCC88, CALCOCO1, Rabaptin5, AKAP10, GRIPAP1, PPP1R37, and the VPS34/VPS15/BECN/ATG14L/NRBF2 PI3K-complex.

5.2.2 Maximising the set of validated Rab1 effectors

The main aim of our study is to gain more understanding of the functioning of the Rab1 paralogues and their effectors. In order to study this, it is essential to maximise the set of true, known Rab1 effectors. As discussed in the previous paragraph, the MitoID approach has highlighted numerous potential novel Rab1A and Rab1B effectors. In order to validate these potential interactors we applied both biochemical and immunofluorescence-based techniques to several of the hits.

First, to confirm the presence of the hits in the MitoID samples and thus validate the identification by mass spectrometry, we performed Western blots of the samples and probed with antibodies to the interactors. We were able to identify the interactions of the putative effectors GCC88, CALCOCO1, Rabaptin5, AKAP10, GRIPAP1 and PPP1R37 in GTP-locked Rab1A and Rab1B samples (Fig. 5.5A). Interestingly, GCC88, Rabaptin5, AKAP10, and GRIPAP1 appear to be strongly enriched in Rab1B samples compared to Rab1A, though this is not reflected in the mass spectrometry data (Fig. 5.2A).

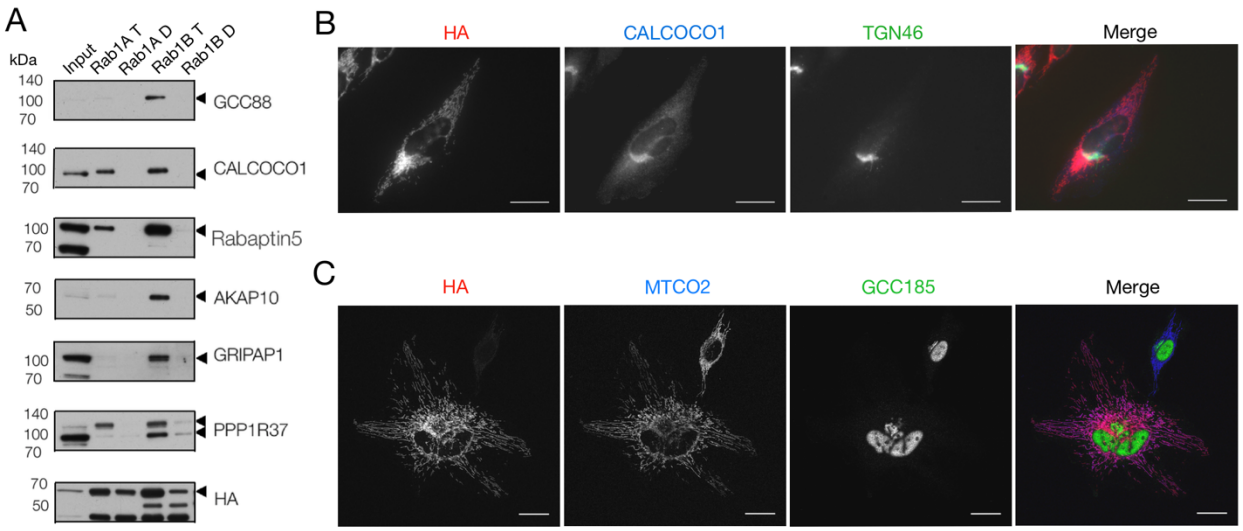

Figure 5.5. Validation of mass spectrometry identification of potential Rab1 interactors. (A) Western blot of MitoID samples of GTP- and GDP-locked Rab1A and Rab1B, probed with antibodies against GCC88, CALCOCO1, Rabaptin5, AKAP10, GRIPAP1, PPP1R37 and HA (loading control), as indicated. Input: wildtype HEK293T lysate. (B) Immunofluorescence micrographs of HeLa cells expressing the GTP-locked Rab1A chimera and stained for HA (internal chimera tag), CALCOCO1, and TGN46 (*trans*-Golgi marker). (C) Immunofluorescence micrographs of HeLa cells expressing GTP-locked Rab2A chimera and stained for HA (internal chimera tag), MTCO2 (mitochondrial marker), and GCC185 (Golgi marker and known Rab2A effector) (of note; this GCC185 antibody shows significant nuclear staining).

We then aimed to validate the potential new Rab1 interactors by visualising whether the hits are effectively recruited to the chimera at the mitochondria. When expressing Rab1A chimeras in HeLa cells and probing against the potential effector CALCOCO1, we found the effector to remain localised at the Golgi (Fig. 5.5B). After testing several potential Rab1 effectors and in all cases observing that the proteins remained at their endogenous location, we decided to test whether a well-established Rab-effector couple could be validated through this method. Interestingly, overexpression of the GTP-locked Rab2A chimera did not result in relocation of its established effector GCC185, which suggests that visualising recruitment might not be an efficient method of validation of interactions with Rabs (Fig. 5.5C) (Hayes et al., 2009).

A possible reason for this is that the interactions between the GTPases and their effectors tend to be transient and don't allow for stable mitochondrial recruitment. In order to try to overcome this, we exogenously over-expressed the potential effectors alongside the Rab chimeras. As shown in Figure 5.6, Rabaptin5-FLAG was recruited by mitochondrially localised GTP-locked Rab1A. Occasionally, partial re-localisation was observed, where Rabaptin5 was found both at the Golgi apparatus and on the mitochondria (Fig. 5.6, middle panel). When co-expressed with GDP-locked Rab1A, Rabaptin5 showed no recruitment to mitochondria, even in highly expressing cells (Fig. 5.6, lower panel).

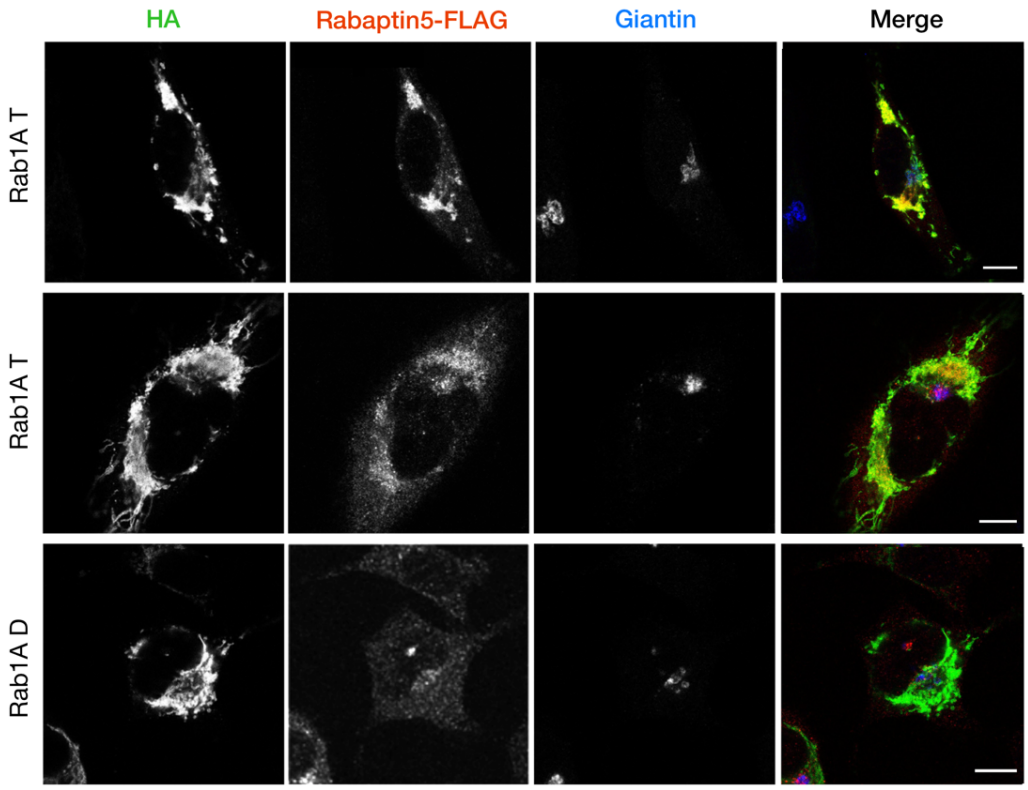

Figure 5.6. Recruitment of Rabaptin5 by mitochondrially localised Rab1A. Confocal micrographs of HeLa cells expressing Rabaptin5-FLAG and Rab1A chimeras, as indicated. Cells are probed against HA (internal chimera tag), FLAG, and the Golgi marker giantin. T: GTP-locked, D: GDP-locked. Scalebars: 10 µm.

CALCOCO1-FLAG, on the other hand, remained dispersed/peri-nuclear when co-expressed with GTP-locked Rab1A but was recruited to the mitochondria by GTP-locked Rab1B. No recruitment was observed by either GDP-locked Rab1 chimeras (Fig. 5.7).

Next, PPP1R37 was N-terminally tagged with the Myc epitope and co-expressed with mitochondrially localised Rab1 chimeras. Clear recruitment is observed for both GTP-locked Rab1 paralogues, whereas GDP-locked Rab1 does not show any mitochondrial recruitment (Fig. 5.8). In cells not expressing GTP-locked Rab1, Myc-PPP1R37 appeared largely dispersed and occasionally punctate. The nature of these puncta will be further examined in Chapter 6.

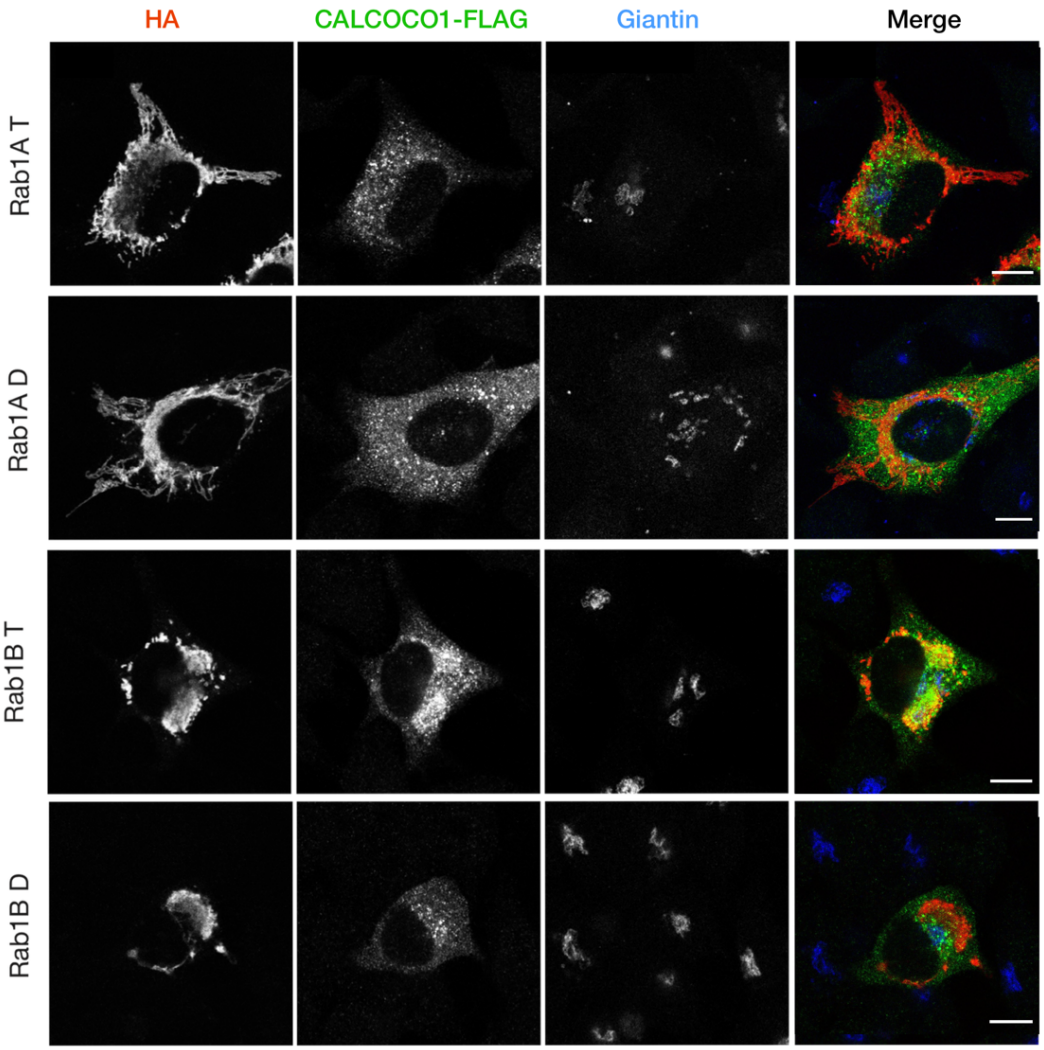

Figure 5.7. Recruitment of CALCOCO1 by mitochondrially localised Rab1. Confocal micrographs of HeLa cells expressing CALCOCO1-FLAG and Rab1 chimeras, as indicated. Cells are probed against HA (internal chimera tag), FLAG, and the Golgi marker giantin. T: GTP-locked, D: GDP-locked. Scalebars: 10 µm.

Another way to validate the interactions is by *in vitro* affinity chromatography experiments. Since Rab1 has proven to be challenging to work with in several *in vitro* experiments, namely when bacterially expressed Rab1 is used, I decided to use a more native expression system. Using Sf9 insect cells and a baculoviral expression system, the GST-fused Rab1 forms were expressed in a background that likely allows for native protein folding and any post-translational modifications. Both N- and C-terminally GST-tagged Rab1 were tested, to maximise the chance of identifying binding interactors. Mixing HEK293T lysate with beads coated in GST-fused Rab1 and then eluting binding proteins off the beads with SDS-based lysis buffer, Rab1-interacting proteins were isolated. Western blots of these samples indicate that CALCOCO1 and CLEC16A specifically interact with GTP-locked Rab1A and Rab1B (Fig. 5.9A).

Interestingly, CALCOCO1 shows additional bands which are smaller than expected, here occurring in GDP-locked GST-Rab1 samples, though these are most likely degradation bands. AKAP10 also shows a clear band for GTP-locked Rab1A-GST at a lower size, and thus more research is needed to test whether this is a true interactor and where this discrepancy arises from.

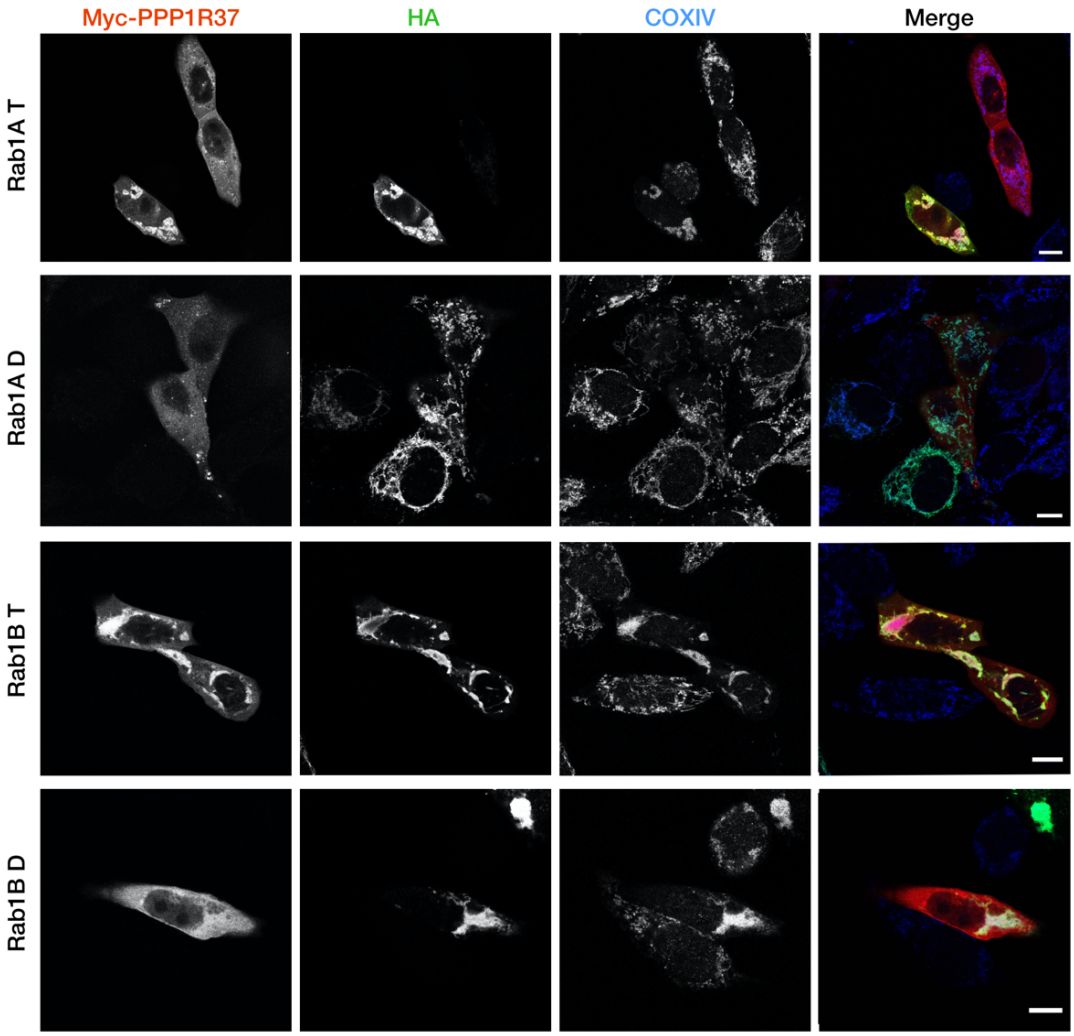

Figure 5.8. Recruitment of PPP1R37 by mitochondrially localised Rab1. Confocal micrographs of HeLa cells expressing Myc-PPP1R37 and Rab1 chimeras, as indicated. Cells are probed against HA (internal chimera tag), Myc, and the mitochondrial marker COXIV. T: GTP-locked, D: GDP-locked. Scalebars: 10 µm.

Although PPP1R37 appears to be a very specific and strong hit for GTP-locked Rab1A and Rab1B, this interaction could not be identified through affinity chromatography with wildtype HEK293T lysate and Sf9-expressed Rab1 (Fig. 5.9A). With the aim to overcome this, affinity chromatography experiments were

performed using Sf9-expressed Rab1 chimeras, now applying lysate from HEK293T cells overexpressing FLAG-PPP1R37. Probing the resulting Western blot with anti-FLAG shows a clear interaction between FLAG-PPP1R37 and GTP-locked Rab1A and Rab1B, tagged with GST on either terminus (Fig. 5.9B).

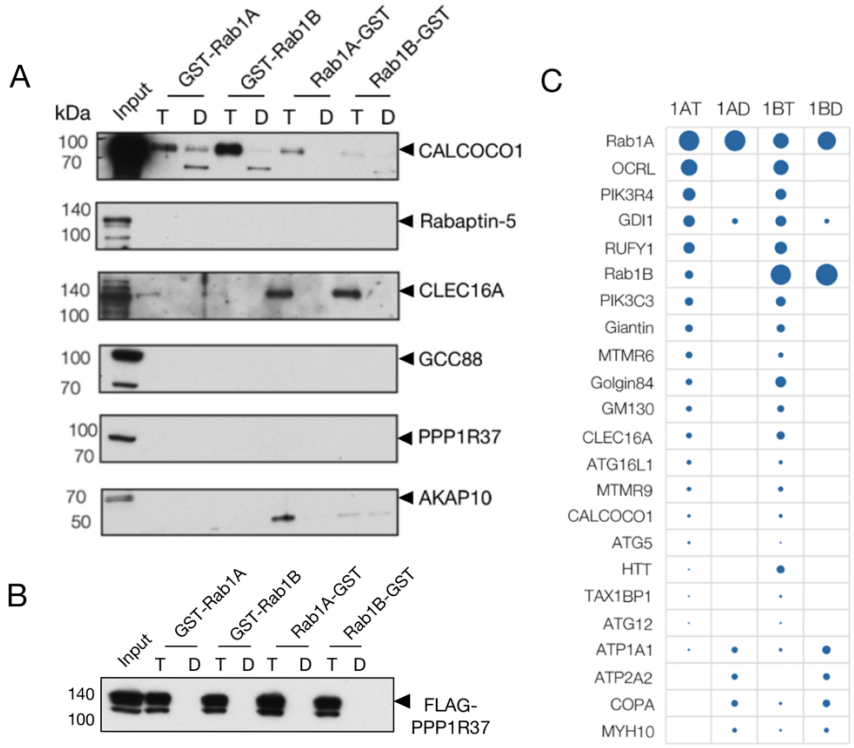

Figure 5.9. In vitro affinity chromatography experiments validate several novel Rab1 effectors. (A) Affinity chromatography of GST-Rab1 and Rab1-GST with wildtype HEK293T lysate. GST-fused Rab1 variants were expressed in Sf9 with the aid of the baculoviral system. Western blots were probed against several antibodies, as indicated. Input: wildtype HEK293T lysate, T: GTP-locked, D: GDP-locked. (B) Affinity chromatography of GST-Rab1 and Rab1-GST with lysate of HEK293T cells overexpressing FLAG-PPP1R37, probed against FLAG. GST-fused Rab1 expressed in Sf9 cells, as in (A). Input: lysate of HEK293T cells expressing FLAG-PPP1R37, T: GTP-locked, D: GDP-locked. (C) Mass spectrometry results of the GST-based affinity chromatography samples used in (A). Several proteins of interest are shown for GTP- (T) and GDP-locked (D) Rab1A and Rab1B. Circle area corresponds to spectral counts.

Examining the samples obtained by affinity chromatography with HEK293T lysate and Rab1-GST by mass spectrometry, validated effectors such as CALCOCO1 and CLEC16A were confirmed (Fig. 5.9C). Furthermore, several previously known Rab1 interactors such as Giantin, MTMR6, OCRL1, and Golgin-84, were also identified. Together, this suggests that the purified Rab1-GST is functional and effective for affinity chromatography experiments.

Further studying the proteins detected by mass spectrometry, several additional interesting hits were identified (Fig. 5.9C). Firstly, the affinity chromatography data suggests that the previously mentioned autophagy receptor TAX1BP1 (also known as CALCOCO2) is a possible effector for both Rab1A and Rab1B, while the MitoID data showed enrichment solely in GTP-locked Rab1B samples (Fig 5.2B, Fig. 5.8C). Moreover, the myotubularin related protein MTMR9 is strongly enriched in GTP-locked Rab1A and Rab1B samples, suggesting an interaction with both Rab1 paralogues. Even though MTMR9 is known to interact with MTMR6, a known Rab1B effector, the interaction between MTMR9 and Rab1A has only very recently been reported (Doubravská et al., 2019; Zou et al., 2009).

With regards to potential new effectors, the three ubiquitin-like proteins Atg5, Atg12, and Atg16L1 were found to be enriched in GTP-locked Rab1A and Rab1B samples (Fig. 5.9C). Interestingly, Atg5, Atg12, and Atg16 are known to form a complex that regulates autophagosome formation by tethering proteins such as Atg8 and Atg3 to the membrane, though any interaction with Rab1 has so far remained unreported (Walczak & Martens, 2013). Furthermore, although the ATPase transport subunits ATP1A1 and ATP2A2 were found to interact specifically with GDP-locked Rab1A and Rab1B, they are unlikely to be true Rab1 regulators. COPA, a subunit of the coatomer complex, is a more likely candidate for truly interacting with inactive Rab1 (Fig. 5.9C). The coatomer is a cytosolic complex that associates with vesicles with the aid of Arf1 and hereby forms the COPI coat (Arakel & Schwappach, 2018). Although an interaction between Rab1 and the coatomer remains unreported, the TRAPPII complex has been reported to interact with both GDP-locked Rab1 and the COPI coat, making this a potential link between the two proteins (Yamasaki et al., 2009). It should be noted, however, that the GST-based affinity chromatography method was unable to identify any TRAPP complex subunits, underscoring the potentiality of a direct link between the coatomer and inactive Rab1 (Fig. 5.9C).

Interestingly, there are some minor inconsistencies when using the different validation methods – some proteins will appear to bind through immunofluorescence but not through affinity chromatography, or the other way around. Most notably, Rabaptin-5 does not appear to show any binding to active Rab1 through affinity chromatography, but shows clear recruitment to active mitochondrial Rab1 when using immunofluorescence (Fig. 5.8, Fig. 5.9A). Conversely, mitochondrial re-localisation experiments suggest that CALCOCO1 is only recruited by mitochondrial active Rab1B and not Rab1A, while the affinity chromatography data shows that CALCOCO1 binds to both GTP-locked paralogues, albeit stronger to Rab1B (Fig. 5.8, Fig. 5.9A).

5.3 Discussion

Using the MitoID approach set out in Chapters 2, and 3, Rab1A and Rab1B were examined – two Rab1 paralogues known to function in ER-to-Golgi and endosomal trafficking, as well as playing an as of yet unknown role in autophagy. By performing triplicate MitoID experiments of GTP- and GDP-locked Rab1A and Rab1B, and comparing them against the full set of tested small GTPases, several previously known Rab1 interactors, as well as numerous potential novel Rab1 effectors, were identified.
As previously discussed, studying Rab1 *in vitro* has been challenging in the past, likely due to a combination of factors including incorrect folding and lack of necessary PTMs of the bacterially expressed protein. It remains unclear which modifications would influence which interactions, although Rab1 has previously been shown to be phosphorylated and can be phosphocholinated or AMPylated during to pathogen invasion (Mukherjee et. al, 2012; Levin et. al, 2016; Du et. al, 2021). Furthermore, the presence or absence of PTMs can greatly affect their ability to bind interaction partners such as GDIs, GEFs, GAPs, or other effectors (Shinde & Maddika, 2018),.

Even though our MitoID set up does not study the true endogenous situation, it allows us to study Rab1 *in vivo* and therefore could highlight novel Rab1 interactors. Moreover, MitoID is a much more sensitive detection method than traditional affinity chromatography – while the background is inherently higher, the *in vivo* proximity labelling approach over a relatively large period of time (48 hours transfection, 18 hours exogenous biotin addition) also inherently allows for the detection of weaker and more transient interactions. It is therefore unsurprising that a relatively large amount of potential new interactors for Rab1A and Rab1B were identified, most notably Rabaptin5, CALCOCO1, GRIPAP1, AKAP10, CLEC16A, PPP1R37, GCC88, and several components of the autophagy-specific PI3-kinase complex (NRBF2, VPS34, and VPS15).

As previously done for Rab6A and Rab11A, the Rab1A interactors identified by the BirA* used in the original BioID method, were compared to those identified with other generations of biotin ligases (BioID2, TurboID). Similar to Rab6A and Rab11A, the Rab1A BioID and BioID2 datasets share a relatively large amount overlap, whereas the TurboID experiment seems to result in more non-specific background. Studying the resulting datasets, I was most interested in proteins that are either present in both BioID and BioID2 or in all three tested biotin ligases. As largely expected, comparing the interactomes did not highlight any additional potential effectors, but rather underscored the proteins I wished to study further, such as CALCOCO1, Rabaptin5, GRIPAP1, and the PI3K complex.

As a first step of validating the potential interactors, the MitoID samples were resolved by Western blot and probed against potential interactors. This confirmed the enrichment of GCC88, CALCOCO1, Rabaptin5, AKAP10, GRIPAP1, and PPP1R37 in GTP-locked Rab1B, while only CALCOCO1, Rabaptin5, and PPP1R37 appeared enriched in GTP-locked Rab1A samples.

Interestingly, the PPP1R37 antibody highlights two bands, one band at approximately 85 kDa and one at approximately 120 kDa. The lower band most likely contains the wildtype, unmodified protein, running slightly higher than the expected molecular weight of 75 kDa. The higher band could represent protein that has been post-translationally modified, and the pattern of binding suggests that Rab1 would preferentially interact with PPP1R37 containing PTMs. It remains unclear which PTM(s) could result in a 35kDa shift in weight, although the considerable size of the shift indicates that numerous modifications occur on the same protein. The platforms iPTMnet proposes 12 phosphorylation sites which are largely located in the C-terminal region of the protein. Although these phosphorylation sites together do not fully add up to the observed shift in weight, considerable protein phosphorylation is known to cause proteins to run slower on SDS-PAGE and thus appear to be (much) bigger than they truly are.
Further research needs to be done to elucidate which modifications PPP1R37 receives, and how these modifications influence its interaction with Rab1.

Next, the interactions between Rab1 and the proteins listed above were validated. For CALCOCO1, Rabaptin5, and PPP1R37, the interactions were validated by ectopically localising active Rab1 to the mitochondria and observe whether the potential interactors are recruited there. However, upon overexpression of AKAP10, GRIPAP1, and CLEC16A, the potential interactors remained dispersed throughout the cell and were not observed to co-localise with any of the Rab1 chimeras (CLEC16A shown in Fig. 6.8A, others not shown). Several immunofluorescence experiments were performed using Rab1A and Rab1B solely tagged with an HA epitope, with the aim of keeping the endogenous localisation of the Rab1 paralogues – perhaps certain potential interactors require their endogenous environment and lipid composition to interact with Rab1. However, no co-localisation was observed of the HA-Rab1 paralogues with the potential interactors, suggesting that the inability to observe the interaction by mitochondrial recruitment is not due its ectopic location (data not shown).

Through affinity chromatography, the interactions between Rab1 and GCC88, CALCOCO1, AKAP10, PPP1R37, and CLEC16A, were confirmed. Although the interaction of Rab1 with GRIPAP1 remained unvalidated, this does not mean that it is not a true interactor. When using affinity chromatography or visualising the recruitment of interactors, only the sufficiently strong and stable interactions will be

detected. The ability to detect weaker and more transient interactions is one of the main advantages of the MitoID technique, however, confirming these types of interactions is a challenge. With the aim of finding a novel method of interaction validation, I attempted to combine the recruitment visualisation with the split-GFP method; fusing the Rab and the potential interactor to GFP fragments, so that when they interact they not only form a functional GFP, but they also remain bound together, solving the problem of visualising transient interactions. As yet, this method needs further improvement and optimisation, hence a combination of affinity chromatography and the visualisation of recruitment was used in this study. Unfortunately, until validation methods are developed that allow for the detection of weaker and transient interactions, it is inevitable that certain interactors might be disregarded. Further research and method development is necessary to overcome this challenge.

Chapter 6: Examining the roles of novel Rab1 effectors on vesicle trafficking and autophagy

6.1 Introduction

In the previous chapter, numerous possible Rab1A and Rab1B binding partners were identified using the MitoID approach, of which several were validated, including CALCOCO1, PPP1R37, and CLEC16A. Since Rab1 is known to play a role in both vesicle trafficking and autophagy, the roles of these effectors on these two distinct processes are further investigated.

The study towards understanding (and manipulating) autophagy is a topic of great interest, particularly since the process of autophagy is involved in metabolic adaptation and can potentially be used as an anti-cancer approach (Kim & Lee, 2014; Kimmelman & White, 2017; Onorati et al., 2008). In order to study the molecular and cellular aspects of autophagy, several different approaches were developed to induce and monitor autophagy in cultured cells.

6.1.1 Inducing autophagy

The most widely used method to induce autophagy in mammalian cultured cells is through starvation. The nutrient-sensing kinase mTOR (mechanistic target of rapamycin) forms a complex called MTORC1 which inhibits autophagy induction in nutrient-rich conditions. Upon glucose starvation, its kinase activity is inhibited which initiates the formation of the phagophore, as schematically shown in Figures 1.3 and 1.4. In mammalian cultured cells, cells are starved by thoroughly removing their growth medium and replacing this with starvation medium (without growth serum) for a few hours (Velazquez & Jackson, 2018).

Other approaches used to induce autophagy also center around the inhibition of mTOR, such as the well-known compound rapamycin. With the kinase named ‘mechanistic target of rapamycin’, it is no surprise that the small compound specifically targets and inhibits the kinase mTOR (Benjamin et al., 2011). Rapamycin has several useful analogues called Rapalogs, which are also commonly used to induce autophagy (Schreiber et al., 2019).

Another group of small compounds which specifically inhibit mTOR are called Torins. While Torin-1 inhibits both mTOR complexes (MTORC1 and MTORC2), Torin-2 specifically inhibits MTORC1 (Wang et al., 2015).

Finally, the disaccharide Trehalose can be used to induce autophagy in an mTOR-independent manner (Sarkar et al., 2007). While the precise mechanism surrounding Trehalose-induced autophagy remains elusive, a recent study has shown that Trehalose rapidly damages and permeabilizes lysosomes which could induce autophagy in an attempt to address lysosomal damage (Rusmini et al., 2019).

6.1.2 Monitoring autophagy

The most widely used method to monitor autophagy in mammalian cultured cells, is through the detection of LC3B-II. LC3B (microtubule-associated protein light chain 3B, a homologue of ATG8) exists as a cytosolic form (LC3B-I) and a lipidated form (LC3B-II), the latter of which is incorporated into the autophagosomal membrane.

Most commonly, LC3B-II levels are measured through Western blot analysis of lysed cells. Since LC3B-II is a key component of the autophagosomal membrane, the intracellular amount of LC3B-II increases as autophagy is induced (Baeken et al., 2020). On the other hand, intra-autophagosomal LC3B-II is degraded by proteases during the fusion of autophagosomes with lysosomes (Mizushima & Yoshimori, 2007). This means that LC3B-II levels are linked to the autophagic flux, and can be hard to interpret. The same issue arises when studying LC3B-II via imaging techniques; the relatively quick turnover can make it hard to properly visualise autophagosomes.

With the aim to halt the autophagic flux and appropriately monitor the induction and effects of autophagy, LC3B-II (and many other autophagic markers) are often studied in the presence of lysosomal inhibitors. Lysosomal inhibitors can either inhibit lysosomal proteases or block autophagosome-lysosome fusion (Mizushima & Yoshimori, 2007). Bafilomycin-A1, the most commonly used lysosomal inhibitor and the one used in this thesis, belongs to the latter category. Other commonly used autophagic markers include p62/SQTM1 and members of the autophagy-related (ATG) protein family.

Besides measuring the accumulation of autophagosomes, as described above, the autophagic flux can be measured to monitor the turnover rate of autophagosome formation and degradation. While this can be accomplished by comparing the amount of lipidated LC3B (or other ATG8-related proteins) with and without lysosomal inhibitors, a perhaps more sophisticated and versatile approach is by using tandem fluorescent tags, as will be further discussed in Chapter 7 (Mizushima & Murphy, 2020). Finally, the

exploration of distinct steps in autophagosomal maturation can be explored by monitoring specific markers such as proteins involved in autophagic induction or lysosomal fusion.

In this thesis, starvation and Trehalose addition are the main approaches used to induce autophagy, and their use will be clearly indicated throughout this chapter. Here, autophagy is almost exclusively monitored after Bafilomycin-A1 addition. The most commonly used autophagy markers used are LC3B-II or p62, and other markers used are clearly indicated where appropriate. All autophagic induction and measuring methods are disclosed in the figure legends.

6.2 Results

6.2.1 Inducing autophagy in cultured mammalian cells

In order to examine the role that Rab1 and its effectors have on the initiation and maturation of autophagy, an efficient and robust protocol is needed to induce autophagy in mammalian cultured cells. The most widely used approach for inducing autophagy is cell starvation. In mammalian cell culture, this involves replacing the incubation medium with media which does not contain any nutrients for several hours (for instance Earle's Balanced Salt Solution, EBSS).

In order to measure a change in autophagic induction and/or flux, the formation and maturation of autophagosomes are studied. As previously mentioned, autophagosomes fuse with lysosomes as they mature, which leads to degradation by the lysosome's acidic components. Thus, as autophagy progresses, the steady state of certain autophagic markers are decreased due to degradation. On the other hand, other commonly used markers such as LC3B-II are upregulated when autophagy is induced (Ravanan et al., 2017). This causes the expression levels of these proteins to be influenced both by the upregulation of expression levels and increased degradation, which complicates the measuring of the autophagic flux rates. To overcome these challenges, the cells can be treated with the lysosomal inhibitor Bafilomycin-A1, which blocks the acidification of the lysosomes and thus inhibits degradation after fusing with autophagosomes (Ravanan et al., 2017). This means that autophagic cells treated with Bafilomycin-A1 should show an increase of the number of autophagosomes, and hereby an increase of LC3B-II levels. The top panel of Figure 6.1A confirms this; showing that HEK293T cells that are starved for 2 or 4 hours show an increase of LC3B-II levels only when Bafilomycin-A1 is added.

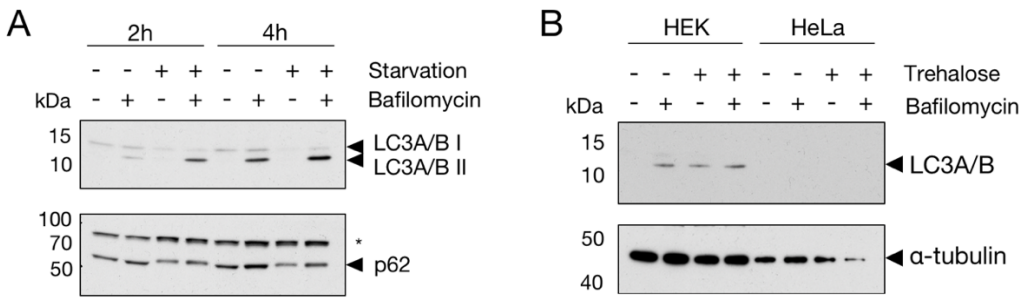

Figure 6.1. Starvation and Trehalose addition both induce autophagy in HEK293T cells. (A) Western blots of lysed HEK293T cells, treated with or without 100 nM Bafilomycin-A1 and grown in either DMEM (fed) or EBSS (starvation medium) for either 2 or 4 hours, all as indicated. Blots were probed for autophagosomal markers LC3A/B (with LC3A/B I being the soluble form, and LC3A/B II being the lipidated, autophagosomal form) and p62. Asterisk indicates non-specific background band (loading control). (B) Western blots of lysed HEK293T and HeLa cells, treated either with or without 100 mM Trehalose and with or without 100 nM Bafilomycin-A1, as indicated. Blots were probed for the autophagosomal marker LC3A/B and α-tubulin (loading control).

Contrarily to LC3B-II, the expression levels of the autophagosome marker p62/SQSTM1 are not solely regulated by the autophagic flux. While certain reports suggest that the expression levels of p62 are strictly regulated by basal autophagic degradation, other reports state that p62 is involved in numerous activities which could affect its expression levels independently of autophagy (Sahani et al., 2014; K. C. Yang et al., 2018). Examining the expression levels of p62 after 2 or 4 hours of starvation, showed that this autophagic marker gives a less straightforward output than LC3B, showing only minor fluctuations in expression levels upon autophagic induction (Figure 6.1A, bottom panel). Taken together, these results underscore the necessity of using multiple assays and approaches to measure autophagic flux. In this study, LC3B-II will be used as the main marker for autophagic induction.

Although starvation is a relatively quick and easy method to induce autophagy, it does not lend itself well to live imaging; in order to adequately starve the cells, all growth medium should be removed and the cells thoroughly washed with EDTA or PBS before the starvation medium is added. Thoroughly washing the cells on a mounted sample is challenging, particularly when aiming to preserve the current location on the slide. Furthermore, this process could be damaging to the microscope if any medium was spilled. While starvation medium could be added before placing the slide under the microscope, this would result in less imaging time of the cells in their fed (i.e. control) state. Therefore, an additional method of autophagic induction was tested; cells were treated with Trehalose, a disaccharide that has been shown to induce autophagy in an mTOR-independent manner (Sarkar et al., 2007). Interestingly, 24 hours of Trehalose induction indeed increased the levels of LC3B-II in HEK293T cells, but not in HeLa cells (Figure 6.1B). Even though the levels of α-tubulin (the loading control) are decreased in HeLa cell samples compared to

those from HEK293T cells, this does not explain the discrepancy of LC3B-II levels between the two cell types.

6.2.2 GTP-locked Rab1 associates with LC3B-positive autophagosomes

Another approach of investigating autophagy induction and maturation, is observing autophagosomes with confocal microscopy. While HEK293T cells are valuable for biochemistry-based approaches requiring large volume of cells, they are not the most useful for microscopy-based techniques since they are quite small and cell structures tend to be more difficult to distinguish. Many mammalian cultured cells have high basal autophagy levels, and several trial experiments with HeLa, CHO and MEFS cells have confirmed this, making them particularly challenging to work with (data not shown). In our hands, visualising autophagosomal structures was the most successful in U2OS cells and hence these were consequently used throughout the study. Vesicular structures labelled by LC3B indicate autophagosomes, as confirmed by the co-labelling of p62 (Fig. 6.2).

Figure 6.2 also shows that GTP-locked HA-tagged Rab1A and Rab1B had considerable overlap with autophagosomes, whereas their GDP-locked counterparts did not. While wildtype and GTP-locked Rab1B have been reported to localise to autophagosomes, the localisation of GDP-locked Rab1B in autophagic cells has remained unreported (Zoppino et al., 2010). However, since GDP-locked Rab1A and Rab1B do not interact with any of the potential autophagy receptors studied in Figures 5.5 and 5.9, it was unsurprising that GDP-locked Rab1 forms are not recruited to autophagosomes (Fig. 6.2).

I next compared autophagosome characteristics and Rab1 localisation in U2OS cells when autophagy was induced with the two distinct approaches mentioned previously. Both Trehalose treatment and cell starvation caused an increase of both size and number of autophagosomes in cells overexpressing GTP-locked Rab1A (Fig. 6.3, left panel). These changes were not observed in cells overexpressing GDP-locked Rab1A (Fig. 6.3, right panel). This is in line with previous reports on the effect of Rab1 overexpression on autophagosomes – overexpression of GTP-locked Rab1 paralogues was shown to result in an increase of size and number of autophagosomes, while overexpression of GDP-locked Rab1 paralogues decreased the autophagosomes in cells (Song et al., 2018; Zoppino et al., 2010).

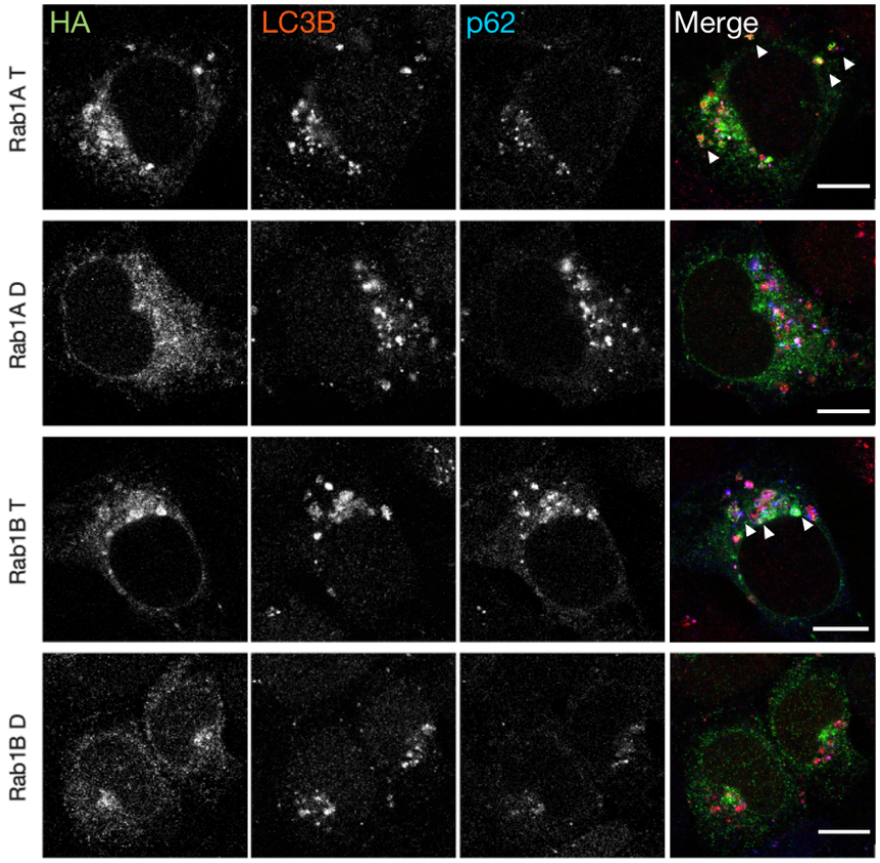

Figure 6.2. Autophagosomes co-localise with GTP-locked Rab1A and Rab1B, but not with their GDP-locked forms. Confocal micrographs of U2OS cells transiently expressing HA-tagged GTP- and GDP-locked Rab1A and Rab1B (as indicated). Cells were treated with 100 mM Trehalose for 24 hours prior to fixing and stained for HA and the autophagosomal markers LC3B and p62. Arrows indicate several puncta of co-localisation with all three antibodies. Scalebars: 10 µm.

With the aim of gaining more understanding of the localisation of Rab1 on autophagosomes, cells were imaged live, expressing fluorescently tagged LC3B and GTP-locked Rab1A. After inducing autophagy by Trehalose treatment for 18 hours, cells expressing eGFP-LC3B and mCherry-Rab1A(QL) were studied on a spinning disc confocal microscope. Figure 6.4 displays a number of time points, showing that LC3B and Rab1A positive puncta are present, that they are mobile, and they occur separately as well as in close proximity of each other and occasionally overlapping (Fig. 6.4).

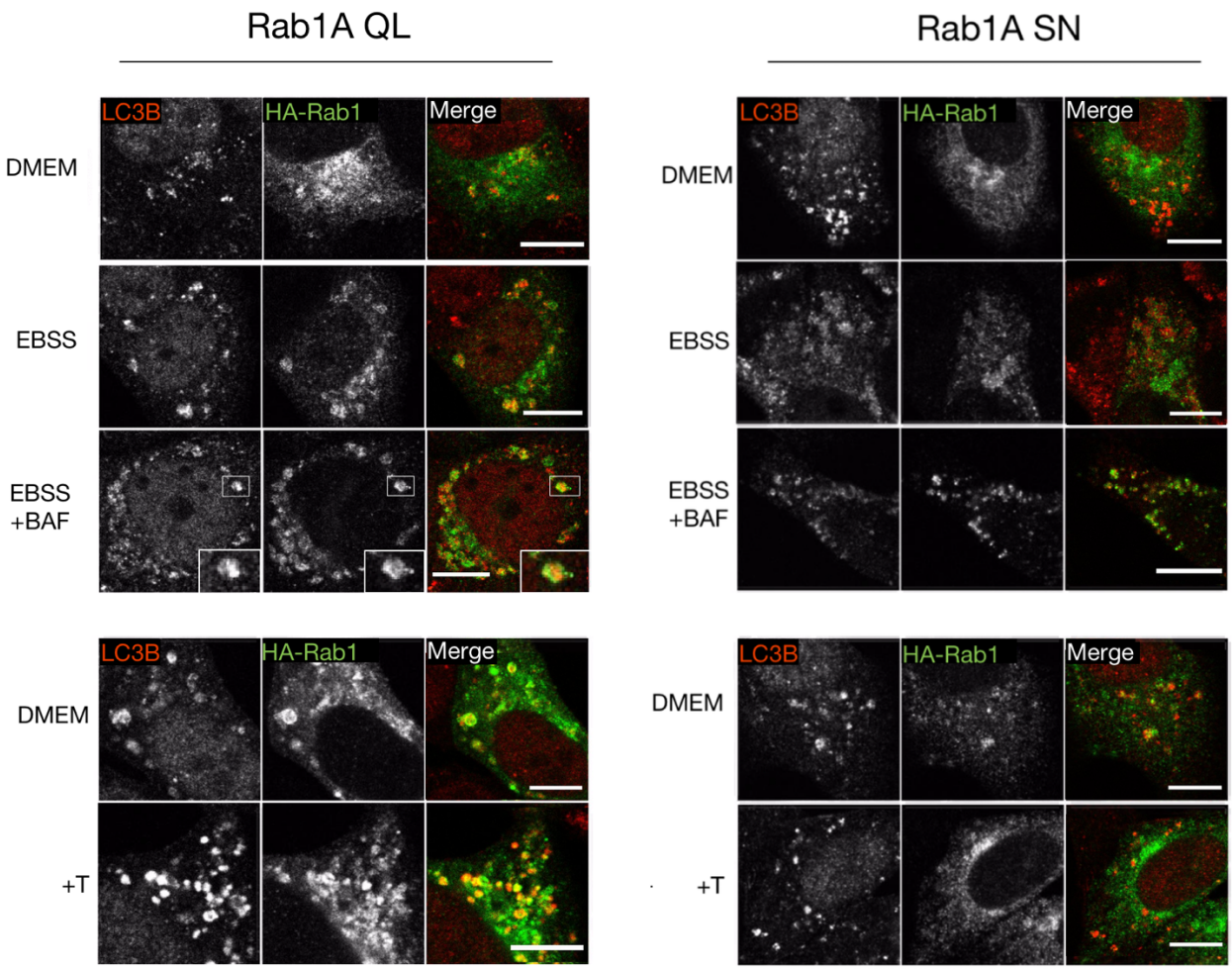

Figure 6.3. Starvation and Trehalose addition both increase size and number of autophagosomes, which co-localise with GTP-locked Rab1A. Confocal micrographs of U2OS cells transiently expressing either GTP- or GDP-locked HA-Rab1A, probed against HA and the autophagosomal marker LC3B. DMEM: untreated cells, EBSS: cells incubating in EBSS for 4 hours, EBSS+BAF: cells incubating in EBSS and treated with 100 nM Bafilomycin-A1 for 4 hours, +T: cells treated with 100 mM Trehalose for 24 hours. All times indicate treatment time before fixation. Scalebars: 10 µm.

The inserts shown in Figure 6.4 highlight four puncta; two Rab1A-positive puncta and two LC3B-positive puncta. The stills indicate that while the four puncta appear to merge into one, the puncta are swiftly transported onwards and actually remain as separate entities, suggesting that the merging is an imaging artifact caused by their increasingly close proximity (Fig. 6.4, inserts). Moreover, closely examining the stills and the time-lapse from which they were taken, it becomes apparent that the Rab1A-positive puncta move in unison with their accompanying LC3B-positive puncta. Whether the Rab1A- and LC3B-positive puncta both coat the same autophagosome, or whether they are simply neighbouring puncta, remains to be clarified. Further research including super-resolution microscopy could gain more insight into this phenomenon, although the observation that they are transported together indicates they might be linked.

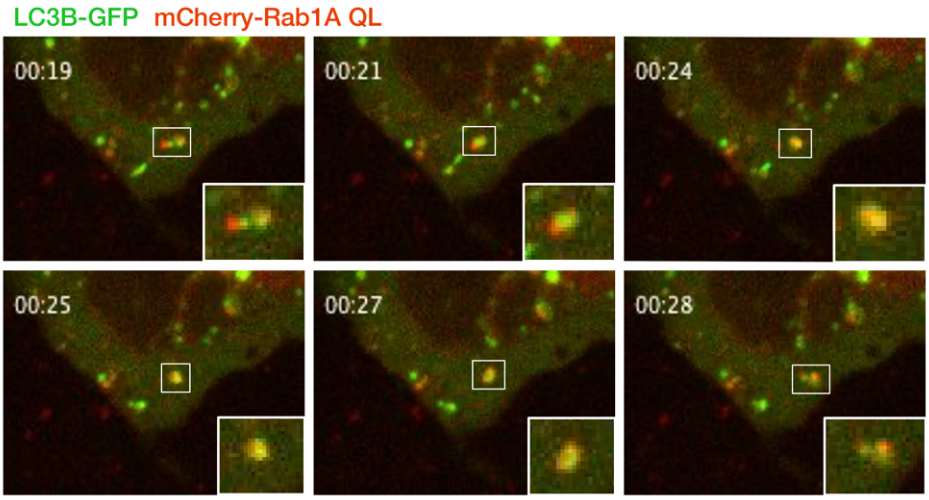

Figure 6.4. Neighbouring GTP-locked Rab1A and LC3B puncta are transported in unison. U2OS cells transiently expressing LC3B and mCherry-Rab1A (QL) were imaged for 30 seconds on a spinning disc confocal microscope.

6.2.3 GTP-Rab1A regulates autophagy by activating PI3-kinase complex I

6.2.3.1 GTP-locked Rab1A recruits and specifically activates PI3K complex I

Having confirmed that active Rab1 associates with autophagosomes, I set out to further investigate what role Rab1 plays in autophagosome formation and/or regulation. Since the functions of small GTPases are performed through their effectors and regulators, studying Rab1 interactors is key in shedding light its function.

Utilising the MitoID approach, numerous potential novel interactors for Rab1 were identified, including multiple subunits of the class III phosphatidylinositol-3-kinase (PI3K) complex (Fig. 5.1, Fig. 5.2A,B). The PI3K complexes phosphorylate phosphatidylinositol (PI) to form phosphatidylinositol-3-phosphate (PI3P) and exist as two related complexes, both of which share a core of PIK3C3 (Vps34), PIK3R4 (Vps15) and BECN1 (Beclin-1), and additionally contain either ATG14L and NRBF2 (complex I) or UVRAG and RUBCN (complex II) (Ohashi et al., 2016, 2018). While complex I is known to be involved in the regulation of autophagy, complex II is found mostly on endosomal membranes and is involved in vesicle trafficking (Ohashi et al., 2018). Recently, a study identified a positive feedback loop where the presence of PI3P aids in the recruitment of Rab5 to endosomal membranes, suggesting that Rab5 itself modifies the local lipid environment to stabilise itself in the membrane (Cezanne et al., 2020).

Two of the core components, PIK3C3 and PIK3R4, as well as the complex I specific protein NRBF2, was found to be present in GTP-locked Rab1A and Rab1B (Fig. 5.1, Fig. 5.2A,B). These components were also identified in GTP-locked Rab5A samples, which is known to be involved in PI3K activity and is thought to mainly interact with complex II (Ohashi et al., 2020; H.-W. Shin et al., 2005) (Fig. 5.1).

Aiming to validate the mass spectrometry data shown in Figure 5.1, and examine if Rab1 binds to one or both subcomplexes, Western blots were performed on the Rab1A and Rab5A MitoID samples. PIK3C3, PIK3R4, BECN1, ATG14L and NRBF2 were identified by Western blot, but not RUBCN or UVRAG, indicating that Rab1 binds specifically to the autophagy-specific PI3K complex (Fig. 6.5A). Moreover, all seven PI3K subunits were found in GTP-locked Rab5A samples, suggesting that active Rab5A interacts with both PI3K complexes (Fig. 6.5A). The GST-based affinity chromatography experiments discussed above further validate the interactions between the Rab1 paralogues and the PI3K complex; mass spectrometry analysis shows the presence of PIK3R4 and PIK3C3 in GTP-locked Rab1A and Rab1B samples (Fig. 5.9C).

While it is suggested that Rab5 aids the recruitment and activation of complex II, its exact mechanism remains unclear (Christoforidis et al., 1999; Murray et al., 2002). The recruitment and activation of complex I, on the other hand, is unknown. Since our data suggest that Rab1 is an interactor of complex I, we aimed to examine the possibility of Rab1 playing a role in PI3K membrane recruitment and activation.

For this study, I collaborated with the group of Roger Williams (MRC LMB, UK), in particular Shirley Tremel and Yohei Ohashi. Tremel, Ohashi, and colleagues have previously designed an assay to study the activation of PI3K on liposomes; PI3K complexes I or II were incubated with giant unilamellar vesicles (GUVs) containing PI and an AlexaFluor647-labelled PX domain which binds specifically to PI3P (Ohashi et al., 2020). By studying the rate of recruitment of the fluorescently labelled PX domain to the GUVs, the generation of PI3P – and thereby the activity of PI3K – can be extrapolated (Fig. 6.5B).

In this study, Rab GTPases were coupled to the GUVs by a covalent bond between the GTPase's C-terminal cysteine and maleimide-fused lipids in the GUV, mimicking the C-terminal geranylgeranylation which anchors the GTPases to membranes *in vivo*. In order to assure correct lipid anchoring solely at the C-terminal cysteine, the remaining cysteines in Rab1A and Rab5A were mutated to serines. The functionality of the mutated Rab GTPases was tested by performing MitoID experiments and studying their interactomes. The identified interactions with GTP- and GDP-locked Rab1A (C26S, C126S) showed identical patterns as compared to their non-mutated forms, which suggests very similar functionality (data not shown).

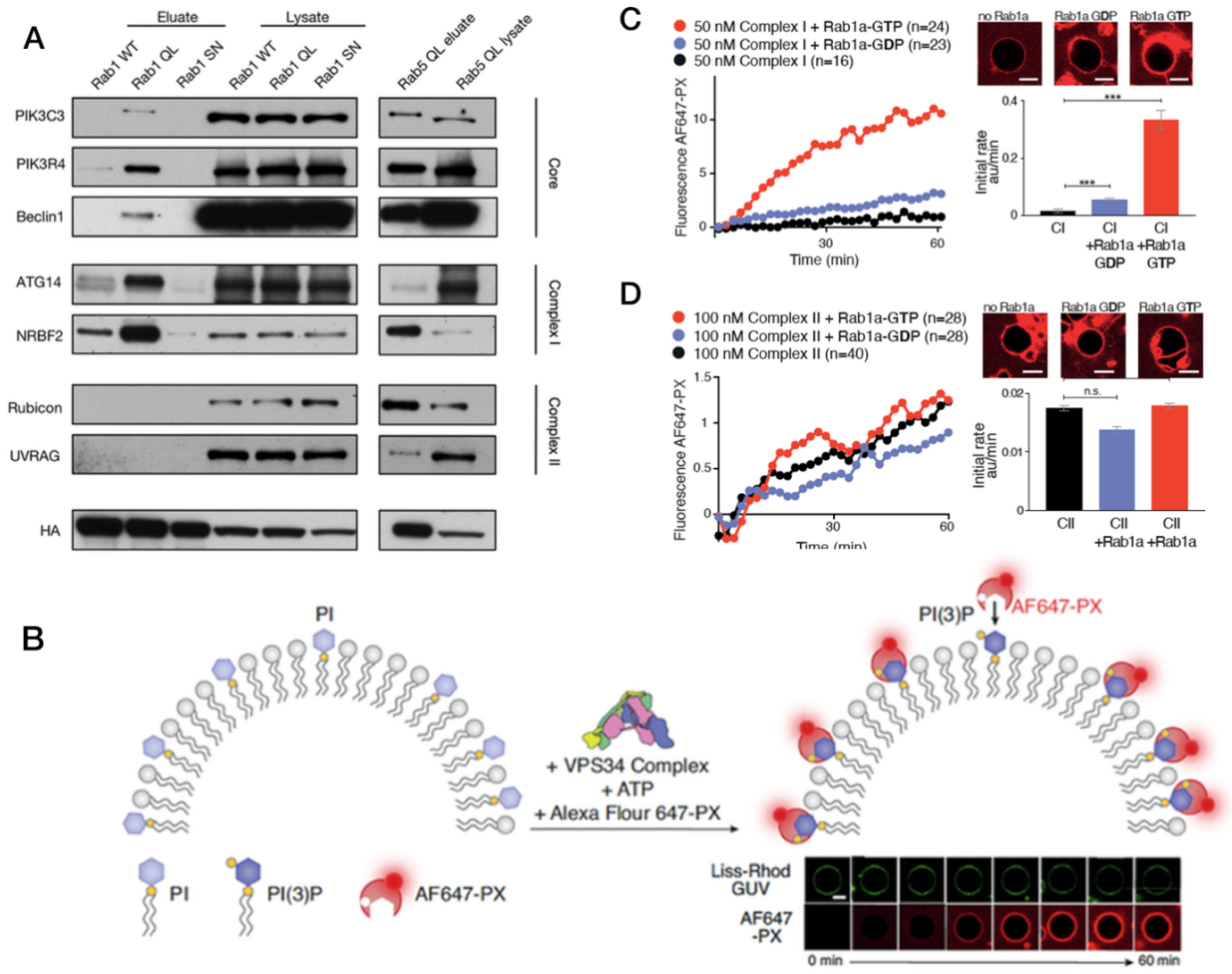

Figure 6.5. Active Rab1A binds and activates PI3K complex I. (A) Western blots of MitoID samples of Wildtype (WT), GTP- (QL) and GDP-locked (SN) Rab1A and Rab5A. Blots were probed with PIK3C3, PIK3R4, BECN1, ATG14L, NRBF2, RUBCN, UVRAG, and HA antibodies, as indicated. (B) Schematic representation of the GUV assay as shown in (Ohashi et al., 2020). Fluorescence from Lissamine-Rhodamine (Liss-Rhod) delineates the GUV membrane, while the AF647-PX channel indicates PI3K activity on the membrane. Scalebar: 5 µm. (C,D) GUV-based activity with membrane-tethered Rab1A with complex I (C) and complex II (D). The reaction progress curves, initial rates, and micrographs showing AF647-PX signals at the end of the reactions are shown. Scalebars: 5 µm. Data obtained by Shirley Tremel, figures as shown in (Tremel et al., 2021).

First examining Rab5A, we found that the presence of the GTP-loaded GTPase was found to increase complex I activity 3-fold, while increasing complex II activity an astonishing 40-fold (data not shown, (Tremel et al., 2021). Contrarily, the presence of GTP-loaded Rab1A was shown to increase complex I activity 11-fold, while not affecting complex II activity (Fig. 6.5C,D, data obtained by Shirley Tremel). GDP-loaded Rab1A showed little activation of PI3K, and neither did soluble Rab1A (Fig 6.5C, data obtained by Shirley Tremel). Together, this shows that membrane-bound Rab5A activates its previously

known effector, PI3K complex II. Interestingly, GTP-bound Rab5A was shown to specifically activate the endosomal complex II but not the autophagy-related complex I. Complex I, on the other hand, was activated specifically by GTP-bound Rab1A.

6.2.3.2 The C2 helical hairpin insertion (C2HH) domain on VPS34 is key for Rab1A binding

Next, we set out to map the Rab1 and Rab5 interaction sites on complex I and II, respectively. Using a combination of unnatural amino acid (UAA) mediated crosslinking and hydrogen/deuterium exchange mass spectrometry (HDX-MS), Tremel, Ohashi, and colleagues were able to identify several binding interfaces – the C2 helical hairpin insertion (C2HH) on VPS34, and the SGD and WD40 domains on VPS15 (Tremel et al., 2021). While the UAA crosslinking method identified C2HH as the sole interaction site, it should be noted that crosslinking occurred much more efficiently to the full complexes (complex I with Rab1 and complex II with Rab5) compared to VPS34 alone. This indicates that other proteins within the PI3K complexes could influence the interaction, potentially the SGD and WD40 domains on VPS15.

Since the VPS34 C2HH domain appears to have the most extensive interface with the Rab5A switch regions, which undergo nucleotide-specific conformational changes, we tested the importance of this domain for binding Rab1A and Rab5A by mutating the 199-REIE-202 residues to alanine (REIE>AAAA). In order to examine the interaction between PI3K and the Rab GTPases, we co-expressed all subunits of complex I or II with GTP-locked Rab1A or Rab5A, respectively. VPS34 was C-terminally tagged with eGFP to allow visualisation of the complexes, and was tested in either its wildtype (WT) or mutated (REIE>AAAA) form. Complex I containing wildtype VPS34-eGFP strongly co-localised with GTP-locked Rab1A, but this was lost completely with VPS34-eGFP (REIE>AAAA) (Fig. 6.6A,B, data obtained by Yohei Ohashi). Surprisingly, Rab5A showed a strongly contrasting pattern of localisation – while wildtype complex II was found to co-localise with GTP-locked Rab5A on enlarged endosomes, using VPS34-eGFP (REIE>AAAA) strongly increased their co-localisation (Fig. 6.6C,D, data obtained by Yohei Ohashi).

To confirm these observations, we performed MitoID proximity labelling experiments, co-expressing mitochondrially localised GTP- and GDP-locked Rab1A and Rab5A chimeras together with all subunits of either complex I or complex II, respectively. VPS34-eGFP, in either its wildtype (WT) or mutated (REIE>AAAA) form, was included to observe the presence of PI3K and the influence of the mutation on the interaction between the Rab GTPases and the PI3K complexes. Performing a Western blot on the MitoID samples and probing with antibodies against GFP and HA, we were able to confirm the immunofluorescence results – mutating 109-REIE-202 to alanines on VPS34 decreases its ability to interact

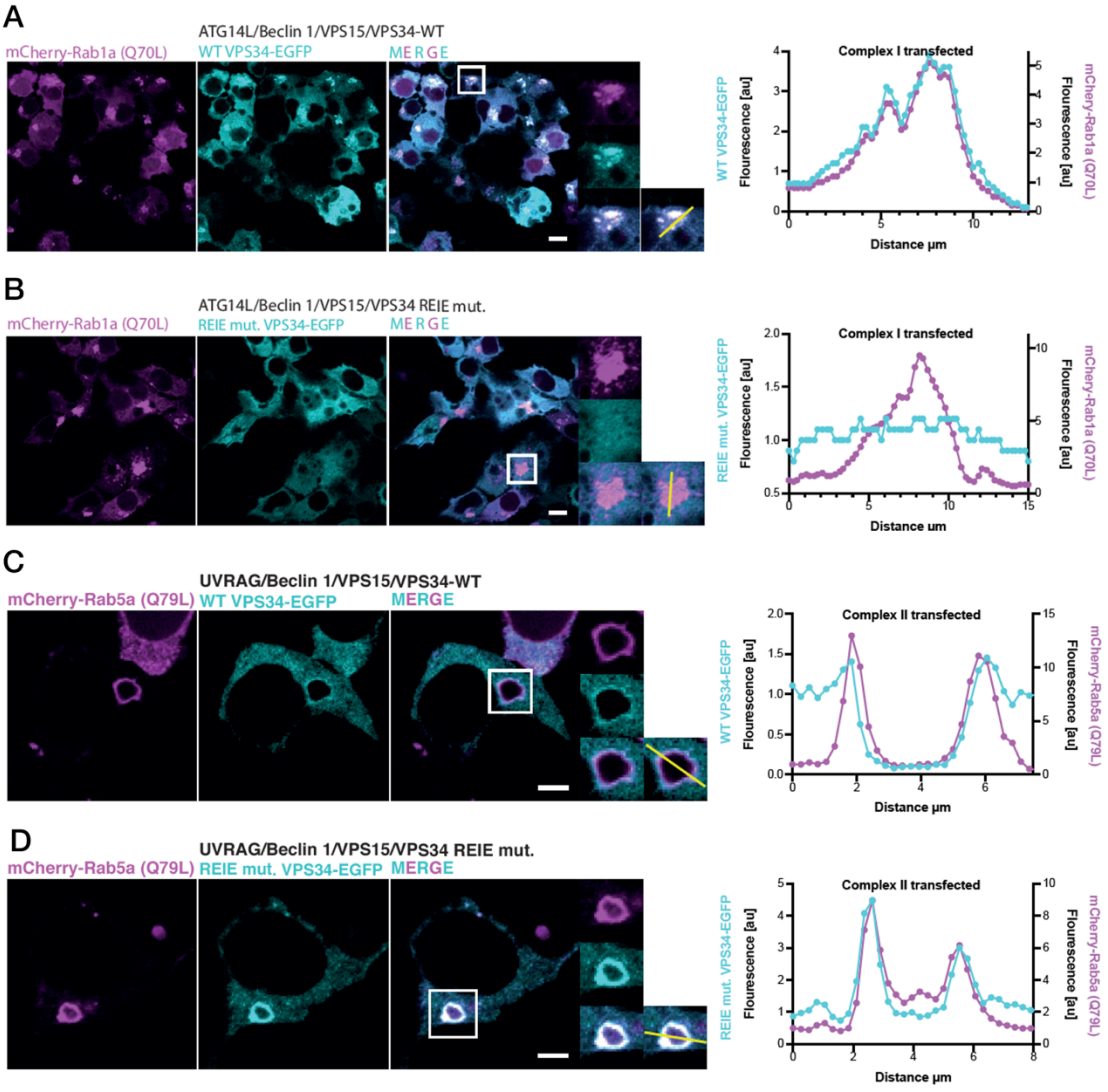

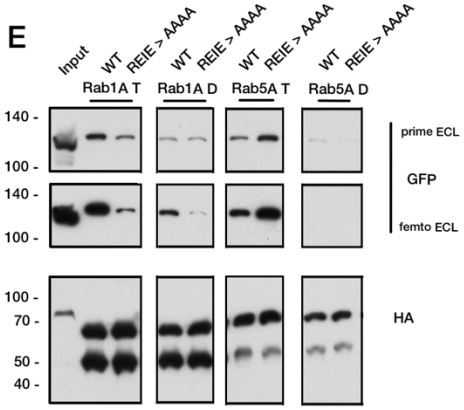

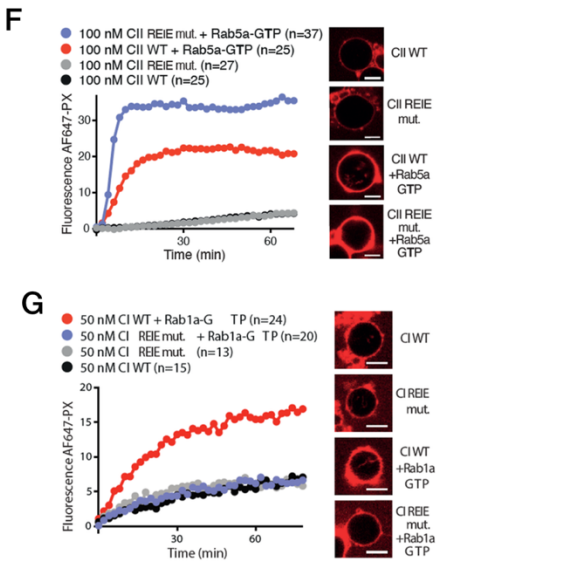

Figure legend on next page.

Figure 6.6. The interaction between Rab1A/Rab5A and VPS34 is regulated through the C2 helical hairpin insertion (C2HH) domain, and is key in activation of the PI3K complex. (A,B) Confocal micrograph images of HEK293T cells co-expressing GTP-locked mCherry-Rab1A and all four components of complex I with wildtype (A) or REIE>AAAA (B) eGFP-VPS34. To the right of each panel, a line plot showing the fluorescence traces is shown. Scalebars: 10 μm. Data obtained by Yohei Ohashi. (C,D) Confocal micrographs of HEK293T cells co-expressing GTP-locked mCherry-Rab5A and all four components of complex II with wildtype (C) or REIE>AAAA (D) eGFP-VPS34. To the right of each panel, a line plot showing the fluorescence traces is shown. Scalebars: 10 μm. Data obtained by Yohei Ohashi. (E) Western blots of MitoID samples of GTP- and GDP-locked Rab1A and Rab5A, as indicated, co-expressed with all four components of either complex I or complex II, respectively. EGFP-VPS34 was used to track PI3K, and was co-transfected in either its wildtype (WT) or REIE>AAAA form. Input: HEK293T lysate expressing GTP-locked Rab1A and WT complex I. Blots were probed with either anti-GFP (eGFP-VPS34) or HA (bait loading control). (F,G) GUV-based activity with membrane-tethered Rab5A with complex II (F) and Rab1A with complex I (G). The reaction progress curves and micrographs showing AF647-PX signals at the end of the reactions are shown. Scalebars: 5 μm. Data obtained by Shirley Tremel. Figures (A,B,C,D,F,G) as shown in (Tremel et al., 2021).

with Rab1A and increases the interaction with Rab5A (Fig. 6.6E). Moreover, Rab5A was shown to more potently activate complex II containing VPS34 (REIE>AAAA) compared to WT, whereas Rab1A showed a strong decrease in activation of VPS34 (REIE>AAAA) compared to WT (Fig. 6.6F,G).

Taken together, these data indicate that the class III phosphatidylinositol-3-kinase complexes I and II are activated by GTP-Rab1A and GTP-Rab5A, respectively. Interestingly, the Rab GTPases bind to the same interface on VPS34 – the C2 helical hairpin – but appear to regulate PI3K activity distinctly. While mutating the C2 helical hairpin in complex I decreases the ability to bind and be activated by Rab1A, the same mutation in complex II strongly increases activation by Rab5A. Identifying Rab1A as an activator of PI3K complex I gives us insight into the mechanisms by which Rab1A might regulate autophagy.

6.2.4 CALCOCO1 partially localises on autophagosomes and binds directly to Rab1

One of the proteins highlighted from our Rab1 MitoID data is CALCOCO1 (Fig. 5.1). The calcium-binding and coiled-coil domain-containing protein was found to co-localise with GTP-locked Rab1B, but not Rab1A, while a GST-based affinity chromatography binding assay showed that CALCOCO1 interacts with both paralogues (Fig. 5.5, Fig. 5.9).

Performing GST-based affinity chromatography, CALCOCO1 was found to bind directly to GTP-locked Rab1A and Rab1B (Fig. 6.7A). To test direct binding, purified FLAG-CALCOCO1 was incubated with beads coated in GTP- or GDP-locked Rab1A or Rab1B. Rab1 was expressed in Sf9 cells using the baculoviral expression system to allow for post-translational modifications, if necessary, and to aid protein

folding by chaperones. The data indicates that CALCOCO1 only binds to N-terminally tagged Rab1B and C-terminally tagged Rab1A, suggesting that CALCOCO1 would bind Rab1B at its C-terminus and Rab1A at its N-terminus (Fig. 6.7A). However, this discrepancy is very unlikely – the high sequence similarity between Rab1A and Rab1B (92%) strongly suggests that any interactors would bind on the same interface. Although further research can shed light on this, I believe that the absence of an interaction with CALCOCO1 with GST-Rab1A and Rab1B-GST is an experimental artefact. Regardless, this data shows that CALCOCO1 binds to GTP-locked Rab1A and Rab1B without any need for intermediate or adaptor proteins.

Until recently, the role of CALCOCO1 was mostly unknown. Indications of CALCOCO1 being involved in autophagy came solely from sequence similarities with the autophagy receptors NDP52 (CALCOCO2) and TAX1BP1 (CALCOCO3) (Y. Yang et al., 2015). Recently, however, a study by Stefely and colleagues found CALCOCO1 to interact with LC3C, and identified CALCOCO1 as a selective autophagy receptor which is regulated by mTOR inhibition (Stefely et al., 2020). Confirming the findings by Stefely and colleagues, CALCOCO1 was found to be partially localised on autophagosomes (Fig. 6.7B).

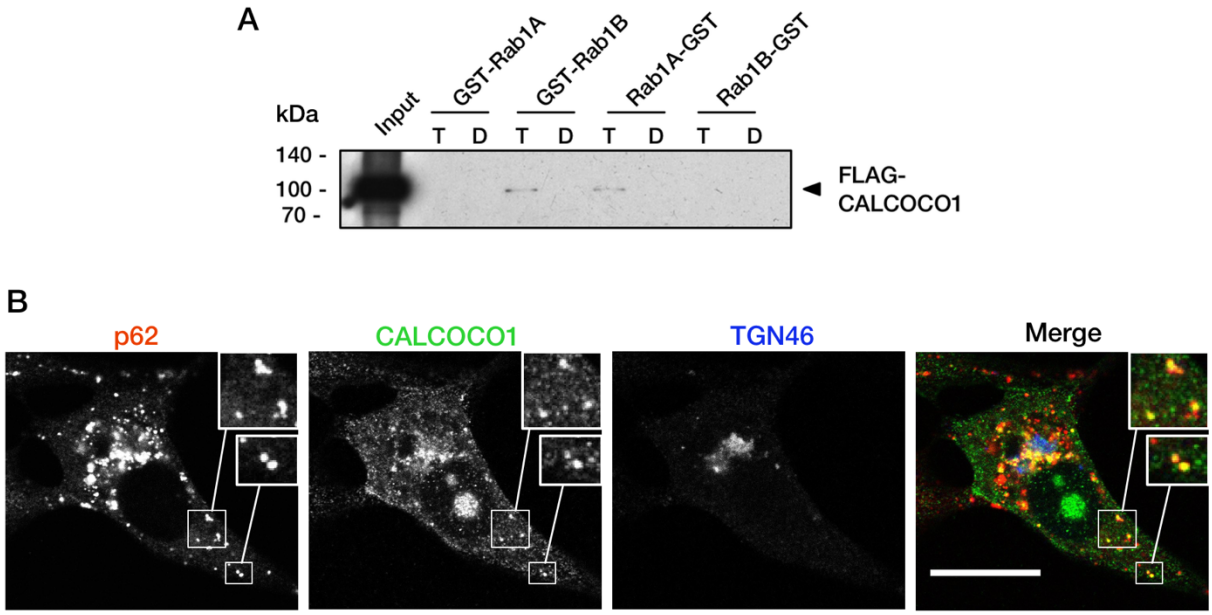

Figure 6.7. CALCOCO1 is a direct Rab1 binder and partially localises on autophagosomes. (A) Western blot of GST-based affinity chromatography samples in which FLAG-CALCOCO1 was washed over beads covered in GST-tagged Rab1 variants expressed in Sf9 cells with the baculoviral expression system. The blot was stained with an antibody against the FLAG epitope tag. Input: purified FLAG-CALCOCO1. (B) Confocal micrographs of U2OS cells treated with 100 mM Trehalose for 24 hours before fixation and staining with antibodies against the autophagosomal marker p62, CALCOCO1, and the *trans*-Golgi network marker TGN46. Scalebar: 20 µm.

As schematically represented in Figure 1.3, mTORC1 and PI3K function in the same pathway of autophagic induction. Interestingly, while we have shown Rab1 to activate PI3K, Stefely and colleagues found that mTOR inhibition causes autophagic CALCOCO1 degradation. More specifically, they found that loss of CALCOCO1 decreases the specific autophagy of the ER (reticulophagy) but increases macro-autophagy (Stefely et al., 2020). While this suggests another route through which Rab1 might affect autophagy in the mTORC1/PI3K pathway, the effect of mTORC1 inhibition degradation on Rab1 and CALCOCO1 appears contradictory – upon mTORC1 inhibition, autophagy is induced, CALCOCO1 is degraded, and Rab1A further activates PI3K to aid in the generation of autophagosomes.

Furthermore, it was shown that CALCOCO1 binds to LC3-family members, particularly LC3C, and is important for lipidation of LC3C (Stefely et al., 2020). How the interaction between CALCOCO1 and Rab1 influences autophagy, and potentially also ER-to-Golgi trafficking, remains to be elucidated. Further research including mapping and mutating the CALCOCO1-Rab1 binding sites would shed light on the role this interaction plays on vesicle trafficking and autophagy.

6.2.5 CLEC16A plays a role in Golgi morphology and binds directly to Rab1

Another protein that was highlighted as a Rab1 effector through our MitoID proximity labelling assays is CLEC16A (Fig. 5.1, Fig. 5.2A,B). CLEC16A is a membrane-associated endo-lysosomal protein which regulates mitophagy (Soleimanpour et al., 2014). Previously, CLEC16A has been shown to down-regulate starvation induced autophagy by stimulating mTOR activity (Tam et al., 2017). Interestingly, Tam and colleagues also found CLEC16A to partially relocate to the Golgi apparatus upon starvation, while Kim and colleagues find the opposite to be true; the *Drosophila melanogaster* orthologue of CLEC16A, Ema, was found to relocate from the Golgi to the autophagosomes upon starvation (S. Kim et al., 2012). Potential explanations for this discrepancy could be that the CLEC16A orthologues play slightly different roles in different organisms, and the different markers used to visualise autophagosomes (LC3B vs Atg8), although both explanations appear unlikely.

Regardless of the exact localisation pattern of CLEC16A, it has become apparent that CLEC16A is found partly on the Golgi and partly on autophagosomes. With the aim of confirming the localisation of CLEC16A under starved and fed conditions, Myc-CLEC16A was expressed in U2OS cells. Unfortunately, whether expressing Myc-CLEC16A alone (data not shown), or co-expressing the Rab1 MitoID chimeras with the aim of observing mitochondrial recruitment, CLEC16A remained fully cytoplasmic and dispersed throughout the cell (Fig. 6.8A). Interestingly, though, overexpression of CLEC16A was found to cause the

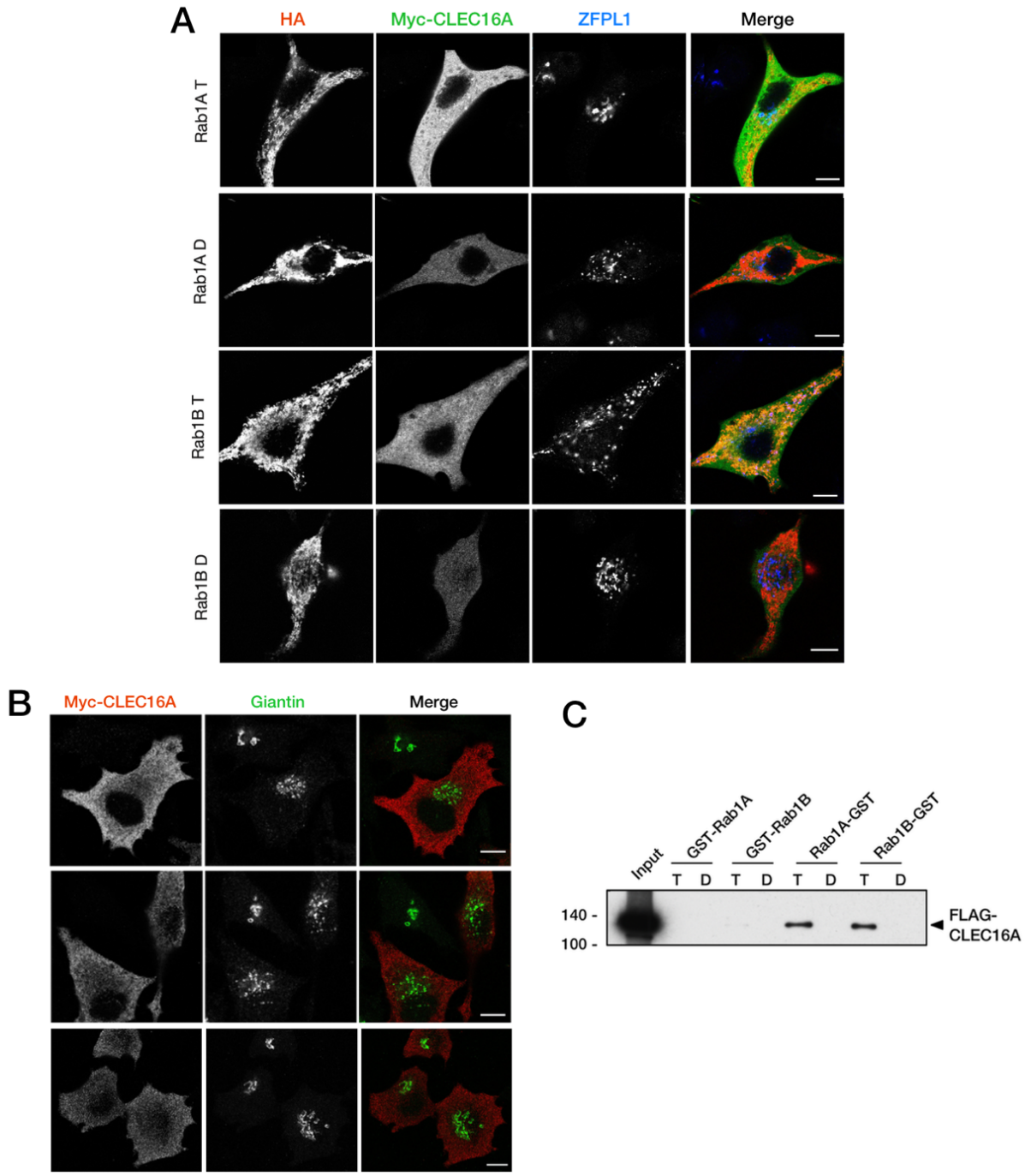

Figure 6.8. CLEC16A plays a role in Golgi morphology and binds directly to Rab1A and Rab1B. (A) Confocal micrographs of U2OS cells overexpressing Myc-CLEC16A and Rab1 MitoID chimeras (Rab1-BirA*-HA-MAO). Cells were probed with antibodies against the HA epitope (Rab1 chimeras), the Myc epitope (Myc-CLEC16A) and the Golgi marker ZFPL1. Scalebars: 10 µm. (B) Confocal micrographs of U2OS cells overexpressing Myc-CLEC16A and probed with antibodies against the Myc epitope and the Golgi marker Giantin. Scalebars: 10 µm. (C) Western blot of GST-based affinity chromatography samples in which FLAG-CLEC16A was washed over beads covered in GST-tagged Rab1 variants expressed in Sf9 cells with the baculoviral expression system. The blot was stained with an antibody against the FLAG epitope tag. Input: purified FLAG-CLEC16A.

Golgi to fragment (Fig. 6.8A,B). Although exceptions remain, Figure 6.8B clearly shows that cells overexpressing CLEC16A have a much more dispersed and fragmented Golgi apparatus compared to surrounding cells not expressing Myc-CLEC16A. While this does not shed light on the question whether CLEC16A is redirected to or from the Golgi upon starvation, it does suggest that CLEC16A might have a role in either establishing or maintaining Golgi morphology.

Finally, in order to study the interaction between Rab1 and CLEC16A further, I set out to examine whether the interaction requires any adaptor proteins or whether they bind directly and unaided. To test this, purified FLAG-CLEC16A was incubated with beads coated in GTP- and GDP-locked Rab1A and Rab1B. Western blots of the resulting samples show us that CLEC16A is able to directly bind GTP-locked Rab1A and Rab1B, but appears to only do so when the Rab1 proteins are C-terminally tagged (Fig. 6.8C). Binding assays of Rab1A, Rab1B, and CLEC16A fragments could elucidate the exact binding site and allow for directed mutagenesis, hereby studying the effect the interaction has on processes such as Golgi morphology, vesicle trafficking, and autophagy.

6.2.6 PPP1R37 binds to Rab1A and Rab1B with its leucine rich repeats

The protein phosphatase inhibitor PPP1R37, also known as leucine-rich repeat-containing protein 68 (LRRC68), was also identified as a novel Rab1 effector through MitoID proximity labelling assays (Fig. 5.1, Fig. 5.2A,B). Besides the presence of five central leucine-rich repeats and a proline-rich stretch near the C-terminus, the protein remains largely uncharacterised and its function unclear, making it an intriguing Rab1 interactor to further investigate.

GST-based affinity chromatography binding assays have confirmed the interaction between Rab1A/Rab1B and PPP1R37 (Fig. 5.9B). To test whether the proteins bind directly or with the aid of an adaptor protein, purified FLAG-PPP1R37 was incubated with beads coated in GTP- and GDP-locked Rab1A and Rab1B. Western blots of these samples show that PPP1R37 indeed binds directly and unaided to GTP-locked Rab1A and Rab1B (Fig. 6.9A, upper panel). Further examining this interaction, the interaction interface was narrowed down by cleaving PPP1R37 and performing binding assays. The platform InterPro predicts PPP1R37 to have two disordered regions flanking a leucine-rich repeat (LRR) domain containing 5 predicted LRR (Fig. 6.9B). Since leucine-rich repeats are well-characterised as frameworks for protein-protein interactions, Rab1 was expected to bind in this domain (Kobe & Kajava, 2001).

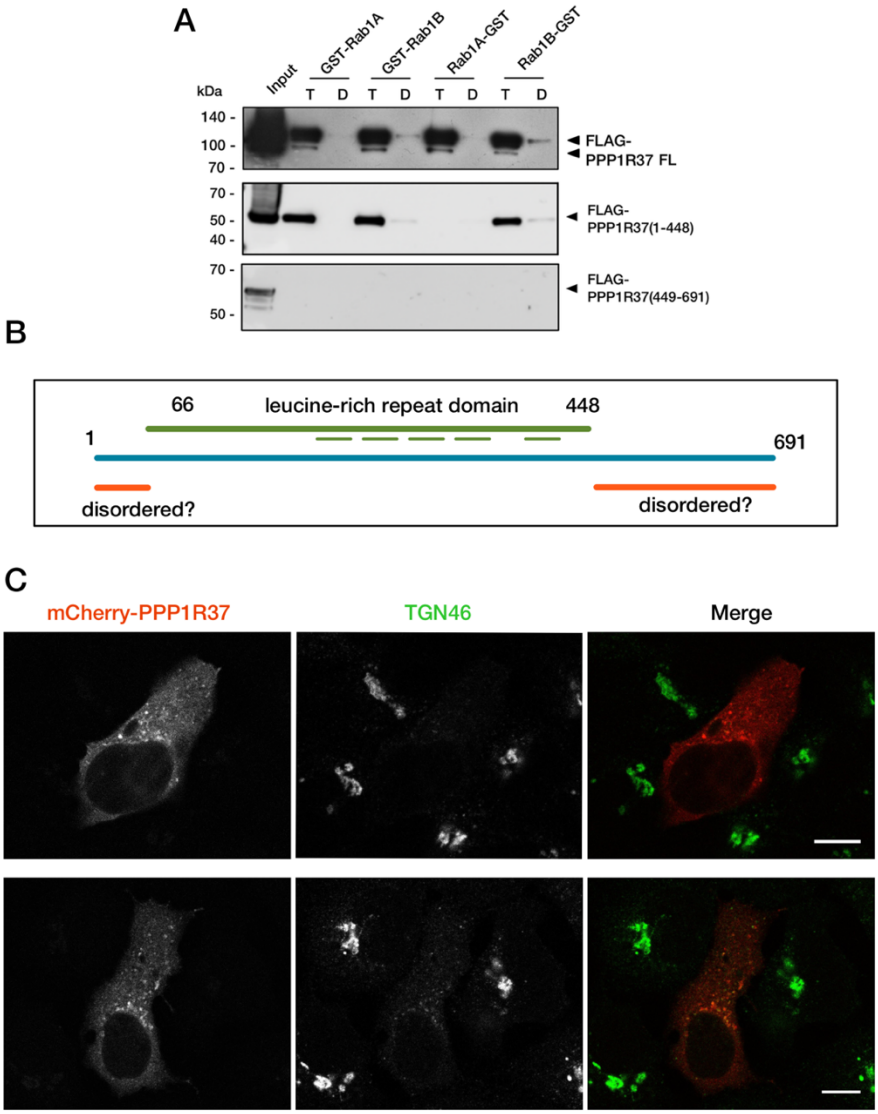

Figure 6.9. PPP1R37 plays a role in Golgi morphology and binds directly to Rab1A and Rab1B with its leucine rich repeats. (A) Western blot of GST-based affinity chromatography samples in which variants of FLAG-PPP1R37 (Full length protein, residues 1-448, and residues 449-691) ware washed over beads covered in GST-tagged Rab1 variants expressed in Sf9 cells with the baculoviral expression system. The blot was stained with an antibody against the FLAG epitope tag. Input: purified FLAG-PPP1R37. (B) Confocal micrographs of U2OS cells transiently expressing mCherry-PPP1R37 and probed with anti-TGN46. Scalebars: 10 µm.

GST-based binding assays were performed on PPP1R37 residues 1-448 and residues 449-691. Since direct binding between PPP1R37 and Rab1A/Rab1B was already established, full HEK293T lysate expressing the PPP1R37 fragments was washed over Rab1-coated beads. Western blots on these samples clearly show that Rab1A and Rab1B bind to the PPP1R37 fragment containing residues 1-448, but not to residues 449-691, suggesting that the binding interface lies at one of the leucine rich repeats (Fig. 6.9A, middle and lower

panels). Further binding essays exploring which of the leucine rich repeats is responsible for Rab1A and Rab1B binding could unfortunately not be completed due to time restraints.

6.2.7 PPP1R37 plays a role in Golgi morphology and partially localises to autophagosomes and the TGN

After validating the interaction between PPP1R37 and Rab1A/Rab1B, I set out to further examine the function of PPP1R37 in cells. While overexpressing mCherry-PPP1R37 in U2OS cells did not appear to disrupt autophagosomal or endosomal expression or localisation (data not shown), the *trans*-Golgi network (TGN) was extremely affected (Fig. 6.9C). The overexpression of PPP1R37 caused extreme Golgi fragmentation, with in some cases causing such severe disruption that the TGN was barely visible anymore (6.9C). Interestingly, the cells remained viable and appeared relatively healthy despite the severe Golgi disruption. This leads us to question whether the entire TGN and/or the entire Golgi apparatus is indeed fragmented, or whether it solely affects the marker chosen here, TGN46. Further research could elucidate this, for instance by co-staining multiple Golgi markers ranging from *cis*- to *trans*- and including several TGN markers.

In general, overexpression of mCherry-PPP1R37 resulted in a diffused, cytoplasmic localisation of PPP1R37. Interestingly, however, a large proportion of cells showed PPP1R37-positive puncta, appearing to be vesicles (Fig. 6.9C). These puncta were visible with or without co-expression of GTP-locked mitochondrial Rab1, where PPP1R37 is recruited to mitochondria (Fig. 5.8, Fig. 6.9C). PPP1R37 puncta appear to partially co-localise to LC3B-positive puncta (Fig. 6.10A). While large subsets of PPP1R37- and LC3B-puncta appear clearly distinct from each other, numerous overlapping or partially overlapping puncta are found. In most cases, the overlap observed between LC3 and PPP1R37 is partial; the two proteins appear to reside on the same vesicle but potentially covering different domains (Fig. 6.10A, inserts). While PPP1R37 and p62 are occasionally observed to be partially overlapping, the pattern is much less clear than for LC3B and PPP1R37 and p62 are mostly found to belong to different vesicle subsets (Fig. 6.10B).

No clear overlap was observed between PPP1R37-positive puncta and EEA1 or CD63 (Fig. 6.10C,D). While Sec16A, indicating ER exit sites, did not show direct overlap with PPP1R37, an intriguing pattern was observed where Sec16A puncta appeared to directly neighbour patches of PPP1R37 (Fig. 6.10E).

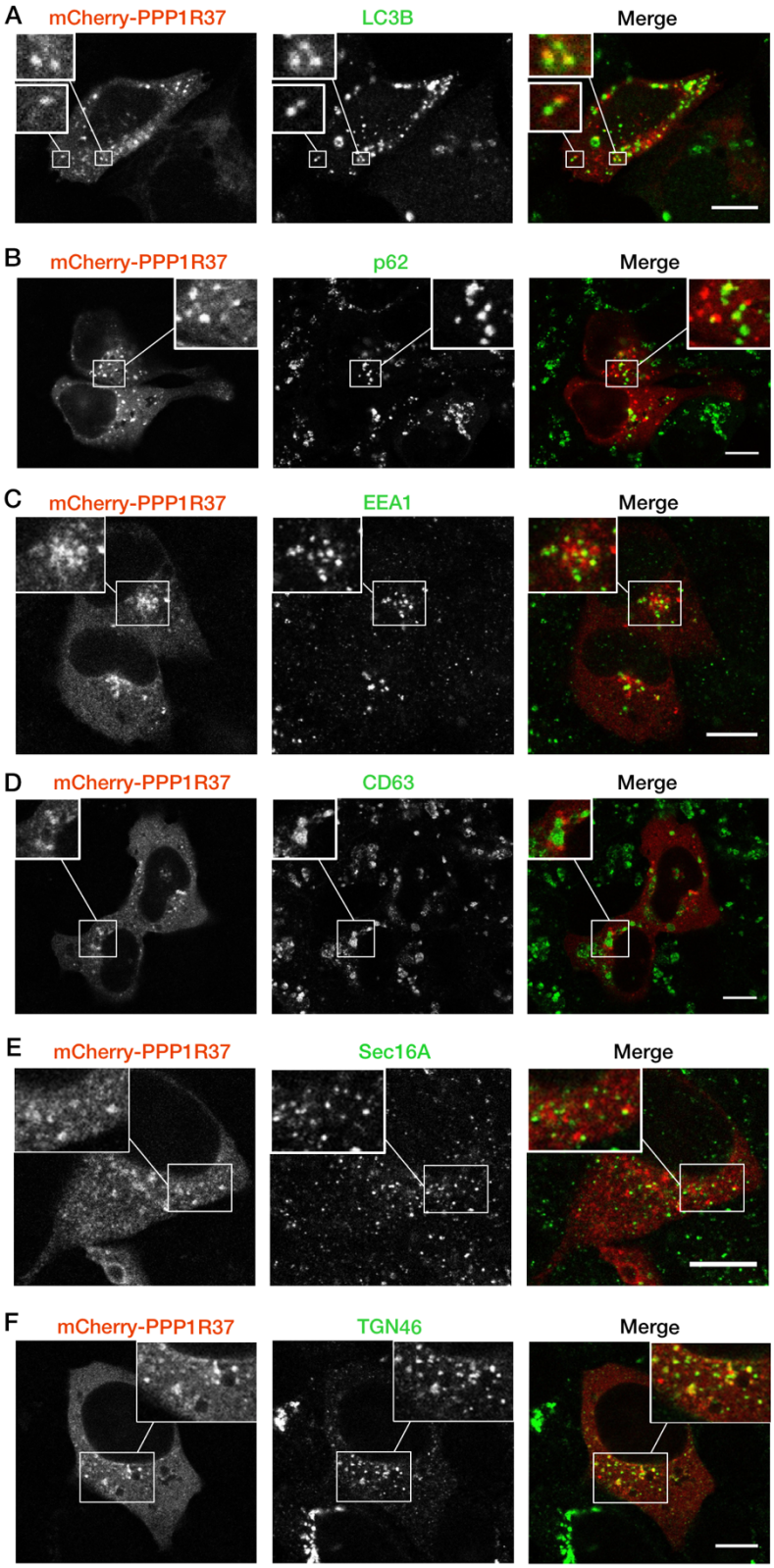

Figure 6.10. PPP1R37 puncta partially co-localise with LC3B and fragmented TGN. (A-F) Confocal micrographs of U2OS cells transiently expressing mCherry-PPP1R37, fixed, and probed with antibodies against LC3B (A), p62 (B), EEA1 (C), TGN46 (D), CD63 (E), and Sec16A (F). Autophagy was induced in (A,B) by 24 hours 100 mM Trehalose incubation. Scalebars: 10 µm.

Finally, I aimed to observe co-localisation of PPP1R37 with the Golgi apparatus, since several images appeared to show a perinuclear, Golgi-esque staining pattern (Fig, 6.10C). As previously mentioned, over-expression of mCherry-PPP1R37 was found to fragment the TGN (Fig. 6.9C). Examining whether the PP1R37 puncta co-localise to fragmented TGN puncta, I indeed found a proportion of the puncta to overlap (Fig. 6.10F). While distinct PPP1R37 and TGN46 puncta remain, as with PPP1R37 and LC3B, a subset of vesicles shows overlap with both, suggesting that PPP1R37 resides both on the Golgi and the autophagosomes.

Taken together, I was able to show several routes through which Rab1A and Rab1B affect autophagy. Firstly, the localisation of active Rab1A and Rab1B to autophagosomes was confirmed, finding a degree of association of Rab1 and LC3B on neighbouring puncta by observing their transport through live imaging. Secondly, in collaboration with the Roger Williams group, Rab1 was shown to recruit and activate the class III PI3K complex I, which plays a key role in initiating autophagosome formation. The binding site between Rab1A and PI3K complex I was identified on the PI3K component VPS34, and, although identical to the Rab5A binding site to PI3K complex II, was found to function in different ways. Furthermore, Rab1A and Rab1B were found to bind the novel interactors CALCOCO1, CLEC16A, and PPP1R37 in a direct, unaided manner. CALCOCO1 and PPP1R37 were shown to partially co-localise to autophagosomes, while CLEC16A and PPP1R37 appear to play a role in Golgi morphology.

6.3 Discussion

Using the MitoID proximity labelling assay, numerous novel potential Rab1A and Rab1B interactors were identified in Chapter 5. Several of these interactors were validated, including CALCOCO1, CLEC16A, PPP1R37, Rabaptin5, GCC88, and AKAP10. Here, I set out to further investigate a number of these interactions, notably CALCOCO1, CLEC16A, and PPP1R37. All three proteins were confirmed to be true direct binders to Rab1A and Rab1B, binding as isolated proteins from mammalian cultured cells to beads covered in Rab1 expressed in insect cells.

CALCOCO1 was found to partially co-localise with autophagosomes, as was PPP1R37. Furthermore, overexpression of either CLEC16A or PPP1R37 lead to fragmentation the Golgi, with at least PPP1R37 partially localising to the resulting puncta. Interestingly, both CLEC16A and CALCOCO1 have been independently shown to negatively influence autophagy by stimulating mTOR activity (Stefely et al., 2020; Tam et al., 2017). What role PPP1R37 might have on the regulation of autophagy remains unknown, but it is likely involved in autophagic regulation since it is partially localised on autophagosomes.

Whether CALCOCO1, CLEC16A, and PPP1R37 share an association with each other, besides all being Rab1 effectors, remains to be examined. While all three proteins could bind Rab1A/B and affect the same processes in manners distinct from each other, it is definitely possible that they might be involved in the same pathway. Examining what effect depletion of one of these proteins has on the other two could shed light on this, as could performing binding assays to see if the effectors might interact with each other independently of Rab1A/B.

Since CALCOCO1 and PPP1R37 were both found to partially co-localise with autophagosomes, the link between these proteins and autophagy is easily drawn. However, after observing the interaction between CALCOCO1 and LC3C, Stefely and colleagues propose an interesting question; since LC3-family members were found to be located to ER exit sites (ERES) where they are involved in the generation of COPII-coated vesicles, could CALCOCO1 play a role in ER-to-Golgi trafficking (Stadel et al., 2015; Stefely et al., 2020)? Having newly identified CALCOCO1 as a Rab1 effector, which is known to be a key player in ER-to-Golgi trafficking, might shed more light on this question. Although, interestingly, while LC3-family members are found to play a role in the formation of COPII-coated vesicles at the ER, Rab1 are only known to aid in the tethering and fusion of COPII vesicles at the ERGIC and the Golgi apparatus. Whether the interaction between Rab1 and CALCOCO1 might facilitate the transfer of recently budded vesicles to p115 remains to be examined.
Moreover, after identifying PPP1R37 as a novel Rab1 interactor and observing it to be partially localised on fragmented Golgi puncta, LC3B-positive puncta, and neighbouring to ERES, the suggestion that could PPP1R37 be involved in COPII vesicle trafficking is not far-fetched. Further research, including mapping and mutating the CALCOCO1-Rab1 and PPP1R37-Rab1 binding sites, would shed light on the role this interaction plays on vesicle trafficking and autophagy.

A widely used method of studying the role of proteins in certain processes is protein depletion by RNAi. Unfortunately, preliminary knockdown experiments were unsuccessful – after testing several methods of siRNA transfection in U2OS cells, including Fugene6 (Promega), FugeneHD (Promega), Lipofectamine RNAiMAX (Thermo Fisher), polyethyleneimine (PEI) (MRC LMB Media Kitchen), and GenMute (SignaGen), only GenMute allowed for enough cell viability to perform further experiments. Due to time constraints, I was unable to optimise this further, and adequate depletion levels were only achieved for siRNAs against Rab1A.
Successful RNAi depletion of CALCOCO1, CLEC16A, PPP1R37, and Rab1B, would be a very useful tool to study the role that these proteins play in vesicle trafficking, Golgi morphology, autophagosome formation

and maturation, and the (co-)localisation of the other proteins including Rab1A/B. Troubleshooting the siRNA transfections in U2OS cells was necessary, since autophagic induction and examination was most effective in these cultured cells. Future investigations could include other cell lines used to study autophagy, such as MEFS or CHO cells, with the aim of increasing the efficiency of RNAi depletion. Ultimately, creating knock-outs using the CRISPR-Cas9 technique will be the most successful way to deplete protein levels. Inducible knock-outs might be most useful to carefully study the exact functions of these proteins, since permanent knock-outs might not be viable.

Aside from the Rab1 effectors discussed above, the class III PI3K complex was also identified as a novel Rab1 effector. In collaboration with the Roger Williams group, Rab1A was found to recruit and activate the autophagy-specific PI3K complex I. Whereas Rab5A was a known PI3K binder, and was shown here to preferentially activate complex II, the identification of Rab1A as a specific activator of complex I is novel and potentially ground-breaking. Opening up new avenues of research, not only to further understand how PI3K complexes I and II are differentially regulated, but also gaining more understanding of the role of Rab1 in the regulation of autophagy.

While Rab1A and Rab1B were primarily known as master regulators of ER-to-Golgi trafficking, in this chapter, several links were shown through which Rab1 might influence the regulation of autophagy, as previously discussed. Investigating Rab1 broadly, I was able to confirm that GTP-locked Rab1A and Rab1B are partially localised on autophagosomes. The localisation of GDP-locked Rab1 on autophagosomes was severely decreased compared to GTP-locked, although studying this was challenging. As previously found by Zoppino and colleagues, overexpressing GTP-locked Rab1B appears to increase the amount of autophagosomes, while GDP-locked Rab1B decreases it (Zoppino et al., 2010). I was able to confirm these findings and extend this further to Rab1A, finding that autophagosomes often appeared bigger and more plentiful when GTP-locked Rab1A/B was expressed, and smaller and fewer when GDP-locked Rab1A/B was expressed. Studying the movement of puncta of GTP-locked Rab1A and LC3B, seemingly neighbouring vesicles were found to move in unison, further confirming their association.

Taken together, our data shows several routes through which Rab1A and Rab1B could be involved in the regulation of autophagy and vesicle trafficking. The identification of GTP-bound Rab1 as a specific activator of the autophagy-specific PI3K complex I, together with the identification and validation of three novel Rab1 effectors that directly bind active Rab1 and show involvement in both autophagy and vesicle trafficking, paves the way for further research which could shed light on one of the great questions in cell biology – how are vesicular processes regulated, and where lies the overlap and distinction.

Chapter 7: Discussion

Membrane trafficking is a highly specialised and tightly regulated process, and it is widely accepted that peripheral membrane proteins and small GTPases of the Arf and Rab families are its key regulators. With Rab GTPases being the largest family of small GTPases in mammals, elucidating their localisation patterns and interaction partners is key to gaining more understanding of how Rab GTPases contribute to membrane trafficking specificity and regulation. In this thesis, a highly effective adaptation to an *in vivo* proximity labelling approach was introduced, resulting in the identification of numerous novel Rab GTPase effectors and regulators. Here, I will discuss the main findings of this thesis and evaluate their broader impact on the field of membrane trafficking, as well as explore future experimental procedures to bring this research further.

7.1 Large-scale MitoID experiments and comparative analyses are able to identify novel interactors

Aiming to increase the array of known Rab GTPase effectors and regulators, the proximity labelling approach BioID, using the promiscuous biotin ligase mutant BirA*, was adapted (Roux et al., 2012; Shin et al., 2017). The novel technique, called MitoID, redirects BirA*-fusion proteins to the unrelated, ectopic location of the outer mitochondrial membrane, where they are stably incorporated (Gillingham et al., 2019). Comparing a large range of small GTPases in their GTP- and GDP-locked states at the same location, followed by a computational scoring analysis, allowed for a relatively clear distinction between potential interactors and background proteins. Using this MitoID screen, several potential novel effectors were identified for many of the tested GTPases. Moreover, several of these proteins were validated to be true interactors, mainly ARFGEF3 and STAMBPL1 for Rab2A, OSBPL9 and TBCK for Rab5A, NDE1 and HPS3 for Rab9A, and Alsin for Rab11A and Rab11B, further highlighting the efficacy of the MitoID approach. Most effective appeared to be the study for novel Rab1A and Rab1B effectors – by performing mitochondrial recruitment assays and GST-based affinity chromatography I was able to validate GCC88, CALCOCO1, Rabaptin5, CLEC16A, PPP1R37, and AKAP10 as Rab1 interactors.

To assess the efficiency of MitoID compared to traditionally used methods, the MitoID-identified interactors of two well-characterised Rabs were compared to those identified through an affinity chromatography screen previously performed in the Munro group (Gillingham et al., 2014). The comparative study found that for both Rab2A and Rab5A, the MitoID approach not only identified more of the previously known effectors compared to the affinity chromatography screen, but was also able to identify several effectors which were not previously reported and were later confirmed to be real interactors

(Gillingham et al., 2019). This analysis indicates that the MitoID approach can be just as, if not more, effective than traditional affinity chromatography methods in identifying Rab GTPase interactors. It should, however, be noted that MitoID, just as any experimental method, comes with its own set of inherent limitations. While we were able to address several BioID-related drawbacks by stably localising BirA*-fusion proteins to the mitochondria, and equalising the backgrounds in comparable samples, the ectopic localisation could also diminish the interactions of certain effectors. For instance, if the association of an effector relies on the composition of the lipid environment, then removing the Rab GTPase from its endogenous membrane compartment could disrupt binding. However, since we were able to identify numerous binding partners for GTPases from several different locations and with different endogenous lipid compositions, it is unlikely to be a common problem.

Furthermore, validating interactions identified through MitoID can be challenging. One of the main advantages of proximity labelling is the ability to detect weaker and transient interactions, which can be notoriously tricky to detect by conventional biochemistry and microscopy techniques. In this thesis, I used a combination of mitochondrial recruitment and affinity chromatography, overexpressing both the GTPase and the potential effector in one system in an attempt to increase detection opportunities. However, the interactions of several MitoID-identified interactors remained unvalidated, which could indicate either that the interaction is false or that the interaction is true but simply not strong or stable enough to be detected through conventional methods. In an attempt to overcome this hurdle, I set out to combine split-GFP with the GTPase:effector pair – coupling GFP fragment to the GTPase, and the other GFP fragment to the potential effector. The idea being that, when effector and GTPase come in close contact, no matter how briefly, the two GFP fragments form a fully functioning GFP molecule and remain bound and fluorescing. Unfortunately, preliminary experiments were unsuccessful and this approach could not be optimised due to time constraints. Until a more sensitive and appropriate validation method will be developed, false negatives are unfortunately inevitable.

Despite these inherent drawbacks, this thesis has shown that the MitoID approach is highly effective for identifying GTPase effectors. The technique has great potential to uncover novel GTPase interactors and hereby potentially gain more understanding in the roles of many less well characterised members of the Ras superfamily. I anticipate that the MitoID approach, as well as the specific interactions identified in this thesis, will aid many labs in working towards their goal of further elucidating the roles of small GTPases and potentially other families of proteins.

7.2 The dual roles of Rab1 in vesicle trafficking and autophagy

Rab1A and Rab1B are key regulators of ER-to-Golgi trafficking, and have increasingly been suggested to play a role in autophagy. With the aim of further uncovering the seemingly dual roles of Rab1A and Rab1B, the MitoID screen was utilised to maximise the set of known Rab1 effectors.

7.2.1 CALCOCO1, CLEC16A, and PPP1R37

As previously described, numerous novel effectors were identified, of which several are known to play a role in vesicle trafficking (Rabaptin5, GCC88, and AKAP10), known or speculated to be involved with autophagy (GCC88, CLEC16A, and CALCOCO1) or remain uncharacterised to date (PPP1R37). Further binding assays found that CALCOCO1, CLEC16A, and PPP1R37 bind Rab1A and Rab1B in a direct and unaided manner. Preliminary data suggests that overexpression of CLEC16A and PPP1R37 causes Golgi fragmentation, suggesting that both proteins are involved in the maintenance of Golgi morphology. Furthermore, CALCOCO1 and PPP1R37 are found to co-localise with autophagosomes, indicating that they may play a role in autophagy.

In the aim to further uncover the exact roles that CALCOCO1, CLEC16A, and PPP1R37 play in vesicle trafficking and autophagy, I set out to deplete protein levels through RNAi. Unfortunately, depletion of these proteins in U2OS cells turned out to be extremely challenging. Due to time constraints, I could not continue working on optimising the protocols. For future research, I suggest using a more stable but inducible system, such as the genome editing techniques CRISPR-Cas9 or Flp-In T-Rex. Other suitable approaches include Trim-Away, auxin-induced degron (AID), and Protacs, which all rapidly degrade proteins, or knocksideways, which swiftly relocalises the protein hereby causing a localised depletion (Clift et al., 2017; Nishimura et al., 2009; Lambrus et al., 2018; Sakamoto et al., 2001; Robinson & Hirst, 2013). The versatility of rapid degradation methods is particularly valuable when combined with time-limited techniques such as the induction of autophagy.

A more sophisticated approach would be to investigate the role that the interaction between Rab1 and the effector plays on membrane trafficking and autophagy. Instead of simply depleting the entire protein from the cell, the binding site could be determined and disrupted through directed mutagenesis. A start was made by examining the binding regions of Rab1 with PPP1R37, although interesting next steps would be to narrow down the binding interface to a particular leucine rich repeat on PPP1R37, and potentially even single residues. Interesting domains on CALCOCO1 to examine would be the N-terminal SKICH domain, the central coiled-coil domains, or the C-terminal C2H2 Zn-finger domain (Ensembl). While coiled-coil domains are common interfaces for Rab GTPase binding, the SKICH domain was shown to bind NAP1, an adaptor protein vital for autophagy regulation, in both of the other CALCOCO family members NDP52

and TAX1BP1, and the Zn-finger is thought to play a role in ubiquitin binding in NDP52 (Fu et al., 2018; Xie et al., 2015). Since CALCOCO1 shares these key domains with its fellow CALCOCO family members, it would be intriguing to study the importance of these domains further, and potentially narrow down the binding site with Rab1A and Rab1B. As discussed for PPP1R37, pinpointing the binding site with Rab1 would allow directed mutagenesis and the precise investigation of the effect of this interaction on autophagy and membrane trafficking. The same is true for CLEC16A; the protein contains an N-terminal domain of highly conserved FPL motifs, which would be interesting to examine further since its function remains unknown to date (UniProt, Pfam).

Further investigation of the roles of CLEC16A, CALCOCO1, and PPP1R37 in vesicle trafficking could be done by observing the endosomes, the Golgi apparatus, and COPI-, COPII- and clathrin-coated vesicles. Visualising these structures and examining their morphology, abundance, and localisation patterns after depleting the Rab1 effectors, or disrupting the specific interaction between Rab1 and its effectors, could give insight into the role that these proteins have in membrane trafficking. Another method to examine the role of proteins in vesicle trafficking would be through the RUSH system (Boncompain et al., 2012). This system is based upon the reversible interaction between a reporter protein and a hook protein, which is stably expressed in a donor membrane compartment. In the assay, the hook protein is fused to streptavidin, while the reporter protein is fused to streptavidin-binding protein (SBP). Addition of biotin will outcompete the binding of streptavidin and allow for the synchronous release of the reporter. Finally, in order to examine the timing of Rab1 effector association, the compound Brefeldin-A could be used. Brefeldin-A functions by inhibiting a subset of Arf1 GEFs, hereby disrupting COPI function. Since COPII function is unaffected, using Brefeldin-A in combination with effector depletion or interaction disruption through mutagenesis could aid in studying the timing or sequence of effector function in depth.

Similarly to vesicle trafficking, studying the role that the identified interactors might have on autophagy can largely be examined by immunofluorescence and live imaging microscopy. While performing co-staining upon effector over-expression has shed some light on the protein's function, studying the morphology and abundance of autophagosomes upon protein depletion or interaction disruption through mutagenesis could give great insight into their roles in the regulation of autophagy. In addition, live imaging would be a great asset in studying dynamics of effector association/disassociation with autophagosomes. Studying co-localisation of the effectors with autophagosomal markers of different stages (phagophore, early autophagosome, mature autophagosome) could aid in studying the timing of effector function or association. Another useful is tandem fluorescence-tagged LC3 or acridine orange, techniques which utilise

changes of the fluorophores in acidic environments, allowing for close examination of the maturation of autophagosomes as they fuse with lysosomes (Kimura et al., 2007; Thomé et al., 2016).

Another route to investigate the functions of CALCOCO1, CLEC16A, and PPP1R37, is by examining whether they have any other interaction partners besides Rab1A and Rab1B. I set out to perform MitoID assays on the three effectors, however, the C-terminally tagged CALCOCO1 chimera did not express well in mammalian cultured cells. An N-terminally fused CALCOCO1 MitoID plasmid would be an alternative, using Tom70-HA-BirA*-bait as previously used for Arf1 and Arl1 by the Munro group, but time constraints did not allow me to perform this. Ideally, the effector MitoID assays would be performed in two situations; one set of assays in healthy, fed cultured cells, and one set of assays in starved or Trehalose induced cultured cells. Comparing the interactomes of the Rab1 effectors in endogenous and autophagic conditions could highlight interaction patterns and give further insights into their roles. However, another difficulty I encountered when trialling the effector MitoID assays, was that autophagic induction for 4-24 hours did not allow for clear comparative output. Because the MitoID assays take approximately 72 hours, the differences in interactomes due to autophagic induction would be minimal and hard to detect. Attempting to shorten the duration of biotinylation, MitoID assays were performed with and without exogenous biotin pulse, as well as using media and FCS depleted in biotin. However, even though the amount of biotinylation was indeed overall decreased, there was still a significant amount of biotinylation occurring in both the bait and several tested effectors (data not shown). Unfortunately, while TurboID is used for shorter biotinylation pulses than the original BioID and BioID2, it showed the same sensitivity issues; the bait and several tested preys were biotinylated even without addition of exogenous biotin (data not shown).

With the aim of making the MitoID approach more useful for short time courses, I set out to adapt MitoID into an inducible system. Combining split-BioID with inducible heterodimerisation system iDimerize, one of the split-BioID fragments to each of the iDimerize domains with the aim to generate a fully functioning BioID only upon addition of the dimerising compound (Schopp et al., 2017). While preliminary results indicate that further optimisation is necessary, I strongly believe that developing this system, or a similar inducible approach, will be extremely useful and beneficial for studying interactomes in time-sensitive systems.

7.2.2 The class III PI3K complex I

The unexpected hits of the Rab1 MitoID assays included components of the class III PI3K complex I. In collaboration with Shirley Tremel and Yohei Ohashi from the Williams group (MRC LMB), we were able to show that Rab1A specifically activates the autophagy-related PI3K complex I. Interestingly, Rab1A and

Rab5A were found to utilise a similar site on VPS34 to interact with complex I and complex II, respectively. Unexpectedly, disruption of the binding interface lead to drastically opposing results – mutating the VPS34 199-REIE-202 residues to alanine (REIE>AAAA) diminished the interaction between complex I and Rab1A, but strengthened the interaction between complex II and Rab5A. Furthermore, we found the WD40 domain in VPS15 to be greatly shifted in complex I compared to complex II, causing the VPS34 C2HH domain to tilt (Tremel et al., 2021). It is possible that the shift of the WD40 domain is due to the binding of ATG14L or UVRAG in complex I or II, respectively, since the binding interface of these proteins lies against WD40. This could partly account for the selectivity of complex I with Rab1 and complex II with Rab5, although the possibility that direct interactions of ATG14L/UVRAG with the Rab GTPases could play a role in selectivity should not be discarded. While direct interactions of this kind were not observed in our study, they would be hard to pick up on if they are transient in nature. Although HDX-MS analyses were performed in our study, it is possible that interactions occurred one of the unobserved regions. Further examinations using HDX-MS and cross-linking, as well as increasing the resolution of the cryo-EM structure, could aid in identifying potential transient interactors. Regardless, the identification of Rab1A as a specific PI3K complex I activator provides great insight into how Rab1 affects autophagy, opening up the fields of study towards PI3-kinases, Rab GTPases, and the intersection of vesicle trafficking and autophagy.

7.3 Concluding remarks

In this thesis, I have shown that the MitoID approach is a very efficient and effective method to identify interactors of small GTPases. Adding to the array of available techniques, MitoID is certainly a valuable tool to study protein-protein interactions, and has the potential to greatly aid many fields of research. Identifying and validating six previously unreported Rab1A and Rab1B effectors greatly increases the set of known Rab1 effectors, which aids us in our journey to closely dissect the seemingly dual roles of Rab1; a master regulator of vesicle trafficking and autophagy.

Acknowledgements

Whew, here we are! Working as PhD student at the LMB, and in Cambridge in general, was a challenging, memorable, and life changing experience for me. There are numerous people without whom I would not have been where I am today, both academically as well as personally.

Thank you Sean, for giving me the opportunity to work in your lab and experience being a student at such a world renowned institute, I really appreciate that you gave me the freedom to explore my scientific interests.

Al, thank you for always being keen to grab a cup of tea and have a chat. Regardless of whether we talked about the current scientific mystery we've got going on, or about personal things, I felt supported. Thank you for your patience, sharing your knowledge, and for luring me to lunchtime body pump.

Lawrence, my bench buddy for most of my time in the LMB! Thank you for some really fun nights out and sharing your plethora of crazy stories. Both your knowledge and your seemingly endless collection of plasmids were extremely helpful, and you've made lab life so much fun!

Thank you Nadine, for being so supportive (and for making me smile when you're laughing out loud to The Guilty Feminist), and Antonio, for always enjoying a chat and bringing a wealth of random history facts to the table!

A big thank you to all the members of the Munro group, past and present, particularly Jérôme, Fiona, João, Igor, Rosa, and John Kilmartin, for all the scientific discussions, coffee chats, and fun Christmas dinners. I also want to thank Shirley, Yohei, and Roger, for a really fruitful and lovely collaboration experience. It was a pleasure working with all of you, and I wish you all the best!

A special thanks goes to Fons, for sparking my love of cell biology all those years ago, and Ivar, whose enthusiasm and patience gave me the confidence to pursue it.

Thank you to all of my friends, both local and abroad, new and old. Your support in my scientific career as well as my personal endeavours has meant so much to me! A special thanks goes out to my support-bubble-buddy Gabby, with whom I navigated most of the rollercoaster that was 2020. Thank you for your patience and support!

Dina. Where do I even start? The support you have given me during my time here in Cambridge is phenomenal. We've been a little team through all of it, and I truly don't know what this PhD would have looked like without you. From making guinea pig cakes to having life changing talks in the microscope room, we made it through. WE DID IT!

And finally, a big thank you to my family. Having a home to return to, no matter what, is invaluable. Dad, Anjo, Fé, Kato, and Sara, your support and love really means the world to me. Thank you, and I can't wait to see you all again!

Materials and Methods

I. Materials

I.I Plasmids

Unique code	Coding region of interest	Description	Vector (Source)
JB74	Rab1AWT-BirA*-HA-MAO	Wildtype (WT) or GTP-locked (QL), or GDP-locked (SN/TN) protein fused at the C-terminus to a GAGAGA linker, the biotin ligase BirA* (BioID), an HA epitope tag, and the transmembrane domain of monoamine oxidase as a mitochondrial targeting sequence.	pcDNA3.1+
JB49	Rab1AQ70L-BirA*-HA-MAO		
JB50	Rab1AS25N-BirA*-HA-MAO		
JB75	Rab1BWT-BirA*-HA-MAO		
JB76	Rab1BQ67L-BirA*-HA-MAO		
JB77	Rab1BS22N-BirA*-HA-MAO		
pH38	Rab2AWT-BirA*-HA-MAO		pcDNA3.1+ (Alison Gillingham)
pN40	Rab2AQ65L-BirA*-HA-MAO		
JB2	Rab2AS20N-BirA*-HA-MAO		pcDNA3.1+
JB39	Rab5AWT-BirA*-HA-MAO		
JB28	Rab5AQ79L-BirA*-HA-MAO		
JB40	Rab5AS34N-BirA*-HA-MAO		
pG38	Rab6AWT-BirA*-HA-MAO		pcDNA3.1+ (Alison Gillingham)
pO40	Rab6AQ72L-BirA*-HA-MAO		
JB4	Rab6AT27N-BirA*-HA-MAO		pcDNA3.1+
JB93	Rab7AQ67L-BirA*-HA-MAO		
JB94	Rab7AT22N-BirA*-HA-MAO		

JB12	Rab8AWT-BirA*-HA-MAO	Wildtype (WT), GTP-locked (QL), or GDP-locked (SN/TN) protein fused at the C-terminus to a GAGAGA linker, the biotin ligase BirA* (BioID), an HA epitope tag, and the transmembrane domain of monoamine oxidase as a mitochondrial targeting sequence.	pcDNA3.1+
JB24	Rab8AQ67L-BirA*-HA-MAO		
JB23	Rab8AT22N-BirA*-HA-MAO		
JB83	Rab9AWT-BirA*-HA-MAO		
JB84	Rab9AQ66L-BirA*-HA-MAO		
JB85	Rab9AS21N-BirA*-HA-MAO		
JB80	Rab10WT-BirA*-HA-MAO		
JB81	Rab10Q68L-BirA*-HA-MAO		
JB82	Rab10T23N-BirA*-HA-MAO		
JB16	Rab11AWT-BirA*-HA-MAO		
JB20	Rab11AQ69L-BirA*-HA-MAO		
JB19	Rab11AS25N-BirA*-HA-MAO		
pX49	Rab11BQ70L-BirA*-HA-MAO		pcDNA3.1+ (Alison Gillingham)
pY49	Rab11BS25N-BirA*-HA-MAO		
JB5	Rab18WT-BirA*-HA-MAO		pcDNA3.1+
JB11	Rab18Q67L-BirA*-HA-MAO		
JB10	Rab18S22N-BirA*-HA-MAO		
JB7	rab19BWT-BirA*-HA-MAO		
JB18	Rab19BQ76L-BirA*-HA-MAO		
JB17	Rab19BT31N-BirA*-HA-MAO		
pG48	Rab21WT-BirA*-HA-MAO		pcDNA3.1+ (Alison Gillingham)
pH48	Rab21Q78L-BirA*-HA-MAO		
pI48	Rab21T33N-BirA*-HA-MAO		

JB89	Rab29WT-BirA*-HA-MAO	Wildtype (WT), GTP-locked (QL), or GDP-locked (SN/TN) protein fused at the C-terminus to a GAGAGA linker, the biotin ligase BirA* (BioID), an HA epitope tag, and the transmembrane domain of monoamine oxidase as a mitochondrial targeting sequence.	pcDNA3.1+
JB90	Rab29T21N-BirA*-HA-MAO		
JB91	Rab29Q67L-BirA*-HA-MAO		
JB92	Rab29A16V-BirA*-HA-MAO		
pI38	Rab30BWT-BirA*-HA-MAO		pcDNA3.1+ (Alison Gillingham)
JB15	Rab30BQ68L-BirA*-HA-MAO		pcDNA3.1+
JB3	Rab30BT23N-BirA*-HA-MAO		
JB13	Rab33BWT-BirA*-HA-MAO		
JB26	Rab33BQ92L-BirA*-HA-MAO		
JB25	Rab33BT47N-BirA*-HA-MAO		
JB6	Rab39BWT-BirA*-HA-MAO		
JB8	Rab39BQ68L-BirA*-HA-MAO		
JB9	Rab39BS22N-BirA*-HA-MAO		
JB14	Rab43WT-BirA*-HA-MAO		
JB21	Rab43Q77L-BirA*-HA-MAO		
JB22	Rab43T32N-BirA*-HA-MAO		
JB41	Rac1WT-BirA*-HA-MAO		
JB42	Rac1Q60L-BirA*-HA-MAO		
JB54	Rac1T17N-BirA*-HA-MAO		
JB47	Cdc42WT-BirA*-HA-MAO		
JB48	Cdc42G12V-BirA*-HA-MAO		
JB57	Cdc42T17N-BirA*-HA-MAO		

JB46	RhoAWT-BirA*-HA-MAO	Wildtype (WT), GTP-locked (QL/GV/GD), or GDP-locked (SN/TN/SA) protein fused at the C-terminus to a GAGAGA linker, the biotin ligase BirA* (BioID), an HA epitope tag, and the transmembrane domain of monoamine oxidase as a mitochondrial targeting sequence.	pcDNA3.1+
JB68	RhoAQ63L-BirA*-HA-MAO		
JB55	RhoAT19N-BirA*-HA-MAO		
JB86	RhebWT-BirA*-HA-MAO		
JB87	RhebQ64L-BirA*-HA-MAO		
JB88	RhebS20N-BirA*-HA-MAO		
JB95	nRasG12D-BirA*-HA-MAO		
JB96	nRasT17N-BirA*-HA-MAO		
JB97	RalBG23V-BirA*-HA-MAO		
JB98	RalBS29A-BirA*-HA-MAO		
JB27 /JJS345	BirA*-HA-MAO	BirA* (BioID) fused at its C-terminus to a GAGAGA linker, an HA epitope tag, and the transmembrane domain of monoamine oxidase as a mitochondrial targeting sequence. Used as a negative control for MitoIDs proximity labelling assays.	pcDNA3.1+ (John Shin)
JB31	Rab1AQ70L-BioID2-HA-MAO	Wildtype (WT), GTP-locked (QL), or GDP-locked (SN/TN) protein fused at the C-terminus to a GAGAGA linker, the biotin ligase BioID2, an HA epitope tag, and the transmembrane domain of monoamine oxidase as a mitochondrial targeting sequence.	pcDNA3.1+
JB32	Rab1AS25N-BioID2-HA-MAO		
JB152	Rab1BQ67L-BioID2-HA-MAO		
JB153	Rab1BS22N-BioID2-HA-MAO		
JB34	Rab6AQ72L-BioID2-HA-MAO		
JB35	Rab6AT27N-BioID2-HA-MAO		
JB37	Rab11AQ69L-BioID2-HA-MAO		
JB38	Rab11AS25N-BioID2-HA-MAO		

JB158	Rab1AQ70L-TurboID-HA-MAO	Wildtype (WT), GTP-locked (QL), or GDP-locked (SN/TN) protein fused at the C-terminus to a GAGAGA linker, the biotin ligase TurboID, an HA epitope tag, and the transmembrane domain of monoamine oxidase as a mitochondrial targeting sequence.	pcDNA3.1+
JB159	Rab1AS25N-TurboID-HA-MAO		
JB150	Rab1BQ67L-TurboID-HA-MAO		
JB151	Rab1BS22N-TurboID-HA-MAO		
JB104	Rab6AQ72L-TurboID-HA-MAO		
JB105	Rab6AS27N-TurboID-HA-MAO		
JB106	Rab11AQ69L-TurboID-HA-MAO		
JB107	Rab11AS25N-TurboID-HA-MAO		
JB44	Rab1AQ70L-GST	GTP-locked (QL) or GDP-locked (SN) protein fused at the C-terminus to a GAGA linker and a GST tag. Used for the baculovirus expression system (MultiBac) in insect cells.	pAceBac1 (Geneva Biotech)
JB45	Rab1AS25N-GST		
JB148	Rab1BQ67L-GST		
JB149	Rab1BS22N-GST		
JB154	GST-Tev-Rab1AQ70L	GTP-locked (QL) or GDP-locked (SN) protein, N-terminally taged with a GST tag, a Tev cleavage site, and a GAGA linker. Used for the baculovirus expression system (MultiBac) in insect cells.	
JB155	GST-Tev-Rab1AS25N		
JB156	GST-Tev-Rab1BQ67L		
JB157	GST-Tev-Rab1BS22N		
JB63	Rab1AQ70L(C26S,C126S)-BirA*-HA-MAO	GTP-locked (QL), or GDP-locked (SN) Rab1A protein with C26S and C126S mutations, C-terminally fused to a GAGAGA linker, BirA* (BioID), an HA epitope tag, and the transmembrane domain of monoamine oxidase (MAO) as a mitochondrial re-localisation tag.	pOPTG (Olga Perisic)
JB65	Rab1AS25N(C26S,C126S)-BirA*-HA-MAO		
JB78	GST-Tev-Rab1AQL (C26S,C126S)	GTP-locked (QL) and GDP-locked (SN) Rab1A protein with C26S and C126S mutations, N-terminally tagged with a GST tag, a Tev cleavage sequence, and a GAGA linker.	
JB79	GST-Tev-Rab1ASN (C26S,C126S)		

JB144	HA-Rab1AQ70L	GTP-locked (QL) and GDP-locked (SN) protein, N-terminally tagged with an HA epitope	pcDNA3.1+
JB145	HA-Rab1AS25N		
JB146	HA-Rab1BQ67L		
JB147	HA-Rab1BS22N		
JB230	HA-Rab5AQ79L		
JB231	HA-Rab5AS34N		
JB180	mCherry2-Rab1AQ70L	GTP-locked (QL) and GDP-locked (SN) Rab1A and Rab1B, N-terminally tagged with red fluorescent protein mCherry2 and a GAGA linker.	
JB181	mCherry2-Rab1AS25N		
JB182	mCherry2-Rab1BQ67L		
JB183	mCherry2-Rab1BS22N		
JB199	mCherry2-Rab1AQ70L-MAO	GTP-locked (QL) and GDP-locked (SN) Rab proteins, N-terminally tagged with red fluorescent protein mCherry2 and C-terminally tagged with the transmembrane domain of monoamine oxidase (MAO) to re-localise to the mitochondrial outer membrane.	
JB200	mCherry2-Rab1AS25N-MAO		
JB201	mCherry2-Rab1BQ67L-MAO		
JB202	mCherry2-Rab1BS22N-MAO		
JB203	mCherry2-Rab5AQ79L-MAO		
JB204	mCherry2-Rab5AS34N-MAO		
JB128	Rabaptin5-FLAG	Rabaptin5 C-terminally tagged with a FLAG epitope	
JB132	FLAG-CALCOCO1	Effector proteins and their fragments, N-terminally tagged with the FLAG epitope.	
JB215	FLAG-Clec16A		
JB137	FLAG-PPP1R37		
JB220	FLAG-PPP1R37 (1-448)		
JB221	FLAG-PPP1R37 (449-end)		
pQ51	FLAG-HPS3		pcDNA3.1+ (Alison Gillingham)

pM51	FLAG-TRAPPC10	Effector proteins and their fragments, N-terminally tagged with the FLAG epitope.	pcDNA3.1+ (Alison Gillingham)
pI51	FLAG-SH3BP5L		
JB170	Myc-PPP1R37	Effector proteins N-terminally tagged with the Myc epitope	pcDNA3.1+
JB171	Myc-CALCOCO1		
JB214	Myc-Clec16A		
N/A	GFP-PX (PI3P)	N-terminally GFP-tagged PX-domain	pcDNA3.1+ (Yohei Ohashi)
pQ49	GFP-FLAG-TBCK	Effector proteins (TBCK, STAMBPL1, ARFGEF3) and PI3P binding domain (PX), N-terminally tagged with the green fluorescence protein GFP and the FLAG epitope	pcDNA3.1+ (Alison Gillingham)
pN49	GFP-FLAG-STAMBPL1		
pO49	GFP-FLAG-ARFGEF3		
pV51	His_6-NDE1	NDE1 N-terminally tagged with polyhistidine	
pYO1296	mCherry-Rab5AQ79L	GTP-locked Rab5A N-terminally tagged with red fluorescent protein mCherry	eGFP-C1 (Yohei Ohashi)
pYO1280	VPS34-eGFP	VPS34 C-terminally tagged with green fluorescent protein eGFP	
pYO1300	VPS34(REIE>AAAA)-eGFP	VPS34, mutated to have its 199-REIE-202 replaced with Alanines, C-terminally tagged with green fluorescent protein eGFP	
pYO1101	BECN and ATG14L	Bicistronic vector containing BECN and ATG14L, both untagged	pCAG (Yohei Ohashi)
pYO1031	BECN and UVRAG	Bicistronic vector containing BECN and UVRAG, both untagged	
pYO350	VPS15	Untagged VPS15	pcDNA4/TO (Yohei Ohashi)
N/A	eGFP-LC3B	LC3B, N-terminally tagged with green fluorescent protein GFP	(Thomas Mund, MRC LMB)

I.II Cell lines

I.II.I Mammalian cell lines

Unique Identifier	Description	Origin
HeLa	Human cell line derived from cervical adenocarcinoma	ATCC
HEK293T	Human cell line derived from embryonic kidney	
U2OS	Human cell line derived from osteosarcoma	
mCherry-Parkin (HeLa)	Human cell line derived from cervical adenocarcinoma with constitutively expressed Parkin (tagged N-terminally with red fluorescent protein mCherry)	(Lazarou et al., 2015)

I.II.II Bacterial cell lines

Unique Identifier	Supplier	Genotype	Used for
α-Select Silver Efficiency	Bio-line (BIO-85027)	F- deoR endA1 recA1 relA1 gyrA96 hsdR17(rk- , mk+) supE44 thi-1 phoA Δ(lacZYA argF)U169 Φ80lacZΔM15λ-	DNA transformation and expression
NEB 5-alpha competent *E. coli*	New England Biolabs	fhuA2 Δ(argF-lacZ)U169 phoA glnV44 Φ80 Δ(lacZ)M15 gyrA96 recA1 relA1 endA1 thi-1 hsdR17	
BL21-CodonPlus(DE3)-RIL competent cells	Agilent Technologies (230132)	E. coli B F– ompT hsdS(rB-mB-) dcm+ Tetr gal λ(DE3) endA Hte [argU ileY leuW Camr]	Protein expression
DH10EMBacY	Geneva Biotech	Request from Supplier	Baculoviral expression

I.III Antibodies

I.III.I Primary antibodies

Antigen	Species	Dilution		Supplier (catalogue number)
		WB	**IF**	
FLAG (M2)	Mouse	1:5000	1:300	Sigma Life Science (F1804)
HA	Rat		1:300	Roche (3F10)
HA	Mouse	1:250		In house (12CA5)
Myc (9E10)	Mouse		1:400	Santa Cruz Biotechnology (sc-40)
α-Tubulin	Rat	1:250		In house (YL1/2)
TGN46	Sheep		1:300	ABD serotec (AHP500G)
Giantin	Goat		1:100	Santa Cruz Biotech (N-18/sc-46993)
Golgin-84	Rabbit		1:300	Atlas Antibodies (HPA000992)
GCC185	Rabbit		1:300	Atlas Antibodies (HPA035849)
GCC88	Rabbit	1:1000	1:300	Sigma Life Science (HPA019369/HPA021323)
ZFPL1	Rabbit		1:300	Sigma Life Science (HPA014909)
COXIV (3E11)	Rabbit		1:200	New England Biolabs (4850S)
TOM20	Mouse		1:300	Santa Cruz Biotechnology (sc-17764)
CI-MPR	Mouse		1:300	Abcam (ab2733)
OSBPL9	Rabbit	1:1000		Abcam (ab151691)
TBCK	Rabbit	1:500		Cambridge Bioscience (HPA039951)
RELCH/KIAA1468	Rabbit	1:1000		Cambridge Bioscience (HPA040038)
RELCH/KIAA1468	Rabbit	1:1000		Atlas Antibodies (HPA014570)
ARFGEF3	Rabbit	1:1000		Thermo Fisher Scientific (PA5-57623)
STAMBPL1	Rabbit	1:1000		Sigma Life Science (SAB4200146)
GBF1	Mouse	1:1000		BD Transduction Laboratory (612116)
NDE1	Rabbit	1:500		Life Technologies (711424)
SIPA1L2	Rabbit	1:1000		Invitrogen (PA5-20848)
ALS2 WB	Rabbit	1:1000		Novus Bio (NBP2-14284)
ARFGEF2	Mouse	1:1000		Santa Cruz Biotechnology (sc-398042)

Antigen	**Species**	**Dilution**		**Supplier (catalogue number)**
		WB	**IF**	
SH3BP5L	Rabbit	1:1000		Aviva Systems Biology (ARP71605-P050)
VPS34	Rabbit	1:1000		Proteintech (12452-1-AP)
VPS15	Rabbit	1:1000		Proteintech (17894-1-AP)
UVRAG	Rabbit	1:1000		Cell Signalling Technology (5320S)
ATG14L	Rabbit	1:1000		Cell Signalling Technology (5504S)
Beclin-1	Rabbit	1:1000		Santa Cruz Biotechnology (sc-11427)
NRBF2	Rabbit	1:1000		GeneTex (GTX54585)
Rubicon	Rabbit	1:1000		Abcam (ab92388)
EEA1	Rabbit		1:300	Abcam (ab109110)
EEA1	Mouse		1:300	BD Transduction Laboratories (610457)
CALCOCO1	Rabbit	1:1000		Atlas Antibodies (HPA038313)
Rabaptin5	Mouse	1:1000		BD Transduction Laboratories (610676)
AKAP10	Rabbit	1:1000		Proteintech (12356-1-AP)
GRIPAP1	Rabbit	1:1000		Proteintech (15806-1-AP)
PPP1R37	Rabbit	1:1000		Atlas Antibodies (HPA041500)
PPP1R37	Rabbit	1:1000		Thermo Scientific (PA5-59597)
CLEC16A	Goat	1:1000		Novus Bio (NBP1-36948)
LC3B	Rabbit		1:300	MBL (PM036)
LC3A/B	Mouse	1:1000		Santa Cruz Biotechnology (sc-398822)
P62	Mouse		1:300	MBL (M162-3)
P62	Mouse	1:1000		BD Transduction Laboratories (610832)
Sec16A	Rabbit		1:300	Atlas Antibodies (HPA005684)
CD63	Mouse		1:250	BD Biosciences (740080)
GFP	Rabbit	1:1000		Sigma Life Science (SAB4301138)

I.III.II Secondary antibodies

Antigen	Species	Dilution	Supplier (catalogue number)
Anti-Rabbit Alexa Fluor 488	Donkey	1:300	Thermo Fisher Scientific (A21206)
Anti-Rabbit Alexa Fluor 555	Donkey	1:300	Thermo Fisher Scientific (A31572)
Anti-Rabbit Alexa Fluor 647	Donkey	1:300	Thermo Fisher Scientific (A31573)
Anti-Rabbit HRP	Donkey	1:3000	GE Life Sciences (NA934V)
Anti-Mouse Alexa Fluor 488	Donkey	1:300	Thermo Fisher Scientific (A21202)
Anti-Mouse Alexa Fluor 555	Donkey	1:300	Thermo Fisher Scientific (A32773)
Anti-Mouse Alexa Fluor 647	Donkey	1:300	Thermo Fisher Scientific (A31571)
Anti-Mouse HRP	Sheep	1:3000	GE Life Sciences (NA931V)
Anti-Rat Alexa Fluor 488	Donkey	1:300	Thermo Fisher Scientific (A21208)
Anti-Rat Alexa Fluor 555	Donkey	1:300	Abcam (ab150154)
Anti-Rat Alexa Fluor 647	Goat	1:300	Thermo Fisher Scientific (A21247)
Anti-Rat HRP	Goat	1:3000	Abcam (ab205720)
Anti-Goat Alexa Fluor 555	Donkey	1:300	Thermo Fiscer Scientific (A21436)
Anti-Goat Alexa Fluor 647	Donkey	1:300	Thermo Fisher Scientific (A32849)
Anti-Sheep Alexa Fluor 647	Donkey	1:300	Thermo Fisher Scientific (A21448)

II. Methods

II.I Molecular cloning

II.I.I DNA manipulation

DNA manipulations were performed using specified kits and carried out according to the manufacturer's protocol. Plasmid DNA was prepared from bacterial liquid cultures using Qiagen plasmid kits and were eluted in TE buffer. Mammalian genomic DNA was purified from cultured cells using the Qiagen DNA extraction kit. DNA amplifications were performed using Phusion High-Fidelity DNA Polymerase (New England Biolabs) with GC buffer, an annealing time of 30 seconds and an extension time of 30s/kbp. DNA digestions were performed for 60 minutes at 37°C using New England Biolabs restriction enzymes and its

corresponding CutSmart buffer. DNA fragments were resolved by gel electrophoresis using a 1.2% agarose gel with SYBR Safe DNA gel stain (Thermo Fisher Scientific). A 1kb+ DNA ladder was loaded together with DNA fragments, and the gels were visualised using a Safe Image Blue-Light Transilluminator (both Thermo Fisher Scientific). Excised bands were purified using the Qiagen gel extraction kit. DNA fragments were ligated using T4 DNA Ligase (New England Biolabs) for 60 minutes at room temperature.

Gibson Assembly backbone and insert DNA were generated by performing PCR DNA amplifications using Gibson-appropriate primers. Gibson Assembly reactions were performed by mixing 3 µL backbone DNA, 1 µL insert DNA and 7.5 µL Gibson Assembly master mix (New England Biolabs). The mixture was incubated for 1 hour at 50°C, and was either stored at 4°C or immediately used for bacterial transformation onto plates.

II.I.II Cloning strategies

Small GTPase chimeras for MitoID assays were generated by fusing the GTPases lacking the C-terminal cysteines to a GAGAGA linker, the promiscuous biotin ligase BirA*, another GAGAGA linker, the HA epitope, a GAGA linker, and the mitochondrial targeting sequence of monoamine oxidase (MAO). These chimeras were cloned into a pcDNA3.1+ vector and used for transiently transfecting mammalian cultured cells.

FLAG-, HA-, Myc-, GFP-, His_6-, and mCherry-tagged proteins were for transient expression in mammalian cultured cells for co-localisation and recruitment experiments by confocal microscopy or to serve as baits for affinity chromatography experiments. All fusion proteins contained a GAGA linker between the tag and the protein of interest, whether tagged on the N- or C-terminus, and were cloned into pcDNA3.1+. Small GTPases were tagged N-terminally whenever possible, with C-terminal tags only being used with mitochondrial re-localisation in combination with the removal of C-terminal cysteines, allowing for proper membrane incorporation. Effector proteins were tagged on either end, after which both chimeras were tested to allow for assay optimisation. All plasmids containing N- or C-terminally tagged proteins were supplied by Alison Gillingham or Lawrence Welch.

GTP- and GDP-locked Rab1A and Rab1B were fused to GST on either their N- or C-terminus, and cloned into pAceBac1 vectors to allow baculoviral expression (see below).

PPP1R37 truncations were created by PCR amplifying residues 1-448 and 449-691 of wildtype PPP1R37 and cloning into pcDNA3.1+ containing an N-terminal FLAG tag (supplied by Lawrence Welch) through traditional restriction enzyme cloning.

II.I.III transformation and growth of bacteria

Bacterial lines stored at -80°C were thawed on ice for 30 minutes and, after which 1-2 µL of plasmid DNA was added to 15 µL of bacterial cells. The mixture was incubated on ice for 30 minutes, heat shocked at 42°C for 45 seconds and placed back on ice. SOB medium was added and the mixtures were incubated at 37°C to allow for antibiotic expression; 1 hour for BL21, α-select and DH5-alpha cells, and 4 hours for DH10EMBacY cells. Bacteria were then plated on 2xTY or LB agar plates with appropriate antibiotics and grown overnight at 37°C. Resulting single colonies of BL21, α-select, and DH5-alpha cells were used for inoculation of liquid cultures of 2 mL 2xTY medium with appropriate antibiotics. DH10EMBacY colonies were screened for successful transposition by blue-white screening.

II.II Mammalian cell biology

II.II.I Cell culture, cryopreservation, transfection, and RNAi

HeLa, HEK293T, and U2OS cells were cultured in Dulbecco's Modified Eagle's Medium with high glucose (DMEM GlutaMAX+, Thermo Fisher Scientific) and 10% supplemented fetal calf serum (FCS) at 37°C and with 5% CO_2. Cell lines were regularly tested to ensure that they were mycoplasma free, using the MycoAlert kit (Lonzo). Cells were passaged consistently to ensure healthy confluency, by washing with EDTA solution and incubating in trypsin solution at 37°C for 2-5 minutes (both MRC LMB media kitchen). Cells were resuspended in culture medium and replated for either maintaining a cell stock or for further experiments. Long term storage was achieved by pelleting resuspended cells for 5 minutes at 1000rpm and resuspending in freezing medium (10% DMSO, 50% FCS, 40% DMEM GlutaMAX+), after which they were stored in cryovials at -80°C.

For immunofluorescence experiments, U2OS or HeLa cells were seeded in 6-well plates to achieve 60-80% confluency at the time of transfection. A total of 1 mg of DNA was mixed with 4 µL FuGENE 6 (Promega) or PEI (MRC LMB media kitchen) and 100 µL Opti-MEM media (Thermo Fisher). The mixture was incubated for 20 minutes and added to the cells for 24 hours. 24 hours prior to fixation, cells were trypsinated, resuspended, and seeded onto microscope slides.

For MitoID and affinity chromatography experiments, HEK293T cells were seeded in T175 flasks in culture medium at 37°C with 5% CO_2. 2 mL Opti-MEM medium was mixed with 75 µL FuGENE 6 or PEI and 25 mg DNA. After gentle mixing and incubating at room temperature for 20 minutes, the mixtures were added to the flasks. 48 hours after transfection, cells require for affinity chromatography were resuspended by tapping of the flask and addition of ice cold PBS. Cells were pelleted by 5 minute centrifugation of 1000rpm at 4°C. Cells were kept on ice prior to immediate use, or snap frozen in liquid nitrogen and kept at -80°C

for long term storage. Cells required for MitoID assays were supplemented with a final concentration of 50 mM biotin, 24 hours before use.

HeLa cells stably expressing mCherry-Parkin were previous described by (Lazarou et al., 2015).

For RNAi protein depletion, U2OS cells were seeded in 6-well plates to achieve 60-70% confluency at time of transfection. One hour prior to transfections, cells were gently washed and given fresh culture medium. 30 nM siRNAs were diluted in 100 µL working solution of GenMute Transfection Buffer (SignaGen). After gentle mixing, 2.4 µL GenMute Reagent was added and the mixture was left to incubate at room temperature for 15 minutes. The mixture was added dropwise to cells and left to incubate for 5 days at 37°C with 5% CO_2. 24 hours before fixation, cells were trypsinised, resuspended, and seeded on microscopy slides.

II.II.II Autophagic induction and lysosomal inhibition

For autophagic induction by starvation, cells were washed twice with EDTA and incubated for 4 hours with EBSS (Earle's Balanced Salt Solution) medium at 37°C and 5% CO_2. Autophagic induction by was performed by washing the cell culture medium off adhered cells and adding 100 mM Trehalose in fresh medium. Cells were incubated at 37°C and 5% CO_2 for 24 hours prior to fixation or lysis. Lysosomal inhibition was achieved by adding 100 nM Bafilomycin-A1 to the autophagic induced cells 4 hours prior to fixation or lysis. Cells were either fixed on microscope slides and used for immunofluorescent staining, or lysed in 6-well plates using 2x Tris-glycine sample buffer (Invitrogen) with 5% β-mercaptoethanol.

II.II.III Mitochondrial stress induction

10 mM CCCP (carbonyl cyanide m-chlorophenylhydrazone) diluted in DMSO was added to HeLa cells stably expressing mCherry-Parkin (Lazarou et al., 2015). The cells were incubated for 3 hours at 37°C and with 5% CO_2, after which they were immediately fixed and used for immunofluorescent staining.

II.III Insect Cell Biology

II.III.I Cell culture

Sf9 cells were cultured and prepared for order by the MRC LMB Baculovirus Facility, and were incubated at 25°C at 140rpm.

II.III.II Baculoviral expression system

Sf9 cells were seeded at a density of 10^6 cells/cm^2 in Insect Xpress culture medium (Lonza) at 27°C and allowed to adhere for 10-15 minutes. Cells were transfected with 2 µg bacmid DNA using Fugene HD (Promega) according to manufacturer's protocol. After incubating at 27°C for 3-5 days, the culture medium was aspirated and added to 50 mL suspended Sf9 cells at a density of $2x10^6$ cells/mL in 250 mL Erlenmeyer flasks. After a further 3-5 days incubation at 27°C with 140rpm, culture medium containing the virus was used to inoculate 500 mL cultures to enhance the viral titer, after which the cells were pelleted at 2500g for 10 minutes and snap frozen in liquid nitrogen. Cell pellets were kept at -80°C until use for protein purification.

II.IV Immunofluorescence microscopy

Cells were seeded onto multisport coated slides (Hendley-Essex) in culture medium at 37°C with 5% CO_2 in a closed humid container. If cells were subjected to autophagic induction, lysosomal inhibition, or mitochondrial stress induction (as described above), this was performed 24 hours after seeding to allow cell adherence. Slides were moved to room temperature and cells were fixed in 4% PFA for 20 minutes. Cells were washed twice in PBS, permeabilised with 0.15% Triton-x100/PBS, washed 3x with PBS, and incubated in blocking buffer (20% FCS, 0.5% Tween-20, PBS) for 1 hour. Primary antibodies (see above) were diluted in blocking buffer and incubated on the cells for 1 hour at room temperature. Cells were washed 5x with 0.05% Tween in PBS after which secondary antibodies diluted in blocking buffer were added to the cells. After incubating for 1 hour at room temperature, cells were washed a further 5x in 0.05% Tween-20/PBS and once in PBS. PBS was fully aspirated and cells were mounted in Vectashield mounting media (Vector Laboratories), after which a coverslip was placed over the microscope slide and sealed by clear nail polish. Microscope slides were imaged using a Leica TCS SP8 confocal microscope using an 63x oil objective.

II.V Biochemistry

II.V.I Protein sample preparation

Pelleted mammalian and insect cells were resuspended in lysis buffer consisting of 50 mM Tris HCl pH 7.4, 150 mM NaCl, 1 mM EDTA, 0.5% Triton X-100, 1 mM PMSF (Sigma) and the cOmplete EDTA-free protease inhibitor cocktail (Roche) on ice. Cells were incubated for 20-30 minutes at 4°C with agitation.

Cells were pelleted by centrifugation at 32.000rpm for 10 minutes at 4°C, after which the supernatant was either immediately used for protein purification or ran on SDS-PAGE protein gels for resolution.

II.V.II GST affinity chromatography of insect cell expressed Rab1A and Rab1B

Glutathione sepharose 4B beads (GE Life Sciences) were washed with lysis buffer and pelletted by centrifugation at 100 x g for 1 minute. Beads were mixed with clarified Sf9 lysate from strains expressing GST-tagged fusion proteins and incubated with agitation at 4°C for 30 minutes. Next, beads were washed once with lysis buffer, once with high salt lysis buffer (lysis buffer with 500 mM NaCl) and another four times with lysis buffer. Mammalian cell lysates, either wildtype or transiently expressing FLAG-tagged proteins, were mixed with the beads coated with GST-tagged proteins and incubated for 1 hour with agitation at 4°C. Beads were washed 5 times with lysis buffer, after which interacting proteins were eluted by boiling the beads at 98°C for 5 minutes in 2x Tris-glycine sample buffer (Invitrogen) with 5% β-mercaptoethanol.

In case of studying direct binding, FLAG-tagged proteins were isolated by incubation with FLAG M2 affinity resin (Sigma) for 1 hour at 4°C with agitation. Beads were washed 5x in lysis buffer and proteins were eluted in 100 mg/ml 3x FLAG peptide (Sigma) in 25 mM Tris-HCl pH 7.4, 250 mM NaCl, and 1 mM EDTA. Isolated FLAG-tagged proteins were mixed with GST-coated beads and continued as described above.

II.V.III Affinity chromatography of E. coli expressed Rab2A, Rab5A, Rab6A, Rab9A, and Rab11A

GTP- and GDP-locked Rab GTPases were expressed in *E. coli* strain BL21-GOLD (DE3; Agilent Technologies) as GST-fusion proteins. Bacteria were grown at 37°C to an OD600 of 0.7 and induced with 100 mM IPTG overnight at 16°C with agitation. Cells were pelleted by centrifugation, dounce homogenised and sonicated in lysis buffer (50 mM Tris-HCl, pH 7.4, 150 mM NaCl, 5 mM MgCl2, 1% Triton X-100, 5 mM β-mercaptoethanol, plus 1 EDTA-free complete protease tablet/50 ml, 1 mM PMSF and either 100 mM non-hydrolysable GTP analog (GppNHp, Sigma) or 100 mM GDP as appropriate). The lysates were clarified by centrifugation at 12,000g for 15 min and GST-Rab proteins were added to washed glutathione Sepharose beads (GE Healthcare) for 30 min at 4°C with agitation. After incubation, beads were washed extensively to remove unbound material. HEK293T cells from 5 T175 cm^2 flasks were collected, washed and lysed in 10 mL lysis buffer (as described above). The lysate was divided equally and applied to 50 ml of GST-Rab coated beads with either 100 mM non-hydrolysable GTP (GppNHp) or 100 mM GDP added as appropriate. Beads were incubated, washed and proteins eluted in high salt buffer (lysis buffer with 500 mM NaCl). Proteins were precipitated and analysed by immunoblotting with the indicated antibodies.

To assess the interaction between Rab9A and HPS3, 1 T175cm^2 flask of HEK293T cells was transfected with FLAG-tagged HPS3 using Fugene 6 (Promega). After 24 hours of incubation, cells were lysed and incubated with beads coated with GST-Rab GTPases, and continued as described above.

II.V.IV Affinity chromatography of GST-Rab2A and purified STAMBPL1

1 T175 cm^2 flask of HEK293T cells was transfected with GFP-FLAG-STAMBPL1 using Fugene 6 (Promega). Cells were lysed as described above and GFP-FLAG-STAMBPL1 was isolated by incubation with FLAG M2 affinity resin (Sigma) for 1 hour at 4°C with agitation. Beads were washed 5x in lysis buffer and proteins were eluted in 100 mg/ml 3x FLAG peptide (Sigma) in 25 mM Tris-HCl pH 7.4, 250 mM NaCl, and 1 mM EDTA. Isolated GFP-FLAG-STAMBPL1 was added to glutathione Sepharose beads (GE Healthcare) coated in GST-Rab2A and incubated at 4°C for 2 hours with agitation. Beads were then washed in lysis buffer, before bound proteins were eluted in high salt buffer (25 mM Tris-HCL, pH7.4, 1.5 M NaCl, 20 mM EDTA, 5 mM β-mercaptoethanol and 1 mM of the opposing nucleotide). Proteins were precipitated with chloroform/methanol, and resuspended in SDS sample buffer with 1 mM β-mercaptoethanol.

II.V.V Affinity chromatography of GST-Rab2A and ARFGEF3 isolated from rat brain

Rat brain was harvested rapidly and placed into ice-cold PBS. Following several washes in PBS, the brain was minced into small pieces and 50 mL of lysis buffer was added (20 mM Tris-HCl, pH8, 150 mM KCl, 5 mM $MgCl_2$,,1 mM PMSF, 1% (w/v) CHAPS, and 1 EDTA-free complete protease tablet/25 ml buffer). The material was dounce homogenised, solubilised by rotation at 4°C for 3 hours and centrifuged at 100.000g for 60 min at 4°C. The supernatant was stored in aliquots at -80°C. For each affinity chromatography experiment, 5 mL of supernatant was applied to 50 mL of GST-Rab coated glutathione Sepharose beads. The beads were then incubated and processed as previously described, except 1% (w/v) CHAPS replaced Triton X-100 in the wash buffer.

II.V.VI Affinity chromatography of GSWT-Rab9A with purified NDE1

NDE1 was expressed BL21-GOLD *E. coli* as a fusion to a N-terminal His_6 tag with a dihydrolipoyl acetyltransferase solubility tag and a TEV cleavage site between the His_6 tag and the NDE1 insert. Lysates containing NDE1 were incubated with glutathione-Sepharose beads to pre-clear the sample prior to incubation with 50 ml GST-Rab coated beads for 2 hours at 4°C with rotation. Beads and protein complexes were washed 5x in lysis buffer, as previously described, and proteins were eluted in SDS sample buffer with 1 mM β-mercaptoethanol.

II.V.VII MitoID assays and streptavidin affinity chromatography

The MitoID protocol was adapted from the BioID method (Roux et al., 2012). Briefly, HEK293T cells were grown in T175 flasks, and transfected using two flasks per bait (as described above). 24h after transfection, biotin was added to a final concentration of 50 µM, and further incubated at 37°C for 18-24 hours. Cells were pelleted by centrifugation for 5 mins at 1000rpm and at 4°C, washed once in ice cold PBS, and resuspended in lysis buffer (25 mM Tris pH 7.4, 150 mM NaCl, 1 mM EDTA, 1% (v/v) Triton X-100, 1 mM PMSF, and 1cOmplete protease inhibitor tablet (Roche) per 50 mL buffer. One pellet containing 2x T175 cells was mixed with 1mL lysis buffer and incubated for 30 mins at 4°C with rotation. After centrifugation at 32.000rpm for 10 minutes at 4°C, the supernatants were added to 500 µL MyOne Streptavidin C1 Dynabead (Invitrogen) that had be pre-washed twice in lysis buffer. The beads were incubated at 4°C overnight and the next morning were washed twice with Wash Buffer 1 (2% SDS, cOmplete inhibitors), three times in Wash Buffer 2 (1% (v/v) Triton X-100, 0.1% (w/v) deoxycholate, 500 mM NaCl, 1 mM EDTA, 50 mM HEPES, cOmplete inhibitors, pH 7.5), and three times in Wash Buffer 3 (50 mM Tris pH 7.4, 50 mM NaCl, cOmplete inhibitors). Finally, beads were incubated in 75 µL SDS sample buffer containing 3 mM biotin and heated for 3 minutes at 98°C, after which 1 mM β-mercaptoethanol was added to the samples. Samples were either used immediately or snap frozen and stored at -20°C. All MitoID experiments were performed as biological triplicates for each GTPase bait; transfection and affinity chromatography assays were performed and processed separately.

II.V.VIII Resolution of protein samples

Protein samples were incubated for 3 minutes at 90°C prior to loading onto Novex 4-20% Tris-Glycine Mini Gels (Thermo Fisher Scientific). After 1 hour at 175V, proteins were either stained by incubating InstantBlue Coomassie stain for 1 hour at room temperature, or transferred onto 0.45 µm nitrocellulose paper using 255 mA. Transferred Western blots were blocked in 5% milk in 0.01% Tween-20/PBS for 1 hour at room temperature with agitation. Blots were incubated with primary antibodies diluted in blocking buffer for 1 hour at room temperature of overnight at 4°C, after which blots were washed 4x for 5 minutes in 0.01% Tween-20/PBS. Next, blots were incubated with HRP-conjugated secondary antibodies diluted in blocking buffer for 1 hour at room temperature, after which blots were washed as described above and once in PBS. Proteins were detected by incubating in ECL detection agent (Amersham) for 3 minutes at room temperature prior to exposure to X-ray films (Photon Imaging Systems). The films were developed using a JP-33 film processor (JPI Healthcare Solutions). Alternatively, Western blots were scanned by the Amersham Typhoon Biomolecular Imager (GE Life Sciences).

II.V.IX GUV assays, cryo-EM, HDX-MS

All GUV assays, cryo-Electron Microscopy, and Hydrogen-Deuterium Exchange experiments were performed by the Williams group (MRC LMB, UK). Detailed descriptions of the protocols and reagents used are stated in (Tremel et al., 2021)

II.VI Mass spectrometry

Protein samples obtained from affinity chromatography and proximity biotinylation were loaded on 4-20% Tris-Glycine SDS-PAGE gels and run for 1-2 centimetres. Gels were stained with Coomassie InstantBlue, after which each gel lane was cut into eight pieces and placed in a 96-well plate. The 96-well plates were handed to the MRC LMB Mass Spectrometry Facility, where the gels were destained with 50% v/v acetonitrile and 50 mM ammonium bicarbonate, reduced with 10 mM DTT, and alkylated with 55 mM iodoacetamide. Proteins were digested with 6 ng/µL trypsin (Promega) by overnight incubation at 37°C, after which peptides were extracted in 2% v/v formic acid and 2% v/v acetonitrile, and analysed by nano-scale capillary LC-MS/MS (Ultimate U3000 HPLC, Thermo Scientific Dionex) at a flow of ~ 300 nL/min. Peptides were trapped (C18 Acclaim PepMap100 5 µm, 100 µm x 20 mm nanoViper) and separated (C18 Acclaim PepMap 100 3 µm, 75 µm x 250 mm nanoViper), after which they were eluted with an acetonitrile gradient. The analytical column outlet was interfaced via a nano-flow electrospray ionisation source with a linear ion trap mass spectrometer (Orbitrap Velos, Thermo Scientific). A resolution of 30.000 for the full MS spectrum was used to perform data dependent analysis, followed by ten MS/MS spectra in the linear ion trap. MS spectra were collected over a m/z range of 300-2000, after which MS/MS scans were collected using a threshold energy of 35 for collision-induced dissociation. LC-MS/MS data were searched against the UniProt KB database using Mascot (Matrix Science), with a precursor tolerance of 5 ppm and a fragment ion mass tolerance of 0.8 Da. The gene RABGAP1L has two entries, RBG1L_HUMAN and RBG10_HUMAN, and so the latter was removed. Variable modifications for oxidised methionine, carbamidomethyl cysteine, pyroglutamic acid, and phosphorylated serine, threonine and tyrosine were included.

II.VII Data analysis

II.VII.I Analysis of confocal micrographs

Confocal micrographs taken on either a laser scanning or spinning disc confocal microscope were processed and analysed using Fiji/ImageJ.

II.VII.II Bubble plot generation

LC-MS/MS data were validated using the Scaffold Programme (Proteome Software Inc). To score the significance of interactors, total spectral counts were converted into WD-scores according to the CompPASS method (Sowa et al., 2009). WD-scores of all tested small GTPases using Bir* were processed in Microsoft Excel, generating so-called bubble plots which visualise the size of the WD-score via the area of the bubbles. When only one or several GTPases are shown in a bubble plot, the WD-scores of the entire comparative dataset were taken, ensuring correct scores. The only exception is for the data described in Chapter 4; when visualising the data of BioID2/TurboID or phospho-mimetic mutants, WD-scores were calculated solely on the GTPases visible in the bubble plots.

II.VII.III Volcano plot generation

Volcano plots were generated as described in (Gillingham et al., 2019). Briefly, LC-MS/MS data were processed in MaxQuant and analysed on the Perseus platform. Two sample Student's t-tests were performed in which GTP-locked GTPases were compared against the entire set of GDP-locked baits, with the number of randomisations set at 250. Analysis was performed by Mark Skehel and Alison Gillingham, and volcano plots were generated by Sean Munro (MRC LMB, UK).

Supplementary material

Table 1. GTP- and GDP-locked mutations for all tested GTPases. Nucleotide-locked point mutations were made, either by using known functional mutants based on previous research or by mutating the equivalent residues in lesser studied GTPases.

GTPase	GTP-locked	GDP-locked
Rab1A	Q70L	S25N
Rab1B	Q67L	S22N
Rab2A	Q65L	S20N
Rab5A	Q79L	S34N
Rab6A	Q72L	T27N
Rab7A	Q67L	T22N
Rab8A	Q67L	T22N
Rab9A	Q66L	S21N
Rab10	Q68L	T23N
Rab11A	Q69L	S25N
Rab11B	Q70L	S25N
Rab18	Q67L	S22N
Rab19B	Q76L	T31N
Rab21	Q78L	T33N
Rab29	Q67L/A16V	T21N
Rab30B	Q68L	T23N
Rab33B	Q92L	T47N
Rab39B	Q68L	S22N
Rab43	Q77L	T32N
Cdc42	G12V	T17N
Rac1	Q60L	T17N
RalB	G23V	S29A
Rheb	Q64L	S20N
RhoA	Q63L	T19N
N-Ras	Q60L	T17N

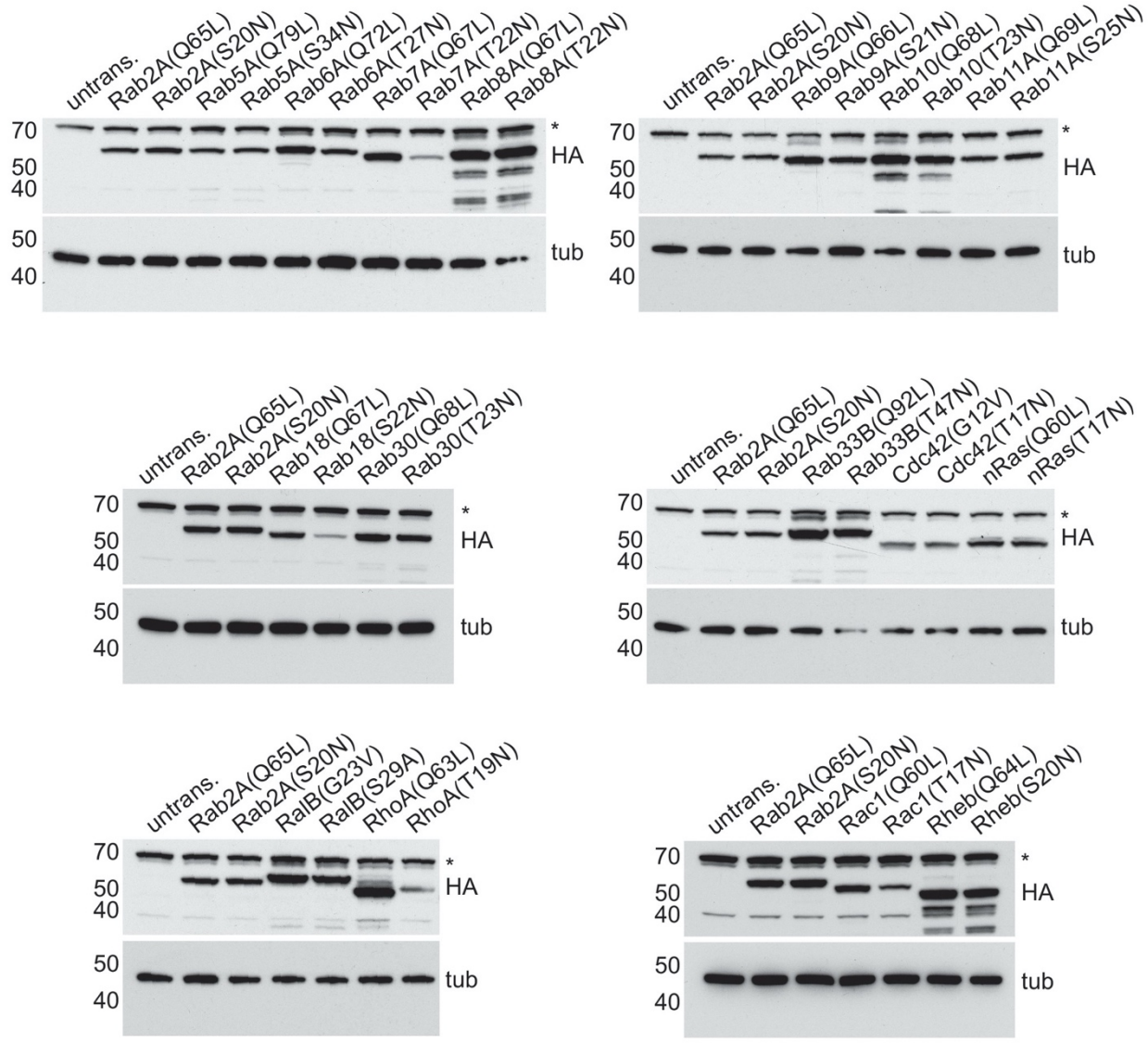

Supplementary Figure 2.1. Expression levels of GTPase-BirA*-HA-MAO chimeras. Immunoblots of whole cell lysate of HEK293T cells expressing mitochondrially-tagged GTPase chimeras, stained for HA (chimera) and α-tubulin (expression level control). Untrans.: untransfected, wildtype HEK293T lysate. The HA antibody has a non-specific background band (also found in untransfected cell lysate), marked with an asterisk (*).

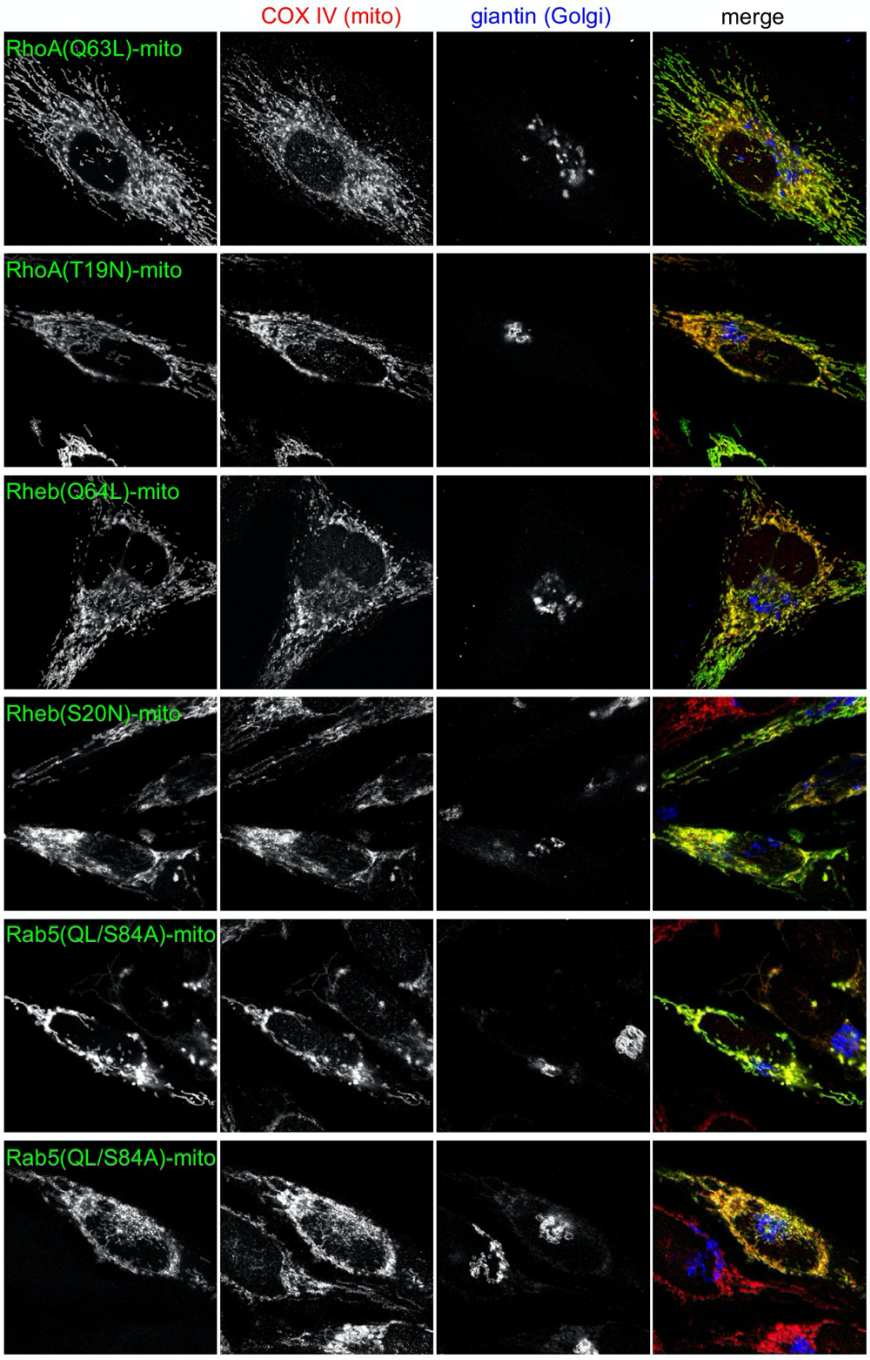

Supplementary Figure 2.2. Representative micrographs of mitochondrially localised GTPase chimeras. Confocal images of HeLa cells expressing mitochondrial GTPase chimeras (as indicated) and stained for HA (internal chimera epitope tag), COXIV (mitochondrial marker) and giantin (Golgi marker).

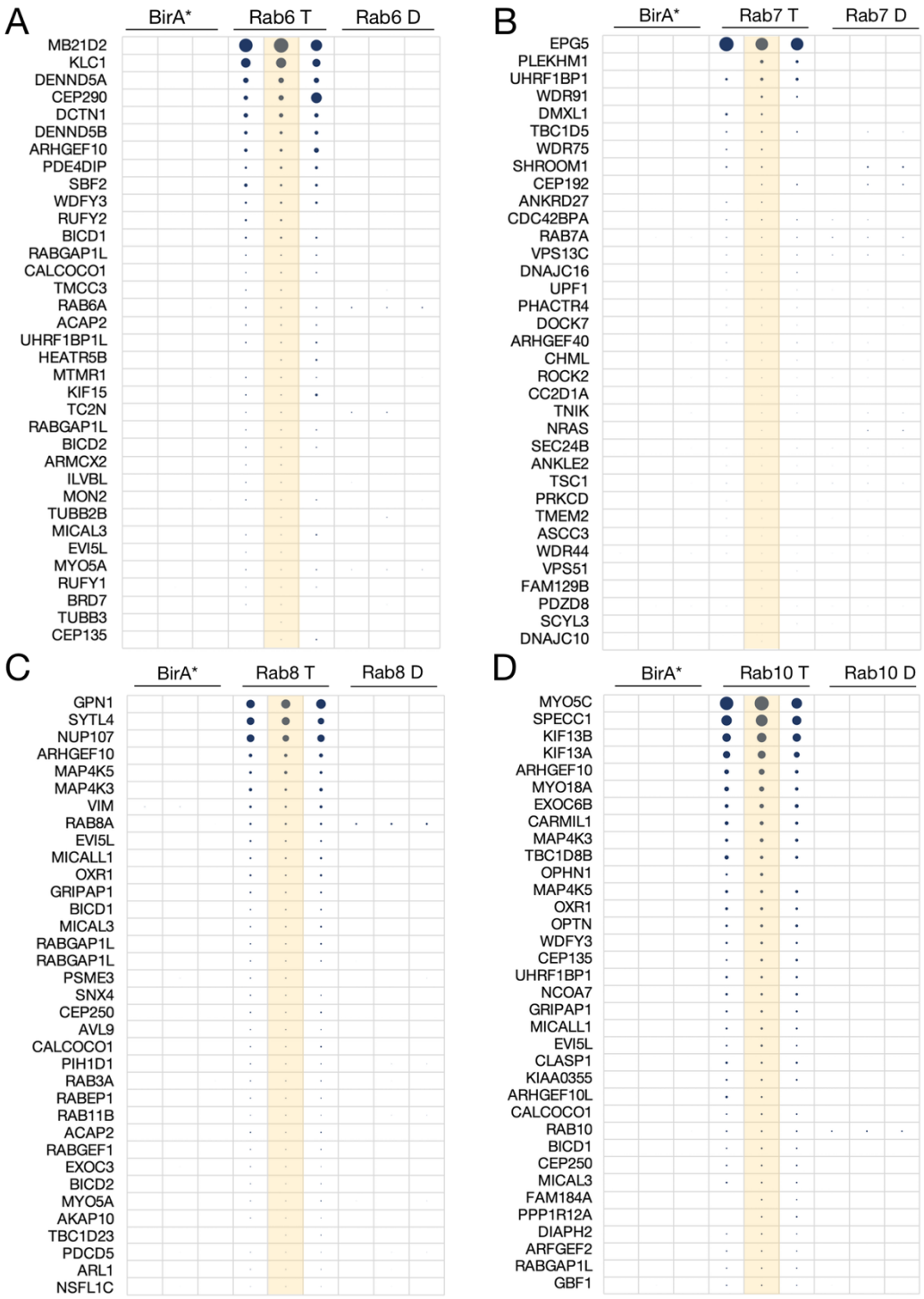

Supplementary Figure 3.1. Analysis of GTP-locked Rab6A, Rab7A, Rab8A, and Rab10 MitoID experiments. (A-D) Bubble-volcano plots showing GTP-locked Rab6A (A), Rab7A (B), Rab8A (C), and Rab10 (D) plotted against all tested GDP-locked GTPases. Circle area corresponds to WD-score. Data analysed by Alison Gillingham, plots generated by Sean Munro.

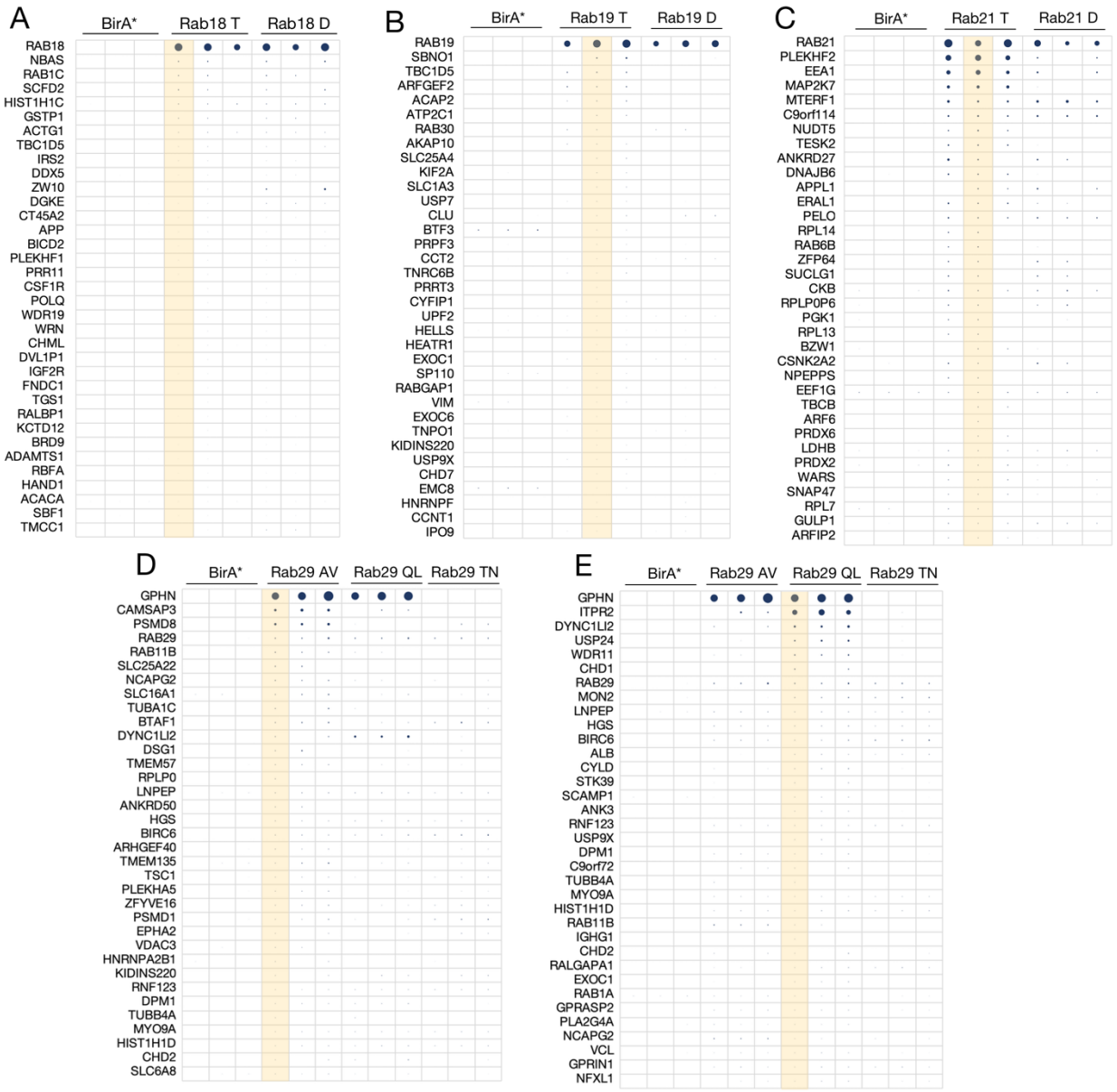

Supplementary Figure 3.2. Analysis of GTP-locked Rab18, Rab19B, Rab21, and Rab29 MitoID experiments. (A-E) Bubble-volcano plots showing GTP-locked Rab18 (A), Rab19B (B), Rab21 (C), Rab29A (Q67L) (D), and Rab29 (A16V) (E) plotted against all tested GDP-locked GTPases. Circle area corresponds to WD-score. Data analysed by Alison Gillingham, plots generated by Sean Munro.

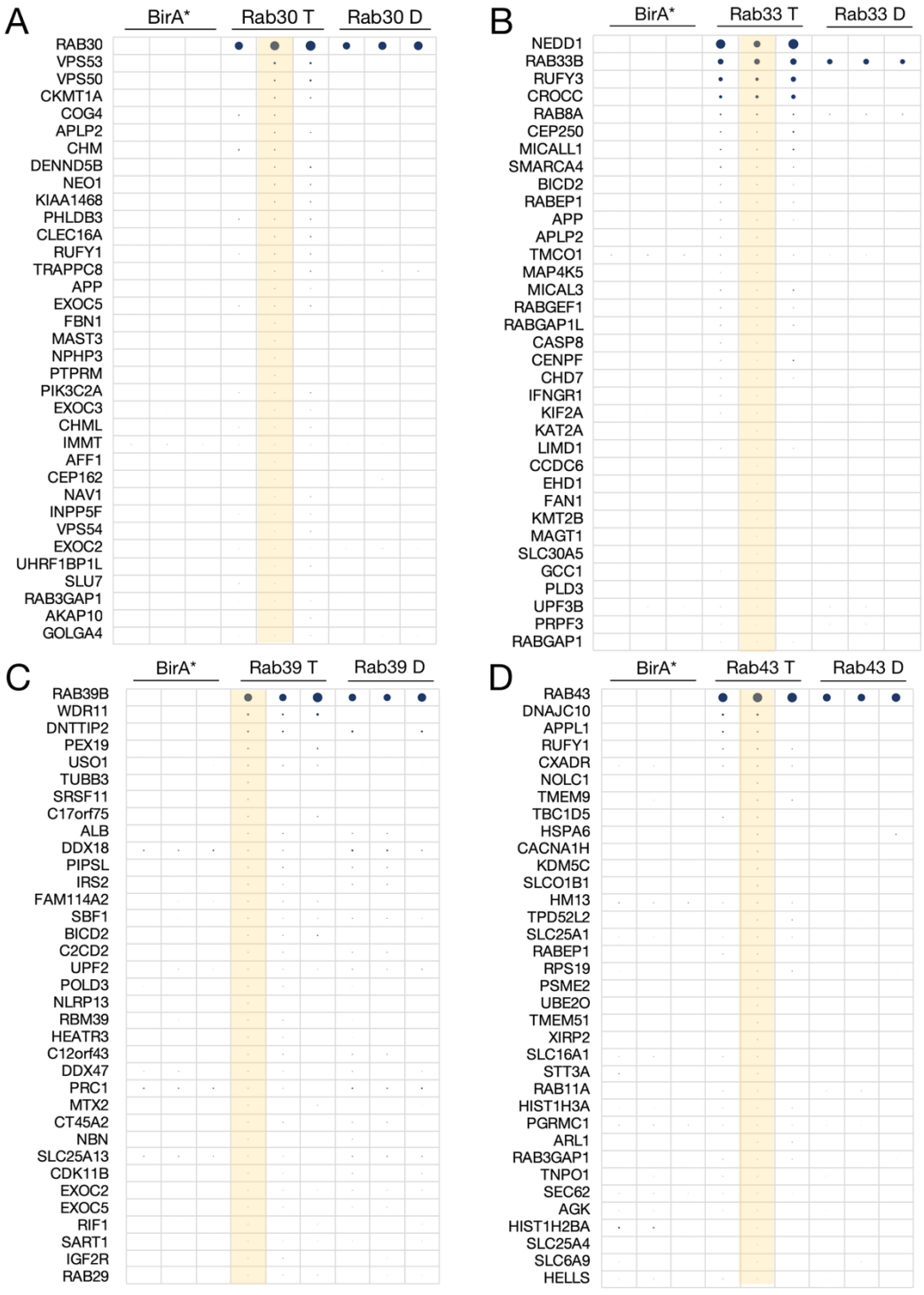

Supplementary Figure 3.3. Analysis of GTP-locked Rab30, Rab33B, Rab39B, and Rab43 MitoID experiments. (A-D) Bubble-volcano plots showing GDP-locked Rab30 (A), Rab33B (B), Rab39B (C), and Rab43 (D) plotted against all tested GDP-locked GTPases. Circle area corresponds to WD-score. Data analysed by Alison Gillingham, plots generated by Sean Munro.

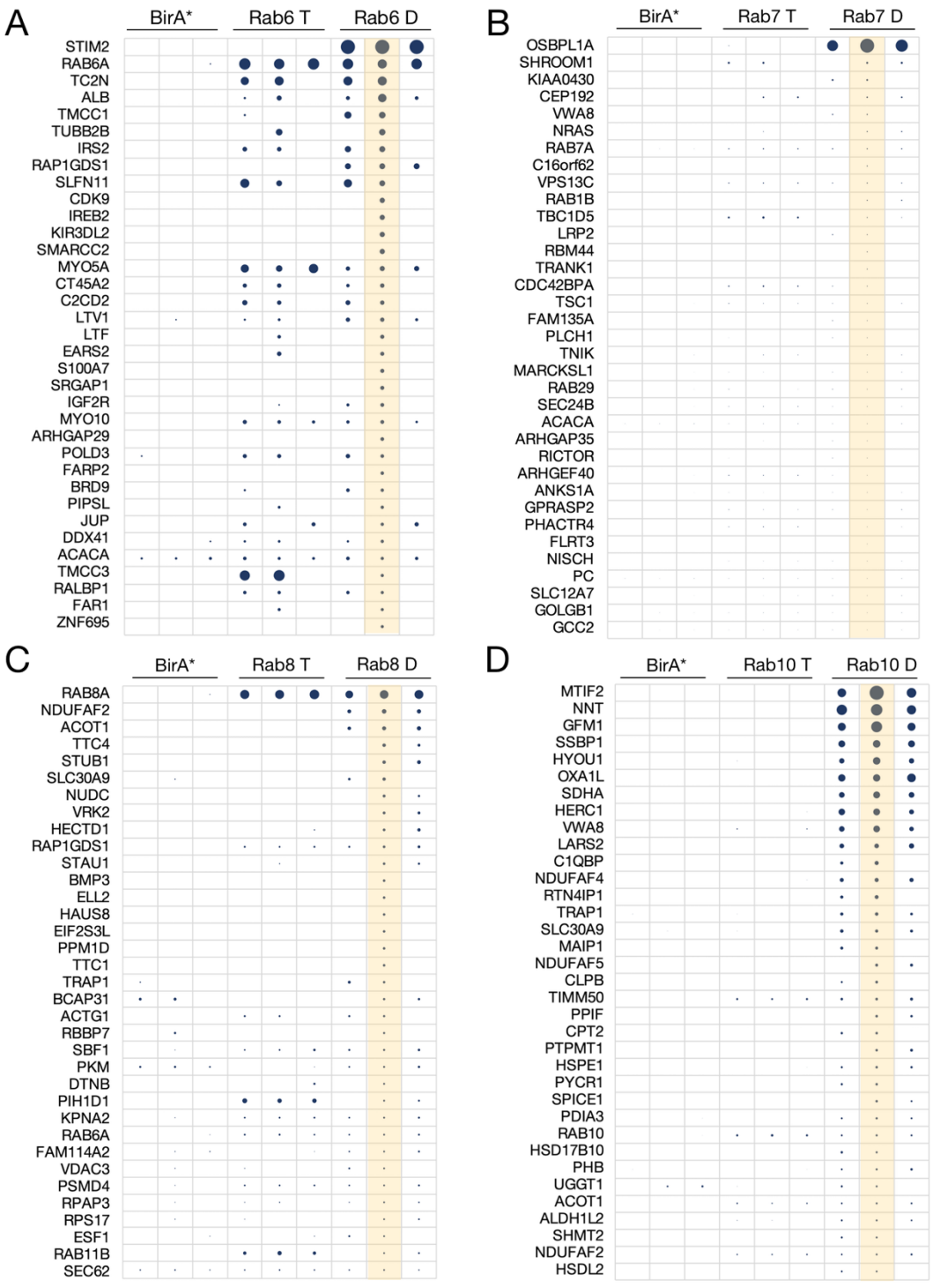

Supplementary figure 3.4. Analysis of GDP-locked Rab6A, Rab7A, Rab8A, and Rab10 MitoID experiments. (A-D) Bubble-volcano plots showing GDP-locked Rab6A (A), Rab7A (B), Rab8A (C), and Rab10 (D) plotted against all tested GDP-locked GTPases. Circle area corresponds to WD-score. Data analysed by Alison Gillingham, plots generated by Sean Munro.

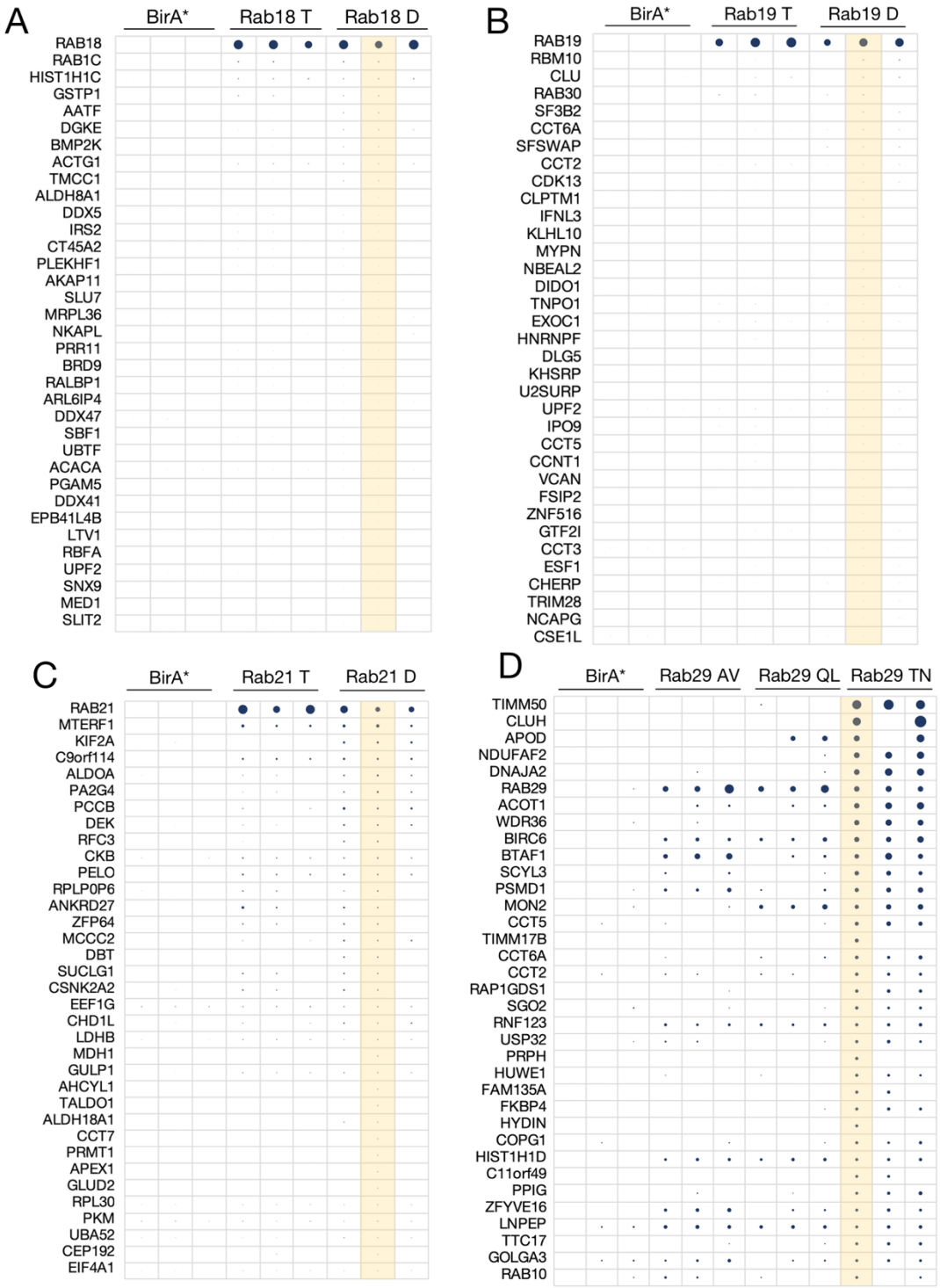

Supplementary figure 3.5. Analysis of GDP-locked Rab18, Rab19B, Rab21 and Rab29 MitoID experiments. (A-D) Bubble-volcano plots showing GDP-locked Rab18 (A), Rab19B (B), Rab21 (C) and Rab29 (D) plotted against all tested GDP-locked GTPases. Circle area corresponds to WD-score. Data analysed by Alison Gillingham, plots generated by Sean Munro.

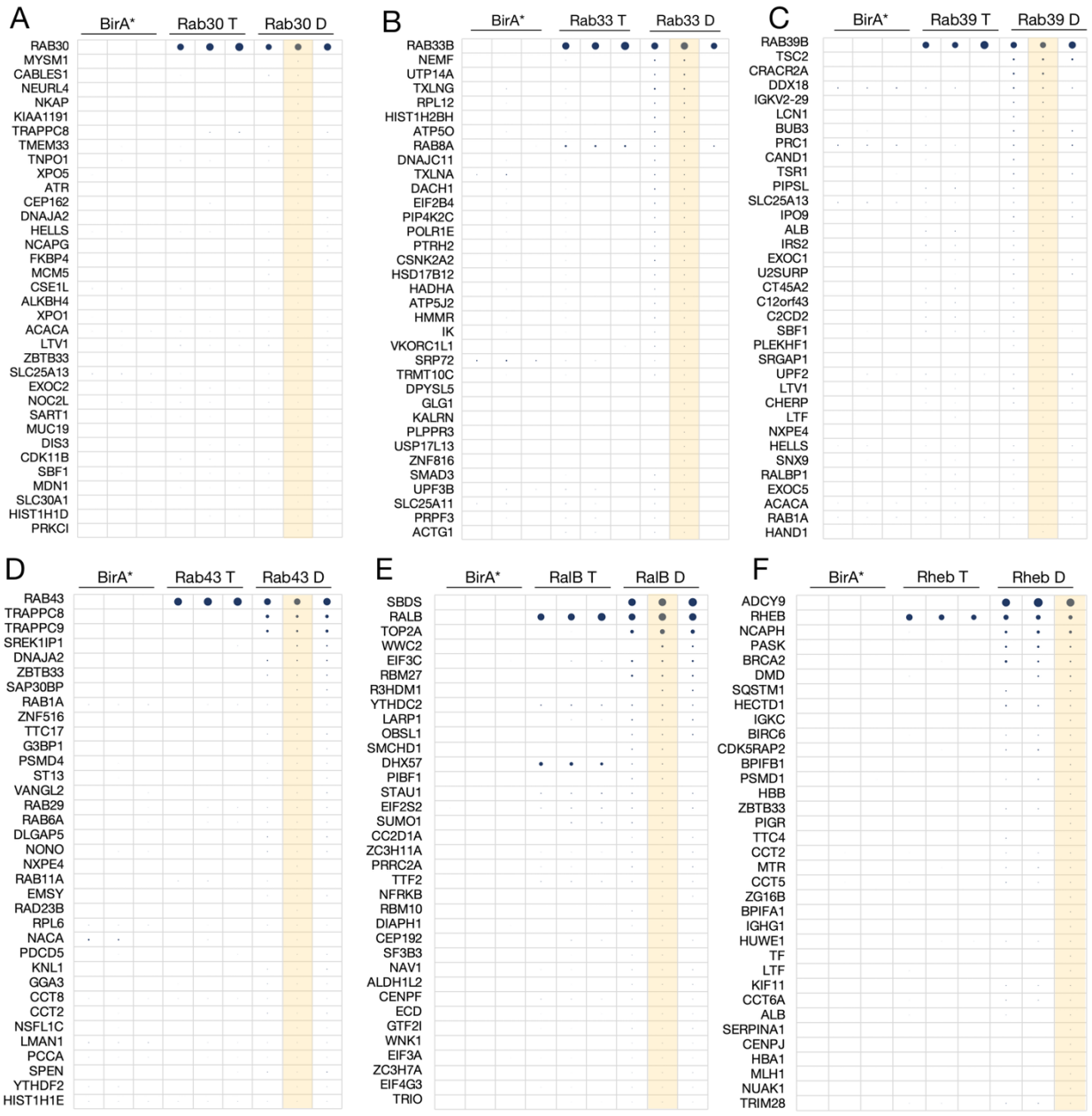

Supplementary figure 3.6. Analysis of GDP-locked Rab30B, Rab33B, Rab39B, Rab43, RalB, and Rheb MitoID experiments. (A-F) Bubble-volcano plots showing GDP-locked Rab30B (A), Rab33B (B), Rab39B (C), Rab43 (D), RalB (E), and Rheb (F) plotted against all tested GDP-locked GTPases. Circle area corresponds to WD-score. Data analysed by Alison Gillingham, plots generated by Sean Munro.

Bibliography

Adolf, F., Herrmann, A., Hellwig, A., Beck, R., Brügger, B., & Wieland, F. T. (2013). Scission of COPI and COPII Vesicles Is Independent of GTP Hydrolysis. *Traffic*, *14*(8), 922–932. https://doi.org/10.1111/tra.12084

Adolf, F., Rhiel, M., Hessling, B., Gao, Q., Hellwig, A., Béthune, J., & Wieland, F. T. (2019). Proteomic Profiling of Mammalian COPII and COPI Vesicles. *Cell Reports*, *26*(1), 250-265.e5. https://doi.org/10.1016/j.celrep.2018.12.041

Ailion, M., Hannemann, M., Dalton, S., Pappas, A., Watanabe, S., Hegermann, J., Liu, Q., Han, H.-F., Gu, M., Goulding, M. Q., Sasidharan, N., Schuske, K., Hullett, P., Eimer, S., & Jorgensen, E. M. (2014). Two Rab2 interactors regulate dense-core vesicle maturation. *Neuron*, *82*(1), 167–180. https://doi.org/10.1016/j.neuron.2014.02.017

Akizu, N., Cantagrel, V., Zaki, M. S., Al-Gazali, L., Wang, X., Rosti, R. O., Dikoglu, E., Gelot, A. B., Rosti, B., Vaux, K. K., Scott, E. M., Silhavy, J. L., Schroth, J., Copeland, B., Schaffer, A. E., Gordts, P. L. S. M., Esko, J. D., Buschman, M. D., Field, S. J., … Gleeson, J. G. (2015). Biallelic mutations in SNX14 cause a syndromic form of cerebellar atrophy and lysosome-autophagosome dysfunction. *Nature Genetics*, *47*(5), 528–534. https://doi.org/10.1038/ng.3256

Alfarsi, L. H., Elansari, R., Toss, M. S., Diez-Rodriguez, M., Nolan, C. C., Ellis, I. O., Rakha, E. A., & Green, A. R. (2019). Kinesin family member-18A (KIF18A) is a predictive biomarker of poor benefit from endocrine therapy in early ER+ breast cancer. *Breast Cancer Research and Treatment*, *173*(1), 93–102. https://doi.org/10.1007/s10549-018-4978-5

Alvarez, C., Garcia-Mata, R., Hauri, H.-P., & Sztul, E. (2001). The p115-interactive Proteins GM130 and Giantin Participate in Endoplasmic Reticulum-Golgi Traffic*. *Journal of Biological Chemistry*, *276*(4), 2693–2700. https://doi.org/10.1074/jbc.m007957200

Anand, I. S., Choi, W., & Isberg, R. R. (2020). Components of the endocytic and recycling trafficking pathways interfere with the integrity of the Legionella-containing vacuole. *Cellular Microbiology*, *22*(4), e13151. https://doi.org/10.1111/cmi.13151

Andres-Alonso, M., Ammar, M. R., Butnaru, I., Gomes, G. M., Sanhueza, G. A., Raman, R., Yuanxiang, P., Borgmeyer, M., Lopez-Rojas, J., Raza, S. A., Brice, N., Hausrat, T. J., Macharadze, T., Diaz-Gonzalez, S., Carlton, M., Failla, A. V., Stork, O., Schweizer, M., Gundelfinger, E. D., … Kreutz, M. R. (2019). SIPA1L2 controls trafficking and local signaling of TrkB-containing amphisomes at presynaptic terminals. *Nature Communications*, *10*(1), 5448. https://doi.org/10.1038/s41467-019-13224-z

Aoki, Y., Manzano, R., Lee, Y., Dafinca, R., Aoki, M., Douglas, A. G. L., Varela, M. A., Sathyaprakash, C., Scaber, J., Barbagallo, P., Vader, P., Mäger, I., Ezzat, K., Turner, M. R., Ito, N., Gasco, S., Ohbayashi, N., Andaloussi, S. E., Takeda, S., … Wood, M. J. A. (2017). C9orf72 and RAB7L1 regulate vesicle trafficking in amyotrophic lateral sclerosis and frontotemporal dementia. *Brain*, *140*(4), 887–897. https://doi.org/10.1093/brain/awx024

Arakel, E. C., & Schwappach, B. (2018). Formation of COPI-coated vesicles at a glance. *J Cell Sci*, *131*(5), jcs209890. https://doi.org/10.1242/jcs.209890

Arancibia, D., Lira, M., Cruz, Y., Barrera, D. P., Montenegro-Venegas, C., Godoy, J. A., Garner, C. C., Inestrosa, N. C., Gundelfinger, E. D., Zamorano, P., & Torres, V. I. (2019). Serine-Arginine Protein Kinase SRPK2 Modulates the Assembly of the Active Zone Scaffolding Protein CAST1/ERC2. *Cells*, *8*(11), 1333. https://doi.org/10.3390/cells8111333

Arasaki, K., Kimura, H., Tagaya, M., & Roy, C. R. (2018). Legionella remodels the plasma membrane–derived vacuole by utilizing exocyst components as tethersInteraction of Legionella DrrA with exocyst. *The Journal of Cell Biology*, *217*(11), 3863–3872. https://doi.org/10.1083/jcb.201801208

ARESTA, S., TAND-HEIM, M.-F. de, BÉRANGER, F., & GUNZBURG, J. de. (2002). A novel Rho GTPase-activating-protein interacts with Gem, a member of the Ras superfamily of GTPases. *Biochemical Journal*, *367*(1), 57–65. https://doi.org/10.1042/bj20020829

Armas-Rillo, L. de, Valera, M.-S., Marrero-Hernández, S., & Valenzuela-Fernández, A. (2016). Membrane dynamics associated with viral infection. *Reviews in Medical Virology*, *26*(3), 146–160. https://doi.org/10.1002/rmv.1872

Asrat, S., Jesús, D. A. de, Hempstead, A. D., Ramabhadran, V., & Isberg, R. R. (2014). Bacterial pathogen manipulation of host membrane trafficking. *Annual Review of Cell and Developmental Biology*, *30*(1), 79–109. https://doi.org/10.1146/annurev-cellbio-100913-013439

Atorino, E. S., Hata, S., Funaya, C., Neuner, A., & Schiebel, E. (2020). CEP44 ensures the formation of bona fide centriole wall, a requirement for the centriole-to-centrosome conversion. *Nature Communications*, *11*(1), 903. https://doi.org/10.1038/s41467-020-14767-2

Backes, S., Hess, S., Boos, F., Woellhaf, M. W., Gödel, S., Jung, M., Mühlhaus, T., & Herrmann, J. M. (2018). Tom70 enhances mitochondrial preprotein import efficiency by binding to internal targeting sequences. *Journal of Cell Biology*, *217*(4), 1369–1382. https://doi.org/10.1083/jcb.201708044

Ballabio, A., & Bonifacino, J. S. (2020). Lysosomes as dynamic regulators of cell and organismal homeostasis. *Nature Reviews Molecular Cell Biology*, *21*(2), 101–118. https://doi.org/10.1038/s41580-019-0185-4

Barac, A., Basile, J., Vázquez-Prado, J., Gao, Y., Zheng, Y., & Gutkind, J. S. (2003). Direct Interaction of p21-Activated Kinase 4 with PDZ-RhoGEF, a G Protein-linked Rho Guanine Exchange Factor. *Journal of Biological Chemistry*, *279*(7), 6182–6189. https://doi.org/10.1074/jbc.m309579200

Bard, F., & Malhotra, V. (2006). The Formation of TGN-to-Plasma-Membrane Transport Carriers. *Annual Review of Cell and Developmental Biology*, *22*(1), 439–455. https://doi.org/10.1146/annurev.cellbio.21.012704.133126

Barlowe, C. K., & Miller, E. A. (2013). Secretory protein biogenesis and traffic in the early secretory pathway. *Genetics*, *193*(2), 383–410. https://doi.org/10.1534/genetics.112.142810

Barr, F. A. (2013). Rab GTPases and membrane identity: Causal or inconsequential?Rab regulation in membrane trafficking. *The Journal of Cell Biology*, *202*(2), 191–199. https://doi.org/10.1083/jcb.201306010

Beck, R., Rawet, M., Ravet, M., Wieland, F. T., & Cassel, D. (2009). The COPI system: Molecular mechanisms and function. *FEBS Letters*, *583*(17), 2701–2709. https://doi.org/10.1016/j.febslet.2009.07.032

Beek, J. van der, Jonker, C., Welle, R. van der, Liv, N., & Klumperman, J. (2019). CORVET, CHEVI and HOPS - multisubunit tethers of the endo-lysosomal system in health and disease. *Journal of Cell Science*, *132*(10), jcs189134. https://doi.org/10.1242/jcs.189134

Beilina, A., Rudenko, I. N., Kaganovich, A., Civiero, L., Chau, H., Kalia, S. K., Kalia, L. V., Lobbestael, E., Chia, R., Ndukwe, K., Ding, J., Nalls, M. A., Consortium, I. P. D. G., Consortium, N. A. B. E., Olszewski, M., Hauser, D. N., Kumaran, R., Lozano, A. M., Baekelandt, V., … Zonderman, A. B. (2014). Unbiased screen for interactors of leucine-rich repeat kinase 2 supports a common pathway for sporadic and familial Parkinson disease. *Proceedings of the National Academy of Sciences of the United States of America*, *111*(7), 2626–2631. https://doi.org/10.1073/pnas.1318306111

Ben-Tekaya, H., Miura, K., Pepperkok, R., & Hauri, H.-P. (2005). Live imaging of bidirectional traffic from the ERGIC. *Journal of Cell Science*, *118*(2), 357–367. https://doi.org/10.1242/jcs.01615

Besemer, A. S., Maus, J., Ax, M. D. A., Stein, A., Vo, S., Freese, C., Nalbach, K., Hilchen, C. von, Pfalzgraf, I. F., Koziollek-Drechsler, I., Silva, B., Huesmann, H., Boukhallouk, F., Florin, L., Kern, A., Behl, C., & Clement, A. M. (2020). Receptor-mediated endocytosis 8 (RME-8)/DNAJC13 is a novel positive modulator of autophagy and stabilizes cellular protein homeostasis. *Cellular and Molecular Life Sciences*, 1–16. https://doi.org/10.1007/s00018-020-03521-y

Bhatt, J. M., Hancock, W., Meissner, J. M., Kaczmarczyk, A., Lee, E., Viktorova, E., Ramanadham, S., Belov, G. A., & Sztul, E. (2019). Promiscuity of the catalytic Sec7 domain within the guanine nucleotide exchange factor GBF1 in ARF activation, Golgi homeostasis, and effector recruitment. *Molecular Biology of the Cell*, *30*(12), 1523–1535. https://doi.org/10.1091/mbc.e18-11-0711

Bi, X., Corpina, R. A., & Goldberg, J. (2002). Structure of the Sec23/24–Sar1 pre-budding complex of the COPII vesicle coat. *Nature*, *419*(6904), 271–277. https://doi.org/10.1038/nature01040

Bi, X., Mancias, J. D., & Goldberg, J. (2007). Insights into COPII Coat Nucleation from the Structure of Sec23•Sar1 Complexed with the Active Fragment of Sec31. *Developmental Cell*, *13*(5), 635–645. https://doi.org/10.1016/j.devcel.2007.10.006

Boal, F., & Stephens, D. J. (2010). Specific functions of BIG1 and BIG2 in endomembrane organization. *PloS One*, *5*(3), e9898. https://doi.org/10.1371/journal.pone.0009898

Boncompain, G., Divoux, S., Gareil, N., Forges, H. de, Lescure, A., Latreche, L., Mercanti, V., Jollivet, F., Raposo, G., & Perez, F. (2012). Synchronization of secretory protein traffic in populations of cells. *Nature Methods*, *9*(5), 493–498. https://doi.org/10.1038/nmeth.1928

Bouchet, B. P., Noordstra, I., Amersfoort, M. van, Katrukha, E. A., Ammon, Y.-C., Hoeve, N. D. T., Hodgson, L., Dogterom, M., Derksen, P. W. B., & Akhmanova, A. (2016). Mesenchymal Cell Invasion Requires Cooperative Regulation of Persistent Microtubule Growth by SLAIN2 and CLASP1. *Developmental Cell*, *39*(6), 708–723. https://doi.org/10.1016/j.devcel.2016.11.009

Bradshaw, N. J., & Hayashi, M. A. F. (2016). NDE1 and NDEL1 from genes to (mal)functions: parallel but distinct roles impacting on neurodevelopmental disorders and psychiatric illness. *Cellular and Molecular Life Sciences*, *74*(7), 1191–1210. https://doi.org/10.1007/s00018-016-2395-7

Brandizzi, F., Snapp, E. L., Roberts, A. G., Lippincott-Schwartz, J., & Hawes, C. (2002). Membrane Protein Transport between the Endoplasmic Reticulum and the Golgi in Tobacco Leaves Is Energy Dependent but Cytoskeleton Independent Evidence from Selective Photobleaching. *The Plant Cell Online*, *14*(6), 1293–1309. https://doi.org/10.1105/tpc.001586

Branon, T. C., Bosch, J. A., Sanchez, A. D., Udeshi, N. D., Svinkina, T., Carr, S. A., Feldman, J. L., Perrimon, N., & Ting, A. Y. (2018). Efficient proximity labeling in living cells and organisms with TurboID. *Nature Biotechnology*, *36*(9), 880–887. https://doi.org/10.1038/nbt.4201

Brooks, S. P., Coccia, M., Tang, H. R., Kanuga, N., Machesky, L. M., Bailly, M., Cheetham, M. E., & Hardcastle, A. J. (2010). The Nance-Horan syndrome protein encodes a functional WAVE homology domain (WHD) and is important for co-ordinating actin remodelling and maintaining cell morphology. *Human Molecular Genetics*, *19*(12), 2421–2432. https://doi.org/10.1093/hmg/ddq125

Buschman, M. D., & Field, S. J. (2017). MYO18A: An unusual myosin. *Advances in Biological Regulation*, *67*, 84–92. https://doi.org/10.1016/j.jbior.2017.09.005

Bykov, Y. S., Schaffer, M., Dodonova, S. O., Albert, S., Plitzko, J. M., Baumeister, W., Engel, B. D., & Briggs, J. A. (2017). The structure of the COPI coat determined within the cell. *ELife*, *6*, e32493. https://doi.org/10.7554/elife.32493

Cabantous, S., Nguyen, H. B., Pedelacq, J.-D., Koraïchi, F., Chaudhary, A., Ganguly, K., Lockard, M. A., Favre, G., Terwilliger, T. C., & Waldo, G. S. (2013). A new protein-protein interaction sensor based on tripartite split-GFP association. *Scientific Reports*, *3*(1), 2854. https://doi.org/10.1038/srep02854

Cao, X., Ballew, N., & Barlowe, C. (1998). Initial docking of ER-derived vesicles requires Uso1p and Ypt1p but is independent of SNARE proteins. *The EMBO Journal*, *17*(8), 2156–2165. https://doi.org/10.1093/emboj/17.8.2156

Carlier, M.-F., Ducruix, A., & Pantaloni, D. (1999). Signalling to actin: the Cdc42-N-WASP-Arp2/3 connection. *Chemistry & Biology*, *6*(9), R235–R240. https://doi.org/10.1016/s1074-5521(99)80107-0

Carter, A. P., Diamant, A. G., & Urnavicius, L. (2016). How dynein and dynactin transport cargos: a structural perspective. *Current Opinion in Structural Biology*, *37*, 62–70. https://doi.org/10.1016/j.sbi.2015.12.003

Casamento, A., & Boucrot, E. (2020). Molecular mechanism of Fast Endophilin-Mediated Endocytosis. *Biochemical Journal*, *477*(12), 2327–2345. https://doi.org/10.1042/bcj20190342

Celona, B., Dollen, J. von, Vatsavayai, S. C., Kashima, R., Johnson, J. R., Tang, A. A., Hata, A., Miller, B. L., Huang, E. J., Krogan, N. J., Seeley, W. W., & Black, B. L. (2017). Suppression of C9orf72 RNA repeat-induced neurotoxicity by the ALS-associated RNA-binding protein Zfp106. *ELife*, *6*, e19032. https://doi.org/10.7554/elife.19032

Cezanne, A., Lauer, J., Solomatina, A., Sbalzarini, I. F., & Zerial, M. (2020). A non-linear system patterns Rab5 GTPase on the membrane. *ELife*, *9*, e54434. https://doi.org/10.7554/elife.54434

Chen, B., Chou, H.-T., Brautigam, C. A., Xing, W., Yang, S., Henry, L., Doolittle, L. K., Walz, T., & Rosen, M. K. (2017). Rac1 GTPase activates the WAVE regulatory complex through two distinct binding sites. *ELife*, *6*, e29795. https://doi.org/10.7554/elife.29795

Chen, F.-T., & Zhong, F.-K. (2019). Kinesin Family Member 18A (KIF18A) Contributes to the Proliferation, Migration, and Invasion of Lung Adenocarcinoma Cells In Vitro and In Vivo. *Disease Markers*, *2019*, 1–9. https://doi.org/10.1155/2019/6383685

Chen, X., Ernst, S. A., & Williams, J. A. (2003). Dominant Negative Rab3D Mutants Reduce GTP-bound Endogenous Rab3D in Pancreatic Acini. *Journal of Biological Chemistry*, *278*(50), 50053–50060. https://doi.org/10.1074/jbc.m309910200

Chen, Y.-A., Murakami, Y., Ahmad, S., Yoshimaru, T., Katagiri, T., & Mizuguchi, K. (2014). Brefeldin A-inhibited guanine nucleotide-exchange protein 3 (BIG3) is predicted to interact with its partner

through an ARM-type α-helical structure. *BMC Research Notes*, *7*(1), 435. https://doi.org/10.1186/1756-0500-7-435

Chiu, S.-L., Diering, G. H., Ye, B., Takamiya, K., Chen, C.-M., Jiang, Y., Niranjan, T., Schwartz, C. E., Wang, T., & Huganir, R. L. (2017). GRASP1 Regulates Synaptic Plasticity and Learning through Endosomal Recycling of AMPA Receptors. *Neuron*, *93*(6), 1405-1419.e8. https://doi.org/10.1016/j.neuron.2017.02.031

Christoforidis, S., Miaczynska, M., Ashman, K., Wilm, M., Zhao, L., Yip, S.-C., Waterfield, M. D., Backer, J. M., & Zerial, M. (1999). Phosphatidylinositol-3-OH kinases are Rab5 effectors. *Nature Cell Biology*, *1*(4), 249–252. https://doi.org/10.1038/12075

Chuang, H.-C., Wang, X., & Tan, T.-H. (2015). MAP4K Family Kinases in Immunity and Inflammation. *Advances in Immunology*, *129*, 277–314. https://doi.org/10.1016/bs.ai.2015.09.006

Chuang, T. H., Xu, X., Kaartinen, V., Heisterkamp, N., Groffen, J., & Bokoch, G. M. (1995). Abr and Bcr are multifunctional regulators of the Rho GTP-binding protein family. *Proceedings of the National Academy of Sciences*, *92*(22), 10282–10286. https://doi.org/10.1073/pnas.92.22.10282

Collier, F. M., Gregorio-King, C. C., Gough, T. J., Talbot, C. D., Walder, K., & Kirkland, M. A. (2004). Identification and characterization of a lymphocytic Rho-GTPase effector: rhotekin-2. *Biochemical and Biophysical Research Communications*, *324*(4), 1360–1369. https://doi.org/10.1016/j.bbrc.2004.09.205

Cormont, M., Mari, M., Galmiche, A., Hofman, P., & Marchand-Brustel, Y. L. (2001). A FYVE-finger-containing protein, Rabip4, is a Rab4 effector involved in early endosomal traffic. *Proceedings of the National Academy of Sciences*, *98*(4), 1637–1642. https://doi.org/10.1073/pnas.98.4.1637

Cuif, M., Possmayer, F., Zander, H., Bordes, N., Jollivet, F., Couedel-Courteille, A., Janoueix-Lerosey, I., Langsley, G., Bornens, M., & Goud, B. (1999). Characterization of GAPCenA, a GTPase activating protein for Rab6, part of which associates with the centrosome. *The EMBO Journal*, *18*(7), 1772–1782. https://doi.org/10.1093/emboj/18.7.1772

Dai, A., Yu, L., & Wang, H.-W. (2019). WHAMM initiates autolysosome tubulation by promoting actin polymerization on autolysosomes. *Nature Communications*, *10*(1), 3699. https://doi.org/10.1038/s41467-019-11694-9

DeBoer, S. R., You, Y., Szodorai, A., Kaminska, A., Pigino, G., Nwabuisi, E., Wang, B., Estrada-Hernandez, T., Kins, S., Brady, S. T., & Morfini, G. (2008). Conventional kinesin holoenzymes are composed of heavy and light chain homodimers. *Biochemistry*, *47*(15), 4535–4543. https://doi.org/10.1021/bi702445j

Dibble, C. C., Elis, W., Menon, S., Qin, W., Klekota, J., Asara, J. M., Finan, P. M., Kwiatkowski, D. J., Murphy, L. O., & Manning, B. D. (2012). TBC1D7 is a third subunit of the TSC1-TSC2 complex upstream of mTORC1. *Molecular Cell*, *47*(4), 535–546. https://doi.org/10.1016/j.molcel.2012.06.009

Ding, X., Jiang, X., Tian, R., Zhao, P., Li, L., Wang, X., Chen, S., Zhu, Y., Mei, M., Bao, S., Liu, W., Tang, Z., & Sun, Q. (2019). RAB2 regulates the formation of autophagosome and autolysosome in mammalian cells. *Autophagy*, *15*(10), 1774–1786. https://doi.org/10.1080/15548627.2019.1596478

Dissmeyer, N., & Schnittger, A. (2011). Methods in Molecular Biology. *Methods in Molecular Biology (Clifton, N.J.)*, *779*, 93–138. https://doi.org/10.1007/978-1-61779-264-9_6

Doherty, G. J., & McMahon, H. T. (2009). Mechanisms of Endocytosis. *Biochemistry*, *78*(1), 857–902. https://doi.org/10.1146/annurev.biochem.78.081307.110540

Donaldson, J. G., & Jackson, C. L. (2011). ARF family G proteins and their regulators: roles in membrane transport, development and disease. *Nature Reviews. Molecular Cell Biology*, *12*(6), 362–375. https://doi.org/10.1038/nrm3117

Doubravská, L., Dostál, V., Knop, F., Libusová, L., & Macůrková, M. (2019). Human myotubularin-related protein 9 regulates ER-to-golgi trafficking and modulates WNT3A secretion. *Experimental Cell Research*, *386*(1), 111709. https://doi.org/10.1016/j.yexcr.2019.111709

Doudna, J. A., & Charpentier, E. (2014). The new frontier of genome engineering with CRISPR-Cas9. *Science*, *346*(6213), 1258096. https://doi.org/10.1126/science.1258096

D'Souza-Schorey, C., & Chavrier, P. (2006). ARF proteins: roles in membrane traffic and beyond. *Nature Reviews Molecular Cell Biology*, *7*(5), 347–358. https://doi.org/10.1038/nrm1910

Dubielecka, P. M., Cui, P., Xiong, X., Hossain, S., Heck, S., Angelov, L., & Kotula, L. (2010). Differential regulation of macropinocytosis by Abi1/Hssh3bp1 isoforms. *PloS One*, *5*(5), e10430. https://doi.org/10.1371/journal.pone.0010430

Duden, R. (2009). ER-to-Golgi transport: COP I and COP II function (Review). *Molecular Membrane Biology*, *20*(3), 197–207. https://doi.org/10.1080/0968768031000122548

Dumaresq-Doiron, K., Savard, M.-F., Akam, S., Costantino, S., & Lefrancois, S. (2010). The phosphatidylinositol 4-kinase PI4KIIIα is required for the recruitment of GBF1 to Golgi membranes. *Journal of Cell Science*, *123*(13), 2273–2280. https://doi.org/10.1242/jcs.055798

Dundas, C. M., Demonte, D., & Park, S. (2013). Streptavidin-biotin technology: improvements and innovations in chemical and biological applications. *Applied Microbiology and Biotechnology*, *97*(21), 9343–9353. https://doi.org/10.1007/s00253-013-5232-z

Eckert, E. S. P., Reckmann, I., Hellwig, A., Röhling, S., El-Battari, A., Wieland, F. T., & Popoff, V. (2014). Golgi Phosphoprotein 3 Triggers Signal-mediated Incorporation of Glycosyltransferases into Coatomer-coated (COPI) Vesicles. *Journal of Biological Chemistry*, *289*(45), 31319–31329. https://doi.org/10.1074/jbc.m114.608182

Edwards, A. S., & Scott, J. D. (2000). A-kinase anchoring proteins: protein kinase A and beyond. *Current Opinion in Cell Biology*, *12*(2), 217–221. https://doi.org/10.1016/s0955-0674(99)00085-x

Edwards, M., Liang, Y., Kim, T., & Cooper, J. A. (2013). Physiological role of the interaction between CARMIL1 and capping protein. *Molecular Biology of the Cell*, *24*(19), 3047–3055. https://doi.org/10.1091/mbc.e13-05-0270

Eggers, C. T., Schafer, J. C., Goldenring, J. R., & Taylor, S. S. (2009). D-AKAP2 interacts with Rab4 and Rab11 through its RGS domains and regulates transferrin receptor recycling. *The Journal of Biological Chemistry*, *284*(47), 32869–32880. https://doi.org/10.1074/jbc.m109.022582

Eidenmüller, J., Fath, T., Hellwig, A., Reed, J., Sontag, E., & Brandt, R. (2000). Structural and Functional Implications of Tau Hyperphosphorylation: Information from Phosphorylation-Mimicking Mutated Tau Proteins †. *Biochemistry*, *39*(43), 13166–13175. https://doi.org/10.1021/bi001290z

Elkin, S. R., Lakoduk, A. M., & Schmid, S. L. (2016). Endocytic pathways and endosomal trafficking: a primer. *Wiener Medizinische Wochenschrift (1946)*, *166*(7–8), 196–204. https://doi.org/10.1007/s10354-016-0432-7

Etoh, K., & Fukuda, M. (2019). Rab10 regulates tubular endosome formation through KIF13A/B motors. *J Cell Sci*, *132*(5), jcs.226977. https://doi.org/10.1242/jcs.226977

Farhan, H., & Hsu, V. W. (2015). Cdc42 and Cellular Polarity: Emerging Roles at the Golgi. *Trends in Cell Biology*, *26*(4), 241–248. https://doi.org/10.1016/j.tcb.2015.11.003

Farrugia, A. J., & Calvo, F. (2016). The Borg family of Cdc42 effector proteins Cdc42EP1–5. *Biochemical Society Transactions*, *44*(6), 1709–1716. https://doi.org/10.1042/bst20160219

Farzana, F., Zalm, R., Chen, N., Li, K. W., Grant, S. G. N., Smit, A. B., Toonen, R. F., & Verhage, M. (2015). Neurobeachin Regulates Glutamate- and GABA-Receptor Targeting to Synapses via Distinct Pathways. *Molecular Neurobiology*, *53*(4), 2112–2123. https://doi.org/10.1007/s12035-015-9164-8

Feig, L. A. (1999). Tools of the trade: use of dominant-inhibitory mutants of Ras-family GTPases. *Nature Cell Biology*, *1*(2), E25–E27. https://doi.org/10.1038/10018

Fenwick, R. B., Campbell, L. J., Rajasekar, K., Prasannan, S., Nietlispach, D., Camonis, J., Owen, D., & Mott, H. R. (2010). The RalB-RLIP76 complex reveals a novel mode of ral-effector interaction. *Structure (London, England : 1993)*, *18*(8), 985–995. https://doi.org/10.1016/j.str.2010.05.013

Fernandes, H., Franklin, E., Recacha, R., Houdusse, A., Goud, B., & Khan, A. R. (2009). Structural aspects of Rab6-effector complexes. *Biochemical Society Transactions*, *37*(Pt 5), 1037–1041. https://doi.org/10.1042/bst0371037

Flaiz, C., Chernoff, J., Ammoun, S., Peterson, J. R., & Hanemann, C. O. (2009). PAK kinase regulates Rac GTPase and is a potential target in human schwannomas. *Experimental Neurology*, *218*(1), 137–144. https://doi.org/10.1016/j.expneurol.2009.04.019

Frémont, S., Romet-Lemonne, G., Houdusse, A., & Echard, A. (2017). Emerging roles of MICAL family proteins - from actin oxidation to membrane trafficking during cytokinesis. *Journal of Cell Science*, *130*(9), 1509–1517. https://doi.org/10.1242/jcs.202028

Fridmann-Sirkis, Y., Siniossoglou, S., & Pelham, H. R. (2004). TMF is a golgin that binds Rab6 and influences Golgi morphology. *BMC Cell Biology*, *5*(1), 18. https://doi.org/10.1186/1471-2121-5-18

Fu, T., Liu, J., Wang, Y., Xie, X., Hu, S., & Pan, L. (2018). Mechanistic insights into the interactions of NAP1 with the SKICH domains of NDP52 and TAX1BP1. *Proceedings of the National Academy of*

Sciences of the United States of America, *115*(50), E11651–E11660. https://doi.org/10.1073/pnas.1811421115

Fuchs, E., Haas, A. K., Spooner, R. A., Yoshimura, S., Lord, J. M., & Barr, F. A. (2007). Specific Rab GTPase-activating proteins define the Shiga toxin and epidermal growth factor uptake pathways. *The Journal of Cell Biology*, *177*(6), 1133–1143. https://doi.org/10.1083/jcb.200612068

Fukuda, M. (2003). Slp4-a/Granuphilin-a Inhibits Dense-core Vesicle Exocytosis through Interaction with the GDP-bound Form of Rab27A in PC12 Cells. *Journal of Biological Chemistry*, *278*(17), 15390–15396. https://doi.org/10.1074/jbc.m213090200

Fukuda, M., Kanno, E., Ishibashi, K., & Itoh, T. (2008). Large scale screening for novel rab effectors reveals unexpected broad Rab binding specificity. *Molecular & Cellular Proteomics : MCP*, *7*(6), 1031–1042. https://doi.org/10.1074/mcp.m700569-mcp200

Fukuda, M., Kobayashi, H., Ishibashi, K., & Ohbayashi, N. (2011). Genome-wide Investigation of the Rab Binding Activity of RUN Domains: Development of a Novel Tool that Specifically Traps GTP-Rab35. *Cell Structure and Function*, *36*(2), 155–170. https://doi.org/10.1247/csf.11001

Gadea, G., & Blangy, A. (2014). Dock-family exchange factors in cell migration and disease. *European Journal of Cell Biology*, *93*(10–12), 466–477. https://doi.org/10.1016/j.ejcb.2014.06.003

Gadila, S. K. G., & Kim, K. (2016). Cargo trafficking from the trans-Golgi network towards the endosome. *Biology of the Cell*, *108*(8), 205–218. https://doi.org/10.1111/boc.201600001

Gao, X., Satoh, T., Liao, Y., Song, C., Hu, C.-D., Kariya, K., & Kataoka, T. (2001). Identification and Characterization of RA-GEF-2, a Rap Guanine Nucleotide Exchange Factor That Serves as a Downstream Target of M-Ras. *Journal of Biological Chemistry*, *276*(45), 42219–42225. https://doi.org/10.1074/jbc.m105760200

Gautam, R., Chintala, S., Li, W., Zhang, Q., Tan, J., Novak, E. K., Pietro, S. M. D., Dell'Angelica, E. C., & Swank, R. T. (2004). The Hermansky-Pudlak Syndrome 3 (Cocoa) Protein Is a Component of the Biogenesis of Lysosome-related Organelles Complex-2 (BLOC-2). *Journal of Biological Chemistry*, *279*(13), 12935–12942. https://doi.org/10.1074/jbc.m311311200

Gentry, L. R., Martin, T. D., Reiner, D. J., & Der, C. J. (2014). Ral small GTPase signaling and oncogenesis: More than just 15minutes of fame. *Biochimica et Biophysica Acta*, *1843*(12), 2976–2988. https://doi.org/10.1016/j.bbamcr.2014.09.004

Georgakopoulos, N. D., Wells, G., & Campanella, M. (2017). The pharmacological regulation of cellular mitophagy. *Nature Chemical Biology*, *13*(2), 136–146. https://doi.org/10.1038/nchembio.2287

Gerondopoulos, A., Bastos, R. N., Yoshimura, S., Anderson, R., Carpanini, S., Aligianis, I., Handley, M. T., & Barr, F. A. (2014). Rab18 and a Rab18 GEF complex are required for normal ER structureRab3GAP is a Rab18 GEF. *The Journal of Cell Biology*, *205*(5), 707–720. https://doi.org/10.1083/jcb.201403026

Gillingham, A. K., Bertram, J., Begum, F., & Munro, S. (2019). In vivo identification of GTPase interactors by mitochondrial relocalization and proximity biotinylation. *ELife*, *8*, e45916. https://doi.org/10.7554/elife.45916

Gillingham, A. K., & Munro, S. (2019). Transport carrier tethering – how vesicles are captured by organelles. *Current Opinion in Cell Biology*, *59*, 140–146. https://doi.org/10.1016/j.ceb.2019.04.010

Gillingham, A. K., Sinka, R., Torres, I. L., Lilley, K. S., & Munro, S. (2014). Toward a comprehensive map of the effectors of rab GTPases. *Developmental Cell*, *31*(3), 358–373. https://doi.org/10.1016/j.devcel.2014.10.007

Girard, M., Poupon, V., Blondeau, F., & McPherson, P. S. (2005). The DnaJ-domain Protein RME-8 Functions in Endosomal Trafficking. *Journal of Biological Chemistry*, *280*(48), 40135–40143. https://doi.org/10.1074/jbc.m505036200

Glick, B. S., & Luini, A. (2011). Models for Golgi Traffic: A Critical Assessment. *Cold Spring Harbor Perspectives in Biology*, *3*(11), a005215. https://doi.org/10.1101/cshperspect.a005215

Goldenring, J. R. (2013). A central role for vesicle trafficking in epithelial neoplasia: intracellular highways to carcinogenesis. *Nature Reviews. Cancer*, *13*(11), 813–820. https://doi.org/10.1038/nrc3601

Gomez-Ferreria, M. A., & Sharp, D. J. (2008). Cep192 and the generation of the mitotic spindle. *Cell Cycle*, *7*(11), 1507–1510. https://doi.org/10.4161/cc.7.11.5957

Gosavi, P., Houghton, F. J., McMillan, P. J., Hanssen, E., & Gleeson, P. A. (2018). The Golgi ribbon in mammalian cells negatively regulates autophagy by modulating mTOR activity. *Journal of Cell Science*, *131*(3), jcs211987. https://doi.org/10.1242/jcs.211987

Grabski, R., Hay, J., & Sztul, E. (2012). Tethering factor P115: a new model for tether-SNARE interactions. *Bioarchitecture*, *2*(5), 175–180. https://doi.org/10.4161/bioa.21702

Grigoriev, I., Splinter, D., Keijzer, N., Wulf, P. S., Demmers, J., Ohtsuka, T., Modesti, M., Maly, I. V., Grosveld, F., Hoogenraad, C. C., & Akhmanova, A. (2007). Rab6 Regulates Transport and Targeting of Exocytotic Carriers. *Developmental Cell*, *13*(2), 305–314. https://doi.org/10.1016/j.devcel.2007.06.010

Grimsey, N. J., Coronel, L. J., Cordova, I. C., & Trejo, J. (2015). Recycling and Endosomal Sorting of Protease-activated Receptor-1 Is Distinctly Regulated by Rab11A and Rab11B Proteins. *The Journal of Biological Chemistry*, *291*(5), 2223–2236. https://doi.org/10.1074/jbc.m115.702993

Groeneweg, F. L., Trattnig, C., Kuhse, J., Nawrotzki, R. A., & Kirsch, J. (2018). Gephyrin: a key regulatory protein of inhibitory synapses and beyond. *Histochemistry and Cell Biology*, *150*(5), 489–508. https://doi.org/10.1007/s00418-018-1725-2

Guo, Y., & Linstedt, A. D. (2013). Binding of the vesicle docking protein p115 to the GTPase Rab1b regulates membrane recruitment of the COPI vesicle coat. *Cellular Logistics*, *3*(1), e27687. https://doi.org/10.4161/cl.27687

Guo, Y., Sirkis, D. W., & Schekman, R. (2014). Protein Sorting at the trans-Golgi Network. *Annual Review of Cell and Developmental Biology*, *30*(1), 1–38. https://doi.org/10.1146/annurev-cellbio-100913-013012

Gupta, M., Kamynina, E., Morley, S., Chung, S., Muakkassa, N., Wang, H., Brathwaite, S., Sharma, G., & Manor, D. (2013). Plekhg4 is a novel Dbl family guanine nucleotide exchange factor protein for rho family GTPases. *The Journal of Biological Chemistry*, *288*(20), 14522–14530. https://doi.org/10.1074/jbc.m112.430371

Gutkowska, M., & Swiezewska, E. (2012). Structure, regulation and cellular functions of Rab geranylgeranyl transferase and its cellular partner Rab Escort Protein. *Molecular Membrane Biology*, *29*(7), 243–256. https://doi.org/10.3109/09687688.2012.693211

Ha, B. H., & Boggon, T. J. (2018). CDC42 binds PAK4 via an extended GTPase-effector interface. *Proceedings of the National Academy of Sciences of the United States of America*, *115*(3), 531–536. https://doi.org/10.1073/pnas.1717437115

Hage, D. S., & Matsuda, R. (2015). Methods in Molecular Biology. *Methods in Molecular Biology (Clifton, N.J.)*, *1286*, 1–19. https://doi.org/10.1007/978-1-4939-2447-9_1

Hall, A. (2012). Rho family GTPases. *Biochemical Society Transactions*, *40*(6), 1378–1382. https://doi.org/10.1042/bst20120103

Hamel, B., Monaghan-Benson, E., Rojas, R. J., Temple, B. R. S., Marston, D. J., Burridge, K., & Sondek, J. (2011). SmgGDS is a guanine nucleotide exchange factor that specifically activates RhoA and RhoC. *The Journal of Biological Chemistry*, *286*(14), 12141–12148. https://doi.org/10.1074/jbc.m110.191122

Hampson, A., O'Connor, A., & Smolenski, A. (2013). Synaptotagmin-like protein 4 and Rab8 interact and increase dense granule release in platelets. *Journal of Thrombosis and Haemostasis : JTH*, *11*(1), 161–168. https://doi.org/10.1111/jth.12068

Hantan, D., Yamamoto, Y., & Sakisaka, T. (2014). VAP-B binds to Rab3GAP1 at the ER: its implication in nuclear envelope formation through the ER-Golgi intermediate compartment. *The Kobe Journal of Medical Sciences*, *60*(3), E48-56.

Hao, F., Itoh, T., Morita, E., Shirahama-Noda, K., Yoshimori, T., & Noda, T. (2015). The PtdIns3-phosphatase MTMR3 interacts with mTORC1 and suppresses its activity. *FEBS Letters*, *590*(1), 161–173. https://doi.org/10.1002/1873-3468.12048

Hardiman, C. A., & Roy, C. R. (2014). AMPylation is critical for Rab1 localization to vacuoles containing Legionella pneumophila. *MBio*, *5*(1), e01035-13. https://doi.org/10.1128/mbio.01035-13

Hariri, H., Bhattacharya, N., Johnson, K., Noble, A. J., & Stagg, S. M. (2014). Insights into the Mechanisms of Membrane Curvature and Vesicle Scission by the Small GTPase Sar1 in the Early Secretory Pathway. *Journal of Molecular Biology*, *426*(22), 3811–3826. https://doi.org/10.1016/j.jmb.2014.08.023

Häsler, S. L.-A., Vallis, Y., Pasche, M., & McMahon, H. T. (2020). GRAF2, WDR44, and MICAL1 mediate Rab8/10/11–dependent export of E-cadherin, MMP14, and CFTR ΔF508. *Journal of Cell Biology*, *219*(5). https://doi.org/10.1083/jcb.201811014

Hatakeyama, J., Wald, J. H., Printsev, I., Ho, H.-Y. H., & Carraway, K. L. (2014). Vangl1 and Vangl2: planar cell polarity components with a developing role in cancer. *Endocrine-Related Cancer*, *21*(5), R345-56. https://doi.org/10.1530/erc-14-0141

Hayes, G. L., Brown, F. C., Haas, A. K., Nottingham, R. M., Barr, F. A., & Pfeffer, S. R. (2009). Multiple Rab GTPase Binding Sites in GCC185 Suggest a Model for Vesicle Tethering at the Trans-Golgi. *Molecular Biology of the Cell*, *20*(1), 209–217. https://doi.org/10.1091/mbc.e08-07-0740

Heard, J. J., Fong, V., Bathaie, S. Z., & Tamanoi, F. (2014). Recent progress in the study of the Rheb family GTPases. *Cellular Signalling*, *26*(9), 1950–1957. https://doi.org/10.1016/j.cellsig.2014.05.011

Hedman, A. C., Smith, J. M., & Sacks, D. B. (2015). The biology of IQGAP proteins: beyond the cytoskeleton. *EMBO Reports*, *16*(4), 427–446. https://doi.org/10.15252/embr.201439834

Henne, W. M., Zhu, L., Balogi, Z., Stefan, C., Pleiss, J. A., & Emr, S. D. (2015). Mdm1/Snx13 is a novel ER-endolysosomal interorganelle tethering protein. *The Journal of Cell Biology*, *210*(4), 541–551. https://doi.org/10.1083/jcb.201503088

Hennig, A., Markwart, R., Esparza-Franco, M. A., Ladds, G., & Rubio, I. (2015). Ras activation revisited: role of GEF and GAP systems. *Biological Chemistry*, *396*(8), 831–848. https://doi.org/10.1515/hsz-2014-0257

Héraud, C., Pinault, M., Lagrée, V., & Moreau, V. (2019). p190RhoGAPs, the ARHGAP35- and ARHGAP5-Encoded Proteins, in Health and Disease. *Cells*, *8*(4), 351. https://doi.org/10.3390/cells8040351

Hobbs, G. A., Der, C. J., & Rossman, K. L. (2016). RAS isoforms and mutations in cancer at a glance. *Journal of Cell Science*, *129*(7), 1287–1292. https://doi.org/10.1242/jcs.182873

Homma, Y., & Fukuda, M. (2016). Rabin8 regulates neurite outgrowth in both GEF activity-dependent and -independent manners. *Molecular Biology of the Cell*, *27*(13), 2107–2118. https://doi.org/10.1091/mbc.e16-02-0091

Homma, Y., Kinoshita, R., Kuchitsu, Y., Wawro, P. S., Marubashi, S., Oguchi, M. E., Ishida, M., Fujita, N., & Fukuda, M. (2019). Comprehensive knockout analysis of the Rab family GTPases in epithelial

cellsComprehensive Rab knockout in epithelial cells. *The Journal of Cell Biology*, *218*(6), 2035–2050. https://doi.org/10.1083/jcb.201810134

Hong, E.-H., Kim, J.-Y., Kim, J.-H., Lim, D.-S., Kim, M., & Kim, J.-Y. (2018). BIG2-ARF1-RhoA-mDia1 Signaling Regulates Dendritic Golgi Polarization in Hippocampal Neurons. *Molecular Neurobiology*, *55*(10), 7701–7716. https://doi.org/10.1007/s12035-018-0954-7

Hoogenraad, C. C., Popa, I., Futai, K., Martinez-Sanchez, E., Sanchez-Martinez, E., Wulf, P. S., Vlijmen, T. van, Dortland, B. R., Oorschot, V., Govers, R., Monti, M., Heck, A. J. R., Sheng, M., Klumperman, J., Rehmann, H., Jaarsma, D., Kapitein, L. C., & Sluijs, P. van der. (2010). Neuron specific Rab4 effector GRASP-1 coordinates membrane specialization and maturation of recycling endosomes. *PLoS Biology*, *8*(1), e1000283. https://doi.org/10.1371/journal.pbio.1000283

Hoogenraad, C. C., & Sluijs, P. van der. (2010). GRASP-1 regulates endocytic receptor recycling and synaptic plasticity. *Communicative & Integrative Biology*, *3*(5), 433–435. https://doi.org/10.4161/cib.3.5.12209

Hoogenraad, C. C., Wulf, P., Schiefermeier, N., Stepanova, T., Galjart, N., Small, J. V., Grosveld, F., Zeeuw, C. I. de, & Akhmanova, A. (2003). Bicaudal D induces selective dynein-mediated microtubule minus end-directed transport. *The EMBO Journal*, *22*(22), 6004–6015. https://doi.org/10.1093/emboj/cdg592

Horgan, C. P., Hanscom, S. R., & McCaffrey, M. W. (2013). GRAB is a binding partner for the Rab11a and Rab11b GTPases. *Biochemical and Biophysical Research Communications*, *441*(1), 214–219. https://doi.org/10.1016/j.bbrc.2013.10.043

Horiuchi, H., Lippé, R., McBride, H. M., Rubino, M., Woodman, P., Stenmark, H., Rybin, V., Wilm, M., Ashman, K., Mann, M., & Zerial, M. (1997). A Novel Rab5 GDP/GTP Exchange Factor Complexed to Rabaptin-5 Links Nucleotide Exchange to Effector Recruitment and Function. *Cell*, *90*(6), 1149–1159. https://doi.org/10.1016/s0092-8674(00)80380-3

Hossain, D., Shih, S. Y.-P., Xiao, X., White, J., & Tsang, W. Y. (2020). Cep44 functions in centrosome cohesion by stabilizing rootletin. *Journal of Cell Science*, *133*(4), jcs239616. https://doi.org/10.1242/jcs.239616

Hsu, F., Spannl, S., Ferguson, C., Hyman, A. A., Parton, R. G., & Zerial, M. (2018). Rab5 and Alsin regulate stress-activated cytoprotective signaling on mitochondria. *ELife*, *7*, e32282. https://doi.org/10.7554/elife.32282

Huang, J., & Manning, B. D. (2008). The TSC1-TSC2 complex: a molecular switchboard controlling cell growth. *The Biochemical Journal*, *412*(2), 179–190. https://doi.org/10.1042/bj20080281

Huber, L. A., Pimplikar, S., Parton, R. G., Virta, H., Zerial, M., & Simons, K. (1993). Rab8, a small GTPase involved in vesicular traffic between the TGN and the basolateral plasma membrane. *The Journal of Cell Biology*, *123*(1), 35–45. https://doi.org/10.1083/jcb.123.1.35

Hunker, C. M., Galvis, A., Kruk, I., Giambini, H., Veisaga, M. L., & Barbieri, M. A. (2006). Rab5-activating protein 6, a novel endosomal protein with a role in endocytosis. *Biochemical and Biophysical Research Communications*, *340*(3), 967–975. https://doi.org/10.1016/j.bbrc.2005.12.099

Huotari, J., & Helenius, A. (2011). Endosome maturation. *The EMBO Journal*, *30*(17), 3481–3500. https://doi.org/10.1038/emboj.2011.286

Hutagalung, A. H., & Novick, P. J. (2011). Role of Rab GTPases in membrane traffic and cell physiology. *Physiological Reviews*, *91*(1), 119–149. https://doi.org/10.1152/physrev.00059.2009

Hyenne, V., Labouesse, M., & Goetz, J. G. (2016). The Small GTPase Ral orchestrates MVB biogenesis and exosome secretion. *Small GTPases*, *9*(6), 445–451. https://doi.org/10.1080/21541248.2016.1251378

Hyvola, N., Diao, A., McKenzie, E., Skippen, A., Cockcroft, S., & Lowe, M. (2006). Membrane targeting and activation of the Lowe syndrome protein OCRL1 by rab GTPases. *The EMBO Journal*, *25*(16), 3750–3761. https://doi.org/10.1038/sj.emboj.7601274

Iacovino, L. G., Magnani, F., & Binda, C. (2018). The structure of monoamine oxidases: past, present, and future. *Journal of Neural Transmission (Vienna, Austria : 1996)*, *125*(11), 1567–1579. https://doi.org/10.1007/s00702-018-1915-z

Itakura, E., Kishi, C., Inoue, K., & Mizushima, N. (2008). Beclin 1 forms two distinct phosphatidylinositol 3-kinase complexes with mammalian Atg14 and UVRAG. *Molecular Biology of the Cell*, *19*(12), 5360–5372. https://doi.org/10.1091/mbc.e08-01-0080

Ito, H., Morishita, R., & Nagata, K. (2018). Functions of Rhotekin, an Effector of Rho GTPase, and Its Binding Partners in Mammals. *International Journal of Molecular Sciences*, *19*(7), 2121. https://doi.org/10.3390/ijms19072121

Itoh, T., Satoh, M., Kanno, E., & Fukuda, M. (2006). Screening for target Rabs of TBC (Tre-2/Bub2/Cdc16) domain-containing proteins based on their Rab-binding activity. *Genes to Cells*, *11*(9), 1023–1037. https://doi.org/10.1111/j.1365-2443.2006.00997.x

Ivics, Z. (2016). Endogenous Transposase Source in Human Cells Mobilizes piggyBac Transposons. *Molecular Therapy : The Journal of the American Society of Gene Therapy*, *24*(5), 851–854. https://doi.org/10.1038/mt.2016.76

Jackson, C. L. (2009). Mechanisms of transport through the Golgi complex. *Journal of Cell Science*, *122*(4), 443–452. https://doi.org/10.1242/jcs.032581

Jain, M., Bhat, G. P., Vijayraghavan, K., & Inamdar, M. S. (2012). Rudhira/BCAS3 is a cytoskeletal protein that controls Cdc42 activation and directional cell migration during angiogenesis. *Experimental Cell Research*, *318*(6), 753–767. https://doi.org/10.1016/j.yexcr.2012.01.016

Janssen, L. M. E., Averink, T. V., Blomen, V. A., Brummelkamp, T. R., Medema, R. H., & Raaijmakers, J. A. (2018). Loss of Kif18A Results in Spindle Assembly Checkpoint Activation at Microtubule-Attached Kinetochores. *Current Biology*, *28*(17), 2685-2696.e4. https://doi.org/10.1016/j.cub.2018.06.026

Johansson, M., Rocha, N., Zwart, W., Jordens, I., Janssen, L., Kuijl, C., Olkkonen, V. M., & Neefjes, J. (2007). Activation of endosomal dynein motors by stepwise assembly of Rab7–RILP–p150Glued, ORP1L, and the receptor βlll spectrin. *The Journal of Cell Biology*, *176*(4), 459–471. https://doi.org/10.1083/jcb.200606077

John, J., Rensland, H., Schlichting, I., Vetter, I., Borasio, G. D., Goody, R. S., & Wittinghofer, A. (1993). Kinetic and structural analysis of the Mg(2+)-binding site of the guanine nucleotide-binding protein p21H-ras. *The Journal of Biological Chemistry*, *268*(2), 923–929.

Jung, J.-H., & Traugh, J. A. (2005). Regulation of the Interaction of Pak2 with Cdc42 via Autophosphorylation of Serine 141. *Journal of Biological Chemistry*, *280*(48), 40025–40031. https://doi.org/10.1074/jbc.m509075200

Kaksonen, M., & Roux, A. (2018). Mechanisms of clathrin-mediated endocytosis. *Nature Reviews Molecular Cell Biology*, *19*(5), 313–326. https://doi.org/10.1038/nrm.2017.132

Kakuta, S., Yamaguchi, J., Suzuki, C., Sasaki, M., Kazuno, S., & Uchiyama, Y. (2017). Small GTPase Rab1B is associated with ATG9A vesicles and regulates autophagosome formation. *FASEB Journal : Official Publication of the Federation of American Societies for Experimental Biology*, *31*(9), 3757–3773. https://doi.org/10.1096/fj.201601052r

Kälin, S., Buser, D. P., & Spiess, M. (2016). A fresh look at the function of Rabaptin5 on endosomes. *Small GTPases*, *7*(1), 34–37. https://doi.org/10.1080/21541248.2016.1140616

Kälin, S., Hirschmann, D. T., Buser, D. P., & Spiess, M. (2015). Rabaptin5 is recruited to endosomes by Rab4 and Rabex5 to regulate endosome maturation. *Journal of Cell Science*, *128*(22), 4126–4137. https://doi.org/10.1242/jcs.174664

Kang, N., Liu, J., & Zhao, Y. (2019). Dissociation mechanism of GDP from Cdc42 via DOCK9 revealed by molecular dynamics simulations. *Proteins*, *87*(6), 433–442. https://doi.org/10.1002/prot.25665

Kato, K., Yazawa, T., Taki, K., Mori, K., Wang, S., Nishioka, T., Hamaguchi, T., Itoh, T., Takenawa, T., Kataoka, C., Matsuura, Y., Amano, M., Murohara, T., & Kaibuchi, K. (2012). The inositol 5-phosphatase SHIP2 is an effector of RhoA and is involved in cell polarity and migration. *Molecular Biology of the Cell*, *23*(13), 2593–2604. https://doi.org/10.1091/mbc.e11-11-0958

Kawabe, H., Sakisaka, T., Yasumi, M., Shingai, T., Izumi, G., Nagano, F., Deguchi-Tawarada, M., Takeuchi, M., Nakanishi, H., & Takai, Y. (2003). A novel rabconnectin-3-binding protein that directly binds a GDP/GTP exchange protein for Rab3A small G protein implicated in Ca2+-dependent exocytosis of neurotransmitter. *Genes to Cells*, *8*(6), 537–546. https://doi.org/10.1046/j.1365-2443.2003.00655.x

Keilhauer, E. C., Hein, M. Y., & Mann, M. (2014). Accurate protein complex retrieval by affinity enrichment mass spectrometry (AE-MS) rather than affinity purification mass spectrometry (AP-MS). *Molecular & Cellular Proteomics : MCP*, *14*(1), 120–135. https://doi.org/10.1074/mcp.m114.041012

Kim, D. I., Jensen, S. C., Noble, K. A., Kc, B., Roux, K. H., Motamedchaboki, K., & Roux, K. J. (2016). An improved smaller biotin ligase for BioID proximity labeling. *Molecular Biology of the Cell*, *27*(8), 1188–1196. https://doi.org/10.1091/mbc.e15-12-0844

Kim, K. H., & Lee, M.-S. (2014). Autophagy—a key player in cellular and body metabolism. *Nature Reviews Endocrinology*, *10*(6), 322–337. https://doi.org/10.1038/nrendo.2014.35

Kim, S., Naylor, S. A., & DiAntonio, A. (2012). Drosophila Golgi membrane protein Ema promotes autophagosomal growth and function. *Proceedings of the National Academy of Sciences*, *109*(18), E1072–E1081. https://doi.org/10.1073/pnas.1120320109

Kimura, S., Noda, T., & Yoshimori, T. (2007). Dissection of the Autophagosome Maturation Process by a Novel Reporter Protein, Tandem Fluorescent-Tagged LC3. *Autophagy*, *3*(5), 452–460. https://doi.org/10.4161/auto.4451

Kitagishi, Y., & Matsuda, S. (2013). RUFY, Rab and Rap Family Proteins Involved in a Regulation of Cell Polarity and Membrane Trafficking. *International Journal of Molecular Sciences*, *14*(3), 6487–6498. https://doi.org/10.3390/ijms14036487

Kiyokawa, E., Hashimoto, Y., Kobayashi, S., Sugimura, H., Kurata, T., & Matsuda, M. (1998). Activation of Rac1 by a Crk SH3-binding protein, DOCK180. *Genes & Development*, *12*(21), 3331–3336. https://doi.org/10.1101/gad.12.21.3331

Klinkert, K., & Echard, A. (2016). Rab35 GTPase: A Central Regulator of Phosphoinositides and F-actin in Endocytic Recycling and Beyond. *Traffic*, *17*(10), 1063–1077. https://doi.org/10.1111/tra.12422

Kloer, D. P., Rojas, R., Ivan, V., Moriyama, K., Vlijmen, T. van, Murthy, N., Ghirlando, R., Sluijs, P. van der, Hurley, J. H., & Bonifacino, J. S. (2010). Assembly of the biogenesis of lysosome-related organelles complex-3 (BLOC-3) and its interaction with Rab9. *The Journal of Biological Chemistry*, *285*(10), 7794–7804. https://doi.org/10.1074/jbc.m109.069088

Klöpper, T. H., Kienle, N., Fasshauer, D., & Munro, S. (2012). Untangling the evolution of Rab G proteins: implications of a comprehensive genomic analysis. *BMC Biology*, *10*(1), 71. https://doi.org/10.1186/1741-7007-10-71

Kluss, J. H., Mamais, A., & Cookson, M. R. (2019). LRRK2 links genetic and sporadic Parkinson's disease. *Biochemical Society Transactions*, *47*(2), 651–661. https://doi.org/10.1042/bst20180462

Ko, J., Yoon, C., Piccoli, G., Chung, H. S., Kim, K., Lee, J.-R., Lee, H. W., Kim, H., Sala, C., & Kim, E. (2006). Organization of the Presynaptic Active Zone by ERC2/CAST1-Dependent Clustering of the

Tandem PDZ Protein Syntenin-1. *Journal of Neuroscience*, *26*(3), 963–970. https://doi.org/10.1523/jneurosci.4475-05.2006

Kobe, B., & Kajava, A. V. (2001). The leucine-rich repeat as a protein recognition motif. *Current Opinion in Structural Biology*, *11*(6), 725–732. https://doi.org/10.1016/s0959-440x(01)00266-4

Koch, D., Rai, A., Ali, I., Bleimling, N., Friese, T., Brockmeyer, A., Janning, P., Goud, B., Itzen, A., Müller, M. P., & Goody, R. S. (2016). A pull-down procedure for the identification of unknown GEFs for small GTPases. *Small GTPases*, *7*(2), 93–106. https://doi.org/10.1080/21541248.2016.1156803

Kourlas, P. J., Strout, M. P., Becknell, B., Veronese, M. L., Croce, C. M., Theil, K. S., Krahe, R., Ruutu, T., Knuutila, S., Bloomfield, C. D., & Caligiuri, M. A. (2000). Identification of a gene at 11q23 encoding a guanine nucleotide exchange factor: Evidence for its fusion with MLL in acute myeloid leukemia. *Proceedings of the National Academy of Sciences*, *97*(5), 2145–2150. https://doi.org/10.1073/pnas.040569197

Krauss, S., So, J., Hambrock, M., Köhler, A., Kunath, M., Scharff, C., Wessling, M., Grzeschik, K.-H., Schneider, R., & Schweiger, S. (2009). Point mutations in GLI3 lead to misregulation of its subcellular localization. *PloS One*, *4*(10), e7471. https://doi.org/10.1371/journal.pone.0007471

Kucera, A., Distefano, M. B., Berg-Larsen, A., Skjeldal, F., Repnik, U., Bakke, O., & Progida, C. (2016). Spatiotemporal Resolution of Rab9 and CI-MPR Dynamics in the Endocytic Pathway. *Traffic (Copenhagen, Denmark)*, *17*(3), 211–229. https://doi.org/10.1111/tra.12357

Kukimoto-Niino, M., Tsuda, K., Ihara, K., Mishima-Tsumagari, C., Honda, K., Ohsawa, N., & Shirouzu, M. (2019). Structural Basis for the Dual Substrate Specificity of DOCK7 Guanine Nucleotide Exchange Factor. *Structure (London, England : 1993)*, *27*(5), 741-748.e3. https://doi.org/10.1016/j.str.2019.02.001

Kumar, Adesh, & Biswas, P. (2019). Effect of site-directed point mutations on protein misfolding: A simulation study. *Proteins: Structure, Function, and Bioinformatics*, *87*(9), 760–773. https://doi.org/10.1002/prot.25702

Kumar, Ambuj, Rajendran, V., Sethumadhavan, R., & Purohit, R. (2013). CEP proteins: the knights of centrosome dynasty. *Protoplasma*, *250*(5), 965–983. https://doi.org/10.1007/s00709-013-0488-9

Kunita, R., Otomo, A., Mizumura, H., Suzuki-Utsunomiya, K., Hadano, S., & Ikeda, J.-E. (2007). The Rab5 Activator ALS2/alsin Acts as a Novel Rac1 Effector through Rac1-activated Endocytosis. *Journal of Biological Chemistry*, *282*(22), 16599–16611. https://doi.org/10.1074/jbc.m610682200

Kurokawa, K., & Nakano, A. (2019). The ER exit sites are specialized ER zones for the transport of cargo proteins from the ER to the Golgi apparatus. *The Journal of Biochemistry*, *165*(2), 109–114. https://doi.org/10.1093/jb/mvy080

Kurokawa, K., Okamoto, M., & Nakano, A. (2014). Contact of cis-Golgi with ER exit sites executes cargo capture and delivery from the ER. *Nature Communications*, *5*(1), 3653. https://doi.org/10.1038/ncomms4653

Kweon, H.-S., Beznoussenko, G. V., Micaroni, M., Polishchuk, R. S., Trucco, A., Martella, O., Giandomenico, D. D., Marra, P., Fusella, A., Pentima, A. D., Berger, E. G., Geerts, W. J. C., Koster, A. J., Burger, K. N. J., Luini, A., & Mironov, A. A. (2004). Golgi Enzymes Are Enriched in Perforated Zones of Golgi Cisternae but Are Depleted in COPI Vesicles. *Molecular Biology of the Cell*, *15*(10), 4710–4724. https://doi.org/10.1091/mbc.e03-12-0881

Lai, F., Stubbs, L., & Artzt, K. (1994). Molecular Analysis of Mouse Rab11b: A New Type of Mammalian YPT/Rab Protein. *Genomics*, *22*(3), 610–616. https://doi.org/10.1006/geno.1994.1434

Lamarche-Vane, N., & Hall, A. (1998). CdGAP, a Novel Proline-rich GTPase-activating Protein for Cdc42 and Rac. *Journal of Biological Chemistry*, *273*(44), 29172–29177. https://doi.org/10.1074/jbc.273.44.29172

Langemeyer, L., Bastos, R. N., Cai, Y., Itzen, A., Reinisch, K. M., & Barr, F. A. (2014). Diversity and plasticity in Rab GTPase nucleotide release mechanism has consequences for Rab activation and inactivation. *ELife*, *3*, e01623. https://doi.org/10.7554/elife.01623

Langemeyer, L., Borchers, A.-C., Herrmann, E., Füllbrunn, N., Han, Y., Perz, A., Auffarth, K., Kümmel, D., & Ungermann, C. (2020). A conserved and regulated mechanism drives endosomal Rab transition. *ELife*, *9*, e56090. https://doi.org/10.7554/elife.56090

Lanoix, J., Ouwendijk, J., Lin, C., Stark, A., Love, H. D., Ostermann, J., & Nilsson, T. (1999). GTP hydrolysis by arf-1 mediates sorting and concentration of Golgi resident enzymes into functional COP I vesicles. *The EMBO Journal*, *18*(18), 4935–4948. https://doi.org/10.1093/emboj/18.18.4935

Lapierre, L. A., Dorn, M. C., Zimmerman, C. F., Navarre, J., Burnette, J. O., & Goldenring, J. R. (2003). Rab11b resides in a vesicular compartment distinct from Rab11a in parietal cells and other epithelial cells. *Experimental Cell Research*, *290*(2), 322–331. https://doi.org/10.1016/s0014-4827(03)00340-9

Lawrence, E. J., Arpag, G., Norris, S. R., & Zanic, M. (2018). Human CLASP2 specifically regulates microtubule catastrophe and rescue. *Molecular Biology of the Cell*, *29*(10), 1168–1177. https://doi.org/10.1091/mbc.e18-01-0016

Lazarou, M., Sliter, D. A., Kane, L. A., Sarraf, S. A., Wang, C., Burman, J. L., Sideris, D. P., Fogel, A. I., & Youle, R. J. (2015). The ubiquitin kinase PINK1 recruits autophagy receptors to induce mitophagy. *Nature*, *524*(7565), 309–314. https://doi.org/10.1038/nature14893

Lee, M. C. S., Orci, L., Hamamoto, S., Futai, E., Ravazzola, M., & Schekman, R. (2005). Sar1p N-Terminal Helix Initiates Membrane Curvature and Completes the Fission of a COPII Vesicle. *Cell*, *122*(4), 605–617. https://doi.org/10.1016/j.cell.2005.07.025

Lee, P. L., Ohlson, M. B., & Pfeffer, S. R. (2015). Rab6 regulation of the kinesin family KIF1C motor domain contributes to Golgi tethering. *ELife*, *4*, e06029. https://doi.org/10.7554/elife.06029

Lévay, M., Bartos, B., & Ligeti, E. (2013). p190RhoGAP has cellular RacGAP activity regulated by a polybasic region. *Cellular Signalling*, *25*(6), 1388–1394. https://doi.org/10.1016/j.cellsig.2013.03.004

Levine, B., & Kroemer, G. (2008). Autophagy in the pathogenesis of disease. *Cell*, *132*(1), 27–42. https://doi.org/10.1016/j.cell.2007.12.018

Levine, B., & Kroemer, G. (2019). Biological Functions of Autophagy Genes: A Disease Perspective. *Cell*, *176*(1–2), 11–42. https://doi.org/10.1016/j.cell.2018.09.048

Li, G., & Stahl, P. D. (1993). Structure-function relationship of the small GTPase rab5. *The Journal of Biological Chemistry*, *268*(32), 24475–24480.

Li, Y., Bakke, J., Finkelstein, D., Zeng, H., Wu, J., & Chen, T. (2018). HNRNPH1 is required for rhabdomyosarcoma cell growth and survival. *Oncogenesis*, *7*(1), 9. https://doi.org/10.1038/s41389-017-0024-4

Liang, Y., Niederstrasser, H., Edwards, M., Jackson, C. E., & Cooper, J. A. (2009). Distinct Roles for CARMIL Isoforms in Cell Migration. *Molecular Biology of the Cell*, *20*(24), 5290–5305. https://doi.org/10.1091/mbc.e08-10-1071

Lim, K. B., Bu, W., Goh, W. I., Koh, E., Ong, S. H., Pawson, T., Sudhaharan, T., & Ahmed, S. (2008). The Cdc42 Effector IRSp53 Generates Filopodia by Coupling Membrane Protrusion with Actin Dynamics. *Journal of Biological Chemistry*, *283*(29), 20454–20472. https://doi.org/10.1074/jbc.m710185200

Lin, Q., Yang, W., Baird, D., Feng, Q., & Cerione, R. A. (2006). Identification of a DOCK180-related Guanine Nucleotide Exchange Factor That Is Capable of Mediating a Positive Feedback Activation of Cdc42. *Journal of Biological Chemistry*, *281*(46), 35253–35262. https://doi.org/10.1074/jbc.m606248200

Lipatova, Z., Belogortseva, N., Zhang, X. Q., Kim, J., Taussig, D., & Segev, N. (2012). Regulation of selective autophagy onset by a Ypt/Rab GTPase module. *Proceedings of the National Academy of Sciences of the United States of America*, *109*(18), 6981–6986. https://doi.org/10.1073/pnas.1121299109

Lis, P., Burel, S., Steger, M., Mann, M., Brown, F., Diez, F., Tonelli, F., Holton, J. L., Ho, P. W., Ho, S.-L., Chou, M.-Y., Polinski, N. K., Martinez, T. N., Davies, P., & Alessi, D. R. (2018). Development of phospho-specific Rab protein antibodies to monitor in vivo activity of the LRRK2 Parkinson's disease kinase. *The Biochemical Journal*, *475*(1), 1–22. https://doi.org/10.1042/bcj20170802

Liu, J.-W., He, C.-Y., Sun, L.-P., Xu, Q., Xing, C.-Z., & Yuan, Y. (2013). The DNA Repair Gene ERCC6 rs1917799 Polymorphism is Associated with Gastric Cancer Risk in Chinese. *Asian Pacific Journal of Cancer Prevention*, *14*(10), 6103–6108. https://doi.org/10.7314/apjcp.2013.14.10.6103

Liu, Tao, Li, H., Hong, W., & Han, W. (2016). Brefeldin A-inhibited guanine nucleotide exchange protein 3 is localized in lysosomes and regulates GABA signaling in hippocampal neurons. *Journal of Neurochemistry*, *139*(5), 748–756. https://doi.org/10.1111/jnc.13859

Liu, Tianyang, Dai, A., Cao, Y., Zhang, R., Dong, M.-Q., & Wang, H.-W. (2017). Structural Insights of WHAMM's Interaction with Microtubules by Cryo-EM. *Journal of Molecular Biology*, *429*(9), 1352–1363. https://doi.org/10.1016/j.jmb.2017.03.022

Liu, Xiaoliang, Yang, X., Li, Y., Zhao, S., Li, C., Ma, P., & Mao, B. (2016). Trip12 is an E3 ubiquitin ligase for USP7/HAUSP involved in the DNA damage response. *FEBS Letters*, *590*(23), 4213–4222. https://doi.org/10.1002/1873-3468.12471

Liu, Xinwei, & Ridgway, N. D. (2014). Characterization of the sterol and phosphatidylinositol 4-phosphate binding properties of Golgi-associated OSBP-related protein 9 (ORP9). *PloS One*, *9*(9), e108368. https://doi.org/10.1371/journal.pone.0108368

Liu, Y., Yan, X., & Zhou, T. (2013). TBCK influences cell proliferation, cell size and mTOR signaling pathway. *PloS One*, *8*(8), e71349. https://doi.org/10.1371/journal.pone.0071349

Liu, Z., Zhan, Y., Tu, Y., Chen, K., Liu, Z., & Wu, C. (2014). PDZ and LIM domain protein 1(PDLIM1)/CLP36 promotes breast cancer cell migration, invasion and metastasis through interaction with α-actinin. *Oncogene*, *34*(10), 1300–1311. https://doi.org/10.1038/onc.2014.64

Lord, C., Ferro-Novick, S., & Miller, E. A. (2013). The Highly Conserved COPII Coat Complex Sorts Cargo from the Endoplasmic Reticulum and Targets It to the Golgi. *Cold Spring Harbor Perspectives in Biology*, *5*(2), a013367. https://doi.org/10.1101/cshperspect.a013367

Lőrincz, P., Tóth, S., Benkő, P., Lakatos, Z., Boda, A., Glatz, G., Zobel, M., Bisi, S., Hegedűs, K., Takáts, S., Scita, G., & Juhász, G. (2017). Rab2 promotes autophagic and endocytic lysosomal degradation. *The Journal of Cell Biology*, *216*(7), 1937–1947. https://doi.org/10.1083/jcb.201611027

Lund, V. K., Madsen, K. L., & Kjaerulff, O. (2018). Drosophila Rab2 controls endosome-lysosome fusion and LAMP delivery to late endosomes. *Autophagy*, *14*(9), 1520–1542. https://doi.org/10.1080/15548627.2018.1458170

Luo, W., Liao, M., Liao, Y., Chen, X., Huang, C., Fan, J., & Liao, W. (2018). The role of kinesin KIF18A in the invasion and metastasis of hepatocellular carcinoma. *World Journal of Surgical Oncology*, *16*(1), 36. https://doi.org/10.1186/s12957-018-1342-5

Ma, M., Liu, J.-J., Li, Y., Huang, Y., Ta, N., Chen, Y., Fu, H., Ye, M.-D., Ding, Y., Huang, W., Wang, J., Dong, M.-Q., Yu, L., & Wang, H.-W. (2017). Cryo-EM structure and biochemical analysis reveal the basis of the functional difference between human PI3KC3-C1 and -C2. *Cell Research*, *27*(8), 989–1001. https://doi.org/10.1038/cr.2017.94

Macaluso, M., Russo, G., Cinti, C., Bazan, V., Gebbia, N., & Russo, A. (2002). Ras family genes: An interesting link between cell cycle and cancer. *Journal of Cellular Physiology*, *192*(2), 125–130. https://doi.org/10.1002/jcp.10109

Machesky, L. M. (2019). Rab11FIP proteins link endocytic recycling vesicles for cytoskeletal transport and tethering. *Bioscience Reports*, *39*(1), BSR20182219. https://doi.org/10.1042/bsr20182219

Macia, E., Luton, F., Partisani, M., Cherfils, J., Chardin, P., & Franco, M. (2004). The GDP-bound form of Arf6 is located at the plasma membrane. *Journal of Cell Science*, *117*(11), 2389–2398. https://doi.org/10.1242/jcs.01090

Madaule, P., Furuyashiki, T., Reid, T., Ishizaki, T., Watanabe, G., Morii, N., & Narumiya, S. (1995). A novel partner for the GTP-bound forms of rho and rac. *FEBS Letters*, *377*(2), 243–248. https://doi.org/10.1016/0014-5793(95)01351-2

Mahajan, D., Tie, H. C., Chen, B., & Lu, L. (2019). Dopey1-Mon2 complex binds to dual-lipids and recruits kinesin-1 for membrane trafficking. *Nature Communications*, *10*(1), 3218. https://doi.org/10.1038/s41467-019-11056-5

Manning, B. D., & Cantley, L. C. (2003). Rheb fills a GAP between TSC and TOR. *Trends in Biochemical Sciences*, *28*(11), 573–576. https://doi.org/10.1016/j.tibs.2003.09.003

Manolea, F., Chun, J., Chen, D. W., Clarke, I., Summerfeldt, N., Dacks, J. B., & Melançon, P. (2010). Arf3 is activated uniquely at the trans-Golgi network by brefeldin A-inhibited guanine nucleotide exchange factors. *Molecular Biology of the Cell*, *21*(11), 1836–1849. https://doi.org/10.1091/mbc.e10-01-0016

Mao, Z., & Nakamura, F. (2020). Structure and Function of Filamin C in the Muscle Z-Disc. *International Journal of Molecular Sciences*, *21*(8), 2696. https://doi.org/10.3390/ijms21082696

Marin-Valencia, I., Gerondopoulos, A., Zaki, M. S., Ben-Omran, T., Almureikhi, M., Demir, E., Guemez-Gamboa, A., Gregor, A., Issa, M. Y., Appelhof, B., Roosing, S., Musaev, D., Rosti, B., Wirth, S., Stanley, V., Baas, F., Barr, F. A., & Gleeson, J. G. (2017). Homozygous Mutations in TBC1D23 Lead to a Non-degenerative Form of Pontocerebellar Hypoplasia. *The American Journal of Human Genetics*, *101*(3), 441–450. https://doi.org/10.1016/j.ajhg.2017.07.015

Markgraf, D. F., Ahnert, F., Arlt, H., Mari, M., Peplowska, K., Epp, N., Griffith, J., Reggiori, F., & Ungermann, C. (2009). The CORVET subunit Vps8 cooperates with the Rab5 homolog Vps21 to induce clustering of late endosomal compartments. *Molecular Biology of the Cell*, *20*(24), 5276–5289. https://doi.org/10.1091/mbc.e09-06-0521

Martelly, W., Fellows, B., Senior, K., Marlowe, T., & Sharma, S. (2019). Identification of a noncanonical RNA binding domain in the U2 snRNP protein SF3A1. *RNA*, *25*(11), 1509–1521. https://doi.org/10.1261/rna.072256.119

Martin, G. A., Viskoohil, D., Bollag, G., McCabe, P. C., Crosier, W. J., Haubruck, H., Conroy, L., Clark, R., O'Connell, P., Cawthon, R. M., Innis, M. A., & McCormick, F. (1990). The GAP-related domain of the neurofibromatosis type 1 gene product interacts with ras p21. *Cell*, *63*(4), 843–849. https://doi.org/10.1016/0092-8674(90)90150-d

Martin, T. D., Chen, X.-W., Kaplan, R. E. W., Saltiel, A. R., Walker, C. L., Reiner, D. J., & Der, C. J. (2014). Ral and Rheb GTPase activating proteins integrate mTOR and GTPase signaling in aging, autophagy, and tumor cell invasion. *Molecular Cell*, *53*(2), 209–220. https://doi.org/10.1016/j.molcel.2013.12.004

Matanis, T., Akhmanova, A., Wulf, P., Nery, E. D., Weide, T., Stepanova, T., Galjart, N., Grosveld, F., Goud, B., Zeeuw, C. I. D., Barnekow, A., & Hoogenraad, C. C. (2002). Bicaudal-D regulates COPI-independent Golgi–ER transport by recruiting the dynein–dynactin motor complex. *Nature Cell Biology*, *4*(12), 986–992. https://doi.org/10.1038/ncb891

Matchett, K. B., McFarlane, S., Hamilton, S. E., Eltuhamy, Y. S. A., Davidson, M. A., Murray, J. T., Faheem, A. M., & El-Tanani, M. (2014). Ran GTPase in nuclear envelope formation and cancer metastasis. *Advances in Experimental Medicine and Biology*, *773*, 323–351. https://doi.org/10.1007/978-1-4899-8032-8_15

Matsunaga, K., Noda, T., & Yoshimori, T. (2009). Binding Rubicon to cross the Rubicon. *Autophagy*, *5*(6), 876–877. https://doi.org/10.4161/auto.9098

Mavioğlu, R. N., Kara, B., Akansel, G., Nalbant, G., & Tolun, A. (2019). FAM160B1 deficit associated with microcephaly, severe intellectual disability, ataxia, behavioral abnormalities and speech problems. *Clinical Genetics*, *96*(5), 456–460. https://doi.org/10.1111/cge.13612

McDonold, C. M., & Fromme, J. C. (2014). Four GTPases differentially regulate the Sec7 Arf-GEF to direct traffic at the trans-golgi network. *Developmental Cell*, *30*(6), 759–767. https://doi.org/10.1016/j.devcel.2014.07.016

McHugh, T., Drechsler, H., McAinsh, A. D., Carter, N. J., & Cross, R. A. (2018). Kif15 functions as an active mechanical ratchet. *Molecular Biology of the Cell*, *29*(14), 1743–1752. https://doi.org/10.1091/mbc.e18-03-0151

Medina, F., Carter, A. M., Dada, O., Gutowski, S., Hadas, J., Chen, Z., & Sternweis, P. C. (2013). Activated RhoA is a positive feedback regulator of the Lbc family of Rho guanine nucleotide exchange factor proteins. *The Journal of Biological Chemistry*, *288*(16), 11325–11333. https://doi.org/10.1074/jbc.m113.450056

Mei, K., & Guo, W. (2018). The exocyst complex. *Current Biology*, *28*(17), R922–R925. https://doi.org/10.1016/j.cub.2018.06.042

Miaczynska, M., Christoforidis, S., Giner, A., Shevchenko, A., Uttenweiler-Joseph, S., Habermann, B., Wilm, M., Parton, R. G., & Zerial, M. (2004). APPL Proteins Link Rab5 to Nuclear Signal Transduction via an Endosomal Compartment. *Cell*, *116*(3), 445–456. https://doi.org/10.1016/s0092-8674(04)00117-5

Miller, E. A., & Barlowe, C. (2010). Regulation of coat assembly—sorting things out at the ER. *Current Opinion in Cell Biology*, *22*(4), 447–453. https://doi.org/10.1016/j.ceb.2010.04.003

Mills, I. G., Jones, A. T., & Clague, M. J. (1999). Regulation of endosome fusion. *Molecular Membrane Biology*, *16*(1), 73–79. https://doi.org/10.1080/096876899294788

Miserey-Lenkei, S., Bousquet, H., Pylypenko, O., Bardin, S., Dimitrov, A., Bressanelli, G., Bonifay, R., Fraisier, V., Guillou, C., Bougeret, C., Houdusse, A., Echard, A., & Goud, B. (2017). Coupling fission and exit of RAB6 vesicles at Golgi hotspots through kinesin-myosin interactions. *Nature Communications*, *8*(1), 1254. https://doi.org/10.1038/s41467-017-01266-0

Miyamoto, Y., Yamauchi, J., Sanbe, A., & Tanoue, A. (2007). Dock6, a Dock-C subfamily guanine nucleotide exchanger, has the dual specificity for Rac1 and Cdc42 and regulates neurite outgrowth. *Experimental Cell Research*, *313*(4), 791–804. https://doi.org/10.1016/j.yexcr.2006.11.017

Mizuno-Yamasaki, E., Rivera-Molina, F., & Novick, P. (2012). GTPase networks in membrane traffic. *Annual Review of Biochemistry*, *81*(1), 637–659. https://doi.org/10.1146/annurev-biochem-052810-093700

Mochizuki, Y., Ohashi, R., Kawamura, T., Iwanari, H., Kodama, T., Naito, M., & Hamakubo, T. (2013). Phosphatidylinositol 3-phosphatase myotubularin-related protein 6 (MTMR6) is regulated by small GTPase Rab1B in the early secretory and autophagic pathways. *The Journal of Biological Chemistry*, *288*(2), 1009–1021. https://doi.org/10.1074/jbc.m112.395087

Moncrieff, C. L., Bailey, M. E. S., Morrison, N., & Johnson, K. J. (1999). Cloning and Chromosomal Localization of Human Cdc42-Binding Protein Kinase β. *Genomics*, *57*(2), 297–300. https://doi.org/10.1006/geno.1999.5769

Monetta, P., Slavin, I., Romero, N., & Alvarez, C. (2007). Rab1b Interacts with GBF1 and Modulates both ARF1 Dynamics and COPI Association. *Molecular Biology of the Cell*, *18*(7), 2400–2410. https://doi.org/10.1091/mbc.e06-11-1005

Moskalenko, S., Tong, C., Rosse, C., Mirey, G., Formstecher, E., Daviet, L., Camonis, J., & White, M. A. (2003). Ral GTPases Regulate Exocyst Assembly through Dual Subunit Interactions. *Journal of Biological Chemistry*, *278*(51), 51743–51748. https://doi.org/10.1074/jbc.m308702200

Moyer, B. D., Allan, B. B., & Balch, W. E. (2001). Rab1 Interaction with a GM130 Effector Complex Regulates COPII Vesicle cis-Golgi Tethering: Rab1-GM130 Complex Regulates COPII-Golgi Transport. *Traffic*, *2*(4), 268–276. https://doi.org/10.1034/j.1600-0854.2001.1o007.x

Mukhopadhyay, A., Quiroz, J. A., & Wolkoff, A. W. (2014). Rab1a regulates sorting of early endocytic vesicles. *American Journal of Physiology-Gastrointestinal and Liver Physiology*, *306*(5), G412–G424. https://doi.org/10.1152/ajpgi.00118.2013

Müller, M. P., & Goody, R. S. (2017). Molecular control of Rab activity by GEFs, GAPs and GDI. *Small GTPases*, *9*(1–2), 5–21. https://doi.org/10.1080/21541248.2016.1276999

Munro, S. (1995). An investigation of the role of transmembrane domains in Golgi protein retention. *The EMBO Journal*, *14*(19), 4695–4704. https://doi.org/10.1002/j.1460-2075.1995.tb00151.x

Murata, T., Delprato, A., Ingmundson, A., Toomre, D. K., Lambright, D. G., & Roy, C. R. (2006). The Legionella pneumophila effector protein DrrA is a Rab1 guanine nucleotide-exchange factor. *Nature Cell Biology*, *8*(9), 971–977. https://doi.org/10.1038/ncb1463

Murray, J. T., Panaretou, C., Stenmark, H., Miaczynska, M., & Backer, J. M. (2002). Role of Rab5 in the Recruitment of hVps34/p150 to the Early Endosome. *Traffic*, *3*(6), 416–427. https://doi.org/10.1034/j.1600-0854.2002.30605.x

Nakamura, M., Tanaka, N., Kitamura, N., & Komada, M. (2006). Clathrin anchors deubiquitinating enzymes, AMSH and AMSH-like protein, on early endosomes. *Genes to Cells*, *11*(6), 593–606. https://doi.org/10.1111/j.1365-2443.2006.00963.x

Nakamura, N., Lowe, M., Levine, T. P., Rabouille, C., & Warren, G. (1997). The Vesicle Docking Protein p115 Binds GM130, a cis-Golgi Matrix Protein, in a Mitotically Regulated Manner. *Cell*, *89*(3), 445–455. https://doi.org/10.1016/s0092-8674(00)80225-1

Nakamura, T., Komiya, M., Sone, K., Hirose, E., Gotoh, N., Morii, H., Ohta, Y., & Mori, N. (2002). Grit, a GTPase-Activating Protein for the Rho Family, Regulates Neurite Extension through Association with the TrkA Receptor and N-Shc and CrkL/Crk Adapter Molecules. *Molecular and Cellular Biology*, *22*(24), 8721–8734. https://doi.org/10.1128/mcb.22.24.8721-8734.2002

Namekata, K., Enokido, Y., Iwasawa, K., & Kimura, H. (2004). MOCA Induces Membrane Spreading by Activating Rac1. *Journal of Biological Chemistry*, *279*(14), 14331–14337. https://doi.org/10.1074/jbc.m311275200

Naslavsky, N., & Caplan, S. (2018). The enigmatic endosome – sorting the ins and outs of endocytic trafficking. *J Cell Sci*, *131*(13), jcs216499. https://doi.org/10.1242/jcs.216499

Nawrotek, A., Zeghouf, M., & Cherfils, J. (2016). Allosteric regulation of Arf GTPases and their GEFs at the membrane interface. *Small GTPases*, *7*(4), 283–296. https://doi.org/10.1080/21541248.2016.1215778

Ng, M. M., Dippold, H. C., Buschman, M. D., Noakes, C. J., & Field, S. J. (2013). GOLPH3L antagonizes GOLPH3 to determine Golgi morphology. *Molecular Biology of the Cell*, *24*(6), 796–808. https://doi.org/10.1091/mbc.e12-07-0525

Nguyen, L. K., Kholodenko, B. N., & Kriegsheim, A. von. (2016). Rac1 and RhoA: Networks, loops and bistability. *Small GTPases*, *9*(4), 316–321. https://doi.org/10.1080/21541248.2016.1224399

Nilsson, T., Au, C. E., & Bergeron, J. J. M. (2009). Sorting out glycosylation enzymes in the Golgi apparatus. *FEBS Letters*, *583*(23), 3764–3769. https://doi.org/10.1016/j.febslet.2009.10.064

Nilsson, T., Slusarewicz, P., Hoe, M. H., & Warren, G. (1993). Kin recognition. *FEBS Letters*, *330*(1), 1–4. https://doi.org/10.1016/0014-5793(93)80906-b

Niu, J., Profirovic, J., Pan, H., Vaiskunaite, R., & Voyno-Yasenetskaya, T. (2003). G Protein betagamma subunits stimulate p114RhoGEF, a guanine nucleotide exchange factor for RhoA and Rac1: regulation of cell shape and reactive oxygen species production. *Circulation Research*, *93*(9), 848–856. https://doi.org/10.1161/01.res.0000097607.14733.0c

Noda, Y., Takeya, R., Ohno, S., Naito, S., Ito, T., & Sumimoto, H. (2001). Human homologues of the Caenorhabditis elegans cell polarity protein PAR6 as an adaptor that links the small GTPases Rac and Cdc42 to atypical protein kinase C. *Genes to Cells*, *6*(2), 107–119. https://doi.org/10.1046/j.1365-2443.2001.00404.x

Nozawa, T., Minowa-Nozawa, A., Aikawa, C., & Nakagawa, I. (2016). The STX6-VTI1B-VAMP3 complex facilitates xenophagy by regulating the fusion between recycling endosomes and autophagosomes. *Autophagy*, *13*(1), 57–69. https://doi.org/10.1080/15548627.2016.1241924

Oguchi, M. E., Noguchi, K., & Fukuda, M. (2017). TBC1D12 is a novel Rab11-binding protein that modulates neurite outgrowth of PC12 cells. *PLOS ONE*, *12*(4), e0174883. https://doi.org/10.1371/journal.pone.0174883

Ogungbenro, Y. A., Tena, T. C., Gaboriau, D., Lalor, P., Dockery, P., Philipp, M., & Morrison, C. G. (2018). Centrobin controls primary ciliogenesis in vertebrates. *The Journal of Cell Biology*, *217*(4), 1205–1215. https://doi.org/10.1083/jcb.201706095

Ohashi, Y., Soler, N., Ortegón, M. G., Zhang, L., Kirsten, M. L., Perisic, O., Masson, G. R., Burke, J. E., Jakobi, A. J., Apostolakis, A. A., Johnson, C. M., Ohashi, M., Ktistakis, N. T., Sachse, C., & Williams, R. L. (2016). Characterization of Atg38 and NRBF2, a fifth subunit of the autophagic Vps34/PIK3C3 complex. *Autophagy*, *12*(11), 1–16. https://doi.org/10.1080/15548627.2016.1226736

Ohashi, Y., Tremel, S., Masson, G. R., McGinney, L., Boulanger, J., Rostislavleva, K., Johnson, C. M., Niewczas, I., Clark, J., & Williams, R. L. (2020). Membrane characteristics tune activities of endosomal and autophagic human VPS34 complexes. *ELife*, *9*, e58281. https://doi.org/10.7554/elife.58281

Ohashi, Y., Tremel, S., & Williams, R. L. (2018). VPS34 complexes from a structural perspective. *Journal of Lipid Research*, jlr.R089490. https://doi.org/10.1194/jlr.r089490

Okabe, T., Nakamura, T., Nishimura, Y. N., Kohu, K., Ohwada, S., Morishita, Y., & Akiyama, T. (2003). RICS, a Novel GTPase-activating Protein for Cdc42 and Rac1, Is Involved in the β-Catenin-N-cadherin and N -Methyl-d-aspartate Receptor Signaling. *Journal of Biological Chemistry*, *278*(11), 9920–9927. https://doi.org/10.1074/jbc.m208872200

O'Loughlin, T., Masters, T. A., & Buss, F. (2018). The MYO6 interactome reveals adaptor complexes coordinating early endosome and cytoskeletal dynamics. *EMBO Reports*, *19*(4). https://doi.org/10.15252/embr.201744884

Onnis, A., Finetti, F., Patrussi, L., Gottardo, M., Cassioli, C., Spanò, S., & Baldari, C. T. (2015). The small GTPase Rab29 is a common regulator of immune synapse assembly and ciliogenesis. *Cell Death and Differentiation*, *22*(10), 1687–1699. https://doi.org/10.1038/cdd.2015.17

Opat, A. S., Houghton, F., & Gleeson, P. A. (2000). Medial Golgi but Not Late Golgi Glycosyltransferases Exist as High Molecular Weight Complexes ROLE OF LUMINAL DOMAIN IN COMPLEX FORMATION AND LOCALIZATION*. *Journal of Biological Chemistry*, *275*(16), 11836–11845. https://doi.org/10.1074/jbc.275.16.11836

O'Rourke, B. P., Gomez-Ferreria, M. A., Berk, R. H., Hackl, A. M. U., Nicholas, M. P., O'Rourke, S. C., Pelletier, L., & Sharp, D. J. (2014). Cep192 controls the balance of centrosome and non-centrosomal microtubules during interphase. *PloS One*, *9*(6), e101001. https://doi.org/10.1371/journal.pone.0101001

Otto, G. P., Razi, M., Morvan, J., Stenner, F., & Tooze, S. A. (2010). A Novel Syntaxin 6-Interacting Protein, SHIP164, Regulates Syntaxin 6-Dependent Sorting from Early Endosomes. *Traffic*, *11*(5), 688–705. https://doi.org/10.1111/j.1600-0854.2010.01049.x

Ozdemir, E. S., Jang, H., Gursoy, A., Keskin, O., Li, Z., Sacks, D. B., & Nussinov, R. (2018). Unraveling the molecular mechanism of interactions of the Rho GTPases Cdc42 and Rac1 with the scaffolding

protein IQGAP2. *The Journal of Biological Chemistry*, *293*(10), 3685–3699. https://doi.org/10.1074/jbc.ra117.001596

Paiano, A., Margiotta, A., Luca, M. D., & Bucci, C. (2018). Yeast Two-Hybrid Assay to Identify Interacting Proteins. *Current Protocols in Protein Science*, *95*(1), e70. https://doi.org/10.1002/cpps.70

Pal, A., Severin, F., Lommer, B., Shevchenko, A., & Zerial, M. (2006). Huntingtin–HAP40 complex is a novel Rab5 effector that regulates early endosome motility and is up-regulated in Huntington's disease. *The Journal of Cell Biology*, *172*(4), 605–618. https://doi.org/10.1083/jcb.200509091

Pan, X., Eathiraj, S., Munson, M., & Lambright, D. G. (2006). TBC-domain GAPs for Rab GTPases accelerate GTP hydrolysis by a dual-finger mechanism. *Nature*, *442*(7100), 303–306. https://doi.org/10.1038/nature04847

Panarella, A., Bexiga, M. G., Galea, G., Neill, E. D. O., Salvati, A., Dawson, K. A., & Simpson, J. C. (2016). A systematic High-Content Screening microscopy approach reveals key roles for Rab33b, OATL1 and Myo6 in nanoparticle trafficking in HeLa cells. *Scientific Reports*, *6*(1), 28865. https://doi.org/10.1038/srep28865

Pantazopoulou, A., & Glick, B. S. (2019). A Kinetic View of Membrane Traffic Pathways Can Transcend the Classical View of Golgi Compartments. *Frontiers in Cell and Developmental Biology*, *7*, 153. https://doi.org/10.3389/fcell.2019.00153

Papanikou, E., & Glick, B. S. (2014). Golgi compartmentation and identity. *Current Opinion in Cell Biology*, *29*, 74–81. https://doi.org/10.1016/j.ceb.2014.04.010

Patel, D. S., Misenko, S. M., Her, J., & Bunting, S. F. (2017). BLM helicase regulates DNA repair by counteracting RAD51 loading at DNA double-strand break sites. *The Journal of Cell Biology*, *216*(11), 3521–3534. https://doi.org/10.1083/jcb.201703144

Pathak, R., & Dermardirossian, C. (2013). GEF-H1: orchestrating the interplay between cytoskeleton and vesicle trafficking. *Small GTPases*, *4*(3), 174–179. https://doi.org/10.4161/sgtp.24616

Patterson, G. H., Hirschberg, K., Polishchuk, R. S., Gerlich, D., Phair, R. D., & Lippincott-Schwartz, J. (2008). Transport through the Golgi Apparatus by Rapid Partitioning within a Two-Phase Membrane System. *Cell*, *133*(6), 1055–1067. https://doi.org/10.1016/j.cell.2008.04.044

Pavlos, N. J., & Jahn, R. (2011). Distinct yet overlapping roles of Rab GTPases on synaptic vesicles. *Small GTPases*, *2*(2), 77–81. https://doi.org/10.4161/sgtp.2.2.15201

Peränen, J. (2011). Rab8 GTPase as a regulator of cell shape. *Cytoskeleton*, *68*(10), 527–539. https://doi.org/10.1002/cm.20529

Pfeffer, S. R. (2010). How the Golgi works: A cisternal progenitor model. *Proceedings of the National Academy of Sciences*, *107*(46), 19614–19618. https://doi.org/10.1073/pnas.1011016107

Pfeffer, S. R. (2017). Rab GTPases: master regulators that establish the secretory and endocytic pathways. *Molecular Biology of the Cell*, *28*(6), 712–715. https://doi.org/10.1091/mbc.e16-10-0737

Pham, N., Cheglakov, I., Koch, C. A., Hoog, C. L. de, Moran, M. F., & Rotin, D. (2000). The guanine nucleotide exchange factor CNrasGEF activates Ras in response to cAMP and cGMP. *Current Biology*, *10*(9), 555–558. https://doi.org/10.1016/s0960-9822(00)00473-5

Pichaud, F., Walther, R. F., & Almeida, F. N. de. (2019). Regulation of Cdc42 and its effectors in epithelial morphogenesis. *Journal of Cell Science*, *132*(10), jcs217869. https://doi.org/10.1242/jcs.217869

Popoff, V., Adolf, F., Brügger, B., & Wieland, F. (2011). COPI Budding within the Golgi Stack. *Cold Spring Harbor Perspectives in Biology*, *3*(11), a005231. https://doi.org/10.1101/cshperspect.a005231

Purlyte, E., Dhekne, H. S., Sarhan, A. R., Gomez, R., Lis, P., Wightman, M., Martinez, T. N., Tonelli, F., Pfeffer, S. R., & Alessi, D. R. (2017). Rab29 activation of the Parkinson's disease-associated LRRK2 kinase. *The EMBO Journal*, *37*(1), 1–18. https://doi.org/10.15252/embj.201798099

Pylypenko, O., Hammich, H., Yu, I.-M., & Houdusse, A. (2017). Rab GTPases and their interacting protein partners: Structural insights into Rab functional diversity. *Small GTPases*, *9*(1–2), 22–48. https://doi.org/10.1080/21541248.2017.1336191

Rabouille, C., & Klumperman, J. (2005). The maturing role of COPI vesicles in intra-Golgi transport. *Nature Reviews Molecular Cell Biology*, *6*(10), 812–817. https://doi.org/10.1038/nrm1735

Rajendran, L., & Annaert, W. (2012). Membrane Trafficking Pathways in Alzheimer's Disease: Membrane Trafficking and Alzheimer's Disease. *Traffic*, *13*(6), 759–770. https://doi.org/10.1111/j.1600-0854.2012.01332.x

Ramalho, J. S., Anders, R., Jaissle, G. B., Seeliger, M. W., Huxley, C., & Seabra, M. C. (2002). Rapid degradation of dominant-negative Rab27 proteins in vivo precludes their use in transgenic mouse models. *BMC Cell Biology*, *3*(1), 26. https://doi.org/10.1186/1471-2121-3-26

Rana, M., Lachmann, J., & Ungermann, C. (2015). Identification of a Rab GTPase-activating protein cascade that controls recycling of the Rab5 GTPase Vps21 from the vacuole. *Molecular Biology of the Cell*, *26*(13), 2535–2549. https://doi.org/10.1091/mbc.e15-02-0062

Ravanan, P., Srikumar, I. F., & Talwar, P. (2017). Autophagy: The spotlight for cellular stress responses. *Life Sciences*, *188*, 53–67. https://doi.org/10.1016/j.lfs.2017.08.029

Reyes, C. C., Jin, M., Breznau, E. B., Espino, R., Delgado-Gonzalo, R., Goryachev, A. B., & Miller, A. L. (2014). Anillin regulates cell-cell junction integrity by organizing junctional accumulation of Rho-GTP and actomyosin. *Current Biology : CB*, *24*(11), 1263–1270. https://doi.org/10.1016/j.cub.2014.04.021

Richter, S., Kientz, M., Brumm, S., Nielsen, M. E., Park, M., Gavidia, R., Krause, C., Voss, U., Beckmann, H., Mayer, U., Stierhof, Y.-D., & Jürgens, G. (2014). Delivery of endocytosed proteins to the cell-division plane requires change of pathway from recycling to secretion. *ELife*, *3*, e02131. https://doi.org/10.7554/elife.02131

Ricketts, M. D., Dasgupta, N., Fan, J., Han, J., Gerace, M., Tang, Y., Black, B. E., Adams, P. D., & Marmorstein, R. (2019). The HIRA histone chaperone complex subunit UBN1 harbors H3/H4- and DNA-binding activity. *Journal of Biological Chemistry*, *294*(23), 9239–9259. https://doi.org/10.1074/jbc.ra119.007480

Riedel, F., Galindo, A., Muschalik, N., & Munro, S. (2017). The two TRAPP complexes of metazoans have distinct roles and act on different Rab GTPases. *The Journal of Cell Biology*, *217*(2), 601–617. https://doi.org/10.1083/jcb.201705068

Rink, J., Ghigo, E., Kalaidzidis, Y., & Zerial, M. (2005). Rab Conversion as a Mechanism of Progression from Early to Late Endosomes. *Cell*, *122*(5), 735–749. https://doi.org/10.1016/j.cell.2005.06.043

Rogerson, C., & Gissen, P. (2016). The CHEVI tethering complex: facilitating special deliveries. *The Journal of Pathology*, *240*(3), 249–252. https://doi.org/10.1002/path.4785

Roosen, D. A., Blauwendraat, C., Cookson, M. R., & Lewis, P. A. (2019). DNAJC proteins and pathways to parkinsonism. *The FEBS Journal*, *286*(16), 3080–3094. https://doi.org/10.1111/febs.14936

Rosing, M., Ossendorf, E., Rak, A., & Barnekow, A. (2007). Giantin interacts with both the small GTPase Rab6 and Rab1. *Experimental Cell Research*, *313*(11), 2318–2325. https://doi.org/10.1016/j.yexcr.2007.03.031

Rossé, C., Hatzoglou, A., Parrini, M.-C., White, M. A., Chavrier, P., & Camonis, J. (2006). RalB Mobilizes the Exocyst To Drive Cell Migration. *Molecular and Cellular Biology*, *26*(2), 727–734. https://doi.org/10.1128/mcb.26.2.727-734.2006

Roux, K. J., Kim, D. I., Raida, M., & Burke, B. (2012). A promiscuous biotin ligase fusion protein identifies proximal and interacting proteins in mammalian cells. *The Journal of Cell Biology*, *196*(6), 801–810. https://doi.org/10.1083/jcb.201112098

Rubino, D., Driggers, P., Arbit, D., Kemp, L., Miller, B., Coso, O., Pagliai, K., Gray, K., Gutkind, S., & Segars, J. (1998). Characterization of Brx, a novel Dbl family member that modulates estrogen receptor action. *Oncogene*, *16*(19), 2513–2526. https://doi.org/10.1038/sj.onc.1201783

Ruggiano, A., Foresti, O., & Carvalho, P. (2014). ER-associated degradation: Protein quality control and beyondER-associated degradation: Protein quality control and beyond. *The Journal of Cell Biology*, *204*(6), 869–879. https://doi.org/10.1083/jcb.201312042

Rümenapp, U., Blomquist, A., Schwörer, G., Schablowski, H., Psoma, A., & Jakobs, K. H. (1999). Rho-specific binding and guanine nucleotide exchange catalysis by KIAA0380, a Dbl family member. *FEBS Letters*, *459*(3), 313–318. https://doi.org/10.1016/s0014-5793(99)01270-3

Russo, A. J., Mathiowetz, A. J., Hong, S., Welch, M. D., & Campellone, K. G. (2016). Rab1 recruits WHAMM during membrane remodeling but limits actin nucleation. *Molecular Biology of the Cell*, *27*(6), 967–978. https://doi.org/10.1091/mbc.e15-07-0508

Sahani, M. H., Itakura, E., & Mizushima, N. (2014). Expression of the autophagy substrate SQSTM1/p62 is restored during prolonged starvation depending on transcriptional upregulation and autophagy-derived amino acids. *Autophagy*, *10*(3), 431–441. https://doi.org/10.4161/auto.27344

Salazar, M. A., Kwiatkowski, A. V., Pellegrini, L., Cestra, G., Butler, M. H., Rossman, K. L., Serna, D. M., Sondek, J., Gertler, F. B., & Camilli, P. D. (2003). Tuba, a Novel Protein Containing Bin/Amphiphysin/Rvs and Dbl Homology Domains, Links Dynamin to Regulation of the Actin Cytoskeleton. *Journal of Biological Chemistry*, *278*(49), 49031–49043. https://doi.org/10.1074/jbc.m308104200

Sandoval, C. O., & Simmen, T. (2012). Rab proteins of the endoplasmic reticulum: functions and interactors. *Biochemical Society Transactions*, *40*(6), 1426–1432. https://doi.org/10.1042/bst20120158

Saraste, J. (2016). Spatial and Functional Aspects of ER-Golgi Rabs and Tethers. *Frontiers in Cell and Developmental Biology*, *4*, 28. https://doi.org/10.3389/fcell.2016.00028

Sarkar, S., Davies, J. E., Huang, Z., Tunnacliffe, A., & Rubinsztein, D. C. (2007). Trehalose, a Novel mTOR-independent Autophagy Enhancer, Accelerates the Clearance of Mutant Huntingtin and α-Synuclein. *Journal of Biological Chemistry*, *282*(8), 5641–5652. https://doi.org/10.1074/jbc.m609532200

Sato, K., Sakaguchi, A., & Sato, M. (2016). REI/SH3BP5 protein family: New GEFs for Rab11. *Cell Cycle (Georgetown, Tex.)*, *15*(6), 767–769. https://doi.org/10.1080/15384101.2015.1137710

Schindler, C., Chen, Y., Pu, J., Guo, X., & Bonifacino, J. S. (2015). EARP is a multisubunit tethering complex involved in endocytic recycling. *Nature Cell Biology*, *17*(5), 639–650. https://doi.org/10.1038/ncb3129

Schlüter, O. M., Khvotchev, M., Jahn, R., & Südhof, T. C. (2002). Localization Versus Function of Rab3 Proteins: EVIDENCE FOR A COMMON REGULATORY ROLE IN CONTROLLING FUSION. *Journal of Biological Chemistry*, *277*(43), 40919–40929. https://doi.org/10.1074/jbc.m203704200

Schneider, T., Martinez-Martinez, A., Cubillos-Rojas, M., Bartrons, R., Ventura, F., & Rosa, J. L. (2018). The E3 ubiquitin ligase HERC1 controls the ERK signaling pathway targeting C-RAF for degradation. *Oncotarget*, *9*(59), 31531–31548. https://doi.org/10.18632/oncotarget.25847

Schoberer, J., & Strasser, R. (2011). Sub-Compartmental Organization of Golgi-Resident N-Glycan Processing Enzymes in Plants. *Molecular Plant*, *4*(2), 220–228. https://doi.org/10.1093/mp/ssq082

Schopp, I. M., Ramirez, C. C. A., Debeljak, J., Kreibich, E., Skribbe, M., Wild, K., & Béthune, J. (2017). Split-BioID a conditional proteomics approach to monitor the composition of spatiotemporally defined protein complexes. *Nature Communications*, *8*(1), 15690. https://doi.org/10.1038/ncomms15690

Schwarz, D. S., & Blower, M. D. (2016). The endoplasmic reticulum: structure, function and response to cellular signaling. *Cellular and Molecular Life Sciences*, *73*(1), 79–94. https://doi.org/10.1007/s00018-015-2052-6

Scott, C. C., Vacca, F., & Gruenberg, J. (2014). Endosome maturation, transport and functions. *Seminars in Cell & Developmental Biology*, *31*, 2–10. https://doi.org/10.1016/j.semcdb.2014.03.034

Segala, G., Bennesch, M. A., Ghahhari, N. M., Pandey, D. P., Echeverria, P. C., Karch, F., Maeda, R. K., & Picard, D. (2019). Vps11 and Vps18 of Vps-C membrane traffic complexes are E3 ubiquitin ligases and fine-tune signalling. *Nature Communications*, *10*(1), 1833. https://doi.org/10.1038/s41467-019-09800-y

Segev, N., & Botstein, D. (1987). The ras-like yeast YPT1 gene is itself essential for growth, sporulation, and starvation response. *Molecular and Cellular Biology*, *7*(7), 2367–2377. https://doi.org/10.1128/mcb.7.7.2367

Seol, W., Nam, D., & Son, I. (2019). Rab GTPases as Physiological Substrates of LRRK2 Kinase. *Experimental Neurobiology*, *28*(2), 134–145. https://doi.org/10.5607/en.2019.28.2.134

Sepulveda, F. E., Burgess, A., Heiligenstein, X., Goudin, N., Ménager, M. M., Romao, M., Côte, M., Mahlaoui, N., Fischer, A., Raposo, G., Ménasché, G., & Basile, G. de S. (2015). LYST controls the biogenesis of the endosomal compartment required for secretory lysosome function. *Traffic (Copenhagen, Denmark)*, *16*(2), 191–203. https://doi.org/10.1111/tra.12244

Sethi, N., Yan, Y., Quek, D., Schupbach, T., & Kang, Y. (2010). Rabconnectin-3 is a functional regulator of mammalian Notch signaling. *The Journal of Biological Chemistry*, *285*(45), 34757–34764. https://doi.org/10.1074/jbc.m110.158634

Shafaq-Zadah, M., Dransart, E., & Johannes, L. (2020). Clathrin-independent endocytosis, retrograde trafficking, and cell polarity. *Current Opinion in Cell Biology*, *65*, 112–121. https://doi.org/10.1016/j.ceb.2020.05.009

Shah, R., Li, F., Voziyanova, E., & Voziyanov, Y. (2015). Target-specific variants of Flp recombinase mediate genome engineering reactions in mammalian cells. *The FEBS Journal*, *282*(17), 3323–3333. https://doi.org/10.1111/febs.13345

Shanthirabalan, S., Chomilier, J., & Carpentier, M. (2018). Structural effects of point mutations in proteins. *Proteins: Structure, Function, and Bioinformatics*, *86*(8), 853–867. https://doi.org/10.1002/prot.25499

Sharpe, H. J., Stevens, T. J., & Munro, S. (2010). A Comprehensive Comparison of Transmembrane Domains Reveals Organelle-Specific Properties. *Cell*, *142*(1), 158–169. https://doi.org/10.1016/j.cell.2010.05.037

Shibata, H., Oishi, K., Yamagiwa, A., Matsumoto, M., Mukai, H., & Ono, Y. (2001). PKNbeta interacts with the SH3 domains of Graf and a novel Graf related protein, Graf2, which are GTPase activating proteins for Rho family. *Journal of Biochemistry*, *130*(1), 23–31. https://doi.org/10.1093/oxfordjournals.jbchem.a002958

Shimizu, H., Toma-Fukai, S., Saijo, S., Shimizu, N., Kontani, K., Katada, T., & Shimizu, T. (2017). Structure-based analysis of the guanine nucleotide exchange factor SmgGDS reveals armadillo-repeat motifs and key regions for activity and GTPase binding. *The Journal of Biological Chemistry*, *292*(32), 13441–13448. https://doi.org/10.1074/jbc.m117.792556

Shin, H.-W., Hayashi, M., Christoforidis, S., Lacas-Gervais, S., Hoepfner, S., Wenk, M. R., Modregger, J., Uttenweiler-Joseph, S., Wilm, M., Nystuen, A., Frankel, W. N., Solimena, M., Camilli, P. D., & Zerial, M. (2005). An enzymatic cascade of Rab5 effectors regulates phosphoinositide turnover in the endocytic pathway. *The Journal of Cell Biology*, *170*(4), 607–618. https://doi.org/10.1083/jcb.200505128

Shin, J. J. H., Gillingham, A. K., Begum, F., Chadwick, J., & Munro, S. (2017). TBC1D23 is a bridging factor for endosomal vesicle capture by golgins at the trans-Golgi. *Nature Cell Biology*, *19*(12), 1424–1432. https://doi.org/10.1038/ncb3627

Shin, Y.-C., Kim, C. M., Choi, J. Y., Jeon, J.-H., & Park, H. H. (2016). Occupation of nucleotide in the binding pocket is critical to the stability of Rab11A. *Protein Expression and Purification*, *120*, 153–159. https://doi.org/10.1016/j.pep.2016.01.001

Shiraishi, A., Uruno, T., Sanematsu, F., Ushijima, M., Sakata, D., Hara, T., & Fukui, Y. (2016). DOCK8 Protein Regulates Macrophage Migration through Cdc42 Protein Activation and LRAP35a Protein

Interaction. *The Journal of Biological Chemistry*, *292*(6), 2191–2202. https://doi.org/10.1074/jbc.m116.736306

Shirakawa, R., Fukai, S., Kawato, M., Higashi, T., Kondo, H., Ikeda, T., Nakayama, E., Okawa, K., Nureki, O., Kimura, T., Kita, T., & Horiuchi, H. (2009). Tuberous sclerosis tumor suppressor complex-like complexes act as GTPase-activating proteins for Ral GTPases. *The Journal of Biological Chemistry*, *284*(32), 21580–21588. https://doi.org/10.1074/jbc.m109.012112

Shirataki, H., Kaibuchi, K., Yamaguchi, T., Wada, K., Horiuchi, H., & Takai, Y. (1992). A possible target protein for smg-25A/rab3A small GTP-binding protein. *Journal of Biological Chemistry*, *267*(16), 10946–10949. https://doi.org/10.1016/s0021-9258(19)49857-8

Shisheva, A., Chinni, S. R., & DeMarco, C. (1999). General Role of GDP Dissociation Inhibitor 2 in Membrane Release of Rab Proteins: Modulations of Its Functional Interactions by in Vitro and in Vivo Structural Modifications †. *Biochemistry*, *38*(36), 11711–11721. https://doi.org/10.1021/bi990200r

Shneyer, B. I., Ušaj, M., & Henn, A. (2015). Myo19 is an outer mitochondrial membrane motor and effector of starvation-induced filopodia. *Journal of Cell Science*, *129*(3), 543–556. https://doi.org/10.1242/jcs.175349

Short, B., Haas, A., & Barr, F. A. (2005). Golgins and GTPases, giving identity and structure to the Golgi apparatus. *Biochimica et Biophysica Acta (BBA) - Molecular Cell Research*, *1744*(3), 383–395. https://doi.org/10.1016/j.bbamcr.2005.02.001

Short, B., Preisinger, C., Körner, R., Kopajtich, R., Byron, O., & Barr, F. A. (2001). A GRASP55-rab2 effector complex linking Golgi structure to membrane traffic. *The Journal of Cell Biology*, *155*(6), 877–884. https://doi.org/10.1083/jcb.200108079

Short, B., Preisinger, C., Schaletzky, J., Kopajtich, R., & Barr, F. A. (2002). The Rab6 GTPase Regulates Recruitment of the Dynactin Complex to Golgi Membranes. *Current Biology*, *12*(20), 1792–1795. https://doi.org/10.1016/s0960-9822(02)01221-6

Simonsen, A., Lippe, R., Christoforidis, S., Gaullier, J.-M., Brech, A., Callaghan, J., Toh, B.-H., Murphy, C., Zerial, M., & Stenmark, H. (1998). EEA1 links PI(3)K function to Rab5 regulation of endosome fusion. *Nature*, *394*(6692), 494–498. https://doi.org/10.1038/28879

Sinka, R., Gillingham, A. K., Kondylis, V., & Munro, S. (2008). Golgi coiled-coil proteins contain multiple binding sites for Rab family G proteins. *The Journal of Cell Biology*, *183*(4), 607–615. https://doi.org/10.1083/jcb.200808018

Sobajima, T., Yoshimura, S.-I., Maeda, T., Miyata, H., Miyoshi, E., & Harada, A. (2018). The Rab11-binding protein RELCH/KIAA1468 controls intracellular cholesterol distribution. *The Journal of Cell Biology*, *217*(5), 1777–1796. https://doi.org/10.1083/jcb.201709123

Soleimanpour, S. A., Gupta, A., Bakay, M., Ferrari, A. M., Groff, D. N., Fadista, J., Spruce, L. A., Kushner, J. A., Groop, L., Seeholzer, S. H., Kaufman, B. A., Hakonarson, H., & Stoffers, D. A. (2014). The Diabetes Susceptibility Gene Clec16a Regulates Mitophagy. *Cell*, *157*(7), 1577–1590. https://doi.org/10.1016/j.cell.2014.05.016

Song, G. J., Jeon, H., Seo, M., Jo, M., & Suk, K. (2018). Interaction between optineurin and Rab1a regulates autophagosome formation in neuroblastoma cells. *Journal of Neuroscience Research*, *96*(3), 407–415. https://doi.org/10.1002/jnr.24143

Sönnichsen, B., Renzis, S. D., Nielsen, E., Rietdorf, J., & Zerial, M. (2000). Distinct Membrane Domains on Endosomes in the Recycling Pathway Visualized by Multicolor Imaging of Rab4, Rab5, and Rab11. *The Journal of Cell Biology*, *149*(4), 901–914. https://doi.org/10.1083/jcb.149.4.901

Sorvina, A., Shandala, T., & Brooks, D. A. (2016). Drosophila Pkaap regulates Rab4/Rab11-dependent traffic and Rab11 exocytosis of innate immune cargo. *Biology Open*, *5*(6), 678–688. https://doi.org/10.1242/bio.016642

Sowa, M. E., Bennett, E. J., Gygi, S. P., & Harper, J. W. (2009). Defining the human deubiquitinating enzyme interaction landscape. *Cell*, *138*(2), 389–403. https://doi.org/10.1016/j.cell.2009.04.042

Spang, A. (2013). Retrograde Traffic from the Golgi to the Endoplasmic Reticulum. *Cold Spring Harbor Perspectives in Biology*, *5*(6), a013391. https://doi.org/10.1101/cshperspect.a013391

Spang, A. (2016). Membrane Tethering Complexes in the Endosomal System. *Frontiers in Cell and Developmental Biology*, *4*, 35. https://doi.org/10.3389/fcell.2016.00035

Spiller, F., Medina-Pritchard, B., Abad, M. A., Wear, M. A., Molina, O., Earnshaw, W. C., & Jeyaprakash, A. A. (2017). Molecular basis for Cdk1-regulated timing of Mis18 complex assembly and CENP-A deposition. *EMBO Reports*, *18*(6), 894–905. https://doi.org/10.15252/embr.201643564

Stadel, D., Millarte, V., Tillmann, K. D., Huber, J., Tamin-Yecheskel, B.-C., Akutsu, M., Demishtein, A., Ben-Zeev, B., Anikster, Y., Perez, F., Dötsch, V., Elazar, Z., Rogov, V., Farhan, H., & Behrends, C. (2015). TECPR2 Cooperates with LC3C to Regulate COPII-Dependent ER Export. *Molecular Cell*, *60*(1), 89–104. https://doi.org/10.1016/j.molcel.2015.09.010

Stagg, S. M., Gürkan, C., Fowler, D. M., LaPointe, P., Foss, T. R., Potter, C. S., Carragher, B., & Balch, W. E. (2006). Structure of the Sec13/31 COPII coat cage. *Nature*, *439*(7073), 234–238. https://doi.org/10.1038/nature04339

Stagg, S. M., LaPointe, P., Razvi, A., Gürkan, C., Potter, C. S., Carragher, B., & Balch, W. E. (2008). Structural Basis for Cargo Regulation of COPII Coat Assembly. *Cell*, *134*(3), 474–484. https://doi.org/10.1016/j.cell.2008.06.024

Stalder, D., & Gershlick, D. C. (2020). Direct trafficking pathways from the Golgi apparatus to the plasma membrane. *Seminars in Cell & Developmental Biology*, *107*, 112–125. https://doi.org/10.1016/j.semcdb.2020.04.001

Stanley, P. (2011). Golgi Glycosylation. *Cold Spring Harbor Perspectives in Biology*, *3*(4), a005199. https://doi.org/10.1101/cshperspect.a005199

Stefely, J. A., Zhang, Y., Freiberger, E. C., Kwiecien, N. W., Thomas, H. E., Davis, A. M., Lowry, N. D., Vincent, C. E., Shishkova, E., Clark, N. A., Medvedovic, M., Coon, J. J., Pagliarini, D. J., & Mercer, C. A. (2020). Mass spectrometry proteomics reveals a function for mammalian CALCOCO1 in MTOR-regulated selective autophagy. *Autophagy*, 15548627.2020.1719746. https://doi.org/10.1080/15548627.2020.1719746

Steger, M., Diez, F., Dhekne, H. S., Lis, P., Nirujogi, R. S., Karayel, O., Tonelli, F., Martinez, T. N., Lorentzen, E., Pfeffer, S. R., Alessi, D. R., & Mann, M. (2017). Systematic proteomic analysis of LRRK2-mediated Rab GTPase phosphorylation establishes a connection to ciliogenesis. *ELife*, *6*, e31012. https://doi.org/10.7554/elife.31012

Steinman, R. M., Mellman, I. S., Muller, W. A., & Cohn, Z. A. (1983). Endocytosis and the recycling of plasma membrane. *The Journal of Cell Biology*, *96*(1), 1–27. https://doi.org/10.1083/jcb.96.1.1

Stenmark, H. (2009). Rab GTPases as coordinators of vesicle traffic. *Nature Reviews Molecular Cell Biology*, *10*(8), 513–525. https://doi.org/10.1038/nrm2728

Stenmark, H., Vitale, G., Ullrich, O., & Zerial, M. (1995). Rabaptin-5 is a direct effector of the small GTPase Rab5 in endocytic membrane fusion. *Cell*, *83*(3), 423–432. https://doi.org/10.1016/0092-8674(95)90120-5

STINTON, L., SELAK, S., & FRITZLER, M. (2005). Identification of GRASP-1 as a novel 97 kDa autoantigen localized to endosomes. *Clinical Immunology*, *116*(2), 108–117. https://doi.org/10.1016/j.clim.2005.03.021

Sumakovic, M., Hegermann, J., Luo, L., Husson, S. J., Schwarze, K., Olendrowitz, C., Schoofs, L., Richmond, J., & Eimer, S. (2009). UNC-108/RAB-2 and its effector RIC-19 are involved in dense core vesicle maturation in Caenorhabditis elegans. *The Journal of Cell Biology*, *186*(6), 897–914. https://doi.org/10.1083/jcb.200902096

Syrbe, S., Harms, F. L., Parrini, E., Montomoli, M., Mütze, U., Helbig, K. L., Polster, T., Albrecht, B., Bernbeck, U., Binsbergen, E. van, Biskup, S., Burglen, L., Denecke, J., Heron, B., Heyne, H. O., Hoffmann, G. F., Hornemann, F., Matsushige, T., Matsuura, R., … Guerrini, R. (2017). Delineating SPTAN1 associated phenotypes: from isolated epilepsy to encephalopathy with progressive brain atrophy. *Brain*, *140*(9), 2322–2336. https://doi.org/10.1093/brain/awx195

Tam, R. C. Y., Li, M. W. M., Gao, Y. P., Pang, Y. T., Yan, S., Ge, W., Lau, C. S., & Chan, V. S. F. (2017). Human CLEC16A regulates autophagy through modulating mTOR activity. *Experimental Cell Research*, *352*(2), 304–312. https://doi.org/10.1016/j.yexcr.2017.02.017

Tammana, T. V. S., Tammana, D., Diener, D. R., & Rosenbaum, J. (2013). Centrosomal protein CEP104 (Chlamydomonas FAP256) moves to the ciliary tip during ciliary assembly. *Journal of Cell Science*, *126*(Pt 21), 5018–5029. https://doi.org/10.1242/jcs.133439

Tao, F., Beecham, G. W., Rebelo, A. P., Svaren, J., Blanton, S. H., Moran, J. J., Lopez-Anido, C., Morrow, J. M., Abreu, L., Rizzo, D., Kirk, C. A., Wu, X., Feely, S., Verhamme, C., Saporta, M. A., Herrmann, D. N., Day, J. W., Sumner, C. J., Lloyd, T. E., … Consortium, I. N. (2019). Variation in SIPA1L2 is

correlated with phenotype modification in Charcot- Marie- Tooth disease type 1A. *Annals of Neurology*, *85*(3), 316–330. https://doi.org/10.1002/ana.25426

Teng, X., Aouacheria, A., Lionnard, L., Metz, K. A., Soane, L., Kamiya, A., & Hardwick, J. M. (2019). KCTD : A new gene family involved in neurodevelopmental and neuropsychiatric disorders. *CNS Neuroscience & Therapeutics*, *25*(7), 887–902. https://doi.org/10.1111/cns.13156

Thomas, J. D., Zhang, Y.-J., Wei, Y.-H., Cho, J.-H., Morris, L. E., Wang, H.-Y., & Zheng, X. F. S. (2014). Rab1A is an mTORC1 activator and a colorectal oncogene. *Cancer Cell*, *26*(5), 754–769. https://doi.org/10.1016/j.ccell.2014.09.008

Thomas, L. L., Joiner, A. M. N., & Fromme, J. C. (2018). The TRAPPIII complex activates the GTPase Ypt1 (Rab1) in the secretory pathway. *The Journal of Cell Biology*, *217*(1), 283–298. https://doi.org/10.1083/jcb.201705214

Thomé, M. P., Filippi-Chiela, E. C., Villodre, E. S., Migliavaca, C. B., Onzi, G. R., Felipe, K. B., & Lenz, G. (2016). Ratiometric analysis of Acridine Orange staining in the study of acidic organelles and autophagy. *J Cell Sci*, *129*(24), 4622–4632. https://doi.org/10.1242/jcs.195057

Tian, X., & Feig, L. A. (2001). Basis for Signaling Specificity Difference between Sos and Ras-GRF Guanine Nucleotide Exchange Factors. *Journal of Biological Chemistry*, *276*(50), 47248–47256. https://doi.org/10.1074/jbc.m107407200

Tong, L. (2012). Structure and function of biotin-dependent carboxylases. *Cellular and Molecular Life Sciences : CMLS*, *70*(5), 863–891. https://doi.org/10.1007/s00018-012-1096-0

Topp, J. D., Gray, N. W., Gerard, R. D., & Horazdovsky, B. F. (2004). Alsin Is a Rab5 and Rac1 Guanine Nucleotide Exchange Factor. *Journal of Biological Chemistry*, *279*(23), 24612–24623. https://doi.org/10.1074/jbc.m313504200

Touchot, N., Zahraoui, A., Vielh, E., & Tavitian, A. (1989). Biochemical properties of the YPT-related rab1B protein. *FEBS Letters*, *256*(1–2), 79–84. https://doi.org/10.1016/0014-5793(89)81722-3

Tremel, S., Ohashi, Y., Morado, D. R., Bertram, J., Perisic, O., Brandt, L. T. L., Wrisberg, M.-K. von, Chen, Z. A., Maslen, S. L., Kovtun, O., Skehel, M., Rappsilber, J., Lang, K., Munro, S., Briggs, J. A.

G., & Williams, R. L. (2021). Structural basis for VPS34 kinase activation by Rab1 and Rab5 on membranes. *Nature Communications*, *12*(1), 1564. https://doi.org/10.1038/s41467-021-21695-2

Trinkle-Mulcahy, L. (2019). Recent advances in proximity-based labeling methods for interactome mapping. *F1000Research*, *8*, F1000 Faculty Rev-135. https://doi.org/10.12688/f1000research.16903.1

Tu, L., Chen, L., & Banfield, D. K. (2012). A Conserved N-terminal Arginine-Motif in GOLPH3-Family Proteins Mediates Binding to Coatomer. *Traffic*, *13*(11), 1496–1507. https://doi.org/10.1111/j.1600-0854.2012.01403.x

Tu, L., Tai, W. C. S., Chen, L., & Banfield, D. K. (2008). Signal-Mediated Dynamic Retention of Glycosyltransferases in the Golgi. *Science*, *321*(5887), 404–407. https://doi.org/10.1126/science.1159411

van Spronsen, M., Mikhaylova, M., Lipka, J., Schlager, M. A., van den Heuvel, D. J., Kuijpers, M., Wulf, P. S., Keijzer, N., Demmers, J., Kapitein, L. C., Jaarsma, D., Gerritsen, H. C., Akhmanova, A., & Hoogenraad, C. C. (2013). TRAK/Milton Motor-Adaptor Proteins Steer Mitochondrial Trafficking to Axons and Dendrites. *Neuron*, *77*(3), 485–502. https://doi.org/10.1016/j.neuron.2012.11.027

Velthuis, A. J. W. te, & Bagowski, C. P. (2007). PDZ and LIM Domain-Encoding Genes: Molecular Interactions and their Role in Development. *The Scientific World JOURNAL*, *7*, 1470–1492. https://doi.org/10.1100/tsw.2007.232

Vetter, M., Stehle, R., Basquin, C., & Lorentzen, E. (2015). Structure of Rab11-FIP3-Rabin8 reveals simultaneous binding of FIP3 and Rabin8 effectors to Rab11. *Nature Structural & Molecular Biology*, *22*(9), 695–702. https://doi.org/10.1038/nsmb.3065

Vidyadhara, D. J., Lee, J. E., & Chandra, S. S. (2019). Role of the endolysosomal system in Parkinson's disease. *Journal of Neurochemistry*, *150*(5), 487–506. https://doi.org/10.1111/jnc.14820

Vikis, H. G., Stewart, S., & Guan, K.-L. (2002). SmgGDS displays differential binding and exchange activity towards different Ras isoforms. *Oncogene*, *21*(15), 2425–2432. https://doi.org/10.1038/sj.onc.1205306

Vitale, G., Rybin, V., Christoforidis, S., Thornqvist, P.-Ö., McCaffrey, M., Stenmark, H., & Zerial, M. (1998). Distinct Rab-binding domains mediate the interaction of Rabaptin-5 with GTP-bound rab4 and rab5. *The EMBO Journal*, *17*(7), 1941–1951. https://doi.org/10.1093/emboj/17.7.1941

Vives, V., Laurin, M., Cres, G., Larrousse, P., Morichaud, Z., Noel, D., Côté, J.-F., & Blangy, A. (2011). The Rac1 exchange factor Dock5 is essential for bone resorption by osteoclasts. *Journal of Bone and Mineral Research : The Official Journal of the American Society for Bone and Mineral Research*, *26*(5), 1099–1110. https://doi.org/10.1002/jbmr.282

Walch, L., Pellier, E., Leng, W., Lakisic, G., Gautreau, A., Contremoulins, V., Verbavatz, J.-M., & Jackson, C. L. (2018). GBF1 and Arf1 interact with Miro and regulate mitochondrial positioning within cells. *Scientific Reports*, *8*(1), 17121. https://doi.org/10.1038/s41598-018-35190-0

Walczak, M., & Martens, S. (2013). Dissecting the role of the Atg12–Atg5-Atg16 complex during autophagosome formation. *Autophagy*, *9*(3), 424–425. https://doi.org/10.4161/auto.22931

Walia, V., Cuenca, A., Vetter, M., Insinna, C., Perera, S., Lu, Q., Ritt, D. A., Semler, E., Specht, S., Stauffer, J., Morrison, D. K., Lorentzen, E., & Westlake, C. J. (2019). Akt Regulates a Rab11-Effector Switch Required for Ciliogenesis. *Developmental Cell*, *50*(2), 229-246.e7. https://doi.org/10.1016/j.devcel.2019.05.022

Wandinger-Ness, A., & Zerial, M. (2014). Rab proteins and the compartmentalization of the endosomal system. *Cold Spring Harbor Perspectives in Biology*, *6*(11), a022616. https://doi.org/10.1101/cshperspect.a022616

Wang, F., Zhan, R., Chen, L., Dai, X., Wang, W., Guo, R., Li, X., Li, Z., Wang, L., Huang, S., Shen, J., Li, S., & Cao, C. (2017). RhoA promotes epidermal stem cell proliferation via PKN1-cyclin D1 signaling. *PLOS ONE*, *12*(2), e0172613. https://doi.org/10.1371/journal.pone.0172613

Wang, Jing, Fedoseienko, A., Chen, B., Burstein, E., Jia, D., & Billadeau, D. D. (2018). Endosomal receptor trafficking: Retromer and beyond. *Traffic (Copenhagen, Denmark)*, *19*(8), 578–590. https://doi.org/10.1111/tra.12574

Wang, Jing, Xu, H., Jiang, Y., Takahashi, M., Takeichi, M., & Meng, W. (2017). CAMSAP3-dependent microtubule dynamics regulates Golgi assembly in epithelial cells. *Journal of Genetics and Genomics*, *44*(1), 39–49. https://doi.org/10.1016/j.jgg.2016.11.005

Wang, Juan, Menon, S., Yamasaki, A., Chou, H.-T., Walz, T., Jiang, Y., & Ferro-Novick, S. (2013). Ypt1 recruits the Atg1 kinase to the preautophagosomal structure. *Proceedings of the National Academy of Sciences of the United States of America*, *110*(24), 9800–9805. https://doi.org/10.1073/pnas.1302337110

Wang, L., Lan, Y., Du, Y., Xiang, X., Tian, W., Yang, B., Li, T., & Zhai, Q. (2020). Plastin 1 promotes osteoblast differentiation by regulating intracellular Ca2. *Acta Biochimica et Biophysica Sinica*. https://doi.org/10.1093/abbs/gmaa027

Wang, S., Ma, Z., Xu, X., Wang, Z., Sun, L., Zhou, Y., Lin, X., Hong, W., & Wang, T. (2014). A role of Rab29 in the integrity of the trans-Golgi network and retrograde trafficking of mannose-6-phosphate receptor. *PloS One*, *9*(5), e96242. https://doi.org/10.1371/journal.pone.0096242

Wang, T., Grabski, R., Sztul, E., & Hay, J. C. (2015). p115–SNARE Interactions: A Dynamic Cycle of p115 Binding Monomeric SNARE Motifs and Releasing Assembled Bundles. *Traffic*, *16*(2), 148–171. https://doi.org/10.1111/tra.12242

Wang, Y., Chai, Z., Wang, M., Jin, Y., Yang, A., & Li, M. (2017). COPB2 suppresses cell proliferation and induces cell cycle arrest in human colon cancer by regulating cell cycle-related proteins. *Experimental and Therapeutic Medicine*, *15*(1), 777–784. https://doi.org/10.3892/etm.2017.5506

Watson, J. R., Owen, D., & Mott, H. R. (2016). Cdc42 in actin dynamics: An ordered pathway governed by complex equilibria and directional effector handover. *Small GTPases*, *8*(4), 237–244. https://doi.org/10.1080/21541248.2016.1215657

Weber, C. K., Slupsky, J. R., Kalmes, H. A., & Rapp, U. R. (2001). Active Ras induces heterodimerization of cRaf and BRaf. *Cancer Research*, *61*(9), 3595–3598.

Webster, C. P., Smith, E. F., Bauer, C. S., Moller, A., Hautbergue, G. M., Ferraiuolo, L., Myszczynska, M. A., Higginbottom, A., Walsh, M. J., Whitworth, A. J., Kaspar, B. K., Meyer, K., Shaw, P. J., Grierson, A. J., & Vos, K. J. D. (2016). The C9orf72 protein interacts with Rab1a and the ULK1 complex to regulate initiation of autophagy. *The EMBO Journal*, *35*(15), 1656–1676. https://doi.org/10.15252/embj.201694401

Webster, C. P., Smith, E. F., Grierson, A. J., & Vos, K. J. D. (2018). C9orf72 plays a central role in Rab GTPase-dependent regulation of autophagy. *Small GTPases*, *9*(5), 399–408. https://doi.org/10.1080/21541248.2016.1240495

Welch, L. G., & Munro, S. (2019). A tale of short tails, through thick and thin: investigating the sorting mechanisms of Golgi enzymes. *FEBS Letters*, *593*(17), 2452–2465. https://doi.org/10.1002/1873-3468.13553

Welz, T., Wellbourne-Wood, J., & Kerkhoff, E. (2014). Orchestration of cell surface proteins by Rab11. *Trends in Cell Biology*, *24*(7), 407–415. https://doi.org/10.1016/j.tcb.2014.02.004

Wennerberg, K., Rossman, K. L., & Der, C. J. (2005). The Ras superfamily at a glance. *Journal of Cell Science*, *118*(5), 843–846. https://doi.org/10.1242/jcs.01660

Westlake, C J, Junutula, J. R., Simon, G. C., Pilli, M., Prekeris, R., Scheller, R. H., Jackson, P. K., & Eldridge, A. G. (2007). Identification of Rab11 as a small GTPase binding protein for the Evi5 oncogene. *Proceedings of the National Academy of Sciences*, *104*(4), 1236–1241. https://doi.org/10.1073/pnas.0610500104

Westlake, Christopher J, Baye, L. M., Nachury, M. V., Wright, K. J., Ervin, K. E., Phu, L., Chalouni, C., Beck, J. S., Kirkpatrick, D. S., Slusarski, D. C., Sheffield, V. C., Scheller, R. H., & Jackson, P. K. (2011). Primary cilia membrane assembly is initiated by Rab11 and transport protein particle II (TRAPPII) complex-dependent trafficking of Rabin8 to the centrosome. *Proceedings of the National Academy of Sciences of the United States of America*, *108*(7), 2759–2764. https://doi.org/10.1073/pnas.1018823108

Williams, C. L. (2003). The polybasic region of Ras and Rho family small GTPases: a regulator of protein interactions and membrane association and a site of nuclear localization signal sequences. *Cellular Signalling*, *15*(12), 1071–1080. https://doi.org/10.1016/s0898-6568(03)00098-6

Wilson, N. H., & Key, B. (2007). Neogenin: One receptor, many functions. *The International Journal of Biochemistry & Cell Biology*, *39*(5), 874–878. https://doi.org/10.1016/j.biocel.2006.10.023

Winslow, A. R., Chen, C.-W., Corrochano, S., Acevedo-Arozena, A., Gordon, D. E., Peden, A. A., Lichtenberg, M., Menzies, F. M., Ravikumar, B., Imarisio, S., Brown, S., O'Kane, C. J., & Rubinsztein,

D. C. (2010). α-Synuclein impairs macroautophagy: implications for Parkinson's disease. *The Journal of Cell Biology*, *190*(6), 1023–1037. https://doi.org/10.1083/jcb.201003122

Witkos, T. M., Chan, W. L., Joensuu, M., Rhiel, M., Pallister, E., Thomas-Oates, J., Mould, A. P., Mironov, A. A., Biot, C., Guerardel, Y., Morelle, W., Ungar, D., Wieland, F. T., Jokitalo, E., Tassabehji, M., Kornak, U., & Lowe, M. (2019). GORAB scaffolds COPI at the trans-Golgi for efficient enzyme recycling and correct protein glycosylation. *Nature Communications*, *10*(1), 127. https://doi.org/10.1038/s41467-018-08044-6

Wixler, V., Wixler, L., Altenfeld, A., Ludwig, S., Goody, R. S., & Itzen, A. (2011). Identification and characterisation of novel Mss4-binding Rab GTPases. *Biological Chemistry*, *392*(3), 239–248. https://doi.org/10.1515/bc.2011.022

Wong, M., Gillingham, A. K., & Munro, S. (2017). The golgin coiled-coil proteins capture different types of transport carriers via distinct N-terminal motifs. *BMC Biology*, *15*(1), 3. https://doi.org/10.1186/s12915-016-0345-3

Wright, P. (2008). Targeting Vesicle Trafficking: An Important Approach to Cancer Chemotherapy. *Recent Patents on Anti-Cancer Drug Discovery*, *3*(2), 137–147. https://doi.org/10.2174/157489208784638730

Wu, B., & Guo, W. (2015). The Exocyst at a Glance. *Journal of Cell Science*, *128*(16), 2957–2964. https://doi.org/10.1242/jcs.156398

Xiao, Y., Peng, Y., Wan, J., Tang, G., Chen, Y., Tang, J., Ye, W.-C., Ip, N. Y., & Shi, L. (2013). The atypical guanine nucleotide exchange factor Dock4 regulates neurite differentiation through modulation of Rac1 GTPase and actin dynamics. *The Journal of Biological Chemistry*, *288*(27), 20034–20045. https://doi.org/10.1074/jbc.m113.458612

Xie, X., Li, F., Wang, Y., Wang, Y., Lin, Z., Cheng, X., Liu, J., Chen, C., & Pan, L. (2015). Molecular basis of ubiquitin recognition by the autophagy receptor CALCOCO2. *Autophagy*, *11*(10), 1775–1789. https://doi.org/10.1080/15548627.2015.1082025

Xiong, X., Liu, X., Li, H., He, H., Sun, Y., & Zhao, Y. (2018). Ribosomal protein S27-like regulates autophagy via the β-TrCP-DEPTOR-mTORC1 axis. *Cell Death & Disease*, *9*(11), 1131. https://doi.org/10.1038/s41419-018-1168-7

Yamaguchi, A., Urano, T., Goi, T., & Feig, L. A. (1997). An Eps Homology (EH) Domain Protein That Binds to the Ral-GTPase Target, RalBP1. *Journal of Biological Chemistry*, *272*(50), 31230–31234. https://doi.org/10.1074/jbc.272.50.31230

Yamamoto, H., Koga, H., Katoh, Y., Takahashi, S., Nakayama, K., & Shin, H.-W. (2010). Functional cross-talk between Rab14 and Rab4 through a dual effector, RUFY1/Rabip4. *Molecular Biology of the Cell*, *21*(15), 2746–2755. https://doi.org/10.1091/mbc.e10-01-0074

Yamasaki, A., Menon, S., Yu, S., Barrowman, J., Meerloo, T., Oorschot, V., Klumperman, J., Satoh, A., & Ferro-Novick, S. (2009). mTrs130 Is a Component of a Mammalian TRAPPII Complex, a Rab1 GEF That Binds to COPI-coated Vesicles. *Molecular Biology of the Cell*, *20*(19), 4205–4215. https://doi.org/10.1091/mbc.e09-05-0387

Yang, F., Chen, Y., & Dai, W. (2015). Sumoylation of Kif18A plays a role in regulating mitotic progression. *BMC Cancer*, *15*(1), 197. https://doi.org/10.1186/s12885-015-1226-9

Yang, K. C., Sathiyaseelan, P., Ho, C., & Gorski, S. M. (2018). Evolution of tools and methods for monitoring autophagic flux in mammalian cells. *Biochemical Society Transactions*, *46*(1), 97–110. https://doi.org/10.1042/bst20170102

Yang, X.-Z., Li, X.-X., Zhang, Y.-J., Rodriguez-Rodriguez, L., Xiang, M.-Q., Wang, H.-Y., & Zheng, X. F. S. (2016). Rab1 in cell signaling, cancer and other diseases. *Oncogene*, *35*(44), 5699–5704. https://doi.org/10.1038/onc.2016.81

Yang, Y., Wang, G., Huang, X., & Du, Z. (2015). Crystallographic and modelling studies suggest that the SKICH domains from different protein families share a common Ig-like fold but harbour substantial structural variations. *Journal of Biomolecular Structure & Dynamics*, *33*(7), 1385–1398. https://doi.org/10.1080/07391102.2014.951688

Ye, B., Liao, D., Zhang, X., Zhang, P., Dong, H., & Huganir, R. L. (2000). GRASP-1 A Neuronal RasGEF Associated with the AMPA Receptor/GRIP Complex. *Neuron*, *26*(3), 603–617. https://doi.org/10.1016/s0896-6273(00)81198-8

Ye, B., Yu, W., Thomas, G. M., & Huganir, R. L. (2007). GRASP-1 is a neuronal scaffold protein for the JNK signaling pathway. *FEBS Letters*, *581*(23), 4403–4410. https://doi.org/10.1016/j.febslet.2007.08.008

Yin, J., Huang, Y., Guo, P., Hu, S., Yoshina, S., Xuan, N., Gan, Q., Mitani, S., Yang, C., & Wang, X. (2017). GOP-1 promotes apoptotic cell degradation by activating the small GTPase Rab2 in C. elegans. *The Journal of Cell Biology*, *216*(6), 1775–1794. https://doi.org/10.1083/jcb.201610001

Yokoyama, N., & Miller, W. T. (2003). Biochemical properties of the Cdc42-associated tyrosine kinase ACK1. Substrate specificity, authphosphorylation, and interaction with Hck. *The Journal of Biological Chemistry*, *278*(48), 47713–47723. https://doi.org/10.1074/jbc.m306716200

Yoshimura, S., Gerondopoulos, A., Linford, A., Rigden, D. J., & Barr, F. A. (2010). Family-wide characterization of the DENN domain Rab GDP-GTP exchange factors. *The Journal of Cell Biology*, *191*(2), 367–381. https://doi.org/10.1083/jcb.201008051

Zago, G., Veith, I., Singh, M., Fuhrmann, L., Beco, S. D., Remorino, A., Takaoka, S., Palmeri, M., Berger, F., Brandon, N., Marjou, A. E., Vincent-Salomon, A., Camonis, J., Coppey, M., & Parrini, M. C. (2018). RalB directly triggers invasion downstream Ras by mobilizing the Wave complex. *ELife*, *7*, e40474. https://doi.org/10.7554/elife.40474

Zerial, M., & McBride, H. (2001). Rab proteins as membrane organizers. *Nature Reviews Molecular Cell Biology*, *2*(2), 107–117. https://doi.org/10.1038/35052055

Zhang, T., Wang, Z., Liu, Y., Huo, Y., Liu, H., Xu, C., Mao, R., Zhu, Y., Liu, L., Wei, D., Liu, G., Pan, B., Tang, Y., Zhou, Z., Yang, C., & Guo, Y. (2020). Plastin 1 drives metastasis of colorectal cancer through the IQGAP1/Rac1/ERK pathway. *Cancer Science*. https://doi.org/10.1111/cas.14438

Zhang, Z., Zhang, T., Wang, S., Gong, Z., Tang, C., Chen, J., & Ding, J. (2014). Molecular mechanism for Rabex-5 GEF activation by Rabaptin-5. *ELife*, *3*, e02687. https://doi.org/10.7554/elife.02687

Zhao, X., Claude, A., Chun, J., Shields, D. J., Presley, J. F., & Melançon, P. (2006). GBF1, a cis-Golgi and VTCs-localized ARF-GEF, is implicated in ER-to-Golgi protein traffic. *Journal of Cell Science*, *119*(18), 3743–3753. https://doi.org/10.1242/jcs.03173

Zhao, Y.-L., Zhong, S.-R., Zhang, S.-H., Bi, J.-X., Xiao, Z.-Y., Wang, S.-Y., Jiao, H.-L., Zhang, D., Qiu, J.-F., Zhang, L.-J., Huang, C.-M., Chen, X.-L., Ding, Y.-Q., Ye, Y.-P., Liang, L., & Liao, W.-T. (2019). UBN2 promotes tumor progression via the Ras/MAPK pathway and predicts poor prognosis in colorectal cancer. *Cancer Cell International*, *19*(1), 126. https://doi.org/10.1186/s12935-019-0848-4

Zhao, Z., & Manser, E. (2015). Myotonic dystrophy kinase-related Cdc42-binding kinases (MRCK), the ROCK-like effectors of Cdc42 and Rac1. *Small GTPases*, *6*(2), 81–88. https://doi.org/10.1080/21541248.2014.1000699

Zhou, W., Li, X., & Premont, R. T. (2016). Expanding functions of GIT Arf GTPase-activating proteins, PIX Rho guanine nucleotide exchange factors and GIT–PIX complexes. *Journal of Cell Science*, *129*(10), 1963–1974. https://doi.org/10.1242/jcs.179465

Zhou, Yeyun, Johnson, J. L., Cerione, R. A., & Erickson, J. W. (2013). Prenylation and membrane localization of Cdc42 are essential for activation by DOCK7. *Biochemistry*, *52*(25), 4354–4363. https://doi.org/10.1021/bi301688g

Zhou, You, Robciuc, M. R., Wabitsch, M., Juuti, A., Leivonen, M., Ehnholm, C., Yki-Järvinen, H., & Olkkonen, V. M. (2012). OSBP-related proteins (ORPs) in human adipose depots and cultured adipocytes: evidence for impacts on the adipocyte phenotype. *PloS One*, *7*(9), e45352. https://doi.org/10.1371/journal.pone.0045352

Zinatizadeh, M. R., Momeni, S. A., Zarandi, P. K., Chalbatani, G. M., Dana, H., Mirzaei, H. R., Akbari, M. E., & Miri, S. R. (2019). The Role and Function of Ras-association domain family in Cancer: A Review. *Genes & Diseases*, *6*(4), 378–384. https://doi.org/10.1016/j.gendis.2019.07.008

Zoppino, F. C. M., Militello, R. D., Slavin, I., Alvarez, C., & Colombo, M. I. (2010). Autophagosome formation depends on the small GTPase Rab1 and functional ER exit sites. *Traffic (Copenhagen, Denmark)*, *11*(9), 1246–1261. https://doi.org/10.1111/j.1600-0854.2010.01086.x

Zou, J., Chang, S.-C., Marjanovic, J., & Majerus, P. W. (2009). MTMR9 Increases MTMR6 Enzyme Activity, Stability, and Role in Apoptosis. *Journal of Biological Chemistry*, *284*(4), 2064–2071. https://doi.org/10.1074/jbc.m804292200

Zulkefli, K. L., Houghton, F. J., Gosavi, P., & Gleeson, P. A. (2019). A role for Rab11 in the homeostasis of the endosome-lysosomal pathway. *Experimental Cell Research*, *380*(1), 55–68. https://doi.org/10.1016/j.yexcr.2019.04.010